

University of Windsor

Scholarship at UWindor

Electronic Theses and Dissertations

Theses, Dissertations, and Major Papers

2008

Methods to mitigate injuries to toddlers in a vehicle crash

Tanya Kapoor
University of Windsor

Follow this and additional works at: <https://scholar.uwindsor.ca/etd>

Recommended Citation

Kapoor, Tanya, "Methods to mitigate injuries to toddlers in a vehicle crash" (2008). *Electronic Theses and Dissertations*. 7871.

<https://scholar.uwindsor.ca/etd/7871>

This online database contains the full-text of PhD dissertations and Masters' theses of University of Windsor students from 1954 forward. These documents are made available for personal study and research purposes only, in accordance with the Canadian Copyright Act and the Creative Commons license—CC BY-NC-ND (Attribution, Non-Commercial, No Derivative Works). Under this license, works must always be attributed to the copyright holder (original author), cannot be used for any commercial purposes, and may not be altered. Any other use would require the permission of the copyright holder. Students may inquire about withdrawing their dissertation and/or thesis from this database. For additional inquiries, please contact the repository administrator via email (scholarship@uwindsor.ca) or by telephone at 519-253-3000ext. 3208.

NOTE TO USERS

This reproduction is the best copy available.

UMI[®]

METHODS TO MITIGATE INJURIES TO TODDLERS IN A VEHICLE
CRASH

by

Tanya Kapoor

A Dissertation
Submitted to the Faculty of Graduate Studies
Through Mechanical Engineering
In Partial Fulfillment of the Requirements for
The Degree of Doctor of Philosophy at the
University of Windsor

Windsor, Ontario, Canada

2008

© 2008 Tanya Kapoor



Library and
Archives Canada

Published Heritage
Branch

395 Wellington Street
Ottawa ON K1A 0N4
Canada

Bibliothèque et
Archives Canada

Direction du
Patrimoine de l'édition

395, rue Wellington
Ottawa ON K1A 0N4
Canada

Your file *Votre référence*
ISBN: 978-0-494-42421-6
Our file *Notre référence*
ISBN: 978-0-494-42421-6

NOTICE:

The author has granted a non-exclusive license allowing Library and Archives Canada to reproduce, publish, archive, preserve, conserve, communicate to the public by telecommunication or on the Internet, loan, distribute and sell theses worldwide, for commercial or non-commercial purposes, in microform, paper, electronic and/or any other formats.

The author retains copyright ownership and moral rights in this thesis. Neither the thesis nor substantial extracts from it may be printed or otherwise reproduced without the author's permission.

AVIS:

L'auteur a accordé une licence non exclusive permettant à la Bibliothèque et Archives Canada de reproduire, publier, archiver, sauvegarder, conserver, transmettre au public par télécommunication ou par l'Internet, prêter, distribuer et vendre des thèses partout dans le monde, à des fins commerciales ou autres, sur support microforme, papier, électronique et/ou autres formats.

L'auteur conserve la propriété du droit d'auteur et des droits moraux qui protègent cette thèse. Ni la thèse ni des extraits substantiels de celle-ci ne doivent être imprimés ou autrement reproduits sans son autorisation.

In compliance with the Canadian Privacy Act some supporting forms may have been removed from this thesis.

Conformément à la loi canadienne sur la protection de la vie privée, quelques formulaires secondaires ont été enlevés de cette thèse.

While these forms may be included in the document page count, their removal does not represent any loss of content from the thesis.

Bien que ces formulaires aient inclus dans la pagination, il n'y aura aucun contenu manquant.


Canada

DECLARATION OF PREVIOUS PUBLICATION

This dissertation includes 9 original papers (6 Journal publications and 3 Conference publications) that have been previously published/submitted for publication in peer reviewed journals, as follows:

Dissertation Chapter	Publication title/full citation	Publication status
<i>Chapter 4</i>	Kapoor T, Altenhof W and Howard A (2005). The effect of using universal anchorages in child restraint seats on the injury potential for children in frontal crash. <i>International Journal of Crashworthiness</i> , Vol. 10, No. 3, pp. 305-314.	<i>Published</i>
<i>Chapter 5</i>	Kapoor T, Wang Q, Chen L, Altenhof W and Howard A (2006). Use of rigid and deformable child restraint seats in finite element simulations of frontal crashes. SAE 2006 Conference, SAE Paper No. 2006-01-1141, April 2006, Detroit, U.S.A.	<i>Published</i>
<i>Chapter 6</i>	Turchi R, Altenhof W, Kapoor T and Howard A (2004). An investigation into the head and neck injury potential of three-year-old children in forward and rearward facing child safety seats. <i>International Journal of Crashworthiness</i> , Vol. 9, No. 4, pp. 419-431.	<i>Published</i>
<i>Chapter 6 and Chapter 7</i>	Kapoor T, Altenhof W, Wang Q and Howard A (2006). Experimental and Numerical investigation into injury potential of three-year-old Hybrid III dummies in forward and rearward facing child safety seats. <i>Accident Analysis and Prevention</i> , Vol. 38, No. 4, pp. 786-800	<i>Published</i>
<i>Chapter 6 and Chapter 10</i>	Kapoor T, Altenhof W, Howard A, Rasico J, Zhu F and Mizuno K (2008). Methods to mitigate injuries to toddlers in Near-side impact crashes. <i>Accident Analysis and Prevention</i> .	<i>In Press: Submitted on 15th January 2008</i>
<i>Chapter 6 and Chapter 10</i>	Kapoor T, Altenhof W and Howard A (2008). The effect of using rigid ISOFIX system on the injury potential of toddlers in near-side impact crashes. 10 th International LS-DYNA Users Conference, June 2008, Dearborn, Michigan.	<i>Accepted for publication</i>
<i>Chapter 6</i>	Kapoor T, Altenhof W, Tot M, Zhang W, Howard A, Rasico J, Zhu F and Mizuno K (2008). Responses of the Q3, Hybrid III and a three year old child finite element model under a simulated 213 test. SAE World Congress 2008, Paper No. 2008-01-1121, April 2008, Detroit, USA.	<i>Published</i>

<i>Chapter 8</i>	Kapoor T, Altenhof W, Tot M, Zhang W, Howard A, Rasico J, Zhu F and Mizuno K (2008). Load limiting behaviour in CRS tether anchors as a method to mitigate head and neck injuries to children in frontal crash. Traffic Injury Prevention Journal.	<i>Accepted for publication</i>
<i>Chapter 8</i>	Kapoor T, Tot M, Altenhof W and Howard A (2007). Use of load limiting tethers in child restraint systems as a method to mitigate injuries to toddlers in frontal crash. Canadian Multidisciplinary Road Safety Conference, 3-6 June, 2007, Montreal, Quebec.	<i>Published</i>

I certify that I have obtained a written permission from the copyright owner(s) to include the above published material(s) in my thesis. I certify that the above material describes work completed during my registration as graduate student at the University of Windsor.

I declare that, to the best of my knowledge, my dissertation does not infringe upon anyone's copyright nor violate any proprietary rights and that any ideas, techniques, quotations, or any other material from the work of other people included in my thesis, published or otherwise, are fully acknowledged in accordance with the standard referencing practices. Furthermore, to the extent that I have included copyrighted material that surpasses the bounds of fair dealing within the meaning of the Canada Copyright Act, I certify that I have obtained a written permission from the copyright owner(s) to include such material(s) in my thesis.

I declare that this is a true copy of my dissertation, including any final revisions, as approved by my dissertation committee and the Graduate Studies office, and that this dissertation has not been submitted for a higher degree to any other University of Institution.

ABSTRACT

This research focuses on methods to reduce injuries, specifically in the head and neck region, sustained by children seated in forward facing child restraint system during a vehicle crash. Three standardized experimental tests were considered in this research for the purpose of model validation and to quantify the injury potential sustained by children in a crash: (i) frontal dynamic sled tests were completed in accordance with FMVSS 213 using a Hybrid III 3-year-old dummy in a five point restraint system, (ii) full frontal vehicle crash test was completed in accordance with the CMVSS 208 with a Hybrid III 3-year-old child dummy, seated behind the passenger seat, restrained in five-point restraint system, and (iii) side impact dynamic sled tests in the presence of a rigid wall and absence of a vehicle body (near side configuration) were conducted by NHTSA using a Hybrid III 3-year-old child dummy seated in a convertible forward/rearward child safety seat. A finite element model of the child restraint seat was developed utilizing CAD data provided by Century/Graco Corporation. Material tests were conducted to obtain the nonlinear material properties of the CRS polypropylene, child seatbelt webbing, and polymeric foams. Numerical simulations were conducted using LS-DYNA, and the simulation results of the frontal and side impact tests were observed to be in a good agreement to the experimental findings. An average percentage error of approximately 20 percent was observed between the numerical and experimental data.

Different countermeasures were investigated to mitigate the head and neck injury potential in frontal and side impact crashes. These methods involved numerical studies utilizing a Hybrid III 3-year-old dummy, Q3/Q3s dummies and a child FE model. Load limiting behaviour into the upper tether and lower LATCH anchors of the CRS in order to reduce the neck injury criteria by increasing forward head excursion in a frontal crash was first examined. It was observed that the implementation of load limiting behaviour in the CRS tethers was effective in reducing the head and neck injury criteria by approximately 60 percent and 35 percent respectively. Secondly, a head and neck restraining device was developed to limit the amount of neck rotation in the dummy's head. A reduction of approximately 50 to 60 percent was observed in the head and neck

injury potential in the presence of the head and neck restraining device. Finally, numerical simulations were completed with rectangular and cross-shaped sections of rigid ISOFIX systems for better side impact protection. In addition, studies were conducted to confine lateral movement of the dummy's head by incorporating energy absorbing foam on the side wings in the vicinity of the contact region of the CRS. It was observed that the use of the rigid ISOFIX system reduced the lateral displacement of the CRS and different injury parameters. Addition of energy absorbing foam blocks was effective in further reducing the lateral displacement of the dummy's head by approximately 50 to 60 mm.

DEDICATION

For my loving parents and my younger brother, without whose patience, love and support the completion of this dissertation would not have been possible. I also dedicate this document to all the people in my life who have inspired me to achieve my PhD degree.

ACKNOWLEDGEMENTS

The author is deeply indebted to her academic advisor, Dr. William Altenhof, for his exceptional motivation and guidance throughout the duration of this research as well as his invaluable knowledge of vehicle crashworthiness and finite element modeling. The author would like to thank participating members of Auto 21 Network Centres of Excellence, especially Dr. Andrew Howard for his child injury data. The in-kind contributions from Graco Corporation are greatly appreciated. I would also like to thank Dr. Koji Mizuno of the Nagoya University, Japan; and Mr. Jim Rasico and Mr. Fuchun Zhu of First Technology Safety Systems for their contributions with the finite element child models. My former colleagues from the Department of Mechanical Engineering supported me in my research work. Especially I am obliged to Mr. Qian Wang, Mr. Miroslav Tot and Mr. Wencheng Zhang for all their help, support, interest and valuable hints.

CLAIMS TO ORIGINALITY

Aspects of this work constitute, in the author's opinion, new and distinct contributions to the technical knowledge pertaining to child safety in vehicle crashes. These include:

- (i) Development of a fully deformable CRS numerical model that incorporates complete deformability of the CRS including material non-linearities and contact definitions amongst different components of the CRS. This model is capable of simulating the experimental testing in both frontal and side impact situations.
- (ii) Implementation of load limiting behaviour in upper tethers and lower LATCH anchors of a forward facing CRS as a method to mitigate severe acceleration induced head and neck injuries to toddlers in a frontal crash.
- (iii) Development of a head and neck restraining device for 3-year-old children, that illustrates a potential of reducing severe inertia based and contact based injuries to children in a frontal crash.
- (iv) Incorporation of a cross-shaped rigid ISOFIX system as a method of anchoring the CRS to the vehicle seat that illustrates a reduction of lateral displacement of the CRS. In addition, use of energy absorbing foam on the side wings of the CRS, in the vicinity of the head of a child, as a method to reduce lateral displacement of the child's head in a near-side impact. Use of energy absorbing foam in conjunction with cross-shaped rigid ISOFIX system illustrates benefits in terms of contact/non-contact based injury reduction in near-side impacts.

TABLE OF CONTENTS

DECLARATION OF PREVIOUS PUBLICATION	iii
ABSTRACT	v
DEDICATION	vii
ACKNOWLEDGEMENTS	viii
CLAIMS TO ORIGINALITY	ix
LIST OF TABLES	xx
LIST OF FIGURES	xxii
LIST OF APPENDICES	xxxiii
LIST OF ABBREVIATIONS	xxxiv
LIST OF NOMENCLATURE	xxxvi
CHAPTER	
1. INTRODUCTION	1
2. LITERATURE REVIEW	4
2.1 Traffic safety facts	4
2.1.1 Automotive crash statistics: Canada	4
2.1.2 Automotive crash statistics: United States	5
2.2 Injury and injury mechanisms	5
2.2.1 Injury to children in MVC's	5
2.2.1.1 Head injuries	5
2.2.1.2 Neck injuries	7
2.2.2 Child anatomy and related injury patterns	8
2.2.2.1 Child anatomy	8
2.2.2.2 Biomechanical structure and properties	11
2.2.2.3 Anatomy related injury mechanisms	13
2.2.3 Child restraint system use	14
2.2.3.1 Types of misuse	14
2.2.3.2 Systematic reviews	16

2.2.3.3 Restraint associated injury mechanisms	18
2.2.4 Child restraint system orientation and related injury patterns	20
2.2.5 Crash factors and related injury patterns	21
2.2.6 Seating positions and related injury risk	22
2.3 Clinical observations	24
2.3.1 Frontal impacts	24
2.3.1.1 Non-catastrophic frontal impacts	25
2.3.1.1.1 Case 1: Forward facing 35 month old child in the rear seat [56]	25
2.3.1.1.2 Case 2: Forward facing 23 month old child in the rear seat [56]	25
2.3.1.2 Vehicle intrusion : Unsurvivable crash	27
2.3.1.2.1 Case 3: Forward facing 3-year-old child in the rear seat [55]	27
2.3.1.3 Vehicle intrusion : Survivable crash	27
2.3.1.3.1 Case 4: Forward facing 2-year, 9-month old child in the rear seat [55]	27
2.3.1.4 Restraint misuse	29
2.3.1.4.1 Case 5: Rear facing infant placed in front passenger side seat of vehicle [67]	29
2.3.1.4.2 Case 6: Toddler placed in front passenger seat of vehicle with no CRS [67]	29
2.3.2 Side impacts	30
2.3.2.1 Vehicle intrusion : Unsurvivable crash	30
2.3.2.1.1 Case 7: A near side crash involving 1-year, 10-month old child [55]	31
2.3.2.1.2 Case 8: A near side crash involving an infant [55]	31
2.3.2.2 Vehicle intrusion : Survivable crash	32
2.3.2.2.1 Case 9: Near side crash involving a 3-year, 6-month old child [55]	32
2.3.2.2.2 Case 10: Near side crash involving 3-year old child [68]	33

2.3.2.2.3 Case 11: Near side crash involving 2-year, 6-month old child [68]	35
2.3.3 Rear impacts	37
2.3.3.1 Vehicle intrusion : Unsurvivable Crash	37
2.3.3.1.1 Case 12: Rear impact involving a 1-year old child [55]	37
2.3.3.2 Vehicle intrusion : Survivable Crash	37
2.4 Injury assessment methods	38
2.4.1 Head injury criteria	38
2.4.2 Neck injury criteria	38
2.4.3 Protection reference values for child dummies	39
2.4.4 Injury risk analysis	41
2.5 Safety standards	41
2.5.1 North American governing bodies	42
2.5.1.1 Transport Canada	42
2.5.1.2 National Highway Traffic Safety Administration	42
2.5.2 Federal motor vehicle safety standard 213: Child restraint systems	43
2.5.2.1 Current FMVSS 213	43
2.5.2.1.1 Aspects of FMVSS 213	43
2.5.2.1.2 Lower anchors and tethers for children	47
2.5.2.1.3 Dummy excursion limits	48
2.5.2.1.4 Dynamic test procedure	49
2.5.2.2 FMVSS 213: ANPRM	51
2.5.3 Federal motor vehicle safety standard 208: Occupant crash protection	52
2.5.3.1 FMVSS 208 and a 3-year-old child test dummy	53
2.5.4 Motor vehicle standards in other parts of the world	54
2.6 Child restraint systems	55
2.6.1 Types of restraint seats	55
2.6.2 Convertible forward/rearward safety seats	57
2.6.3 Installing a forward-facing CRS	58

2.7 Anthropomorphic testing devices	59
2.7.1 History of crash test dummies	61
2.7.2 Hybrid III dummy family	62
2.7.3 Child dummies	65
2.7.3.1 Hybrid III 3-year-old	66
2.7.3.2 Q3 child dummy	67
2.7.3.3 Q3s child dummy	68
2.8 Experimental testing applicable to this research	69
2.8.1 New car assessment program	69
2.8.1.1 Child restraint systems rating in NCAP	69
2.8.2 Frontal impact testing	71
2.8.2.1 Cadaver testing at University of Heidelberg	71
2.8.2.2 Sled testing at Graco Corporation	72
2.8.2.3 Sled testing to evaluate different belt retractors	74
2.8.2.4 Sled testing to evaluate different anchorage systems	75
2.8.3 Side impact testing	77
2.8.3.1 Side impact vehicle tests by Rockwell	77
2.8.3.2 Side impact testing by NHTSA (Test No. 4585)	78
2.8.3.3 Side impact testing to evaluate different anchorage systems	80
2.8.4 Head and neck safety device	84
2.9 Numerical studies applicable to this research	85
2.9.1 Modeling techniques	85
2.9.2 Frontal impact testing	86
2.9.2.1 Forward/rearward facing CRS configuration	86
2.9.2.2 Finite element model of a 3-year-old child	88
2.9.3 Side impact testing	92
2.9.3.1 Side impact multi-body simulations	92
2.9.3.2 Countermeasure development for far-side impact situations	93
3. FOCUS OF RESEARCH	95

4. EXPERIMENTAL TESTING	98
4.1 Sled testing: FMVSS 213	98
4.2 Sled testing: ANPRM 213 (Test No. 4585)	98
4.3 Full vehicle crash test: CMVSS 208	99
4.3.1 Experimental set-up	99
4.3.2 Extraction of data	101
4.3.3 Data analysis/injury parameters	102
4.3.3.1 Head injury criteria	103
4.3.3.2 Neck injury criteria	103
4.3.3.3 Protection reference values	104
4.3.3.4 Injury risk analysis	104
4.3.4 Experimental observations	104
4.3.4.1 Qualitative comparison	104
4.3.4.2 Quantitative comparison	107
4.3.4.2.1 Head accelerations	107
4.3.4.2.2 Chest accelerations and deflection	108
4.3.4.2.3 Seatbelt loads	110
4.3.4.2.4 Resultant upper and lower neck forces	111
4.3.4.2.5 Resultant upper and lower neck moments	111
4.3.4.2.6 Head injury criteria	114
4.3.4.2.7 Neck injury criteria	115
4.3.4.3 Discussion	116
4.3.4.3.1 Injury risk analysis	116
4.3.4.3.2 Protection reference values	117

5. NUMERICAL MODEL DEVELOPMENT	119
5.1 Simplified rigid model	119
5.1.1 Modeling of the rigid CRS	119
5.1.2 Modeling of the seatbelt restraints	120
5.1.3 Modeling of the foam insert	122
5.1.4 Contact definitions	123
5.2 Deformable CRS model	124
5.2.1 Modeling of the deformable child seat	124
5.2.2 Modeling of the seatbelt restraints	128
5.2.3 Modeling of the foam insert	131
5.2.4 Modeling of the seat buck	131
5.2.4.1 Parametric Study on Seat Buck Foam	132
5.3 Anthropomorphic testing devices	135
5.3.1 Hybrid III 3-year-old dummy	135
5.3.2 Q3 3-year-old child dummy	136
5.3.3 Q3s 3-year-old child dummy	138
5.3.4 Child FE model	138
5.4 Simulation procedure	139
5.5 Data extraction	141
6. NUMERICAL MODEL VALIDATION	146
6.1 Validation technique utilized in this research	146
6.2 Finite element model validation – CMVSS 208 vehicle crash test	149
6.2.1 Qualitative Comparison	149
6.2.2 Quantitative comparison	152
6.2.2.1 Head accelerations	152
6.2.2.2 Chest accelerations	154
6.2.2.3 Resultant upper and lower neck forces	155
6.2.2.4 Resultant upper and lower neck moments	157

6.3 Finite element model validation – FMVSS 213 sled test	159
6.3.1 Qualitative comparison	159
6.3.2 Quantitative comparison	161
6.3.2.1 Head accelerations	161
6.3.2.2 Chest accelerations	163
6.4 Comparison between Hybrid III, Q3 and child FE model	166
6.4.1 Qualitative analysis	166
6.4.2 Quantitative analysis	169
6.4.2.1 Resultant head accelerations	169
6.4.2.2 Resultant chest accelerations	170
6.4.2.3 Head injury criteria	171
6.4.2.4 Head trajectories	172
6.4.2.5 Upper neck resultant forces and moments	173
6.4.2.6 Neck injury criteria	175
6.4.3 Discussion	177
6.5 Finite element model validation - CRS compressive test	177
6.5.1 Experimental CRS compressive test	177
6.5.2 Simulation procedure	179
6.5.3 Numerical model validation - CRS compressive test	180
6.6 Finite element model validation – 4585 near-side impact sled test	182
6.6.1 Qualitative analysis	183
6.6.2 Quantitative analysis	186
6.6.2.1 Head acceleration in the local y -direction	186
6.6.2.2 Chest acceleration in the local y -direction	187
6.6.2.3 Resultant upper and lower neck forces	188
6.6.2.4 Resultant upper and lower neck moments	190

7. FRONTAL IMPACT PROTECTION - REARWARD FACING	193
7.1 Simulation procedure	193
7.2 Qualitative analysis	195
7.3 Quantitative analysis	197
7.3.1 Resultant head and chest accelerations	197
7.3.2 Resultant neck forces and moments	198
7.3.3 Head injury criteria	200
7.3.4 Neck injury criteria	201
7.4 Discussion	203
7.4.1 Injury risk analysis	203
7.4.2 Protection reference values	203
8. FRONTAL IMPACT PROTECTION - LOAD LIMITING OF TETHERS	206
8.1 Load limit evaluation	206
8.1.1 Injury based approach	206
8.1.2 Energy based approach	207
8.2 Qualitative analysis	210
8.3 Quantitative analysis	215
8.3.1 Resultant head accelerations	215
8.3.2 Resultant chest accelerations	215
8.3.3 Resultant upper neck forces and cross-sectional forces	217
8.3.4 Head injury criteria	219
8.3.5 Neck injury criteria	220
8.3.6 Head trajectories	222
8.4 Discussion	224
8.4.1 Injury risk analysis	224
8.4.2 Protection reference values	224

9. FRONTAL IMPACT PROTECTION - HEAD AND NECK	227
RESTRAINING DEVICE	
9.1 Model development	227
9.2 Simulation procedure	229
9.3 Qualitative analysis	230
9.4 Quantitative analysis	235
9.4.1 Resultant head accelerations	235
9.4.2 Resultant chest accelerations	236
9.4.3 Resultant upper neck forces and cross-sectional forces	237
9.4.4 Resultant upper and lower neck moments	239
9.4.5 Head injury criteria	239
9.4.6 Neck injury criteria	240
9.4.7 Head trajectories	242
9.5 Discussion	243
9.5.1 Injury risk analysis	243
9.5.2 Protection reference values	244
10. SIDE IMPACT PROTECTION	246
10.1 Countermeasure development	246
10.1.1 Rigid ISOFIX system	246
10.1.2 Energy absorbing foam	247
10.2 Qualitative analysis	249
10.3 Quantitative analysis	252
10.3.1 Resultant head accelerations	252
10.3.2 Resultant chest accelerations	253
10.3.3 Lateral shear	259
10.3.4 Lateral bending	262
10.4 Discussion	267

11. CONCLUSION AND FUTURE WORK	269
11.1 Experimental Testing	269
11.2 Countermeasures	271
11.2.1 Frontal impact protection - rearward facing	271
11.2.2 Frontal impact protection - load limiting of tethers	272
11.2.3 Frontal impact protection - head and neck restraining device	273
11.2.4 Side impact protection	275
11.3 Limitations	277
11.3.1 Frontal impact protection – rearward facing	277
11.3.2 Frontal impact protection – load limiting of tethers	277
11.3.3 Frontal impact protection – head and neck restraining device	278
11.3.4 Side impact protection	278
11.4 Future work	279
REFERENCES	281
APPENDICES	298
APPENDIX A – Contents of the associated DVD	299
APPENDIX B – Injury scales and Prasad and Mertz injury risk curves	300
APPENDIX C – Numerical algorithms	303
APPENDIX D – Material models and sample input data from LS-Dyna	305
APPENDIX E – Contact definitions	312
APPENDIX F – Copyright permission	324
VITA AUCTORIS	328

LIST OF TABLES

Table		Page
1	Protection reference values for Hybrid III 3-year-old dummy [32].	41
2	Anthropomorphic test devices [89].	61
3	Instrumentation provided in 3-year-old Hybrid III child dummies and the SAE-J211 filters used	102
4	Probability of severe injuries (AIS 3+) to both the dummies using Prasad and Mertz injury risk analysis	117
5	Yield stress and ultimate tensile stress for the polypropylene tensile testing.	125
6	Peak values for different injury parameters for the simulated FMVSS 213 crash involving a Hybrid III 3-year-old dummy for different material properties of the seat buck.	135
7	Summary of the peak values of experimental and numerical results from CMVSS 208 test.	158
8	Summary of the peak values of experimental and numerical results from FMVSS 213 test.	164
9	Peak values for the parametric study on the seatbelt slack for a simulated FMVSS 213 crash.	166
10	Summary of peak values of all injury parameters for the Hybrid III, Q3 and child FE model for the simulated 213 test.	176
11	Summary of peak values of all injury parameters for experimental and numerical sled tests (Test No. 4585) incorporating Hybrid III 3-year-old dummy.	191
12	Peak values predicted by the Hybrid III 3-year-old dummy in both forward and rearward facing CRS configurations.	203
13	Load limit values obtained for the top tether and the lower LATCH anchor.	209

Table	Page
14 Summary of peak values of various injury parameters predicted for the Hybrid III and the Q3 child dummies for load limiting and no load limiting situations.	222
15 Summary of peak values of various injury parameters predicted for the child FE model for load limiting and no load limiting situations.	222
16 Summary of peak values of various injury parameters predicted for the Hybrid III and the Q3 child dummies in the absence and presence of the HANS device.	242
17 Summary of peak values of various injury parameters predicted for the child FE model in the absence and presence of the HANS device.	242
18 Peak values predicted for the flexible LATCH, rigid ISOFIX (rectangular section) and rigid ISOFIX (cross-shaped section) configurations for the Hybrid III 3-year-old dummy.	265
19 Peak values predicted for the flexible LATCH, rigid ISOFIX (rectangular section) and rigid ISOFIX (cross-shaped section) configurations for the Hybrid III 3-year-old dummy in the presence of energy absorbing foam blocks.	265
20 Peak values predicted for the flexible LATCH, rigid ISOFIX (rectangular section) and rigid ISOFIX (cross-shaped section) configurations for the Q3s child dummy.	265
21 Peak values predicted for the flexible LATCH, rigid ISOFIX (rectangular section) and rigid ISOFIX (cross-shaped section) configurations for the Q3s dummy in the presence of energy absorbing foam blocks.	266
22 Peak values predicted for the flexible LATCH, rigid ISOFIX (rectangular section) and rigid ISOFIX (cross-shaped section) configurations for the child FE model.	266
23 Peak values predicted for the flexible LATCH, rigid ISOFIX (rectangular section) and rigid ISOFIX (cross-shaped section) configurations for the child FE model in the presence of energy absorbing foam blocks.	266

LIST OF FIGURES

Figure		Page
1	Proportion of the human body in relation to different ages. From left to right: newborn infant, 2-year old child, 6 year old child, 12 year old child and 25 year old adult [33]	9
2	Skull Profiles showing changes in size and shape [32].	9
3	Medial sagittal plane of the Occ-C2 complex [36].	11
4	Typical cervical vertebrae for ages one, three, six, eleven, and adult [37].	13
5	Angulated fracture of the cervical spine (C2) in child of Case 1 [56].	26
6	Occipitocervical dislocation in the 23-month-old male involved in Case 2 [56].	26
7	Unsurvivable frontal impact with pickup truck, Case 3 [55].	28
8	Frontal impact with some instrument panel intrusion, Case 4 [55].	28
9	Lap belt injuries in frontal impact crashes [68].	30
10	The unsurvivable side impact with a SUV, Case 7 [55].	31
11	The unsurvivable side impact with tractor-trailer, Case 8 [55].	32
12	Side impact with a tree, Case 9 [55].	33
13	Pontiac Bonneville, Case 10 [68].	34
14	Right femur fracture sustained by child of Case 10 [68].	34
15	Right frontal lobe contusions and skull fractures to the child of Case 10 [68].	34
16	Scene diagram of the side impact, Case 11 [68].	35
17	Pontiac Grand-Prix, Case 11 [68].	36
18	Cervical dislocation sustained by child of Case 11 [68].	36
19	Rear impact with extreme crush, Case 12 [55].	37

Figure	Page
20 Belt anchorage point locations on the standard seat assembly [78].	45
21 FMVSS 213 sled test corridor [78].	46
22 Top tether and lower anchors for children [81].	48
23 Location of universal child restraint anchorage systems and forward excursion limits for the standard seat assembly [82].	49
24 Suggested modes of restraint for various ages and sizes of children: (a) rear facing car seat, (b) convertible child safety seat, (c) booster seat, and (d) child weighing 36 kg or over eight years of age should fit properly in adult restraints [85].	56
25 Three harness types available on convertible child safety seats: (a) five-point, (b) tray-shield, and c) T-shield [66].	58
26 Different ways of installing the CRS to the vehicle seat: (a) car seatbelt, (b) flexible LATCH, (c) top tether and (d) rigid ISOFIX [86].	59
27 Hybrid III dummy family (from left to right: Hybrid III 6-year-old, CRABI 12-month-old, 50th-percentile male, 5th-percentile female and Hybrid III 3-year-old) [90].	63
28 Hybrid III 3-year-old child dummy [89].	67
29 (a) Q3 and (b) Q3s child dummy [91 and 94].	68
30 Dynamic test procedures: (a) Vehicle crash, and (b) Sled Test in NCAP [96].	70
31 Sled acceleration for the 2½ year old cadaver test [98].	71
32 Pneumatically powered sled test device [100].	73
33 Sled acceleration pulse for FMVSS 213 sled tests [100].	73
34 Forward displacement of the Hybrid III dummy [102].	75
35 Vehicle body shell/ buck mounted on crash sled [103].	76
36 Side Impact vehicle test results [104].	77
37 Test 4585 side impact acceleration pulse [105].	79

Figure	Page
38 Test configuration for the 4585 side impact test [105].	79
39 Visual observations from 4585 side impact test [105].	80
40 Side impact tests (far-side) for forward facing with seatbelt, flexible and rigid anchorages showing maximum lateral head displacement during impact and rebound [106].	81
41 CLEPA side impact test configuration [107].	82
42 Peak lateral head excursions for (a) lap belt, (b) flexible LATCH, and (c) rigid ISOFIX anchorages in forward facing configurations [108].	83
43 Peak lateral head excursions for (a) lap belt, (b) flexible LATCH, and (c) rigid ISOFIX anchorages in rearward facing configurations [108].	83
44 HANS device anatomy [109].	84
45 The maximum forward head excursion in the crash test dummy for (a) without HANS device and (b) with HANS device [110].	85
46 3-year-old TNO P3 child dummy restrained in a four point safety seat in (a) forward facing, and (b) rearward facing configuration [111].	87
47 Hybrid III 3-year-old dummy model restrained in a five-point restraint in forward facing CRS configuration [101].	88
48 Finite element model of a 3-year-old child [113].	89
49 Child occupant kinematics in five-point harness CRS [114].	90
50 Sectional comparison of the behaviour of the head, neck and thorax of the (a) Hybrid III 3-year-old dummy and the (b) 3-year-old child FE model at different intervals of time [115].	91
51 Child restraint system and vehicle body model with intrusion [116].	93
52 (a) Front and (b) side view of the two Hybrid III 3-year-old child dummies restrained in the five-point restrained child seat in the vehicle, and (c) location of different instrumentation in a Hybrid III 3-year-old dummy.	100
53 Average vehicle acceleration in local x -direction.	101

Figure		Page
54	Experimental observations (frontal and side view) at different time intervals.	106
55	Experimental head acceleration in local x -axis direction as a function of time.	107
56	Experimental head acceleration in local z -axis direction as a function of time.	108
57	Experimental chest acceleration in local x -axis direction as a function of time.	109
58	Experimental chest deflection in local x -axis direction as a function of time.	110
59	Experimental seatbelt loads as a function of time.	111
60	Experimental upper neck resultant force as a function of time.	112
61	Experimental lower neck resultant force as a function of time.	113
62	Experimental upper neck resultant moment as a function of time.	113
63	Experimental lower neck resultant moment as a function of time.	114
64	Experimental HIC_{36} as a function of time.	115
65	Experimental N_{ij} as a function of time.	116
66	(a) Meshed portion of the simplified rigid CRS model, and (b) numerical model of the seatbelt and clasps for the simplified rigid CRS model.	120
67	The FE mesh of the foam insert.	122
68	Hybrid III 3-year-old dummy model restrained in the simplified rigid CRS model using a five-point restraint in a forward facing position.	123
69	Engineering stress/strain curve for CRS polypropylene tensile tests.	125
70	Elastic/Plastic behaviour of the CRS polypropylene.	126
71	Front (a) numerical and (b) actual; Rear (c) numerical and (d) actual view of the deformable Child Restraint System (CRS).	127

Figure	Page
72 The seatbelt, LATCH, top tether, and the five point restraint system.	129
73 Force versus engineering strain response of the CRS webbing.	130
74 Side view of the deformable CRS model including the seat buck and the Hybrid III 3-year-old dummy.	132
75 Engineering stress versus engineering strain response for the 213 seat bench foam.	133
76 Maximum head excursion observed for the Hybrid III 3-year-old dummy for seat buck with material properties of (a) automotive seat, and (b) 213 seat bench.	134
77 (a) Finite element model of the Hybrid III 3-year-old dummy, and (b) the complete FE model of the dummy seated in the CRS.	136
78 (a) Finite element model of the Q3 3-year-old dummy, and (b) the complete FE model of the Q3 dummy seated in the CRS.	137
79 (a) The child FE model, and (b) the child FE model seated in the CRS.	139
80 Accelerometer locations in the (a) head and (b) chest of the Hybrid III 3-year-old dummy model.	142
81 Upper and lower neck areas of the Hybrid III 3-year-old finite element dummy model.	143
82 Location of the nodes in the head and chest of the Child FE model used to track accelerations.	144
83 Location of the section planes in the neck of the Child FE model.	144
84 Validation metric as a function of relative error.	147
85 (a) Simplified rigid model, (b) complex model and (c) experimental observations for the full vehicle crash test in accordance with CMVSS 208.	151
86 Experimental and numerical head accelerations in the local <i>x</i> -axis direction.	152

Figure		Page
87	Experimental and numerical head accelerations in the local z-axis direction.	154
88	Experimental and numerical chest accelerations in the local x-axis direction.	155
89	Experimental and numerical upper neck resultant forces.	156
90	Experimental and numerical lower neck resultant forces.	156
91	Experimental and numerical upper neck resultant moments.	157
92	Experimental and numerical lower neck resultant moments.	158
93	(a) Simplified rigid model, (b) complex model and (c) experimental observations for the full vehicle crash test in accordance with FMVSS 213.	160
94	Experimental and numerical head accelerations in the local x-axis direction.	162
95	Experimental and numerical head accelerations in the local z-axis direction.	162
96	Experimental and numerical chest accelerations in the local x-axis direction.	163
97	Experimental and numerical chest accelerations in the local z-axis direction.	164
98	Numerical observations (side view) for the (a) Hybrid III 3-year-old dummy, (b) Q3 child dummy and (c) the child FE model at different durations of time.	168
99	Resultant head acceleration for Hybrid III, Q3 and child FE model as a function of time.	169
100	Resultant chest acceleration for Hybrid III, Q3 and child FE model as a function of time.	170
101	HIC_{36} for Hybrid III, Q3 and child FE model as a function of time.	171
102	Head trajectories of the center of mass of the head for the Hybrid III, Q3 and child FE model.	172

Figure	Page
103 Resultant upper neck forces for the Hybrid III and Q3 dummy, and cross sectional forces for the child FE model as a function of time.	173
104 Resultant upper neck moments for the Hybrid III and Q3 dummy as a function of time.	175
105 N_{ij} for the Hybrid III and Q3 as a function of time.	176
106 Isometric view of the testing configuration of the CRS compressive test.	178
107 Rear view of the testing configuration of the CRS compressive test.	179
108 Isometric view of the numerical model of the CRS compressive test.	180
109 Force versus displacement curves of the compressive test.	181
110 Hybrid III 3-year-old child dummy seated in the CRS for the rigid-wall near-side impact test.	183
111 Numerical observations for the 4585 near-side impact test.	185
112 Experimental and numerical head acceleration in local y-axis direction as a function of time.	187
113 Experimental and numerical chest acceleration in local y-axis direction as a function of time.	188
114 Experimental and numerical resultant upper neck force as a function of time.	189
115 Experimental and numerical resultant lower neck force as a function of time.	189
116 Experimental and numerical resultant upper neck moment as a function of time.	190
117 Experimental and numerical resultant lower neck moment as a function of time.	191
118 Hybrid III 3-year-old dummy model in (a) forward and (b) rearward facing configurations.	194
119 Numerical observations (side view) for the (a) forward facing and (b) rearward facing CRS configuration under a simulated CMVSS 208 crash.	196

Figure	Page
120 Forward and rearward resultant head accelerations as a function of time.	197
121 Forward and rearward resultant chest accelerations as a function of time.	198
122 Forward and rearward resultant upper neck forces as a function of time.	199
123 Forward and rearward resultant upper neck moments as a function of time.	200
124 Forward and rearward HIC_{36} as a function of time.	201
125 Forward and rearward (upper neck) N_{ij} as a function of time.	202
126 Loads observed in top tether and LATCH anchors for FMVSS 213 simulations as a function of time.	207
127 Side view of the CRS illustrating the Z-point, SORL and the head/knee excursion limits.	208
128 Load limiting curves for the upper tether and lower LATCH anchors.	210
129 Numerical observation (side view) of Hybrid III 3-year-old dummy for (a) No load limiting and (b) Load limiting conditions.	212
130 Numerical observation (side view) of Q3 dummy for (a) No load limiting and (b) Load limiting conditions.	213
131 Numerical observation (side view) of child FE model for (a) No load limiting and (b) Load limiting conditions.	214
132 Resultant head accelerations for load limiting and no load limiting conditions for (a) Hybrid III dummy, (b) Q3 dummy and (c) Child FE model as a function of time.	216
133 Resultant chest accelerations for load limiting and no load limiting conditions for (a) Hybrid III dummy, (b) Q3 dummy and (c) Child FE model as a function of time.	217
134 Resultant upper neck forces for load limiting and no load limiting conditions for (a) Hybrid III dummy and (b) Q3 dummy and (c) resultant cross-sectional force for the child FE model as a function of time.	218
135 Head Injury Criteria (HIC_{15} and HIC_{36}) for load limiting and no load limiting conditions for (a) Hybrid III dummy, (b) Q3 dummy and (c) child FE model as a function of time.	220

Figure	Page
136 Neck Injury Criteria (N_{ij}) for load limiting and no load limiting conditions for (a) Hybrid III dummy and (b) Q3 dummy as a function of time.	221
137 Head trajectories of the center of mass for load limiting and no load limiting conditions for (a) Hybrid III dummy, (b) Q3 dummy and (c) Child FE model.	223
138 Finite Element mesh of the HANS device.	228
139 Positioning of the HANS device around the Hybrid III 3-year-old dummy.	229
140 Numerical observation (side view) of Hybrid III 3-year-old dummy in the (a) absence, and (b) presence of the HANS device.	232
141 Numerical observation (side view) of Q3 child dummy in the (a) absence, and (b) presence of the HANS device.	233
142 Numerical observation (side view) of child FE model in the (a) absence, and (b) presence of the HANS device.	234
143 Resultant head accelerations in the presence and absence of the HANS device for (a) Hybrid III dummy, (b) Q3 dummy, and (c) Child FE model as a function of time.	236
144 Resultant chest accelerations in the presence and absence of the HANS device for (a) Hybrid III dummy, (b) Q3 dummy, and (c) Child FE model as a function of time.	237
145 Resultant upper neck forces in the absence and presence of the HANS device for (a) Hybrid III dummy and (b) Q3 dummy, and (c) Resultant cross-sectional forces for child FE model as a function of time.	238
146 Resultant lower neck moments in the absence and presence of the HANS device for (a) Hybrid III dummy, and (b) Q3 dummy.	239
147 Head Injury Criteria (HIC_{15} and HIC_{36}) in the absence and presence of HANS device for (a) Hybrid III dummy, (b) Q3 dummy and (c) child FE model as a function of time.	240
148 Neck Injury Criteria (N_{ij}) in the absence and presence of the HANS device for (a) Hybrid III dummy and (b) Q3 dummy as a function of time.	241

Figure		Page
149	Head trajectories of the center of mass in the absence and presence of a HANS device for (a) Hybrid III dummy, (b) Q3 dummy and (c) Child FE model.	243
150	Different anchoring methods: (a) flexible LATCH, (b) rigid ISOFIX rectangular section, and (c) rigid ISOFIX cross-shaped section.	247
151	Finite element model of the CRS with additional energy absorbing foam blocks.	248
152	Maximum head and CRS displacement observed by the Hybrid III 3-year-old dummy for: <ol style="list-style-type: none"> 1. Flexible LATCH (a) without foam blocks, and (b) with foam blocks 2. Rigid ISOFIX rectangular section (a) without foam blocks, and (b) with foam blocks 3. Rigid ISOFIX cross-shaped section (a) without foam blocks, and (b) with foam blocks 	250
153	Maximum head and CRS displacement observed by the Q3s dummy for: <ol style="list-style-type: none"> 1. Flexible LATCH (a) without foam blocks, and (b) with foam blocks 2. Rigid ISOFIX rectangular section (a) without foam blocks, and (b) with foam blocks 3. Rigid ISOFIX cross-shaped section (a) without foam blocks, and (b) with foam blocks. 	251
154	Maximum head and CRS displacement observed by the child FE model for: <ol style="list-style-type: none"> 1. Flexible LATCH (a) without foam blocks, and (b) with foam blocks 2. Rigid ISOFIX rectangular section (a) without foam blocks, and (b) with foam blocks 3. Rigid ISOFIX cross-shaped section (a) without foam blocks, and (b) with foam blocks. 	252
155	Resultant head acceleration profiles for the Hybrid III 3-year-old dummy as a function of time in the absence and presence of foam blocks for (a) flexible latch, (b) rigid ISOFIX rectangular section and (c) rigid ISOFIX cross-shaped section.	254
156	Resultant head acceleration profiles for the Q3s child dummy as a function of time in the absence and presence of foam blocks for (a) flexible latch, (b) rigid ISOFIX rectangular section and (c) rigid ISOFIX cross-shaped section.	255

Figure		Page
157	Resultant head acceleration profiles for the child FE model as a function of time in the absence and presence of foam blocks for (a) flexible latch, (b) rigid ISOFIX rectangular section and (c) rigid ISOFIX cross-shaped section.	256
158	Resultant chest acceleration profiles for the Hybrid III 3-year-old dummy as a function of time in the absence and presence of foam blocks for (a) flexible latch, (b) rigid ISOFIX rectangular section and (c) rigid ISOFIX cross-shaped section.	257
159	Resultant chest acceleration profiles for the Q3s dummy as a function of time in the absence and presence of foam blocks for (a) flexible latch, (b) rigid ISOFIX rectangular section and (c) rigid ISOFIX cross-shaped section.	258
160	Resultant chest acceleration profiles for the child FE model as a function of time in the absence and presence of foam blocks for (a) flexible latch, (b) rigid ISOFIX rectangular section and (c) rigid ISOFIX cross-shaped section.	259
161	Lateral shear profiles for the Hybrid III child dummy as a function of time in the absence and presence of foam blocks for (a) flexible latch, (b) rigid ISOFIX rectangular section and (c) rigid ISOFIX cross-shaped section.	260
162	Lateral shear profiles for the Q3s child dummy as a function of time in the absence and presence of foam blocks for (a) flexible latch, (b) rigid ISOFIX rectangular section and (c) rigid ISOFIX cross-shaped section.	261
163	Lateral shear profiles for the child FE model as a function of time in the absence and presence of foam blocks for (a) flexible latch, (b) rigid ISOFIX rectangular section and (c) rigid ISOFIX cross-shaped section.	262
164	Lateral bending profiles for the Hybrid III child dummy as a function of time in the absence and presence of foam blocks for (a) flexible latch, (b) rigid ISOFIX rectangular section and (c) rigid ISOFIX cross-shaped section.	263
165	Lateral bending profiles for the Q3s child dummy as a function of time in the absence and presence of foam blocks for (a) flexible latch, (b) rigid ISOFIX rectangular section and (c) rigid ISOFIX cross-shaped section.	264

LIST OF APPENDICES

APPENDIX A – Contents of the associated DVD

APPENDIX B – Injury scales and Prasad and Mertz injury risk curves

APPENDIX C – Numerical algorithms

APPENDIX D – Material models and sample input data from LS-Dyna

APPENDIX E – Contact definitions

APPENDIX F – Copyright permission

LIST OF ABBREVIATIONS

AIS	Abbreviated Injury Scale
ABS	Acrylonitrile Butadiene Styrene
ANCAP	Australian New Car Assessment Program
ANPRM	Advanced Notice of Proposed Rule Making
AOD	atlanto-occipital dislocation
AS	Australia Standards
ASCII	American Standard Cord for Information Interchange
ASTM	American Society for Testing and Materials
ATD	Anthropomorphic Test Device
BPB	Belt Positioning Booster
CAD	Computer Aided Design
CDC	Centres for Disease Control and Prevention
CDWG	Child Dummy Working Group
CHILD	CHild Injury Led Design
CIREN	Crash Injury Research Engineering Network
CLEPA	Construction d'Equipements et de Pièces d'Automobiles
CMVSS	Canadian Motor Vehicle Safety Standards
CRABI	Child Restraint Air Bag Interaction Dummy
CREST	Child REstraint System sTandard
CRS	Child Restraint System
ECE	Economic Commission for Europe
EURO-NCAP	European New Car Assessment Program
FARS	Fatality Analysis Reporting System
FE	Finite Element
FEMB	Finite Element Model Builder
FMVSS	Federal Motor Vehicle Safety Standards
FFCRS	Forward Facing Child Restraint Systems
FTSS	First Technology Safety Systems
GM	General Motors

GSI	Gadd severity index
HANS	Head and Neck Safety device
ISO	International Standards Organization
LATCH	Lower Anchors and Tethers for Children
LUAS	Lower Universal Anchorage System
LVDT	Linear Voltage Differential Transformer
MAIS	Maximum Abbreviated Injury Scale
MVC's	Motor Vehicle Crashes
NCAP	New Car Assessment Program
NCSA	National Centre for Statistics and Analysis
NHTSA	National Highway Traffic Safety Administration
NPRM	Notice of Proposed Rule Making
NSKC	National Safe Kids Campaign
OOP	Out Of Position
OSA	National Organization for Automotive Safety & Victims' Aid
PRV	Protection Reference Values
RSSR	Restraint Systems and Booster Cushions Safety Regulations
SAE	Society of Automotive Engineers
SID	Side Impact Dummy
SORL	Seat Orientation Reference Line
THUMS	Total Human Model for Safety
TRC	Transportation Research Centre
TREAD	Transportation Recall Enhancement, Accountability and Documentation
UAS	Universal Anchorage System
UMTRI	University of Michigan Transportation Research Institute
UNECE	United Nations Economic Commissions for Europe
VRTC	Vehicle Research and Test Centre
WSTC	Wayne State Tolerance Curve

LIST OF NOMENCLATURE

a	Acceleration
$a_{resultant}$	Resultant Acceleration
ΔV	Change in speed
E	Young's Modulus
E	Average relative error
$F_{resultant}$	Resultant Force
F_x	Force in the x direction
F_y	Force in the y direction
F_z	Force in the z direction/Axial Force
F_{zc}	Critical Axial Force
HIC	Head Injury Criteria
HIC_{15}	Head Injury Criteria over 15 ms time duration
HIC_{36}	Head Injury Criteria over 36 ms time duration
$HIC_{unlimited}$	Head Injury Criteria over unlimited time duration
$M_{resultant}$	Resultant Moment
M_x	Moment in the x direction
M_y	Moment in the y direction/Bending Moment
M_{yc}	Critical Bending Moment
M_z	Moment in the z direction
N_{ij}	Neck injury criteria
v	Velocity
ρ	Density
ν	Poisson's Ratio
V	Validation Metric
X, Y, Z	Global coordinate system axes
x, y, z	Local coordinate system axes for Hybrid III 3-year-old child dummy
$y(x)$	Measured value
$Y(x)$	Expected value

1. INTRODUCTION

Many people, among them children, are killed or seriously injured in road traffic everyday, which constitutes a major public health problem. Automobile travel is a part of everyday life that begins in early infancy. Journeys to and from kindergarten, school and leisure activities become more frequent as the age of the child increases. Hence, children are frequent users of the road transport system and are thus exposed to the inherent risks associated with motor vehicle transportation.

According to Bureau of Reproductive & Child Health, and statistics from Fatality Analysis Reporting System (FARS), motor vehicle crashes are the leading cause of deaths for children in Canada and the United States [1, 2]. National Highway Traffic Safety Association (NHTSA) has determined that each year in the United States, 1,400 children under the age of 14 are killed in vehicle collisions and over 280,000 are injured [2]. According to the Traffic safety facts [3], everyday in the United States, on an average 5 children age 14 and under were killed and 640 were injured everyday in motor vehicle crashes in 2005. In the year 2005, there were 2,923 deaths and 210,629 injuries due to automobile accidents in Canada [4]. Children under the age of 14 accounted for 3.5 percent (103) of all the traffic fatalities in that year. In the year 2005, National Centre for Statistics and Analysis (NCSA), reported 43,443 deaths and 2,699,000 injuries due to automobile crashes in the United States [2]. Children under the age of 15 accounted for 5.4 percent (2,348) of all the traffic fatalities in the United States in 2005. It is evident from these statistics that the younger population is at an increased risk of death and loss of life expectancy.

In a study released by the University of Michigan Transportation Research Institute (UMTRI), Weber [5] determined that young children are at risk for devastating head and neck injuries due to the neck's fragile physiology and weak neck musculature. These factors reduce the tolerance of a child to withstand high crash forces. In a study done by Gotschall and Luchter [6], it was determined that head injuries are the leading cause of death among children in the United States. Although head injuries are the most

common injury to children in Motor Vehicle Crashes (MVC's), approximately 50 percent of injuries to the pediatric cervical spine sustained in MVC's are fatal [7]. Mousny et al. [8] found that almost one third of all neck injuries occur in frontal impacts in the United States. Injuries to the head and neck account for a greater number and severity of abbreviated injury scale (AIS) 2+ injuries [9]. According to traffic safety facts [10], when a child dies in an accident the injury location is recorded on the death certificate by the coroner/medical examiner and is captured in mortality databases under what are known as axis codes. While the severity of the injuries is not recorded, the location of injuries is recorded. Dr. Howard [11] from the Hospital of Sick Kids in a personal communication stated that MVC's which result in death to a child, prior to hospitalization, generally are classified as a fatal MVC without any physical examination as to the reason/mechanism for death. Thus, since cervical spine injuries in MVC's typically result in death of a child the actual number of neck injuries may actually be underestimated to true values.

Child restraint systems (CRS) are extremely effective when correctly installed and used in passenger cars, reducing the risk of death by 71 percent for infants and 54 percent for children ages 1 to 4, and reducing the need for hospitalization by 69 percent for children ages 4 and under [12]. In North America, the recommended standard for the seating of children in child safety seats states that children should remain rearward facing until the age of 12 months. After this age, governing bodies recommend that children may be positioned in a forward facing child safety seat. In Sweden, children remain rear facing until the ages of three and four. In fact, the rear facing car seats are designed very differently than those in North America. A study done by Skold [13] explains a Swedish system ISOFIX for rearward facing seats, which incorporates the child safety seat and anchorage points within the vehicle. Skold suggested that the development of the rearward facing child safety seat for toddlers has reduced the risk of serious injuries. An Australian CRS features a mandatory top tether strap, single point of adjustment for the body harness and the most notable design difference being a six-point harness with double groin straps as compared to a five point harness design as seen in the North American market [14]. These Australian designs have proved to provide exceptional protection to child occupants in severe crashes. Therefore design modifications to the

current CRS are required to mitigate the occurrence of severe head and neck injuries to toddlers in a frontal crash.

For passenger vehicle child occupants aged birth through 8 years, data from the FARS from 1991–2000 showed that regardless of whether the child was seated in the front seat or rear seat, frontal and side crashes accounted for most child occupant fatalities [3]. For rear seat child occupants, frontal impacts and side impact crashes accounted for 44 percent and 42 percent of the fatalities respectively. Of the 3,826 rear seat fatalities, 25 percent involved near side impacts [15]. Studies have shown that approximately twice as many crashes with a child fatality are frontal compared to lateral, but side impacts are nearly twice as likely to result in a child fatality as frontal impacts, regardless of restraint status or seating position [16]. The net result is that the number of children killed in each type of crash is about the same. Most child restraints provide good protection in frontal impacts when used properly. Unfortunately, side impact testing is not mandated and has not been a main design feature for most car seats and boosters in the United States [17].

The above mentioned statistics and issues show that there is a considerable scope of improvement in the current North American child safety norms for both the frontal and side impact situations. The purpose of this research is to shed light on the injury mechanisms for children and thereby develop methods to mitigate head and neck injuries to children in frontal and side impact crashes.

2. LITERATURE REVIEW

2.1 Traffic safety facts

Traffic related injuries are a major public health challenge globally that requires intensive efforts for effective and sustainable prevention [18]. Worldwide, 1.2 million people are killed and 50 million injured annually in road crashes. In the year 2002, road traffic injuries accounted for 2.1 percent for all global deaths, making them the eleventh leading cause of global deaths. According to the world report on road traffic injury prevention [18], projections indicate an increase of approximately 65 percent in traffic related fatalities over the next 20 years unless there is a new commitment to prevention. According to Bureau of Reproductive & Child Health, and statistics from FARS, motor vehicle crashes are the leading cause of deaths for children in Canada and the United States [1, 2]. This section details the traffic related statistics for children in the Canada and the United States.

2.1.1 Automotive crash statistics: Canada

Unintentional injury is the leading cause of death for persons between the ages of 1 through 34 years of age in Canada [19]. In the year 1996, unintentional injuries accounted for 69.6 percent of all injury related deaths among children and youth less than 20 years of age. MVC's accounted for 60.9 percent of all the unintentional injuries for persons between the ages of 1 through 20 years of age [19]. According to Statistics Canada [1] MVC's are the leading cause of death for children under the age of 4 in Canada. In the year 2005, there were 2,923 deaths and 210,629 injuries due to automobile accidents in Canada [4]. There were a total of 103 deaths and 13,649 injuries to children under the age of 14 in the year 2005 due to vehicle crashes. Children under the age of 4 accounted for 23.3 percent (24) of traffic fatalities and 19.4 percent (2,649) of injuries to children in that year. Child restraint laws came into effect between 1982 and 1987. According to Chouinard et al. [20], the number of fatalities for children under the age of 14 has been under 100 per year since 1998 and major injuries have been under 700 since

1999. There were a total of 402 fatalities for child occupants of light duty vehicles between 1998 and 2002. For children who were fatally injured, unsuitable restraint was found to be approximately 66 percent for infants (under 1 year old), 50 percent for toddlers (1 to 4 years old), 97 percent for school-age children (4 to 8 years old) and 31 percent for older children (9 to 14 years old) [20].

2.1.2 Automotive crash statistics: United States

Injury is recognized as the principal public health problem in the United States affecting children and accounts for almost 50 percent of fatalities to children aged one through four. Motor vehicle crashes are the major cause of injuries to children belonging to this age group [21]. Statistics from NHTSA confirm that vehicle crashes are the leading cause of death to children in the United States [2]. In the year 2005, NCSA reported 43,443 deaths and 2,699,000 injuries due to automobile crashes in the United States [2]. According to the 2005 statistics by NCSA in the year 2005 there were 2,348 deaths and 271,000 injuries to children under the age of 15 in automobile crashes in the United States [3]. Children under the age of 5 accounted for 25 percent (590) of these traffic fatalities and 20.6 percent (56,000) of all the children injured in vehicle crashes in the United States. It was found that only 62 percent of the children killed and 81 percent of the children injured were restrained using child safety seats.

2.2 Injury and injury mechanisms

2.2.1 Injury to children in MVC's

2.2.1.1 Head injuries

According to National Safe Kids Campaign (NSKC) [12], most motor vehicle deaths result from fatal head injuries; and serious non-fatal injuries most frequently include brain and spinal cord trauma and facial disfigurement. In a study released by the UMTRI, Weber [5] determined that young children are at risk for devastating head and

neck injuries due to the neck's fragile physiology and weak neck musculature. In a study done by Gotschall and Luchter [6], it was found that head injuries are the leading cause of death among children in the United States. It was determined that 23 percent of the total head injuries to children aged 0-4 years were traffic related. According to Weber [5], 75 percent of all traumatic injury deaths to children are the direct result of brain injury. Klinich et al. [22] found that head injury is the leading cause of health care costs in the United States. Even in minor frontal impacts infants sustain serious head injuries [22].

According to a study carried out by Arbogast et al. [9], 19 percent of the children in Forward Facing Child Restraint Systems (FFCRS) with injuries sustained injuries to the head. The head injuries include both contact induced injuries as well as inertial injuries. Injuries such as skull fracture, epidural hematoma, and frontal lobe contusion are contact injuries [23, 24] that are most likely due to excursion of the head and subsequent impact with the vehicle interior. Arbogast et al. [9] demonstrated that substantial intrusion alters the space available for the child, thus allowing for contact.

The primary concern of head trauma is injury to the brain caused by acceleration induced contusions to the cerebral cortex [9]. The major mechanisms of brain injury are positive pressure, negative pressure and shear due to pressure gradients [25]. When the head is impacted, positive pressure is developed as a result of compressive stress. Similarly, at the site opposite to the location of injury, negative pressure develops due to tensile loading. Shear injuries are often the result of large angular accelerations of the head. Injuries to the brain due to motion of the brain relative to the skull result in contusions on the surface of the brain which are attributed to shear caused by pressure gradients. The injury that occurs at the point of impact due to brain movement in the skull is called coup injury, and the injury that occurs at the side opposite the area that was impacted is called contrecoup injury [25]. Children in FFCRS also sustain inertial injuries to the head such as subdural hematomas [9]. Subdural hematomas are most often caused when fast changing velocities within the skull may stretch and tear small bridging veins.

2.2.1.2 Neck injuries

Mousny et al. [8] found that approximately 40 percent of children's cervical spine injuries occur in motor vehicle collisions and almost one third of all neck injuries occur in frontal impacts in the United States. Further, clinical observations documented from the Crash Injury Research Engineering Network (CIREN) calculated that motor vehicle accidents account for 50 percent of all pediatric trauma and 30-40 percent of pediatric cervical spine injuries [7, 26]. Although head injuries are the most common injury to children in MVC's, approximately 50 percent of injuries to the pediatric cervical spine sustained in MVC's are fatal [7]. For children under 11 years of age, motor vehicle accidents account for 38 percent of all cervical spine injuries [26]. Para vertebral soft tissue injuries are the most common type of injury to the cervical spine, accounting for 68 percent of all spinal injuries. The most common spinal injury level was the high cervical spine, the occiput through the fourth cervical vertebrae [27]. More specifically, injuries of the Occipitoatlantoaxial (Occ-C2) complex (also known as atlanto-occipital injuries) are the most common form of cervical spine injury in children aged 10 years and younger [28]. Approximately 80 percent of all cervical spine injuries in children occur at levels above C2. In contrast, 84 percent of all cervical spine injuries to adults occur in the C3-C7 region [29]. Traumatic cervical spine injuries to children include atlanto-occipital dislocations, fractures to the odontoid process and spinal cord lesions [8, 27 and 30].

Injuries to the head and neck account for a greater number and severity of Abbreviated Injury Scale (AIS) 2+ injuries [9]. Injury mechanisms for children in vehicle crashes depend on various factors that include child anatomy, restraint usage, impact direction and the severity of impact. This Section details all these factors as well as their associated injury patterns.

2.2.2 Child anatomy and related injury patterns

2.2.2.1 Child anatomy

Anatomical differences between children and adults place children at an increased risk of head and neck injury as compared to adults. According to Tingval [31], unintentional accidents amongst children account for a greater percentage of injuries than all other factors combined. The proportion of accidents as a main cause of death has grown and today accidents account for more than 30 percent of the deaths among children 1-14 years of age in the United States. He established that children differ from adults not only in size but also in body segment proportion and anatomy. Hence ribs will bend rather than break, resulting in collision energy being transferred to heart and lungs. A child has a higher centre of gravity which decreases the tolerance of the child to withstand high forces in the event of an accident. According to Tingval's study child restraint use was found to be effective in reducing injuries, especially the use of rearward-facing restraints. Figure 1 illustrates the variation in body segment proportions for a child relative to an adult. Klinich et al. [32] established that one of the major differences in anatomy between children and adults is the proportion of total mass in the head. The relative size of the head of a child represents a greater percentage of the overall body mass as compared to an adult. At birth, the head comprises 30 percent of body weight while the adult head makes up only 6 percent of body weight. Figure 2 exhibits the variation in size and shape of a skull from birth to maturity. The relatively large head may particularly affect neck loads, as a larger proportion of mass is being supported by a smaller structure. As a result of the larger proportion of mass found in the heads of children, their overall centres of gravity are higher, as previously found by Tingval [31]. This can lead to a different interaction with a restraint system compared to adults, as a child is more likely to bend over a lap belt or around a shoulder belt in a crash.

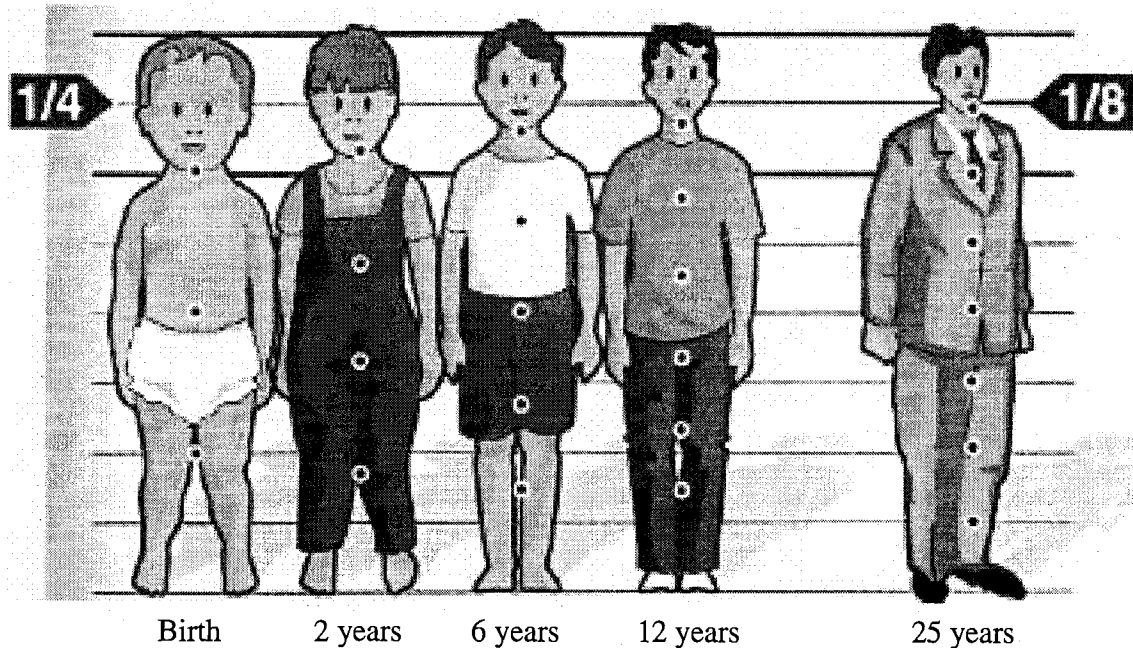


Figure 1. Proportion of the human body in relation to different ages. Left to right: infant, 2-year old child, 6 year old child, 12 year old child and 25 year old adult [33].

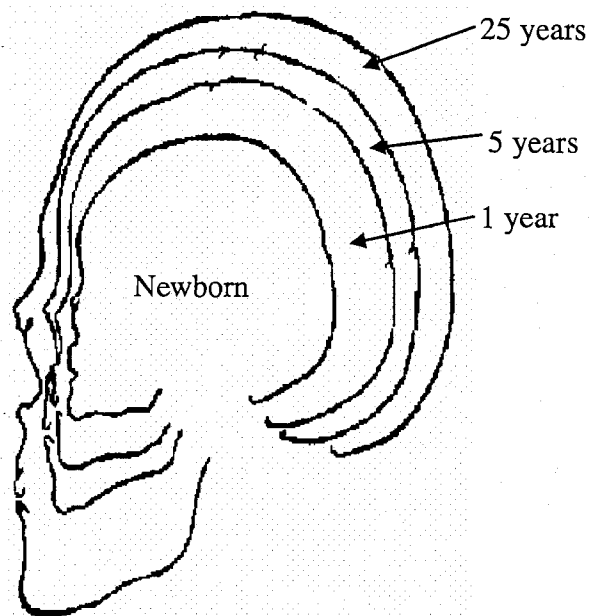


Figure 2. Skull Profiles showing changes in size and shape [32].

A number of case studies have shown that severe neck injuries occur very often to young child occupants in a crash. For children under 11 years of age, motor vehicle

accidents account for 38 percent of all cervical spine injuries [26]. The biomechanical structure and properties of the upper cervical spine of children place them at an increased risk for acceleration induced injury. Figure 3 shows the medial sagittal plane of the Occ-C2 complex. The ligaments are lax, the vertebrae are not ossified and are more likely to separate, the facets are predominately horizontal providing limited restriction of subluxation and the posterior-lateral contours of the vertebral bodies are not developed to restrict flexion forces. Eman et al. [34] stated that infants and young children have a disproportionately large head, with a high centre of gravity and a weaker neck structure resulting in relatively poor head support. Huelke et al. [35] also confirmed that due to the large size of a child's head compared to its body, the weak cervical spine musculature, and ligamentous laxity the infant could be subjected to uncontrolled and passive cervical spine movements and possibly to compressive or distraction forces in impact deceleration environments. These factors contribute to a high incidence of injury to the upper cervical spine.

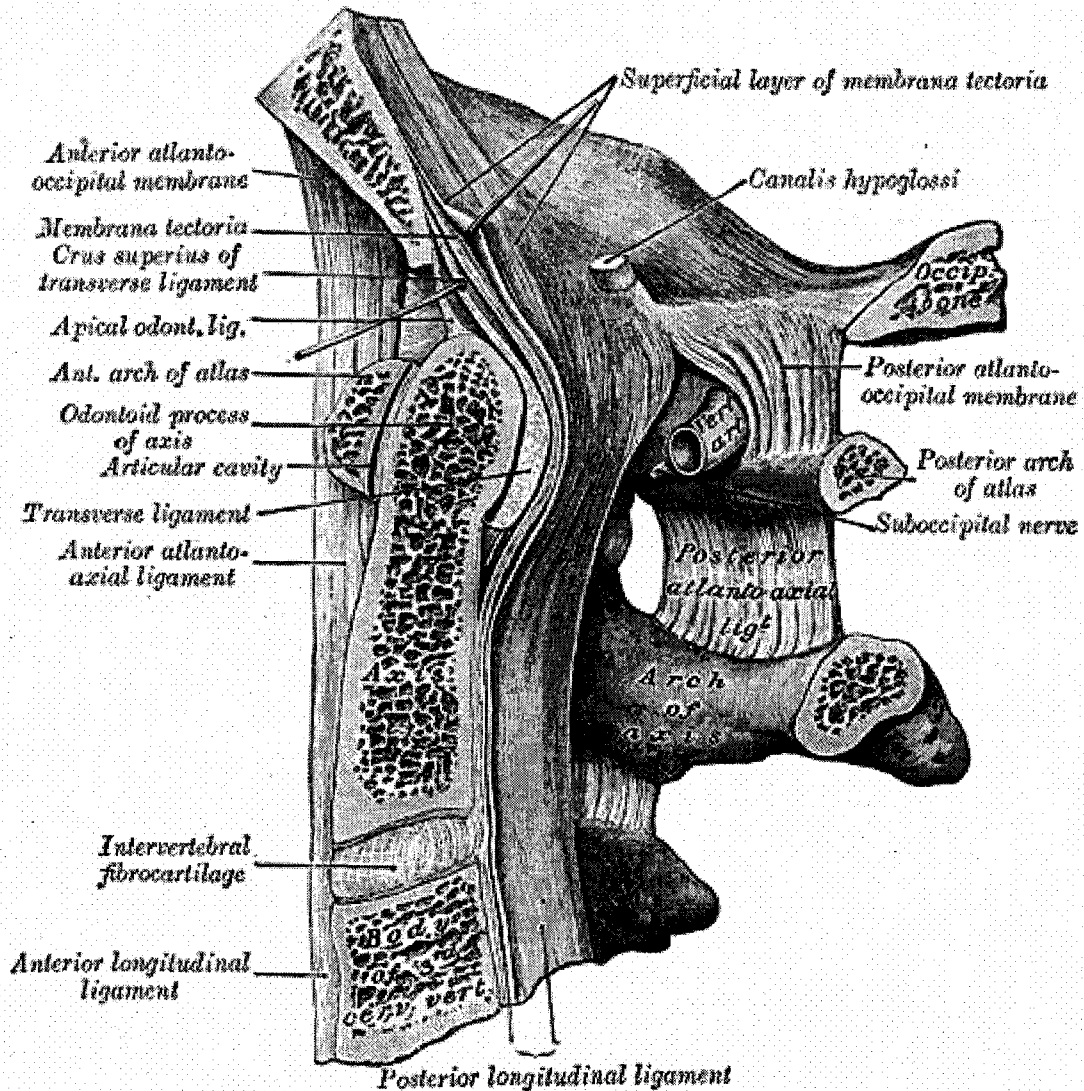


Figure 3. Medial sagittal plane of the Occ-C2 complex [36].

2.2.2.2 Biomechanical structure and properties

Mechanical properties of biological tissues, such as modulus of elasticity, ultimate strength and percentage elongation often vary with age. This also greatly influences the injury mechanisms observed for children in vehicle crashes [32]. Burdi et al. [37] noted that not only does the head change in size, it also changes in composition. At birth the infant skull has open suture lines and the effect of trauma on the infant skull is local, with reduced transmission through the brain. As the skull develops, the suture lines are joined but ossification is incomplete. In this intermediate stage of development the skull will

absorb some of the energy of trauma and lessen the forces transmitted to the brain. When the skull has become completely ossified it can be considered a rigid structure. At this stage the forces of trauma are transmitted in all directions through the brain and its fluid envelope. The stiffness ratio for the skull of a 1-year-old, 3-year-old and 6-year-old is 0.312, 0.588 and 0.733 respectively [38]. These ratios have been calculated as a comparison to the skull stiffness of an adult. Less stiff skull properties are likely to increase the magnitude of intracranial strains that occur during head injuries involving impact. This makes the head of a child less resistant to impact trauma compared to adults [37].

The biomechanical structure and biomaterial properties of the pediatric cervical spine place children at an increased risk of acceleration induced injury as experienced in MVC's [35, 38, and 39]. The ligaments of the paediatric cervical spine are lax and do not effectively contribute to the structural integrity of the cervical column. The cervical vertebrae are not yet completely ossified making them more prone to separation. In children, cervical vertebrae are connected by synchondrosis, which is a temporary cartilaginous joint that exists during normal growth and development. As the child grows older, this soft tissue undergoes ossification. In infants and toddlers, there is curtailed ossification of the synchondrosis, which makes their necks more prone to fracture [37]. Figure 4 shows the top view, side view and the front view of cervical vertebrae for different age groups. The light gray portion represents the cartilage and black portion represents the bones. It can be seen that for children there is curtailed ossification in the cervical vertebrae. This implies pictorially that as a person ages, their neck becomes stiffer, and therefore mechanically behaves differently. In addition, the relatively large head and shorter neck of children places the fulcrum of the cervical spine within the Occ-C2 complex increasing the risk for Occ-C2 dislocation injuries [30]. As a result of these biomechanical factors, 60-80 percent of all paediatric vertebral injuries are in the cervical region.

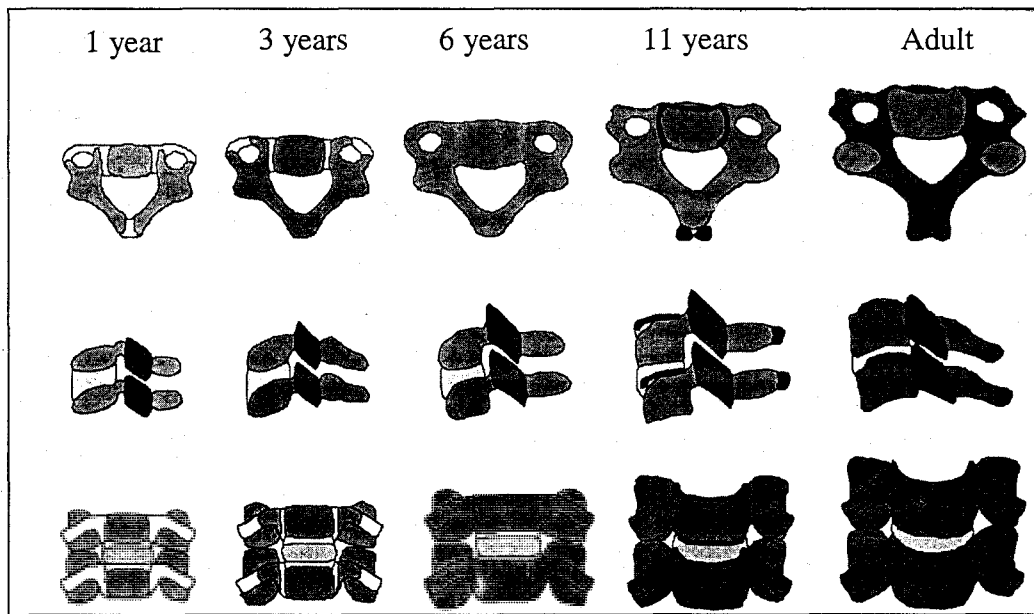


Figure 4. Typical cervical vertebrae for ages one, three, six, eleven, and adult [37].

2.2.2.3 Anatomy related injury mechanisms

Anatomical, physiological and developmental differences between children and adults place children at an increased risk of head and neck injury as compared to adults. Mechanisms of neck injury include extreme hyperflexion which leads to rupture of the tectorial membrane and separation of vertebrae which leads to atlanto-occipital dislocation (AOD) [40]. Separation occurs in the immature paediatric cervical spine due to the column not yet having formed a contiguous interlocking structure through the normal processes of growth and development such as ossification and geometric changes. This structural inadequacy in high axial tension-forward flexion environments as experienced in MVC's damages the spinal cord by placing it in a state of tension or complete transaction [9]. The disproportionate size of the child's head relative to the rest of the body increases the relative moment of inertia per unit of acceleration for children as compared to adults. This in combination with the under-developed musculoskeletal pediatric cervical spine put children at an increased risk for cervical injuries in MVC's.

The combination of tension and forward flexion in and of itself is an injury mechanism for Occ-C2 dislocation injuries. Research conducted on primates has determined the tolerance of the cervical spine to Occ-C2 dislocation injuries is estimated to occur at approximately 120 g's [41]. Occ-C2 dislocations occur more frequently in children due to their relatively small occipital condyles, ligamentous laxity and flat articulation between the occiput and the atlas.

2.2.3 Child restraint system use

CRS provide specialized protection for small occupants whose body structures are still immature and growing [16]. The primary goal of an occupant protection system is to protect injury to the central nervous system. Rapid deceleration of the body and the impact of the vehicle's structure on body surfaces are both associated with severe injury during collisions. All CRS work on the principle of creating a tight coupling of the restrained child and the crushing vehicle, and to distribute the remaining load as widely as possible over the child's strongest anatomical structures. Restraints in vehicles are designed to limit and control the body's rate of deceleration during a crash, thus reducing the forces acting on the body's surface to minimize the differential motion between the skeleton and the internal organs [16].

2.2.3.1 Types of misuse

Child safety seats are extremely effective when correctly installed and used in passenger cars, reducing the risk of death by 71 percent for infants and 54 percent for children ages 1 to 4, and reducing the need for hospitalization by 69 percent for children ages 4 and under [12]. FF CRS effectively reduce the risk of serious injury by 78 percent in MVC's compared to children restrained by using only seat belts [42]. Weber determined that in North America, 80 percent of child restraints were not being used as intended [16]. Different types of misuse can have different effects on child restraint performance. The most common forms of misuse are relatively minor, resulting in sub-optimal levels of protection. Some extreme forms of misuse can themselves lead to

injury in a crash where otherwise no injury would have occurred [16]. If all child passengers aged 4 years and younger were restrained, each year an additional 162 lives could be saved and 20,000 injuries could be prevented. Approximately 29 percent of children aged 4 years and younger do not ride in appropriate restraints, placing them at twice the risk of fatal and nonfatal injuries of those riding restrained. In addition, approximately 85 percent of children riding in child safety seats are improperly restrained [43].

Misuse rates have ranged from 44 percent to 81 percent for child safety seats and 33 percent to 50 percent for booster seats in different jurisdictions of United States [44 – 46]. There were a total of 3201 major injuries for child occupants of light duty vehicles between 1998 and 2002 in Canada [20]. For child occupants suffering a major injury, unsuitable restraint was found to be approximately 92 percent for infants, 74 percent for toddlers and 96 percent for school-age children. The forms of misuse found to produce the greatest degradation are related to non-use of the restraint's shoulder harness and the introduction of slack into the harness or anchorage system. In terms of injury outcome, non-use of a restraint is the most dangerous form of inappropriate restraint use. Rate of restraint use fall as children grow older. Nonuse of CRS and seatbelts for children is estimated to be 13 percent in Canada and 11.8 percent in the United States [20]. The other "gross forms" of misuse that can make the role of the CRS useless are: not anchoring the CRS to the vehicle, positioning an infant facing forward in the vehicle and placing an infant rear-facing in front of an airbag [47].

The most common form of misuse for CRSs is loose harness straps and loose vehicle safety belts. Critical misuse was much lower for CRSs used by young children between 18 and 36 kg (40 and 80 pounds). This may be attributed to the fact that there are fewer CRS parts that need to be adjusted on booster seats. The most common forms of critical misuse for boosters were loose vehicle shoulder and lap belts [44 – 46]. Presence of slack in the restraint systems, incorporating both child restraints and the use of adult seatbelts for children, generally leads to a greater extent of head excursion

(displacement of the head relative to the torso) putting both the head and spinal regions at greater risk of injury.

Usually children are commonly “graduated” to inappropriate restraints too early. This is called premature graduation and it leads to greater torso motion together with the belt loading regions of the child’s body in an undesirable manner resulting in abdominal injuries [48]. Premature movement of the child from CRS to seat belts remains a serious problem. While children less than 18 kg (40 pounds) are predominantly in CRSs, the same does not hold true for children between the age group of 4 – 8 years [44 – 46]. Though premature graduation is more commonly observed in children between the age group of 4 – 8 years age, younger children are at a higher risk of injury than older children if both categories of children are inappropriately restrained. In particular, children aged 4 and under using adult belts are at a significantly greater risk of injury than children of the same age in a child restraint or booster [48 and 49]. Premature graduation results in a 3.5-fold increased risk of significant injury and a more than 4-fold increased risk of significant head injury [48]. This suggests that the younger children are more susceptible to the effects of misuse and inappropriate restraint use.

2.2.3.2 Systematic reviews

Parents often move their children out of child restraints too early, or choose not to use them, because their children don’t like the car seat or booster seat [50]. School-age children are likely to view themselves as too old or too big for booster seats; this perception is shared by many Canadian parents, as indicated by Safe Kids Canada’s survey results [50]. Studies show that infants, toddlers, and preschoolers are restrained in car seats, but when they outgrow these restraints, usually between the ages of 4 and 5, the majority are transitioned into seat belts prematurely, with parents completely unaware of the risks or believing they have made the right choice [50]. Studies show that parents who place their children in booster seats are more aware of the potential for injury than those whose children use seat belts alone [50 and 51].

Systematic reviews have been conducted to examine the effectiveness of community-based intervention programs, interventions to increase the use of booster seats and child safety seats. A systematic review of 3,500 citations examined all intervention studies designed to increase the effectiveness of safety seats [43]. The review specifically examined the effectiveness of interventions relative to the correct use of safety seats or injury outcomes in 72 studies that met the inclusion criterion. The findings of this study state that “there is strong evidence of the effectiveness of child safety seat legislation and distribution of safety seats in combination with education programs.” There was only 1 Canadian study that examined the effectiveness of an infant car seat loan program. This study did not examine the effect of the intervention on actual use of safety seats for children. Another systematic review of 1,320 studies examining the effectiveness of intervention programs specifically for booster seat use reviewed all randomized controlled studies and controlled pretest-posttest intervention studies for 4 – 8 year old children [51]. Only 5 studies met the criteria for the review. Evidence “supports the use of multiple intervention approaches to effectively increase acquisition and use.” There was only 1 Canadian study cited in this systematic review that examined the effectiveness of a media campaign on the correct use of safety seats for children. Findings in this study were not significant, and there have been few intervention studies completed in Canada.

Parent’s knowledge and perceptions about safety seat use are not well documented in Canada. Snowdon et al. [52] carried out a survey to examine parental knowledge and perceptions of the use of safety systems for children in 2 communities in the province of Ontario. Parents of children aged newborn to 9 years were recruited from 3 urban/rural school boards and from daycare centres and hospitals. Data analysis revealed that only 68 percent of children used correct seats for their weight and that as the child advanced in age the rate of misuse increased significantly due to high rates of premature transitioning into safety seats inappropriate for the child's height and weight. The results also revealed that parents had limited knowledge concerning the correct use of safety seats and frequently used non-professional sources of information for vehicle safety information. Following this survey, Snowdon et al. [53] conducted a multisite

intervention study using pretest-posttest design in four Ontario cities to test the effectiveness of an educational program on parents' knowledge of safety system use for children (0 – 12 years) 6 weeks following the educational intervention. Results of this study indicated that knowledge increased significantly following the intervention [53]. Therefore use of professional sources of information is an important factor that is linked with increased parents' knowledge [53].

2.2.3.3 Restraint associated injury mechanisms

The head, chest, spine, abdomen and extremities are the most commonly seriously injured regions. Brown et al. [54] carried out an analysis of injury data from medical records from two specialist pediatric hospitals, in combination with an interview with the vehicle driver and a car inspection in Australia. This study focused on children 3 to 8 years of age. Analysis of injury mechanisms showed that head injuries were typically caused by head contacts with the vehicle interior. These head contacts generally occurred when there was excessive head excursion because of poor upper body restraint, due to misuse of a restraint, or when there was intrusion. The more serious spinal injuries also occurred in conjunction with excessive head motion, and were also associated with restraint misuse. For correctly restrained children, intrusion only becomes a problem when the intrusion occurs into the child's seating position. In this case study, head injuries due to intrusion occurred to inappropriately restrained children in frontal, side and rollover crashes. In another study carried out by Arbogast et al. [9], head injuries were observed to occur due to looseness of both the vehicle seatbelt attaching the child restraint and of the child restraint harness. With loose vehicle belt attachment, the time and space for "ride down" is reduced. With a loose CRS harness, the thoracic spine is allowed to flex and there is relative movement between the torso of the child and the back of the child seat [9].

Abdominal injuries occurred by two main mechanisms [54] - the first being loading of the abdomen by the lap belt which was poorly located across the abdomen of children in adult belts, and the second being from intruding structures in severe side

impacts. The former mechanism was more commonly seen in younger children, and the latter in older children. Lap belt injuries include bruising of the abdominal wall, abdominal viscous injury and vertebral fracture. Children are prone to lap belt injuries because they often slouch with the belt loose and across the abdomen [49]. Correct seat belt fit is not usually achieved until a child is 9 years old, the age at which the child's femur length is long enough for the child to sit against the back of the seat, the anterior superior iliac spines are sufficiently developed to anchor the belt, and the child's sitting height is sufficient for the shoulder belt to fit properly over the shoulder and sternum [48]. A booster seat corrects these problems by lifting the child up and forward, allowing better fit of both the lap and the shoulder belts. For many of the children suffering serious abdominal injury in crashes where intrusion was not a factor, the use of an appropriate restraint system would almost certainly have completely removed the risk of injury [55].

Spinal injuries mostly occur in the cervical and thoracic spine and are associated with poor fit of the seatbelt, poor pre-crash posture and misuse [54]. However, the most severe spinal injuries occur when child restraints and booster seats are misused, due to which excessive head excursion results. Brown et al. [54] stated that, the use of a system such as a high back booster that adequately corrects poor belt fit, and assists in maintaining an acceptable pre-crash posture would have assisted most of the children who suffer bony cervical and thoracic injuries.

The most serious chest injuries observed tended to occur as a result of direct contact between the thorax and the vehicle interior, either in incorrectly restrained children or when major intrusion occurred [54].

Children in loose seat belts or loose child safety seat harnesses are at risk of ejection from a vehicle, especially if it rolls over [49]. Optimizing protection of children against ejection injuries requires universal use of restraints and better understanding of how restraints can prevent ejection. The restraint type influences the injury mechanism, particularly for children in adult belts [54]. Interaction of vulnerable body parts, such as the abdomen and neck, with the adult belt in younger children gives rise to abdominal

and cervical spine injuries [55]. Children using restraints with side wings (CRS and high back boosters) are protected from thoracic and abdominal/pelvic injuries in side impacts, which are seen in children in forms of restraint with no side structure.

2.2.4 Child restraint system orientation and related injury patterns

Child restraint systems provide specialized protection for small occupants whose body structures are still immature and growing. There is a wide variety of systems from which to choose, and different types of restraints are appropriate for children of different ages and sizes. Even with the most appropriate CRS, however, the way in which it is installed and used can have an effect on its performance. Child restraint designs vary with the size of the child, the direction the child faces, the type of internal restraining system, and the method of installation. All CRS, however, work on the principle of coupling the child as tightly as possible to the vehicle. Historically in North America, the CRS has been attached to the vehicle with the existing seatbelts, sometimes supplemented by an additional top tether strap. The child is then secured to the CRS with a separate harness and/or other restraining surface (shield). This results in two links between the vehicle and the occupant, rather than only one. It is therefore critical that both the seatbelt and the harness, for instance, be as tight as possible to allow the child to ride down the crash with the vehicle [16]. Different types of CRS and the North American norms will be discussed in details later in Section 2.6.

In Canada and the United States, it is recommended that children in safety seats should remain rearward facing until the age of 12 months. After this age, governing bodies recommend that children may be positioned in a forward facing child safety seat. However, a comparison investigating the injury potential for children over the age of 12 months in forward and rearward facing configurations during frontal vehicle crash has not been documented. Howard et al. [56] studied the cervical spine injuries in children restrained in forward facing child safety seats and determined that children should be in a rearward facing configuration as long as it is physically possible and comfortable. North American manufactured child safety seats do not allow for proper legroom for older

children whereas in other parts of the world, namely Sweden, children are positioned in rearward facing child seats until the age of approximately 3 years. In a study by Skold [13], it was stated that the child safety seats in Sweden are manufactured in such a way that they are physically able to contain a 3-year-old child and can be properly restrained in a passenger vehicle. Skold suggested that the development of the rearward facing child safety seat for toddlers has reduced the risk of serious injuries. In a study by Weber [16] dealing with rear facing restraint systems for children, it was stated that child safety seats that face the rear of the vehicle are very effective in preventing serious and fatal injuries to small children. They are especially effective in preventing injuries to the upper spinal cord. Injuries to the spinal cord typically occur in children in forward facing child restraint systems. Weber [16] has found that tensile forces acting on the neck can be reduced by half when forward facing child dummies are turned to face the rear.

2.2.5 Crash factors and related injury patterns

Crash factors that influence the injury mechanism include intrusion, impact direction, and crash severity [54]. Nance et al. [57] examined the association between change in speed (ΔV) and risk of injury to children involved in frontal motor vehicle crashes. Nance et al., defined ΔV as the difference in initial velocity at the instant prior to impact and the final velocity, assumed to be zero, for the MVC. The probability of an AIS 2 injury increased on average 56 percent for each 10 kph increase in ΔV . The ΔV at which 50 percent of child occupants would be expected to sustain an AIS 2 injury was 37 kph and that of an AIS 3 injury was 63 kph. The researchers concluded that ΔV is strongly positively correlated with and predictive of injury risk for child occupants.

Research done by Klinich et al. [32] found an inversely proportional relationship between the duration of time a load was applied and the critical load to cause injury. As the time duration increases, the critical load to cause injury decreases. As an example, axial tensile neck loads of approximately 2,500 N imparted on the neck of a 3-year-old can be sustained from 0 to approximately 20 ms. After 20 ms, the critical load that can be sustained is greatly reduced. For example, after 30 ms, the critical load that can be

sustained without causing injury is approximately 1,000 N. Higher severity crashes are associated with a higher risk of injury [54], particularly for sub-optimally restrained children.

Impact direction greatly affects the pattern of injury. Spinal injuries predominantly involve bony injuries and tend to be associated with frontal crashes [54]. The more serious injuries occur when excessive head excursion resulted in the neck being subjected to large tension forces (due to head inertia) at which time head contact occurs, typically with the vehicle interior. Rotation of the head at any time during this process increases the likelihood of serious neck injuries. In the most extreme examples of this mechanism, spinal cord disruption also occurs. Intra-abdominal injuries were seen in frontal, side and rear impacts [54]. Serious head injuries occur only in the more severe frontal and side crashes and are related to impact with the vehicle interior and intruding structures. Side impact crashes, where intrusion occurs at the child's seating position are associated with injuries to the torso, head and extremities from contact with the intruding structure.

2.2.6 Seating positions and related injury risk

For passenger vehicle child occupants aged 0 through 8 years, data from the FARS from 1991–2000 showed that regardless of whether the child was seated in the front seat or rear seat, frontal and side crashes accounted for most child occupant fatalities [3]. Fifty one percent of front seat child occupant fatalities were in frontal crashes, and 31 percent were in side impact crashes. For rear seat child occupants, frontal impacts and side impact crashes accounted for 44 percent and 42 percent of the fatalities respectively.

Smith et al. [58] determined that the rear seat passenger position may reduce the risk of death in a motor vehicle crash by about 39 percent and reduce the risk of death or serious injury in a crash by 33 percent, compared with the front seat passenger position.

Many other researchers also concluded [59 – 61], that occupants in rear seating positions had a reduced risk of fatality and injury when compared to front seated occupants.

Literature shows that seating position relative to the point of impact is one of the major factors in side impact crash fatalities. Data from NHTSA demonstrated that 22 percent of the 3,018 front seat child fatalities were killed in near side impacts [15]. Of the 3,826 rear seat fatalities, 25 percent involved near side impacts. Of the 682 children ages 0 to 8 years old who were killed in side impacts and were secured in child restraints, 64 percent (434) were seated in the near side position. The remaining 36 percent of the fatalities (248) for children in child restraints were seated either in the middle seating position or in the far side position.

Howard et al. [62] found that positioning a child or CRS at the centre of the rear seat was statistically safer than the near-side seat, particularly for restrained child occupants. This conclusion is based on the hypothesis that during vehicle crashes near-side child occupants may have contact with intruding structures. It is also expected that a child positioned in either the centre or far-side location have a greatly reduced possibility of contact with the vehicle interior and injuries more typical of protected motor vehicle occupants may result. A crash study was carried out for 71 collision investigations. It was found that severe injuries to near-side seated children occurred in both the presence and absence of the vehicle wall intrusion. In the first situation with the intrusion of the vehicle wall into the occupant compartment, severe head, chest, abdominal, and extremity injuries are observed. In the absence of intrusion, lateral translation of the child's body can result in injurious contact with the vehicle interior or other occupants, or in severe non-contact head and neck injuries. Newgard et al. [63] found that occupants seated on the near-side or middle-seat of a lateral crash had a higher probability of serious thoraco-abdominal injury compared to far-side occupants, with the probability of thoracic injury being higher than that of abdominal injury at all seat positions.

The severity of the injury is correlated to the relative velocity between the child occupant and the vehicle structure [64]. The relative velocity also depends on the time when the contact occurs between the child occupant and the door. Occupant contact with the door usually occurs prior to the door achieving its maximum velocity. Coupling the child to the vehicle seat tends to move the child along with the vehicle structure resulting in less potential of injury.

According to a study carried out by Roberta Glass [65], fully powered passenger side airbags pose a significant risk to children. Unrestrained children exposed to airbags are found to be 84 percent more likely to die than unrestrained children in the front seat without airbags. Restrained infants are 254 percent more likely to die if placed in front of an airbag. Children occupying the front seat have been killed or severely injured by front passenger air bags, even in minor crashes [49]. The bag inflates quickly from a chemical explosion that results in a contact between the airbag fabric and the child at a relative speed of 300 kph. Children in the zone of inflation can suffer fatal injuries to the head and cervical spine. Therefore children should not be seated in the front seat to avoid injury to children.

2.3 Clinical observations

Clinical data of injured and dead children is usually reviewed to obtain basic crash information and to determine the factors responsible for injury or fatality. This helps researchers better understand the mechanism of injury and modify the current designs to enhance child occupant safety in vehicles.

2.3.1 Frontal impacts

Sherwood et al. [55] carried out a study involving 92 children that died in vehicle crashes in 2000. They found that 34 percent of the child fatalities occurred in frontal crashes. Almost half of these crashes were considered unsurvivable. Restraint misuse was judged to be a factor in 16 percent of the frontal crashes. 39 percent of the fatalities

occurred in potentially survivable frontal crashes in which no other factors played a clear role (non-catastrophic frontal impact).

2.3.1.1 Non-catastrophic frontal impacts

The frontal impact is called non-catastrophic when there is minimum or no vehicle intrusion. In these cases the injury is not contact related. Therefore the principal mechanism of injury in these cases is inertial loading.

2.3.1.1.1 Case 1: Forward facing 35 month old child in the rear seat [56]

This case involved a 35-month-old female in a 5 point child restraint in the rear seat of a vehicle involved in a frontal collision with a ΔV of 80 kph. The driver of the vehicle sustained minor injuries while the front seat passenger required hospitalization. The 35 month old child sustained C2 fracture through the base of the odontoid. This child had no neurological injury and was successfully treated with halo vest immobilization. Figure 5 shows the x-ray for the child with an evident fracture at C2.

2.3.1.1.2 Case 2: Forward facing 23 month old child in the rear seat [56]

In this case a previously healthy 23 month old child was seated in an overhead shield style child restraint in the rear seat of a vehicle involved in an offset frontal collision with a ΔV of 40 kph. The adult front seat occupants were minimally injured. The 23 month old child suffered from an atlanto-occipital dissociation and died as a result of this injury. Figure 6 shows the x-ray of the child exhibiting the atlanto-occipital dislocation

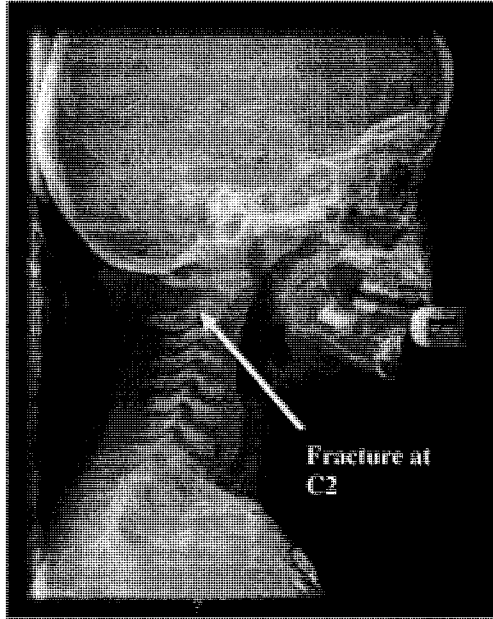


Figure 5. Angulated fracture of the cervical spine (C2) in child of Case 1 [56].

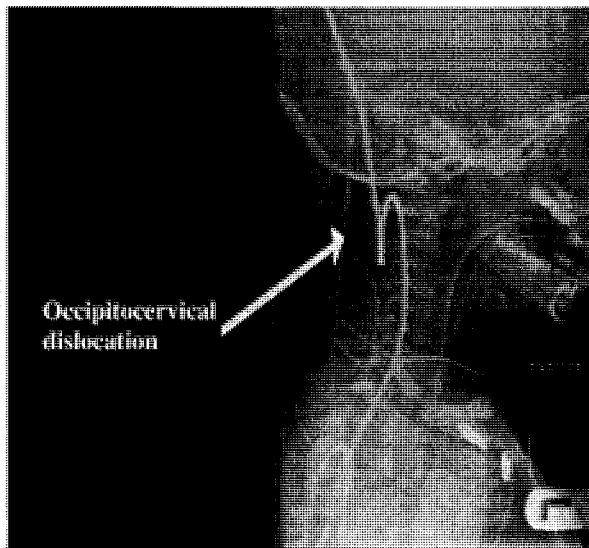


Figure 6. Occipitocervical dislocation in the 23-month-old male involved in Case 2 [56].

Both of the above mentioned cases had children properly restrained in the CRS and yet sustained serious injury. Howard et al. [56] determined that motor vehicle crashes cause a large proportion of children's cervical spine injuries. 20 percent of the injuries are fatal. It has been observed that children facing the rear of the vehicle do not suffer from the same cervical spine injuries as those children that face forward. Heavy head and weak

neck musculature make properly restrained children prone to serious or fatal injuries. Howard [56] suggested that “raising the age at which children are turned from rear to forward facing might prevent catastrophic neck injuries among North American toddlers”. Arbogast et al. [66] also suggested that parents should be encouraged to keep their children facing the rear of the vehicle for as long as possible.

2.3.1.2 Vehicle intrusion: Unsurvivable crash

Cases are considered to be unsurvivable if there is no survival space left at the child’s seating position [55].

2.3.1.2.1 Case 3: Forward facing 3-year-old child in the rear seat [55]

In this case the 3-year-old child was seated in a shield booster in the left rear seating position. The passenger car was struck in the left front by a pickup truck, and the severe crush eliminated the survival space. The driver and 5-year-old child in the middle seat of the second row were killed. Figure 7 shows the amount of crush in the passenger car.

2.3.1.3 Vehicle intrusion: Survivable crash

Intrusion cases are considered to be survivable when the intrusion does not completely compromise the child occupant’s space [55].

2.3.1.3.1 Case 4: Forward facing 2-year, 9-month old child in the rear seat [55]

In this case, the 2-year, 9-month-old child was seated in a forward facing restraint. The vehicle sustained some intrusion of the instrument panel, but the entire survival space was not eliminated. The child died due to the intrusion of the vehicle as well as head contact in the remaining survival area. Figure 8 shows the amount of intrusion in the vehicle.

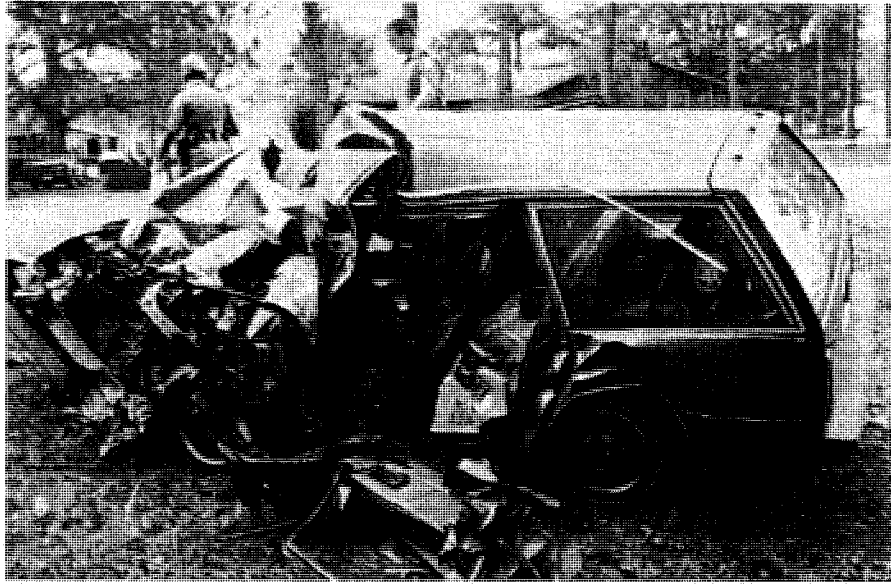


Figure 7. Unsurvivable frontal impact with pickup truck, Case 3 [55].



Figure 8. Frontal impact with some instrument panel intrusion, Case 4 [55].

2.3.1.4 Restraint misuse

2.3.1.4.1 Case 5: Rear facing infant placed in front passenger side seat of vehicle [67]

In this case, an infant less than one year of age, was properly positioned in the car seat and was also rear facing, following the recommended standard for a child of his age in Canada. However, the child was placed in the front passenger seat of the vehicle instead of in the rear seat. This child suffered a skull fracture and subdural haemorrhage caused by the deployment of the airbag.

2.3.1.4.2 Case 6: Toddler placed in front passenger seat of vehicle with no CRS [67]

In this case, a four year old boy was sitting in the front seat with an adult seatbelt and suffered a fractured left orbit and maxilla, laceration of the left scalp, bruising to the right arm, and a right brachial plexus traction palsy due to airbag deployment. The airbag accelerated the child's head against the vehicle interior.

Both of these children might have been spared the injuries they sustained if they were properly restrained or located in the rear seat of the vehicle. Although the injuries incurred to the children were attributed to airbag deployment, there are other factors involved. In Case 5, the child should have been placed in the rear seat of the car. It is believed that the child would have suffered less injury this way due to being placed away from the airbag as well as being far removed from the impact site of the crash. In the Case 6, the child might have been better restrained if placed in a booster seat as well as if he was placed in the rear seat of the vehicle. Again, this child's injuries could have been avoided if recommended restraint precautions were taken into consideration. Some other cases of misuse have been reported by other researchers. For instance, Howard [68] has reported seatbelt injuries to children in frontal crashes. Figure 9 illustrates x-ray reports with evident lap belt injuries sustained by toddlers. Three other cases investigated by Sherwood et al. [55] involved children who were not buckled into the internal harness, and two cases involved child restraints that were loosely attached to the vehicle.

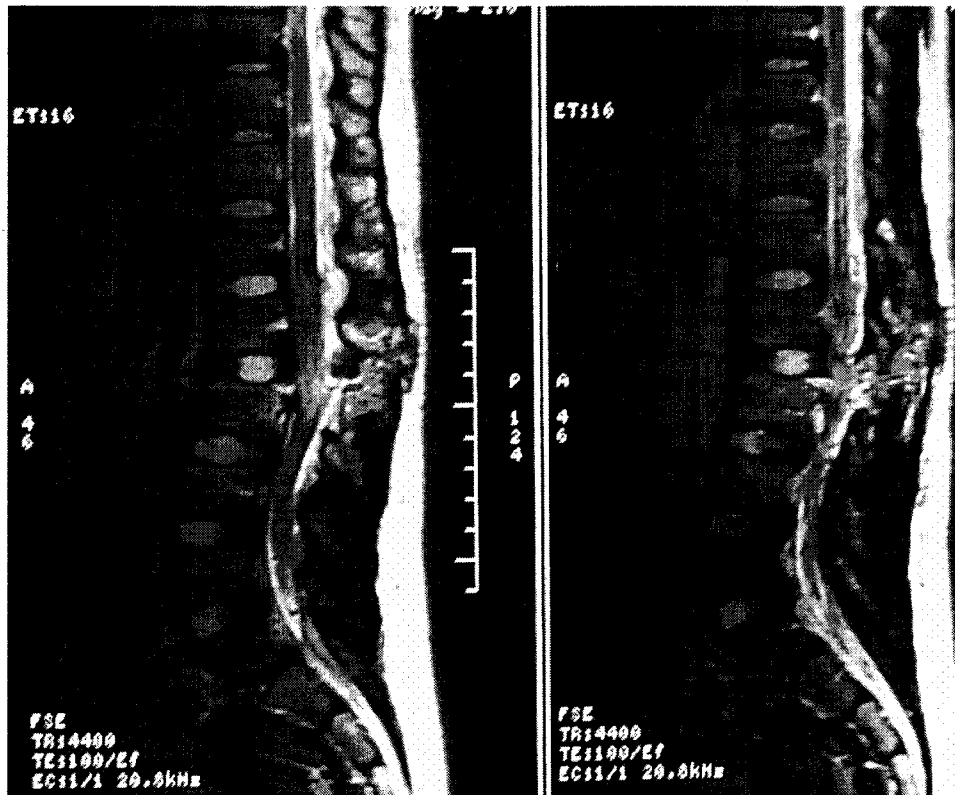


Figure 9. Lap belt injuries in frontal impact crashes [68].

2.3.2 Side impacts

According to Sherwood's study [55] side impacts accounted for the largest number (40 percent) of fatalities; in 70 percent of these crashes, the child was seated on the struck side (near side). Almost half of the side impacts were unsurvivable.

2.3.2.1 Vehicle intrusion: Unsurvivable crash

As it has been mentioned previously, cases are considered to be unsurvivable if there is no survival space left at the child's seating position [55]. The following two cases, reviewed by Sherwood et al. were defined as unsurvivable. These crashes were so severe that even the most sophisticated countermeasures could not have prevented the fatalities.

2.3.2.1.1 Case 7: A near side crash involving 1-year, 10-month old child [55]

In this case, the 1-year, 10-month-old child was seated in the rear outboard seat on the struck side of a passenger car that was hit by an SUV. Figure 10 shows the amount of crush in the child's side for this case.



Figure 10. The unsurvivable side impact with a SUV, Case 7 [55].

2.3.2.1.2 Case 8: A near side crash involving an infant [55]

In this case, the infant was seated in a rear-facing restraint in the rear outboard seat on the struck side. The passenger car was hit by a tractor-trailer with such energy that the car was split into three pieces. The driver also died. The final condition of the passenger car is shown in Figure 11.

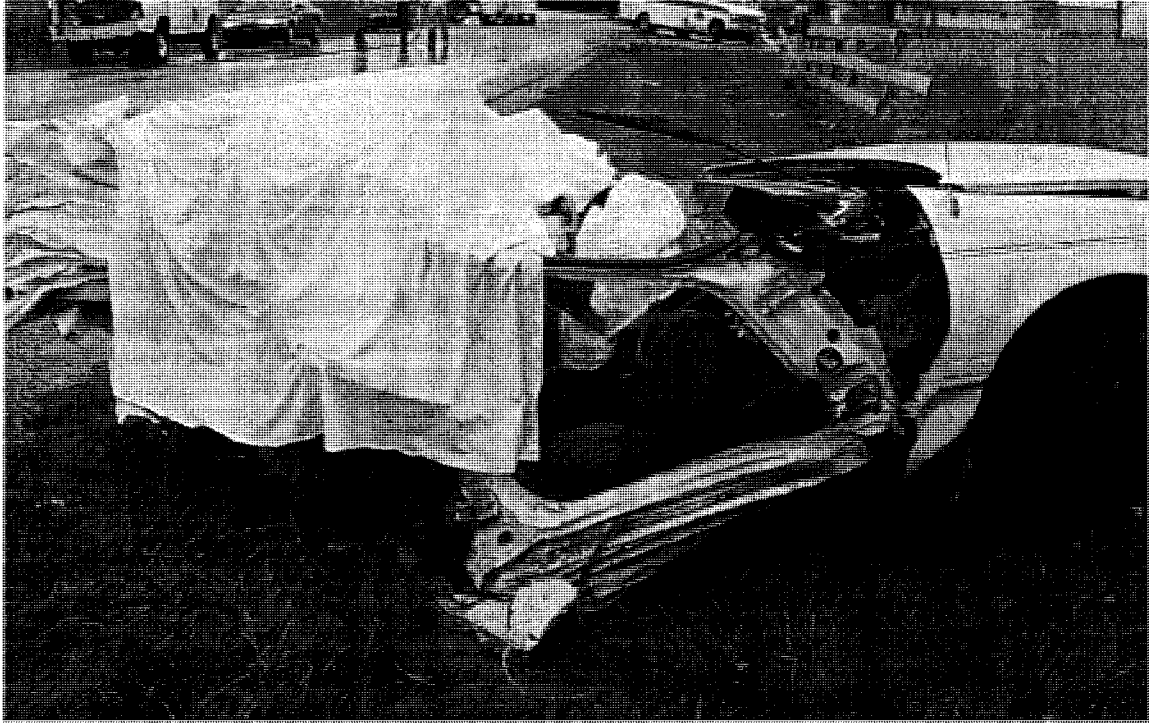


Figure 11. The unsurvivable side impact with tractor-trailer, Case 8 [55].

2.3.2.2 Vehicle intrusion: Survivable Crash

Sherwood found 14 side crashes without excessive amounts of intrusion [55]. Each of these 14 crashes had the primary intrusion located at the child's seating position, and it is possible that the head contacted an external object through the window. In addition, at least 11 of these crashes involved a forward crash component. In the majority of deaths, the fatal injury location was unknown; but in the six cases of known injury, the fatality was due to head trauma.

2.3.2.2.1 Case 9: Near side crash involving a 3-year, 6-month old child [55]

In this case, the 3-year, 6-month-old male was seated in a shield booster directly at the site of impact with a tree. The child died from severe head trauma. Figure 12 shows the amount of crush in the vehicle.



Figure 12. Side impact with a tree, Case 9 [55].

2.3.2.2.2 Case 10: Near side crash involving 3-year old child [68]

In this case the driver of 1995 Pontiac Bonneville proceeded through an intersection without stopping which resulted in an impact on the right side by a Chevrolet R30 tilt-bed pickup towing a trailer with 2 lawnmowers. Bonneville had a maximum crush of 53 cm and a maximum intrusion of 40 cm. Figure 13 shows the deformations associated with the Bonneville. A 3 year old female (20 kg) was seated in a high back booster seat. She sustained a right femur fracture (Figure 14) and right frontal lobe contusions and right skull fractures as presented in Figure 15.



Figure 13. Pontiac Bonneville, Case 10 [68].



Figure 14. Right femur fracture sustained by child of Case 10 [68].



Figure 15. Right frontal lobe contusions and skull fractures to the child of Case 10 [68].

2.3.2.2.3 Case 11: Near side crash involving 2-year, 6-month old child [68]

In a side crash involving three vehicles, a 2 and 1/2 years old child occupant sustained severe cervical dislocation, brain stem injury, and left rib fracture, which are illustrated in Figure 18. These injuries were a result of multiple impacts that occurred when a Pontiac Grand Prix, which the child was seated in struck a Honda Accord, followed by impact between the Grand Prix and Dodge Caravan. Figure 16 illustrates the scene diagram of the side impact. The Pontiac Grand Prix had a maximum crush of 30 cm on the left side of vehicle and a secondary impact crush of 25 cm on the right rear quarter panel (Figure 17). The child occupant was seated in the rear location of the vehicle in a forward facing child restraint with a top tether.

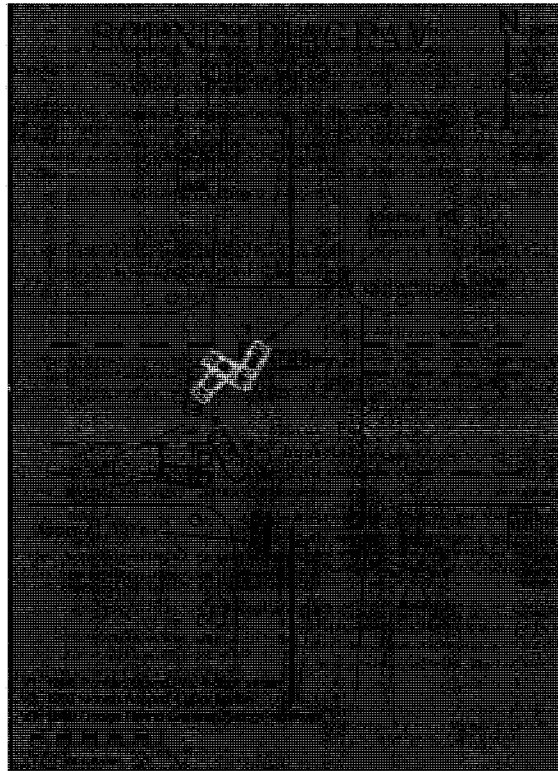


Figure 16. Scene diagram of the side impact, Case 11 [68].



Figure 17. Pontiac Grand-Prix, Case 11 [68].



Figure 18. Cervical dislocation sustained by child of Case 11 [68].

The study done by Sherwood et al. [55] found three side impact crashes that were deemed fatal due to misuse of the child restraint. In one case, the child was restrained in a device that was not approved for vehicle use. In another case, the child restraint was not attached to the vehicle. In the third case, the internal harness was not used. Other reasons for the child fatality were found to be contact with other passengers or ejection from the vehicle.

2.3.3 Rear impacts

Sherwood et al. [55] concluded that rear impacts accounted for 12 percent of the child fatalities. Nine of these 11 cases had massive amounts of vehicle intrusion and were deemed unsurvivable.

2.3.3.1 Vehicle intrusion: Unsurvivable crash

2.3.3.1.1 Case 12: Rear impact involving a 1-year old child [55]

In this case, the passenger car was struck in the rear by a tractor-trailer (Figure 19). The left rear seating position of the 1-year-old child suffered catastrophic intrusion.



Figure 19. Rear impact with extreme crush, Case 12 [55].

2.3.3.2 Vehicle intrusion: Survivable crash

Two of the rear impact fatalities [55] were caused by contact with occupants or cargo. In one case, the relatively minor rear impact propelled an air tank from the rear of a pickup truck, through the rear glass, and into the child in the front seat of the pickup. In the second case, it was judged that the force of the rear impact caused the driver to rotate rearward and strike the child sitting behind the driver.

2.4 Injury assessment methods

2.4.1 Head injury criteria

This Head Injury Criterion (*HIC*) has a historical basis in the work of Gadd who used the Wayne State Tolerance Curve (WSTC) to develop what eventually became known as the Gadd severity index (GSI) [69]. The WSTC is based on the average resultant translational head acceleration. Versace [70] proposed a version of the current *HIC* in 1971 as a measure of average acceleration that correlates with the WSTC. *HIC* was then proposed by NHTSA as a replacement for the GSI in FMVSS No. 208 [71] and is computed according to the following expression:

$$HIC_{t_2-t_1} = \left[\frac{1}{t_2 - t_1} \int_{t_1}^{t_2} a_{\text{resultant}} \cdot dt \right]^{2.5} \cdot (t_2 - t_1) \quad (1)$$

where

$$a_{\text{resultant}} = \sqrt{a_x^2 + a_y^2 + a_z^2} \quad (2)$$

t_2 and t_1 are any two arbitrary times during the acceleration pulse. Acceleration is the resultant acceleration measured in multiples of the acceleration of gravity (g) and time is measured in seconds. The *HIC* measures the effects of head acceleration and duration. These parameters are easily measured by accelerometers on Anthropomorphic Testing Devices (ATD's). The criterion is valid for linear acceleration impacts. In most MVC's, both linear and angular accelerations are present, however, due to lack of another acceptable measure, this criteria is accepted by researchers and government regulatory agencies in both frontal and side impact crash testing.

2.4.2 Neck injury criteria

Injuries to the cervical spine of children in motor vehicle crashes are rare [31, 35 and 39]. However, the biomechanical structure and properties of the upper

cervical spine of the young child place the neck at increased risk for acceleration-induced injury. Neck injuries can range from mild to catastrophic. Generally, the injuries involving the spinal cord at the higher cervical levels are life threatening whereas those at the lower levels can lead to paralysis [25].

The normalized neck injury criterion (N_{ij}) was developed to determine a combination of forces and moments subjected to the neck that would cause injury. According to Schmitt et al. [72], N_{ij} was proposed to assess severe neck injuries in frontal impacts. The N_{ij} was defined by NHTSA [73] as a linear combination of the normalized neck axial load (tension or compression) and normalized neck moment about the occipital condyle. The equation used to calculate N_{ij} is as follows:

$$N_{ij} = \left(\frac{F_z}{F_{zC}} \right) + \left(\frac{M_y}{M_{yC}} \right) \quad (3)$$

F_{zC} and M_{yC} are the critical values of force and moment, respectively.

2.4.3 Protection reference values for child dummies

In a document released by NHTSA and written by DeSantis-Klinich et al. [32], it was stated that the duration of time to which one is subjected to a force or torque has an effect on the potential injury incurred. This study attempted to generate injury criteria for children and protection reference values for child dummies. An important point of distinction is the difference between injury criteria and protection reference values (PRV). Injury criteria apply to humans, while PRV apply to crash test dummies. If dummies were perfectly biofidelic, the injury criteria and PRV would be the same. Since dummies only approximate human response to varying degrees, PRV are usually different from injury criteria. In addition, PRV developed for a particular dummy in a particular situation may or may not apply to other dummies of that size, or to other impact conditions.

The HIC and N_{ij} presented in Sections 2.4.1 and 2.4.2 were developed based on a number of techniques. These include volunteer testing, cadaver testing, animal testing and accident reconstruction [32]. A combination of these techniques has led to the development of injury criteria for adults and for protection reference values for the 50th percentile dummy. There have been only eleven cadaver tests on children that have been reported [32]. Animal testing can generate more information because of the closeness in size to children, but anatomy differences still exists. Reconstruction of accidents is a more viable method of assessing child injury. Since there is so little biomechanical data on children, it is difficult to have a child dummy perfectly represent the actual child.

An additional way to develop injury criteria or PRV for children is by scaling adult data. This has been accomplished by using geometry, mass and biomechanical material property ratios through dimensional analysis. This method assumes that children and adults have similar geometries, which is less appropriate for small children. However, there is such a lack of biomechanical properties of children and it has become an essential way in developing design specifications for constructing child dummies.

Two slightly different approaches to dimensional analysis scaling are available, termed “human-based” and “dummy-based” techniques. A “human-based” approach starts with adult injury criteria or protection reference values, and uses published anatomical and human material modulus data to scale according to dimensional analysis. The “dummy-based” scaling approach assumes that the design of child dummies has been scaled from adult data, so the effects of differing modulus should already be accounted for in the child dummy response [32]. Scaling techniques have been used to develop the PRV’s and injury criteria for child dummies [32, 73]. Table 1 tabulates the PRV’s developed for the Hybrid III 3-year-old dummy. These values are only applicable for frontal impact situations.

Table 1. Protection reference values for Hybrid III 3-year-old dummy [32].

Parameter	PRV
Head injury criteria (<i>HIC-36</i>)	1000
Peak head acceleration (g's)	80
Chest acceleration (spinal) (g's)	60
Neck injury criteria (N_{ij})	$N_{ij} < 1$ $N_{ij} < 1 - 0.0222 \cdot t$ for $0 < t < 30$ ms $N_{ij} < 0.333$ for $t > 30$ ms

The specific values of injury criteria applicable to different safety standards will be discussed in Section 2.5.

2.4.4 Injury risk analysis

The injury risk curves obtained from the test dummy in the crash demonstrate the probability of injury to a real person in that crash. AIS is one of the injury scales used to find the probability of injury to an occupant during a crash. The AIS labels vary from 0 (no injury) to 6 (fatal injury) [73]. Prasad and Mertz [73, 74] have proposed probability curves that help assess the severity of injury to an occupant during a frontal vehicle crash. Appendix B further details the various injury scales as well as the expressions for calculating the probability of injury incurred to a 3-year-old child during a crash (Prasad and Mertz injury risk curves).

2.5 Safety standards

There are different laws and recommendations on child safety in different parts of the world. In the US, the regulations about the technical construction of CRS are referred to as Federal Motor Vehicle Safety Standards (FMVSS), which were issued by NHTSA. In Canada, Transport Canada issues their regulations the Canadian Motor Vehicle Safety Standards (CMVSS), which are very similar to FMVSS. In Australia it is referenced as Australia Standards (AS) 1754. Every child safety seat on the European market has to be approved and labelled according to Economic Commission for Europe (ECE) R44.03.

2.5.1 North American governing bodies

2.5.1.1 Transport Canada

Transport Canada's mission is to develop and administer policies, regulations and services for the best transportation system for Canada and Canadians - one that is safe and secure, efficient, affordable, integrated and environmentally friendly. The Safety and Security Group of Transport Canada is responsible for the development of regulations and national standards, as well as for the implementation of monitoring, testing, inspections and subsidy programs, which contribute to safety and security in the aviation, marine, rail and road modes of transport. Transport Canada sets and monitors the CMVSS which deals with all aspects of vehicle safety. CMVSS 213 specifically deals with testing the performance of motor vehicle child restraint systems. Every child restraint system must conform to the applicable standards set out in CMVSS 213 [75]. On May 1, 2007, this standard was made a part of Motor Vehicle Restraint Systems and Booster Cushions Safety Regulations (RSSR) [76].

2.5.1.2 National Highway Traffic Safety Administration

NHTSA is included within the Department of Transportation and was established by the Highway Safety Act of 1970 [77]. NHTSA is responsible for reducing deaths, injuries and economic losses resulting from MVC's. NHTSA's responsibilities include setting and enforcing safety standards for motor vehicles and motor vehicle equipment. Safety standards for motor vehicles and motor vehicle equipment are referred to as FMVSS, which are established and modified through a process of petition, public notification, public comment, and final ruling. Interested parties can petition NHTSA to take action with respect to the FMVSS. If NHTSA is considering or proposing a change or addition to the FMVSS, NHTSA will publish a notice in the Federal Register and solicit comments. Anyone can submit comments regarding a NHTSA proposal. NHTSA then considers comments before issuing a final rule on a proposed change or addition to the FMVSS. If the proposal is preliminary and lacks sufficient detail to lead directly to a

final rule, the notice is typically referred to as an Advanced Notice of Proposed Rule Making (ANPRM). On the other hand, if the notice proposes specific changes or additions to the FMVSS that will likely lead to a final rule, the proposal is typically referred to as a Notice of Proposed Rule Making (NPRM). Once NHTSA has made a final decision, the public is notified using a Final Rule.

2.5.2 Federal motor vehicle safety standard 213: Child restraint systems

FMVSS 213 specifies requirements for child restraint systems used in motor vehicles and was first introduced by the National Highway Safety Bureau in 1971 [78]. In 1981, the standard was modified to require dynamic testing of child restraints.

2.5.2.1 Current FMVSS 213

2.5.2.1.1 Aspects of FMVSS 213

The final rule makes a number of revisions to the previous version of FMVSS 213, "Child restraint systems". These amendments have been effective from 22nd December, 2003. The revisions incorporate four elements into the standard:

- (i) An updated bench seat used to dynamically test add-on child restraint systems.
- (ii) A sled pulse that provides a wider test corridor.
- (iii) Improved child test dummies.
- (iv) Expanded applicability to child restraint systems recommended for use by children weighing up to 29.5 kg (65 lbs).

The final rule strengthens the technical underpinnings of the standard and ensures that a firmer foundation is laid for possible technical improvements in the future. Child restraints will be tested using the most advanced test dummies available today and tested to conditions representing current model vehicles. The final rule does not adopt the scaled injury criteria developed for the occupant protection standard (FMVSS 208), except that

the time interval used to calculate the head injury criterion is amended from an unlimited time interval to 36 ms, during which the maximum calculated head injury criteria (HIC_{36}) shall not exceed 1000. Other than that, the resultant chest acceleration should not exceed 60 g's, except for intervals whose cumulative duration is not more than 3 ms. The HIC is calculated using Equation 1 and resultant acceleration is calculated using Equation 2.

- (i) Based on data collected on 35 vehicles, NHTSA proposed that the seat bottom angle be increased from 8 to 15 degrees off the horizontal, the seat back angle be increased from 15 to 22 degrees off the vertical, and the spacing of the lap belt anchors be increased from 222 mm (8.7 in.) to 392 mm (15.2 in.) in the centre and from 356 mm (14 in.) to 472 mm (18.6 in.) in the outboard positions. In addition, NHTSA proposed that the seat back should be fixed rather than flexible.

In the current FMVSS 213 rule, NHTSA adopted the revised bench seat as proposed in the NPRM, except that the lap belt anchor points for the centre seating position were specified to be 400 mm (15.7 in.) apart rather than 392 mm (15.4 in.) as proposed. Figure 20 illustrates the revised test bench in FMVSS 213 Final Rule.

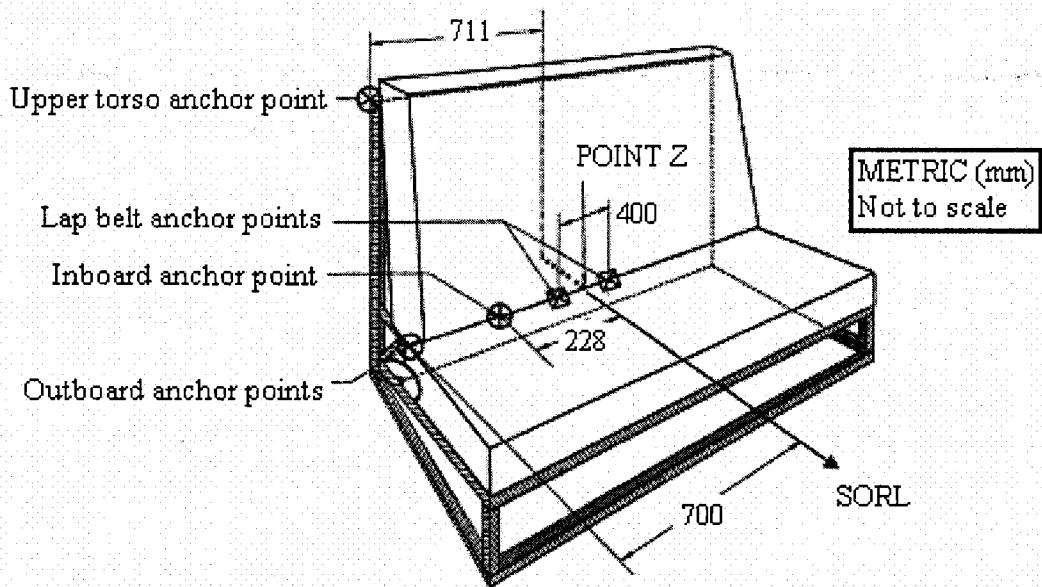


Figure 20. Belt anchorage point locations on the standard seat assembly [78].

- (ii) NHTSA proposed to widen the corridor of the sled acceleration pulse to make it easier for more testing facilities to reproduce this input. The wider corridor extends the pulse from 80 ms to approximately 90 ms in duration. NHTSA believed that the expanded corridor would not reduce the stringency of the test, and would also make it easier to conduct compliance tests at speeds closer to 48 kph (30 mph).

In the final rule, NHTSA adopted the wider corridor proposed in the NPRM, and concluded that the severity of the pulse should not be increased or decreased at this time. Figure 21 shows the revised sled test corridor in FMVSS 213 Final Rule. The lower bound equals 19 g's and the upper bound equals 25 g's.

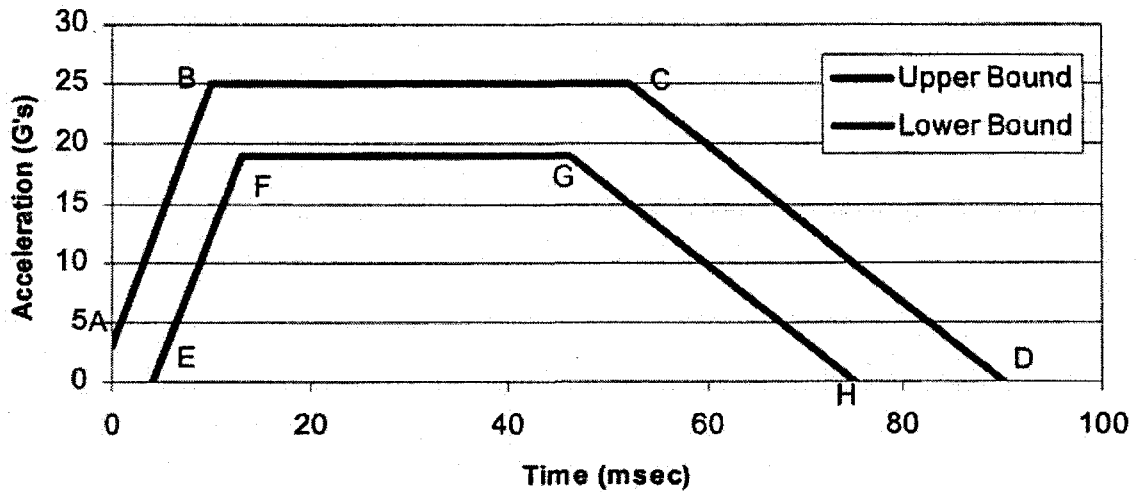


Figure 21. FMVSS 213 sled test corridor [78].

- (iii) NHTSA proposed replacing the 9-month-old test dummy with the Child Restraint Air Bag Interaction Dummy (CRABI) 12-month-old dummy and replacing the Hybrid II 3-year-old and 6-year-old dummies with the Hybrid III 3-year-old and 6-year-old dummies. In addition, NHTSA proposed the use of a weighted Hybrid III 6-year-old dummy weighing 28 kg (62 lb) to test child restraints intended for children weighing 23 to 29 kg (50 to 65 lb). The newborn dummy would still be used as it had been in the past.

In the final rule, NHTSA adopted the new test dummies as proposed in NPRM, effective August 1, 2005 (two years from the publication of the final rule).

- (iv) FMVSS 213 previously only covered child restraints designed for children weighing up to 23 kg (50 lb). NHTSA proposed to amend FMVSS 213 to regulate child restraints recommended for children weighing up to 29 kg (65 lb). The NPRM stated that NHTSA was proposing this modification in order to subject Belt Positioning Booster (BPB) seats that are intended for children weighing 23 to 29 kg (50 to 65 lb) to the same dynamic test requirements as other CRSs.

In the final rule, NHTSA amended FMVSS 213 to regulate child restraints for children weighing up to 29 kg (65 lb) as proposed in the NPRM.

2.5.2.1.2 Lower anchors and tethers for children

Child safety seats are affixed to car seats using various anchorage devices. According to the Motor Vehicle Safety Act, Standard 210.2 [79] and FMVSS 213 [78] as of September 1st 2002, two rear seating positions on all cars, minivans and light trucks are equipped with lower child safety seat anchorage points located between a vehicle's seat cushion and seat back. New child safety seats have two attachments which will connect to the vehicle's lower anchorage attachment points. In addition, all new vehicles have top anchor points that connect to a child safety seat's top tether strap. Together, the lower anchors and upper tethers for children make up the LATCH system. In older vehicle models, the child safety seats are secured to the car seat using seat lap belt. A top tether strap is mandatory in both cases. Top tethers provide additional protection by limiting the motion of the CRS during a severe crash. Weber at UMTRI found that use of a top tether keeps the child head from traveling beyond a safe limit during a severe frontal crash [16]. FMVSS 225 outlines the specifications for the LATCH system [80]. Figure 22 shows the use of a top tether and lower anchors with a CRS in a vehicle.

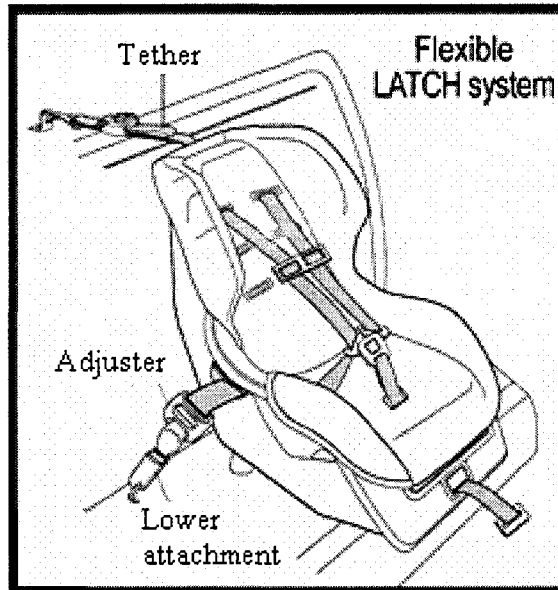


Figure 22. Top tether and lower anchors for children [81].

2.5.2.1.3 Dummy excursion limits

The forward direction of the standard seat is defined by the Seat Orientation Reference Line (SORL), which is the horizontal line through point Z as illustrated in Figure 20 [82]. Additional belt anchor points and forward dummy excursion limits for dynamic test compliance are illustrated in Figure 23. Point Z defines the location from where the dummy excursions are measured. According to the Final Rule, for each add-on child restraint system:

- (i) No portion of the test dummy's head shall pass through a vertical transverse plane that is 720 mm (in the presence of a top tether) or 813 mm (in the absence of a top tether) forward of point Z on the standard seat assembly, measured along the centre SORL.
- (ii) Neither knee pivot point shall pass through a vertical transverse plane that is 915 mm forward of point Z on the standard seat assembly, measured along the centre SORL.

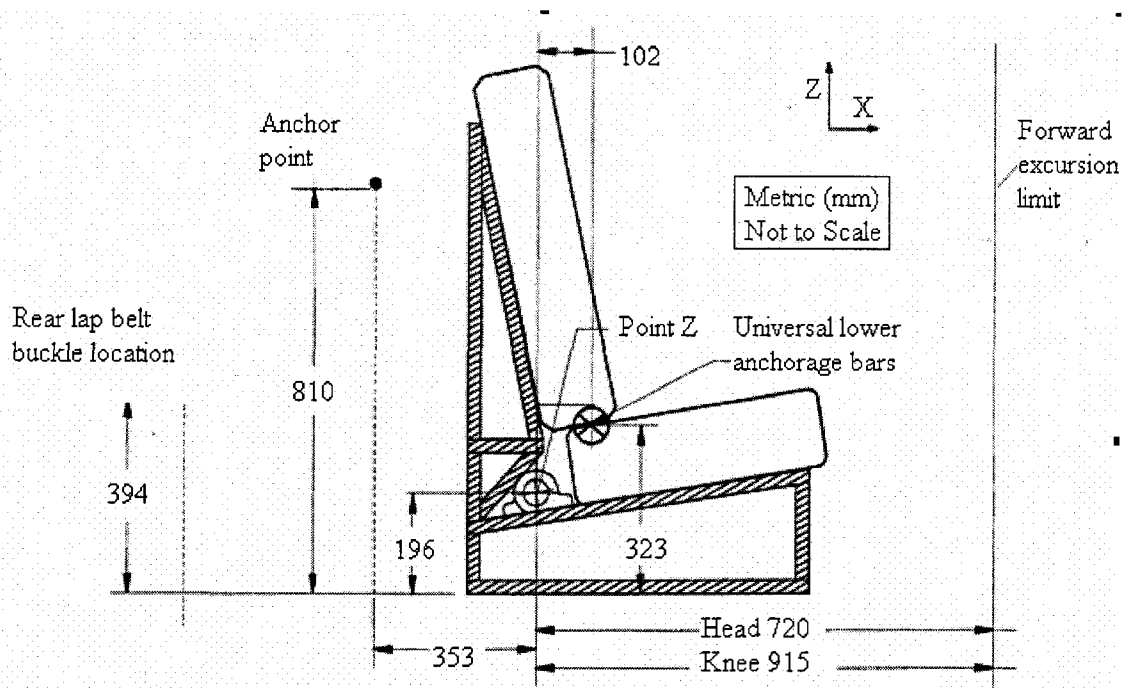


Figure 23. Location of universal child restraint anchorage systems and forward excursion limits for the standard seat assembly [82].

2.5.2.1.4 Dynamic test procedure

This Section outlines the dynamic test procedure outlined by NHTSA that has been effective from November, 2005 [82].

- (i) **Impact Velocity:** A dynamic impact test is conducted at a velocity change of 48 kph (30 mph), lying within the corridor illustrated in Figure 21.
- (ii) **Dummy Dressing:** The 3-year-old dummy is clothed in thermal knit waffle-weave polyester and cotton underwear, a size 4 long-sleeved shirt weighing 0.01 kg, a size 4 pair of long pants weighing 0.01 kg and cut off just far enough above the knee to allow the knee target to be visible, and size 7M sneakers with rubber toe caps, uppers of dacron and cotton or nylon and a total weight of 0.495 kg.
- (iii) **Restraint Installation:** Beginning September 1, 2002, in the case of each add-on child restraint system other than a harness, backless booster seat, belt-positioning seat, or a restraint designed for use by physically handicapped children, install the

child restraint system at the centre seating position of the standard seat assembly in accordance with the manufacturer's instructions provided with the system. The tether strap, if one is provided, is attached to the tether anchorage.

(iv) Dummy Installation:

- a. Holding the test dummy torso upright until it contacts the system's design seating surface, place the test dummy in the seated position within the system with the midsagittal plane of the test dummy head.
- b. Extend the arms of the test dummy as far as possible in the upward vertical direction. Extend the legs of the dummy as far as possible in the forward horizontal direction, with the dummy feet perpendicular to the centreline of the lower legs.
- c. Using a flat square surface with an area of 2580 square millimeters (4 square inches), apply a force of 178 N (40 lbs), perpendicular to the plane of the back of the standard seat assembly, in the case of an add-on system.

(v) Belt adjustment:

- a. Place the dummy in the child restraint for testing. Tighten the child restraint belts until a 9 N (2 lbs.) force applied to the webbing at the top of each dummy shoulder and to the pelvic webbing 50 mm (2 inches) on either side of the torso midsagittal plane pulls the webbing 7 mm (1/3 inch) from the dummy.
- b. Tighten all belt systems used to attach the restraint to the tether anchorage and the child restraint anchorage system on the standard seat assembly to a tension of not less than 53.5N (12 lb) and not more than 67 N (15 lb), as measured by a load cell used on the webbing portion of the belt.

(vi) Before conducting the Dynamic Impact Test, ensure that:

- a. The restraint system and dummy are properly installed on the standard seat, and all belts are adjusted and tensioned as required.
- b. Restraint and dummy targeting required to measure performance are properly installed.
- c. All required calibrations of instrumentation, transducers, and high-speed movie/video camera field are completed and recorded.

- d. All parameters relating to the required impact severity and velocity have been correctly set.
- e. The environmental requirements are met.
- f. When all pretest requirements are met, conduct the dynamic impact test.

2.5.2.2 FMVSS 213: ANPRM

On May 1, 2002, concurrent with the publication of the NPRM and in further response to Section 14(b) of the Transportation Recall Enhancement, Accountability and Documentation (TREAD) Act, NHTSA issued an ANPRM seeking public comments on NHTSA's work on developing a near-term possible side impact protection standard for child restraint systems [15].

The ANPRM primarily addressed the uncertainties in side impact protection for children in child restraints [15]:

- (i) Determination of child injury mechanisms in side impacts, and crash characteristics associated with serious and fatal injuries to children in child restraints.
- (i) Development of test procedures, a suitable test dummy and appropriate injury criteria.
- (ii) Identification of cost beneficial countermeasures.

Uncertainties in these areas, together with the statutory schedule for this rulemaking, made it difficult for NHTSA to assess and make judgments on the benefits and costs of a rulemaking on side impact protection. The ANPRM also requested comments on the appropriateness of proposing to incorporate a rear impact test procedure into FMVSS 213 for rear-facing child restraint systems.

Upon further consideration of the comments on the ANPRM and NHTSA's side impact test program, NHTSA decided not to issue an NPRM and final rule on side and

rear impact protection at the time and thus withdrew the action. A full explanation of NHTSA's reasons for this decision is set forth in a report to Congress that NHTSA has issued concurrently with the final rule. To summarize, NHTSA found that for side crashes [15]:

- (i) Data are not widely available as to how children are being injured and killed in side impacts (e.g., to what degree injuries are caused by intrusion of an impacting vehicle or other object).
- (ii) Potential countermeasures for side impact intrusion have not been developed.
- (iii) There is not a consensus on an appropriate child test dummy and associated injury criteria for side impact testing.

There was widespread support for NHTSA to monitor the progress of the International Standards Organization (ISO) to develop a harmonized side impact test procedure. A preliminary draft of an ISO side impact test procedure includes specifications for an intruding door member. However, no dummies are available at the present time whose construction is designed for side impact validation. Given the lack of an approved test device, and corresponding injury criteria, a final version of an ISO test procedure is not expected in the near future.

The level and amount of effort needed to further develop and validate the ISO side impact test procedure far exceeds what could be accomplished within the time constraints of the TREAD Act. While an NPRM is not feasible, NHTSA's research into improved side impact protection requirements for child restraints will continue as an ongoing program.

2.5.3 Federal motor vehicle safety standard 208: Occupant crash protection

FMVSS 208 specifies performance requirements for the protection of vehicle occupants in crashes [71]. The purpose of the standard is to reduce the number of deaths of vehicle occupants, and the severity of injuries, by specifying vehicle crashworthiness

requirements in terms of forces and accelerations measured on a variety of anthropomorphic dummies in test crashes and static airbag deployment tests, and by specifying equipment requirements for active and passive restraint systems. The frontal barrier impact test is conducted at a test speed of 56 kph (35 mph).

2.5.3.1 FMVSS 208 and a 3-year-old child test dummy

FMVSS 208 outlines the following guidelines when testing a vehicle with a 3-year-old dummy [71].

- (i) All portions of the test dummy shall be contained within the outer surfaces of the vehicle passenger compartment.
- (ii) For any two points in time, t_1 and t_2 , during the event which are separated by not more than a 15 millisecond time interval and where t_1 is less than t_2 , the head injury criterion (HIC_{15}) shall be determined using the resultant head acceleration at the centre of gravity of the dummy head, $a_{resultant}$, expressed as a multiple of g. HIC can be calculated using equation 1 and $a_{resultant}$ can be calculated using equation 2. The maximum calculated HIC_{15} should not exceed 570.
- (iii) The resultant acceleration calculated from the output of the thoracic instrumentation shall not exceed 55 g's, except for intervals whose cumulative duration is not more than 3 milliseconds.
- (iv) Compression deflection of the sternum relative to the spine, as determined by instrumentation, shall not exceed 34 millimeters (1.3 in).
- (v) The neck injury criteria can be measured using equation 3. The critical values for F_{zc} and M_{yc} , are: $F_{zc} = 2120$ N (477 lbf) when F_z is in tension, $F_{zc} = 2120$ N (477 lbf) when F_z is in compression, $M_{yc} = 68$ N·m (50 lbf·ft) when a flexion moment exists, and $M_{yc} = 27$ N·m (20 lbf·ft) when an extension moment exists. N_{ij} values should not exceed 1.0 at any time during the event. The suggested neck tension and compression limits are 1130 N (254 lbf) for peak tension and 1380 N (310 lbf) for peak compression. These values are typical for the Hybrid III 3-year-old dummy.

2.5.4 Motor vehicle standards in other parts of the world

In Sweden, children remain rear facing until the ages of three and four. In fact, the rear facing car seats are designed very differently than those in North America. A study done by Skold [13] explains a Swedish system called ISOFIX for rearward facing seats, which incorporates the child safety seat and anchorage points within the vehicle. ISOFIX is a system for the connection of child restraint systems to vehicles which has two vehicle rigid anchorages, two corresponding rigid attachments on the child restraint system and a mean to limit the pitch rotation of the child restraint system. ISOFIX system is outlined in United Nations Economic Commissions for Europe (UNECE) Regulation 14 [83]. The seats are larger and can be set up in such a way that there is sufficient leg room for a three or four year old toddler. A study that explored the current issues with the ISOFIX system determined that there are some design aspects that need to be changed, including the anchorage points since they are not easily visible and therefore hard to find. In addition, the system is not entirely ergonomic. The system was designed based on the in-car components, in that the anchors are strong enough to hold the seat in place. Also, modifications were made to offer the most possible legroom for the child. There is a high demand for rearward facing child seats due to their superior protection effect. Skold [13] also stated that while restraint systems have been observed as an integrated part of the crashworthiness of an automobile, child safety seats are considered to be add-on systems made to fit in any car. The European regulations still adhere to this identification; however, more recently, the European New Car Assessment Program (EURO-NCAP), the European crash safety rating system, has integrated the protection of children into the rating of a complete vehicle.

In Australia, design standards for CRS anchorages in vehicles have some significant outcomes that set it apart from other standards in North America and Europe [14]. An Australian CRS features a mandatory top tether strap, single point of adjustment for the body harness and the most notable design difference being a six-point harness with double groin straps as compared to a five point harness design as seen in the North American market. Children are anchored to the vehicle seat using the vehicle

seatbelt. These Australian designs have proved to provide exceptional protection to child occupants in severe crashes. In Australia, no cases of severe injuries have been reported with the six-point harness system [14].

2.6 Child restraint systems

2.6.1 Types of restraint seats

Child restraint systems provide specialized protection for small occupants whose body structures are still immature and growing. There is a wide variety of systems from which to choose, and different types of restraints are appropriate for children of different ages and sizes. Even with the most appropriate CRS, however, the way in which it is installed and used can have an effect on its performance. NHTSA and Transport Canada have recommended standards in North America regarding the restraining of children in passenger cars. The growing phase of a child can be divided into four phases [84 and 85]. The following are the four recommended child restraints that should be used from birth till the age of 12. It should be noted that till the age of 12 a child should be seated in the “kid-zone” [85]. The “kid-zone” is the rear seat of the vehicle, which is far away from the front seat airbag. Also, the child should be seated with side-airbags deactivated [85].

- (i) Rear-facing infant seat: Infant seats (Figure 24 (a)) are recommended to be used for infants up to the age of 1, or till the child weighs 10 kg. For heavier babies, a forward/rearward convertible safety seat is used. Babies have relatively large heads and weak neck muscles. An infant’s seat cradles the babies head to protect it against sudden stops or turns. Infant seats are placed backwards so that in a collision, the back of the infant seat takes the force of the impact.
- (ii) Forward-facing child seat: A forward-facing CRS (Figure 24 (b)) is used for children weighing 10 kg to 18 kg, generally from 1 year to 4 years of age. A properly installed FFCRS is safe and effective because its three different parts work together. The harness absorbs the forward motion of the child at the moment

of impact. The LATCH or the vehicle seat belt keeps the base in place. The top tether secures the top of the child seat to the vehicle.

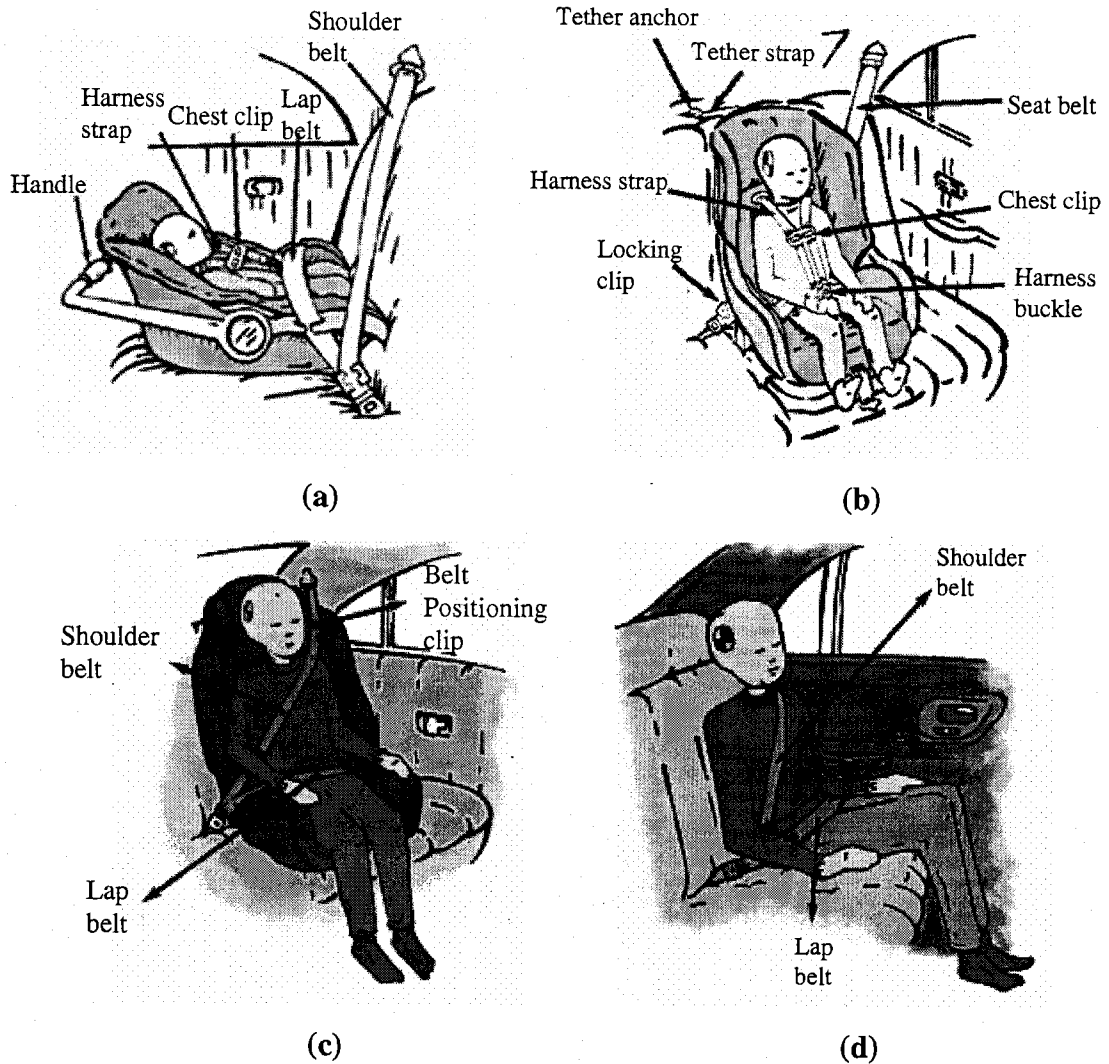


Figure 24. Suggested modes of restraint for various ages and sizes of children: (a) rear facing car seat, (b) convertible child safety seat, (c) booster seat, and (d) child weighing 36 kg or over eight years of age should fit properly in adult restraints [85].

- (iii) Booster seat: A booster seat (Figure 24 (c)) is recommended to be used for children weighing more than 18 kg and less than 4 feet 9 inches tall, generally from 4 years to 8 years of age. Booster seats are the safest way to position a seat belt correctly over a child's body.

- (iv) Seat belt: A seat belt (Figure 24 (d)) is recommended to be used for children beyond 8 years of age and weighing more than 27 kg. The lap and shoulder parts of the seatbelt work together to keep both the lower and upper body secure in a sudden stop and collision.

2.6.2 Convertible forward/rearward safety seats

Convertible child safety seats can be used both forward facing and rear facing and may be a more economical option because they can be used from birth up to 18 kg (40 lb). These seats are generally larger and heavier than infant-only seats. Convertible seats can be turned to face forward when a child reaches 1 year of age and 9 kg (20 lb). When the seat is turned to face forward a change is often required in the threading of the shoulder straps and the vehicle seat belt securing the child safety seat to the vehicle. For children under 1 year and over 9 kg (20 lb), many convertible seats are approved for rear-facing use until the child reaches 13.5–15.75 kg (30–35 lb) [66]. Although children may face forward at 1 year of age and 9 kg (20 lb), it is recommended to keep them rear-facing for as long as possible within the weight and height guidelines for the child safety seat.

Convertible seats come in three harness types: the T-shield, the tray shield, and the five-point harness (Figure 25). The five-point harness has five attachment points, two at the shoulder, two at the hips, and one between the legs. The tray-shield harness has a wide, curved padded surface that swings down around the child's body and is attached to the shoulder straps and crotch buckle. The T-shield harness has a roughly triangular or T-shaped pad that is attached to shoulder straps, fits over the child's abdomen and hips, and latches between the legs [66]. Although all three harness types meet the same federal motor vehicle safety standards, the five-point harness typically fits best for an infant. The five-point harness can be adjusted to the infant's small body, better distributing the forces of a crash [66]. It is usually more difficult to get a tight harness fit for a small infant in a T-shield or tray shield child safety seat because the harness straps are not close to the

body of the infant. In addition, the plastic shield often lies too close to the child's face and neck.

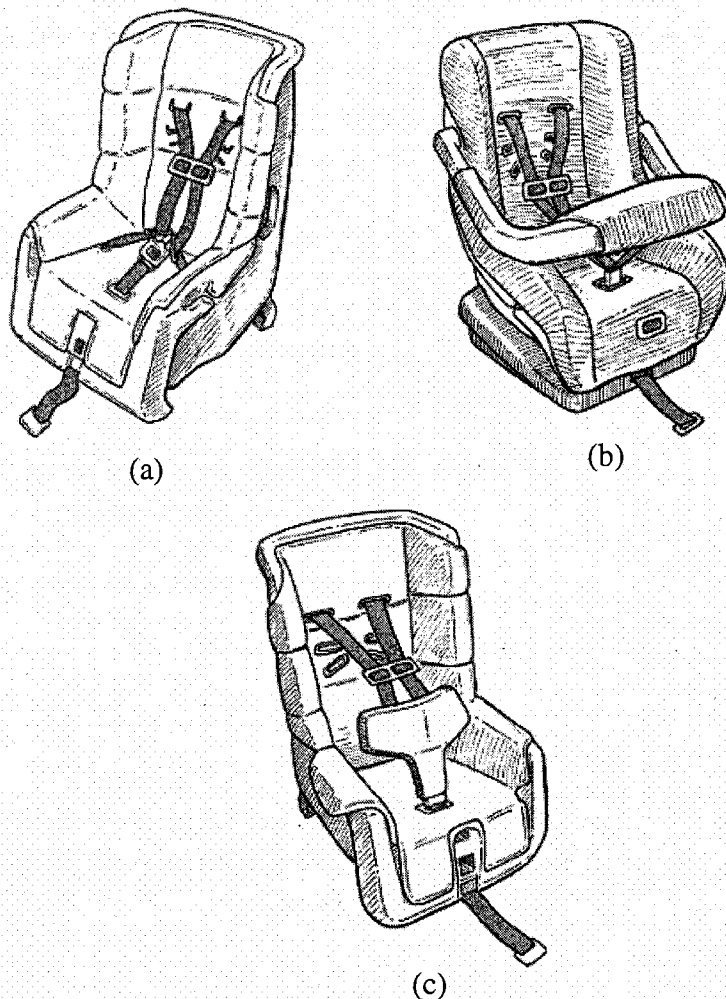


Figure 25. Three harness types available on convertible child safety seats:
(a) five-point, (b) tray-shield, and (c) T-shield [66].

2.6.3 Installing a forward-facing CRS

To minimize possible injuries, the seat must be installed tightly in the vehicle, and the child must be secured tightly in the seat. The harness straps should be very snug against the child's body and the chest clip should be placed at armpit level [66]. All the car seats manufactured after September 1, 2002 have two LATCH connectors that attach

to the LATCH anchor bars in newer vehicles [86]. Otherwise the CRS is anchored using the seat belt. A top tether is mandatory in both the cases. Figure 26 shows different ways of anchoring the CRS to the safety seat. The LATCH system was originally called ISOFIX, a term still used in Europe. In Canada, it is called the Lower Universal Anchorage System (LUAS) or CANFIX [87]. It has also been called the Universal Child Safety Seat System or UCSSS, and Universal Anchorage System (UAS). The advantage of the LATCH system is that it should make it much easier to get a proper installation. The LATCH system can be either flexible or rigid as illustrated in Figure 26.

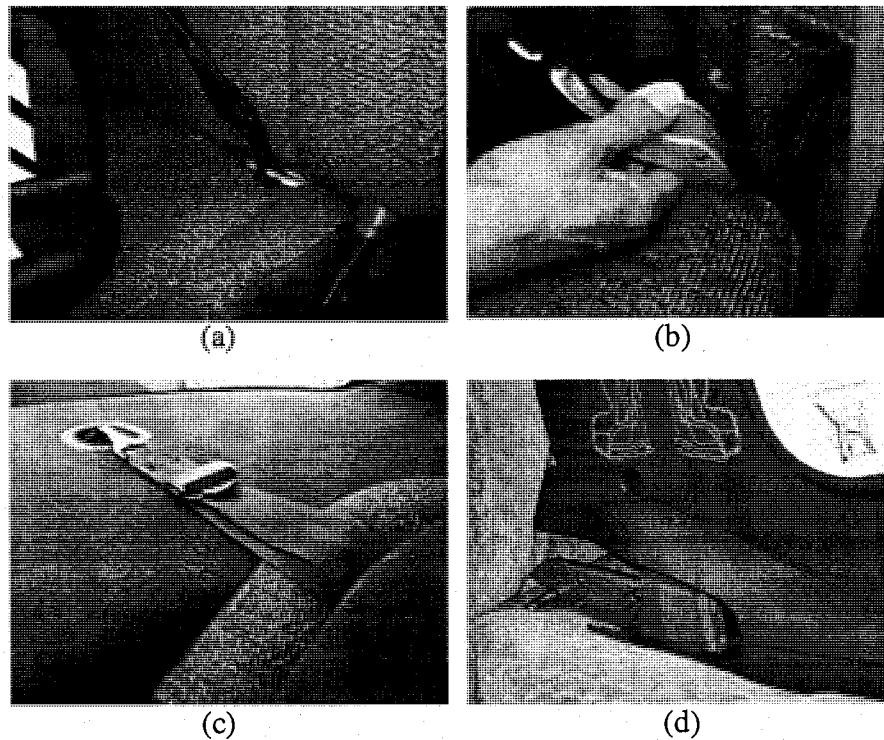


Figure 26. Different ways of installing the CRS to the vehicle seat: (a) car seatbelt, (b) flexible LATCH, (c) top tether and (d) rigid ISOFIX [86].

2.7 Anthropomorphic testing devices

ATDs, better known as crash test dummies, are used to assess the risk of injury in motor-vehicle collisions. They are full-scale replicas of humans that record acceleration and loads during biomechanical testing. Current ATD are designed to be biofidelic, meaning they imitate pertinent human physical characteristics such as size, shape, mass,

stiffness, and energy absorption and dissipation [88]. The dummies' mechanical responses simulate corresponding human responses of trajectory, velocity, acceleration, deformation, and articulation when the dummies are exposed to prescribed simulated collision conditions. Dummies are equipped with transducers that measure accelerations, deformations and loading of various body parts. Analyses of these measurements are used to assess the effectiveness of restraint system designs.

Dummies are classified according to size, age, sex and impact direction. Adult male and female dummies are of different sizes and child dummies represent different ages. Some dummies are used to assess frontal collision protection and others are used to evaluate side impact collisions. The most current frontal impact dummies have sufficient biofidelity to be used to evaluate rear-end collision protection. However, neither the current frontal nor side impact dummies have the necessary biofidelity, measurement capacity nor durability to evaluate the other impact direction. Most often, test engineers use the mid-size adult male dummy for automotive restraint testing. It approximates the median height and weight of the 50th-percentile adult male population. The heights and weights of the small female and large male adult dummies are approximately those of the 5th-percentile female and the 95th-percentile male, respectively. Child dummies have the median heights and weights of children of the specific age groups they represent without regard to gender [88].

Table 2 tabulates different types of dummies available today according to durability in different impact test direction.

Table 2. Anthropomorphic test devices [89].

Frontal Impact ATD's	Side Impact ATD's	Rear Impact ATD's	Children ATD's
Hybrid III 5th Female	SID-IIs	RID2	CAMI
Hybrid III 50th Male	BioSID	TRID –	CRABI 6 Month Old
Hybrid III 95th Male	EuroSID-1	(Rear Impact Neck)	CRABI 12 Month Old
Hybrid II 50th Male	DOT SID		CRABI 18 Month Old
VIP Test Dummies	ES-2		Hybrid III 3 Year Old
TNO-10 Dummy			Hybrid III 6 Year Old
			Hybrid III 10 Year Old
			VIP 3 Year Old
			Hybrid II 6 Year Old
			Q3 Child Dummy
			P0 Newborn
			P3/4 9 Month Old
			P1 1/2 18 Month Old
			P3 3 Year Old
			P6 6 Year Old
			P10 10 Year Old

2.7.1 History of crash test dummies

The first crash test dummy was the Sierra Sam created in 1949. This 95th percentile adult male crash test dummy was developed by Sierra Engineering Co. under a contract with the United States Air Force, to be used for evaluation of aircraft ejection seats on rocket sled tests [88 and 89]. Engineers used early versions of dummies to assess the integrity of restraint systems during simulated frontal collisions. These dummies mimicked human shape and weight and were quite durable. However, they lacked human-like stiffness in the important areas such as the head, neck, thorax and knee. They also were not extensively instrumented to measure responses that could be associated with all pertinent injury concerns. Current dummies have been designed to be biofidelic in their impact responses and are extensively instrumented.

The most used of the early frontal impact dummies was the Hybrid II mid-size adult male dummy developed by General Motors (GM) in 1972 to assess the integrity of lap/shoulder belt systems [88]. This dummy mimicked the size, shape, mass and ranges of arm and leg motion of the 50th-percentile adult male. The dummy was quite durable and gave repeatable responses of coefficient of variations of 10 percent or less when subjected to repeat tests. In 1973, the GM Hybrid II was specified in the FMVSS 208 as the dummy to be used for compliance testing of vehicles equipped with passive restraints. It remained as a compliance dummy until 1997. In addition to the mid-size male, Humanoid Systems developed Hybrid II type small adult female and large adult male dummies by scaling the shapes and features of the mid-size male [88]. These dummies had instrumentation capabilities similar to the Hybrid II mid-size adult male. At the same time, engineers developed 3-year-old and 6-year-old child dummies. The child dummies, along with the three sizes of adult dummies, became known as the Hybrid II Dummy Family. The Hybrid II Dummy Family had two major deficiencies that limited their usefulness in assessing the efficacy of restraint systems. They lacked humanlike response stiffness for their heads, necks, thoraxes and knees and they were sparsely instrumented.

2.7.2 Hybrid III dummy family

In 1997, GM's Hybrid III crash test dummies officially became the industry standard for testing to comply with government frontal impact regulations and air bag safety [89]. The Hybrid III Dummy Family consists of a small adult (5th percentile) female dummy, a mid-size adult (50th percentile) male dummy, a large adult (95th percentile) male dummy, a 3-year-old child dummy and a 6-year-old child dummy. Figure 27 shows the Hybrid III dummy family.

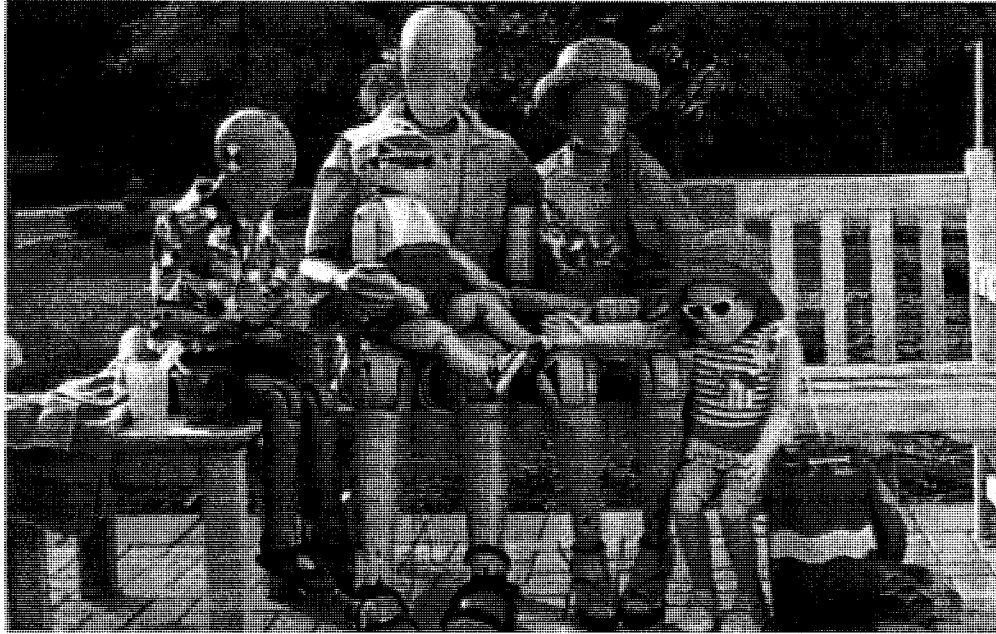


Figure 27. Hybrid III dummy family (from left to right: Hybrid III 6-year-old, CRABI 12-month-old, 50th-percentile male, 5th-percentile female and Hybrid III 3-year-old) [90].

In 1972, General Motors initiated a research program to define and develop a biofidelic mid-size adult male dummy, called Hybrid III, to replace the GM Hybrid II dummy [88]. The Hybrid III was designed to mimic human responses for forehead impacts, fore and aft neck bending, distributed sternal impacts and knee impacts. Its head consists of an aluminum shell covered by vinyl skin having constant thickness over the cranium. The thickness of the skin was chosen to give human-like head accelerations when the forehead is impacted. The neck is made up of asymmetric rubber segments bonded to aluminum disks. A braided wire cable attached to end plates passes through the neck centre. The top end plate is linked to the head with a single pivot joint to represent the atlantooccipital joint of the human. This construction allows the neck to mimic human neck bending responses for flexion, extension, and lateral bending. The chest comprises of six steel ribs linked on one end to a leather part representing the sternum and on the other end to a rigid spine. Dampening material is bonded to the inside of each rib to copy the energy dissipation of the human thorax. The ribs are sized to mimic the sternal force-deflection response of the human thorax. The shoulder structure is designed to

provide an appropriate interface with the shoulder belt. The abdomen is made of polymeric foam. The lumbar spine is represented by a cylindrical curved rubber piece with two braided steel cables running through the centre and attached to end plates. The curvature of the spine gives the dummy a human-like seated posture. The pelvis is an aluminum casting of a human pelvic bone covered with vinyl skin. Femurs and legs are made of steel shafts covered with vinyl skin. Rubber pads are inserted in both knee areas under the skin to give human-like impact response. Ball joints are used for the hip and ankle. Other joints are constant torque pin-joints.

Due to its excellent biofidelity and measurement capability, General Motors petitioned NHTSA in 1983 to allow the use of the Hybrid III mid-size adult male dummy as an alternative test device to the Hybrid II for FMVSS 208 compliance testing of passive restraints [88]. Its use was allowed in 1986. Since its creation in 1976, the Hybrid III mid-size male dummy has undergone design changes to improve the biofidelity of its hips and ankles and to increase its measurement capacity [88]. Since the Hybrid III is specified in worldwide regulations, several regulatory bodies must approve all design changes. After NHTSA allowed the use of the Hybrid III mid-size adult in FMVSS 208 compliance testing, the Centres for Disease Control and Prevention (CDC) awarded a grant to The Ohio State University in 1987 to develop a multi-sized Hybrid III-based dummy family. To support this effort, the Mechanical Human Simulation Subcommittee of the Human Biomechanics and Simulation Standards Committee of the Society of Automotive Engineers (SAE) formed a Dummy Family Task Group of biomechanics, test dummy, transducer, and restraint-system experts. They defined the specifications for a small adult (5th percentile) female dummy, a large adult (95th percentile) male dummy and a 6-year-old child dummy having the same level of biofidelity and measurement capacity as the Hybrid III mid-size adult male dummy. Key body segment lengths and weights were defined based on anthropometry data for the United States population. Biofidelity response requirements for the head, neck, thorax, and knee of each size of dummy were scaled from the respective biofidelity requirements of the Hybrid III, mid-size adult male dummy.

In 1990, a second SAE Task Group of the Human Mechanical Simulation Subcommittee convened to develop instrumented 6-month, 12-month, and 18-month-old infant dummies [88]. The dummies would be used to assess the injury potential to infants due to the interactions of deploying passenger air bags and rearward-facing child restraints placed in the front seat of vehicles.

In 1992, the SAE Hybrid III Dummy Family Task Group initiated a program to develop a Hybrid III 3-year-old child dummy [88]. Again, this dummy was designed to have the same level of biofidelity and measurement capacity as the other Hybrid III type dummies, except for the knee impact requirement and the leg instrumentation. These items were omitted from the design requirements since knee impact is an unlikely event for a properly restrained 3-year-old child. This dummy was designed to replace the GM 3-year-old “airbag” dummy for evaluating unrestrained child interactions with deploying passenger airbags. It would also be used to assess the efficacy of child restraints. For these reasons, its sternum was instrumented to measure its response to the punch-out forces of deploying passenger airbags. In June 2000, the SAE Hybrid Dummy Family Task Group provided specifications for the dummy and has since overseen the development of the 10 year old [89]. The dummy, the Hybrid III 10-year-old child or HIII-10C, has been designed to weigh approximately 34.5 kg (76 lbs) with an estimated height of 137 cm [91].

2.7.3 Child dummies

The P-series is a series of crash test dummies representing children in the age of six weeks (P0), 9 month (P3/4), 3 year (P3), 6 year (P6) and 10 year (P10) old. The P-dummies were the first European child dummies to become official in 1981, when the ECE-R44 regulation came into force [92]. Later, the dummies were also adopted by other standards. The P-series, despite being simple in design and limited in measurement capability, gave a substantial contribution to the protection of children in cars. However, more knowledge on biomechanics related to children and the changing nature of exposure (airbags, belt systems) meant that the P-series became less appropriate over time. In the

nineties the CRABI and Hybrid III child dummies were developed in particular to address the growing problem of child-airbag interaction in the United States. In 1993, the international Child Dummy Working Group (CDWG) was formed with the mission to develop the Q-series as the successor of the P-dummy series. In 1997, this work was continued under the EC sponsored CREST (Child REstraint System sTandard) research program. Within the CREST and the consecutive CHILD (CHild Injury Led Design) projects, altogether the new-born (Q0), the 12-month (Q1), 3-year-old (Q3) and 6-year-old (Q6) dummies were delivered and used in accident reconstruction.

2.7.3.1 Hybrid III 3-year-old

The Hybrid III 3-year-old child dummy (Figure 28) was designed to be used in testing child restraints and assessing the injury risks associated with air bag interactions [93]. The dummy's final design was based on a combination of designs from the 3-year-old "Air Bag" dummy, scaled-down versions of the Hybrid III 50th percentile male and scaled-up versions of the CRABI dummy. The dummy's current design includes some changes made by GM, First Technology Safety Systems (FTSS) and the Vehicle Research and Test Centre (VRTC) to maximize permissible chest deflection and protect instrumentation, and further changes made by the SAE as a result of this evaluation. Some of the distinguishing characteristics of the 3-year-old Hybrid III design are a segmented neck with a steel cable to limit elongation, a set of ribs and rib stiffeners made of 1095 steel for increased durability, upper and lower rib guides to deter vertical movement of the ribs for improved accuracy of chest deflection measurement and sternum-to-spine bumpers to prevent instrumentation destruction caused by metal-to-metal contact in the event of extreme chest deflection. As the dummy was intended to be used while properly restrained in child restraint systems as well as out-of-position with air bags, the dummy's pelvis allows sitting, standing and kneeling postures. The dummy weighs 15.5 kg (34.1 lbs) and its stature height is 94.5 cm (37.2 in) [89]. The dummy has a total of 50 data channels that include a tri-axial accelerometer in the head and chest, and a multi-axial load cell in the upper and lower neck.

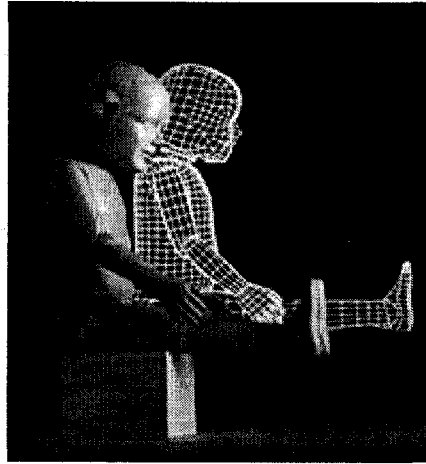
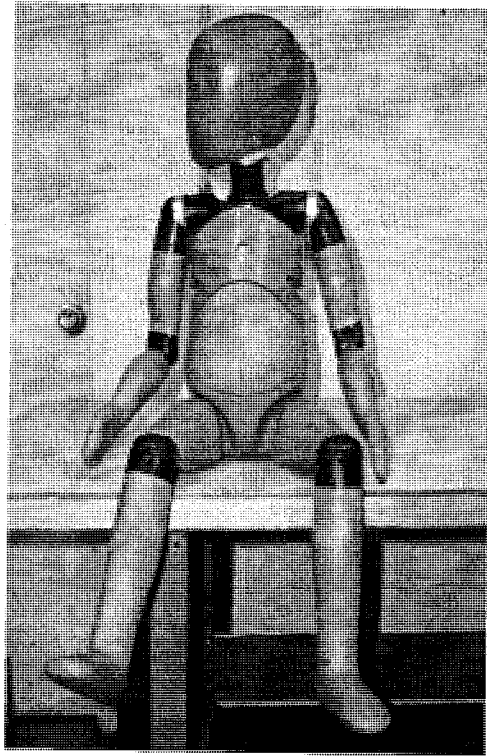


Figure 28. Hybrid III 3-year-old child dummy [89].

2.7.3.2 Q3 child dummy

Specific design features of the Q-dummies are the anatomical representation of body regions, use of advanced materials, dummy-interchangeable instrumentation, multi-directional use (frontal & side impact) and easy handling properties (limited components, easy assembly/disassembly, and simple calibration) [92]. The design of the head, the neck, the shoulder, the clavicle, the thorax, the lumbar spine, the abdomen and the extremities show a realistic anatomy compared to the human anatomy. The head and the clavicle are made entirely from plastics. The neck and the lumbar spine have a similar design: a combination of metal and a natural rubber. It is flexible and allows shear and bending in all directions. The thorax consists of a deformable ribcage and a rigid metal thoracic spine. The plastic clavicle is connected to the thorax at the front of the ribcage and to the shoulders at the arm side. The shoulders are made of natural rubber with metal end plates which are connected to the upper arm on one side and the thoracic spine on the other side. The lumbar spine is mounted between the pelvis and the thoracic spine. The abdomen is skin covered foam, which is enclosed by the ribcage and the pelvis. The pelvis consists of two parts: a metal pelvic bone and a plastic pelvis flesh. Figure 29 (a) shows the Q3 child dummy.



(a)



(b)

Figure 29. (a) Q3 and (b) Q3s child dummy [91 and 94].

2.7.3.3 Q3s child dummy

Q3s is a 3-year-old child dummy specifically designed for side impact. The new Q3s dummy incorporates improved lateral impact performance and enhanced instrumentation for side impact testing [94]. Construction of this dummy is based on Q3 platform, though several of the original Q3 components have been replaced by more compliant yet durable components. Figure 29 (b) shows the Q3s child dummy. Q3s is equipped with 35 data channels. Q3s has shown improved biofidelity in the lateral direction compared to Hybrid III 3-year-old and Q3 child dummies.

2.8 Experimental testing applicable to this research

2.8.1 New car assessment program

In 1978, NHTSA began crash-testing popular vehicle models in the United States. Their protocol (FMVSS 208) involved a full frontal collision into a fixed barrier at 56 kph (35 mph) [95]. Results were published for the information of consumers, as the US arm of the international New Car Assessment Program (NCAP). Today's passenger vehicles are designed to be more crashworthy than they used to be because of this testing. NHTSA provides safety information for a large number of vehicles through their NCAP, using a crash-testing procedure and featuring only vehicles built after 1994. NCAP is conducted by a number of entities around the world, although the test procedure and regulations followed may be different to some extent. In Europe, the most popular models are crash-tested by the European NCAP. The Euro NCAP was established in 1997, and is funded by governments, the European Commission, and consumer organizations. In Australia, the Australian NCAP (ANCAP) has recently adopted the Euro-NCAP testing procedures. In Japan, the National Organization for Automotive Safety & Victims' Aid (OSA) sponsors Japanese NCAP tests (full-frontal, frontal offset, and side impact) on the most popular Japanese home-market vehicles [95].

2.8.1.1 Child restraint systems rating in NCAP

The child restraint seats are rated in order to provide consumers proper information about the efficiency of the CRS. In 2002, in response to the TREAD Act, NHTSA concluded that the most effective consumer information system is one that gives the consumer a combination of information about child restraints' ease of use and dynamic performance [96]. NHTSA examined three dynamic tests for determining the CRS rating that include:

- (i) A sled test at 48 kph (30 mph) in compliance with FMVSS 213
- (ii) A high-speed sled test at 56 kph (35 mph) in compliance with FMVSS 213

- (iii) A full-scale crash test in compliance with FMVSS 208

The dynamic rating is based on the injury parameters of the dummy, head and knee excursion, CRS and dummy containment in the vehicle. The other method of rating the CRS is the ease of use. Under the new rating system, child restraints are given an overall ease-of-use rating at the "A", "B" or "C" levels [97]. The overall rating is determined from the letter grades the child restraint receives in each of five categories:

- (i) Whether the restraint is pre-assembled or requires assembly after purchase.
- (ii) Clarity of the labeling attached to the restraint.
- (iii) Clarity of the written instructions on the restraint's proper use.
- (iv) Ease of securing a child correctly in the restraint.
- (v) Whether the seat has features that make it easier to install in a vehicle.

Figure 30 shows the experimental set-up used for the dynamic testing of a CRS in NCAP.

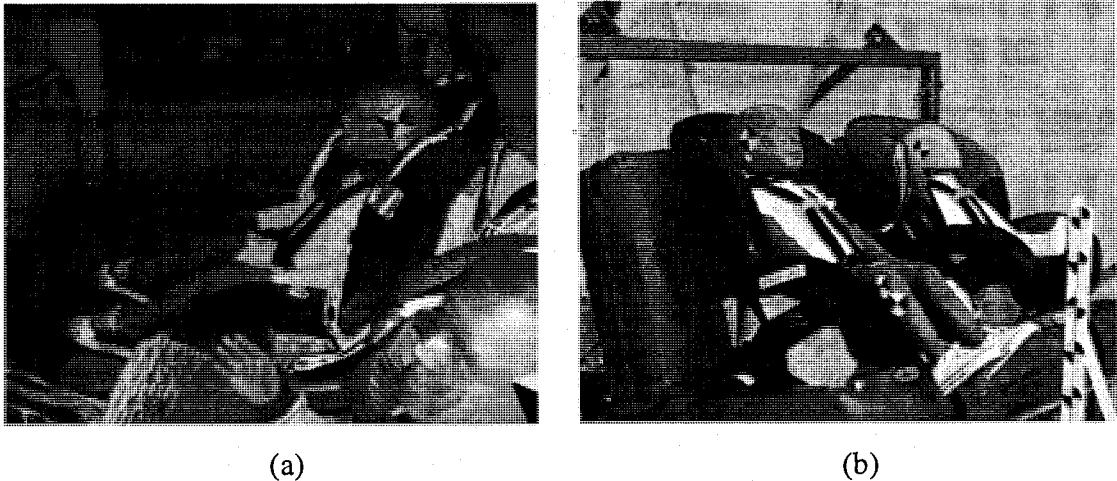


Figure 30. Dynamic test procedures: (a) Vehicle crash, and (b) Sled Test in NCAP [96].

2.8.2 Frontal impact testing

2.8.2.1 Cadaver testing at University of Heidelberg

Experimental child cadaver testing [98] was completed at the University of Heidelberg. The experimental child cadaver tests involved 4 child cadavers in the age of 2½ up to 11 years. The tests were conducted at impact velocities ranging between 30 – 40 kph. One of the cadaver tests was conducted with a 2½ year old male with a mass of 16 kg and a length of 97 cm. The acceleration pulse which this child cadaver was subjected to is illustrated in Figure 31. The pulse was of trapezoidal shape and had an average deceleration of 18g's over the pulse of approximately 75 ms and the impact velocity of the sled was 8.6 m/s. The cadavers were equipped with instrumentation in the head to record the head accelerations and head trajectories of the centre of mass of the head.

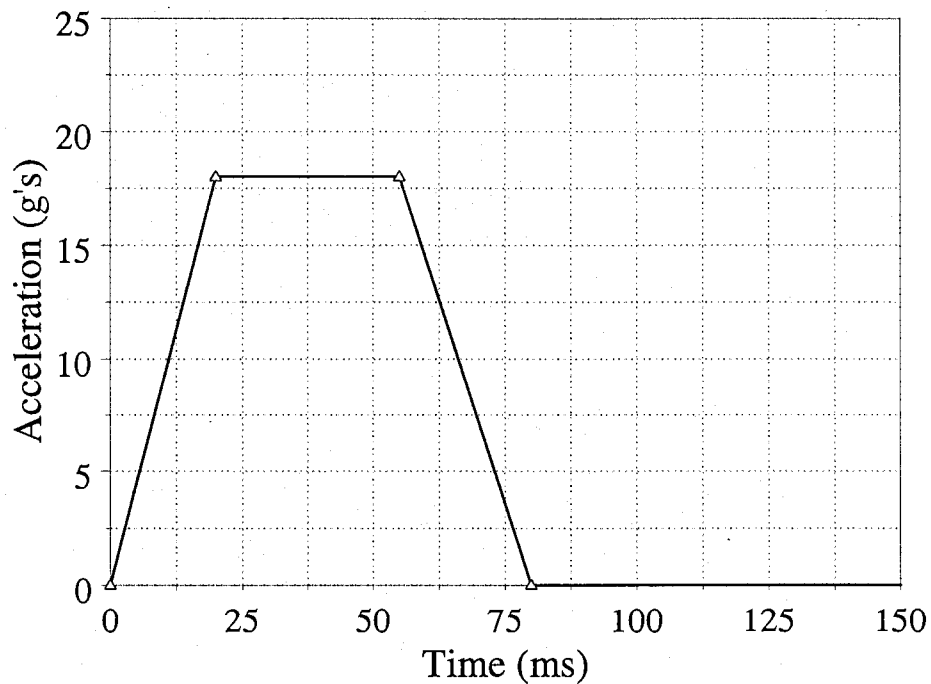


Figure 31. Sled acceleration for the 2½ year old cadaver test [98].

Cassan et al. [99] have completed a comparison study of the kinematics observed in restrained child dummies and child cadavers in frontal crashes. A total of 8 tests were conducted with 3-year old child dummies (TNO P3 and CRABI 3-year-old) with similar test configurations to the above mentioned cadaver tests. This work showed that neither of the two dummies produced exactly the kinematics of the cadavers. P3 exhibited closer reactions compared to the CRABI dummy.

2.8.2.2 Sled testing at Graco Corporation

Experimental sled testing was completed by Turchi [100 and 101] at Graco Corporation's sled testing facilities. The testing apparatus consisted of a sled with an approximate mass of 635 kg. The length of the rails which permit sled translation was measured to be 30.5 m. During a typical impact test, the sled is accelerated towards a fixed seismic mass using pneumatic pressure. The acceleration pulse experienced by the sled during the impact was controlled by a hydraulic damper at the front of the sled. High speed digital cameras were fastened to either side of the sled that acquired photographs at a rate of 1000 frames per second. An additional overhead high speed camera, which was not mounted to the sled, also acquired photos at the same rate. Figure 32 illustrates the crash testing facilities which were used in the experimental portion of this research. Sled impact testing was completed at a speed of 11.6 m/s and the magnitude of the acceleration pulse which the sled experienced in a direction opposite to the impact velocity is illustrated in Figure 33. Also presented in Figure 33 are the lower and upper limits of sled acceleration outlined in FMVSS 213.

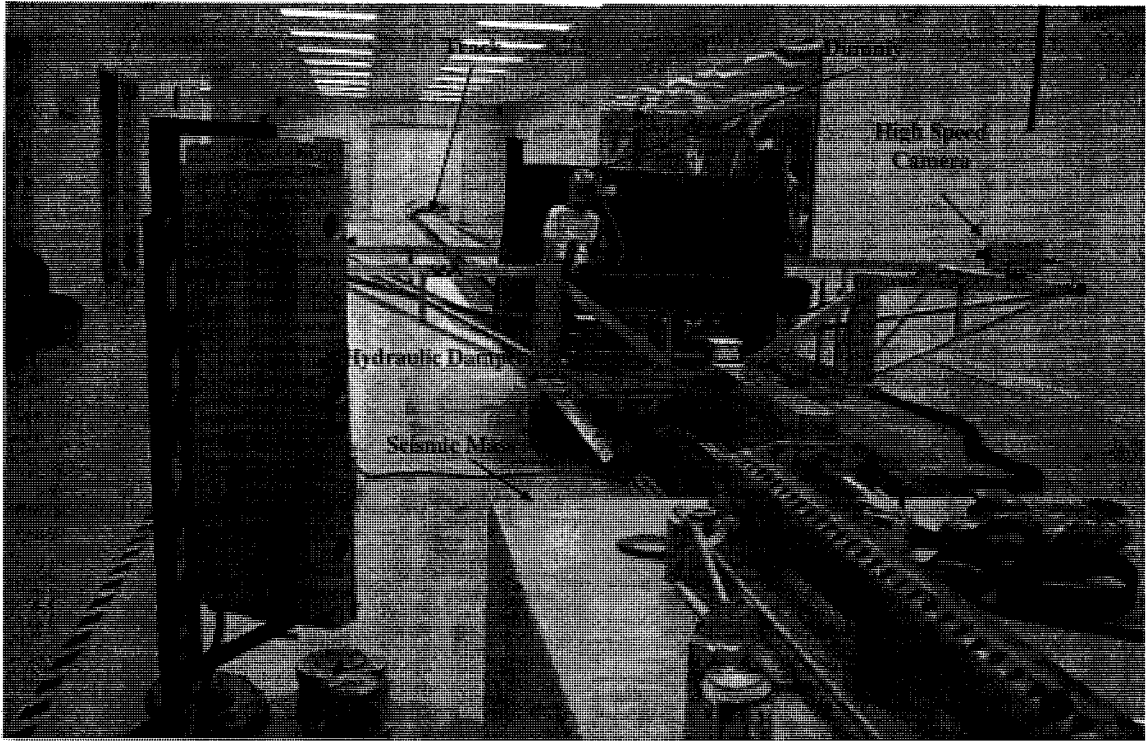


Figure 32. Pneumatically powered sled test device [100].

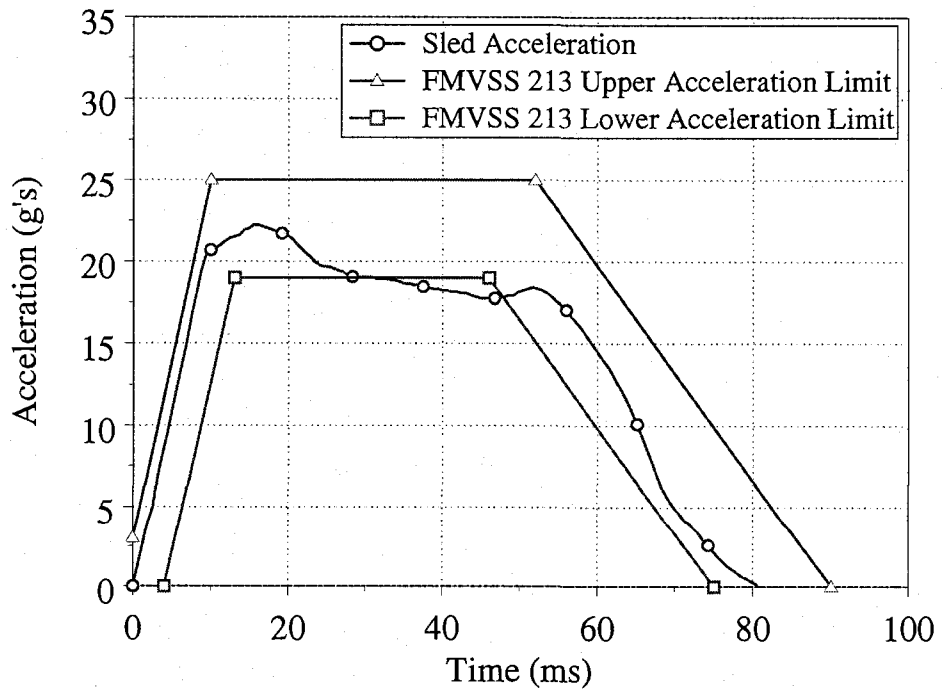
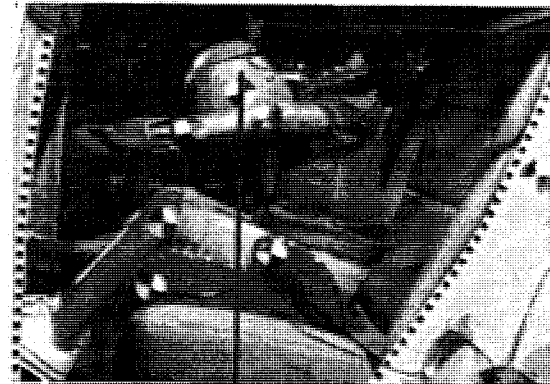


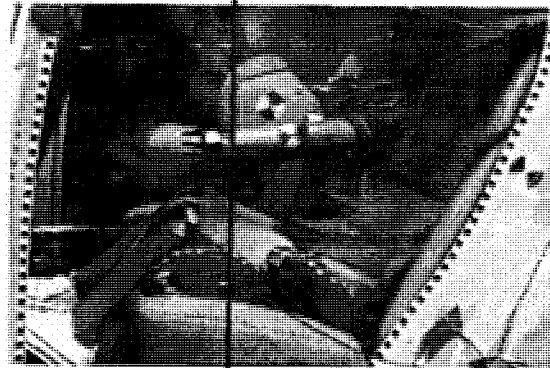
Figure 33. Sled acceleration pulse for FMVSS 213 sled tests [100].

2.8.2.3 Sled testing to evaluate different belt retractors

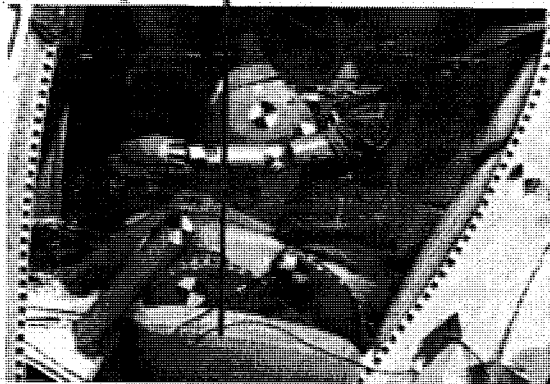
Bohman et al. [102] carried out a study to evaluate the effect of different belt retractors in Sweden. Frontal sled tests were performed with a reinforced car body, having both front and rear seats included. A Hybrid III 6-year-old child dummy was positioned on the left outboard position in the rear seat. Three different 3-point belt retractors were used: a standard configuration, a retractor with pretensioner and a retractor with both pretensioner and load limiter. The acceleration pulse had a mean velocity of 55 kph, peak acceleration 27g at 25ms and a mean acceleration of 12.1g. This study found that when adding a pretensioner to the retractor it was possible to reduce the head excursion and with addition of a load limiter it was possible to keep the head excursion shorter than with a standard retractor. Figure 34 shows the forward displacement observed by the Hybrid III dummy for all the three above mentioned cases.



No pretensioner



With pretensioner



With pretensioner and load limiter

Figure 34. Forward displacement of the Hybrid III dummy [102].

2.8.2.4 Sled testing to evaluate different anchorage systems

A series of 28 frontal impact sled tests were conducted by Belcher et al. in Australia, based on the Australian Standard AS/NZS 3629 child restraint dynamic test method [103]. A further series of 15 tests were conducted in a vehicle body mounted on

an impact sled with an acceleration-time history representative of a 56 kph full frontal rigid barrier crash. Three different models of forward-facing child restraint were tested, with varying anchorage configurations including rigid ISOFIX outlined in UNECE Regulation 14 [83], flexible LATCH strap (as outlined in FMVSS 225) [80] and 3-point seatbelt. P3 and Hybrid III 3-year-old dummies were used. Figure 35 shows the experimental set-up for these sled tests. The results using a rigid ISOFIX connection with a Hybrid III 3-year-old dummy showed a reduced risk of head injury, but a slightly increased risk of extension injury to the upper neck and chest injury (thorax deflection and thoracic spine acceleration) when compared to other mounting systems. In terms of restraint performance and dummy injury measures from the tests reported in this paper, flexible LATCH strap does not seem to offer any significant benefits when compared with 3-point seatbelts. Injury measures for restraints mounted using flexible LATCH straps indicated a higher risk of injury than for 3-point seatbelts. The use of flexible LATCH for mounting of child restraints does not provide increased loading on top tether anchorages when compared to mounting child restraints using the adult 3-point seatbelt. This study suggested that further modifications are required to the existing UNECE and LATCH systems to ensure compatibility with existing Australian child restraint systems without a degradation of child safety [103].

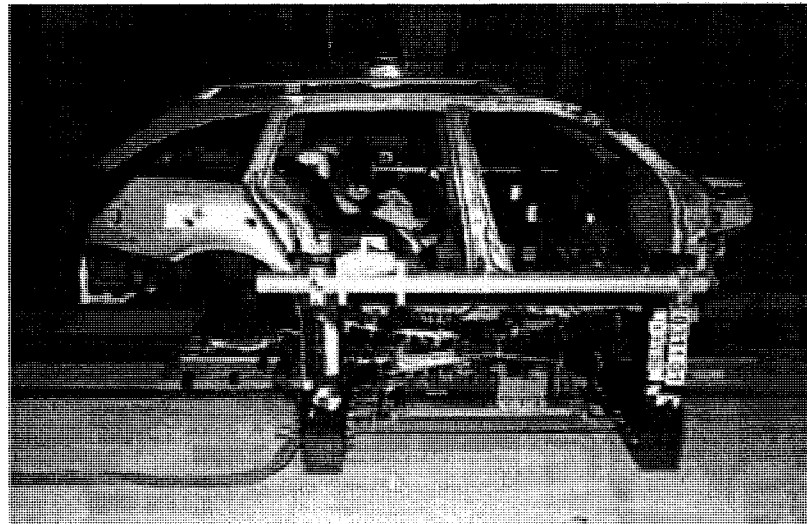


Figure 35. Vehicle body shell/ buck mounted on crash sled [103].

2.8.3 Side impact testing

2.8.3.1 Side impact vehicle tests by Rockwell

Side impact vehicle tests by Rockwell et al. [104] were performed to develop a lateral test procedure for child restraints and to address some of the issues raised in the FMVSS 213 ANPRM that include, determining child injury mechanisms in side impact vehicle tests, and comparing performance in vehicle tests to that of the suggested 90 degree sled tests. Eight vehicles were selected for the research. For any one particular vehicle, the model of CRS, CRS orientation, CRS belt configuration, and child dummy were identical for both outboard rear seating positions. Hybrid III 3-year-old child dummies and CRABI 12-month-old child dummies were used in the tests. The side NCAP test procedure was followed to simulate a car moving at 55 kph hitting another car moving at 27 kph. The observations from one of the side impact vehicle tests are shown in Figure 36. It was observed that the CRS were able to withstand severe side impact crash conditions without mechanical failure. Also, dummies located in the near side crash location exhibited larger injury criteria than those for far side dummies. The circles in the Figure 36 indicate the contact made by the dummy with the vehicle interior and the CRS side wings.



Figure 36. Side Impact vehicle test results [104].

2.8.3.2 Side impact testing by NHTSA (Test No. 4585)

Sled tests were conducted by NHTSA in 2001 at the Transportation Research Centre (TRC). This test, labeled 4585, was a sled test without a vehicle body and in the presence of a side rigid wall [105]. The side impact testing requirements in the presence of a rigid wall are outlined in ANPRM 213 [15]. In this test, use of a rigid structure represents the location of a vehicle's side structure, positioned 508 mm (20 inches) from Point Z1 (location of the further located LATCH anchorage), and adjacent to the child restraint. The structure is essentially rigid, flat surface adjacent to the seat assembly, extending from the seat cushion to a height of approximately 762 mm (30 inches). The height is intended to be high enough so that if the dummy's head were to contact the structure, the head would contact a flat surface and not an edge or curve. The structure extends forward a distance of approximately 813 mm (32 inches), to ensure that head contact would only be with a flat surface. The structure should be unyielding, and should not bend or flex when loaded, and is covered with an aluminum plate. An acceleration pulse with a closing speed of 24.1 kph was used in the tests and is illustrated in Figure 37. The test incorporated a Hybrid III 3-year-old child dummy restrained in a forward facing child safety seat, and anchored with the LATCH system and a top tether. The dummy was equipped with accelerometers in the head and the chest, and load cells were located in the dummy's upper and lower neck region. The accelerometers were set up to acquire the data in the local x , y , and z coordinate systems for the head and the chest. The load cells were utilized to obtain the forces and moments in the local coordinate systems. Figure 38 shows the test configuration and Figure 39 shows the result of the side impact test. The test results exhibit a contact between the dummy's head and the side wings of the CRS. Also, a minor contact between the dummy's head and the rigid wall was observed.

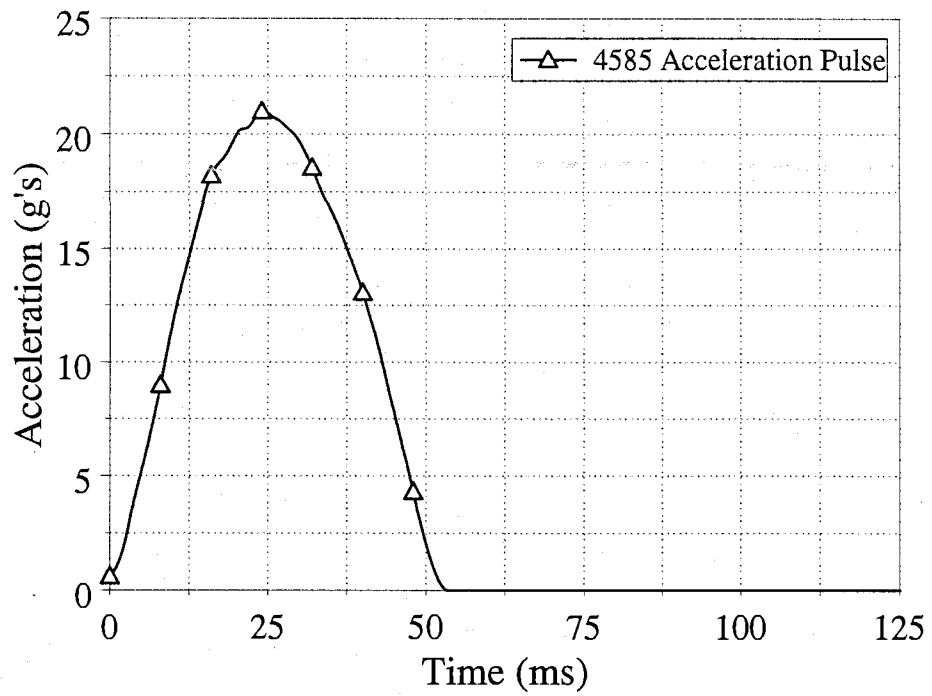


Figure 37. Test 4585 side impact acceleration pulse [105].



Figure 38. Test configuration for the 4585 side impact test [105].



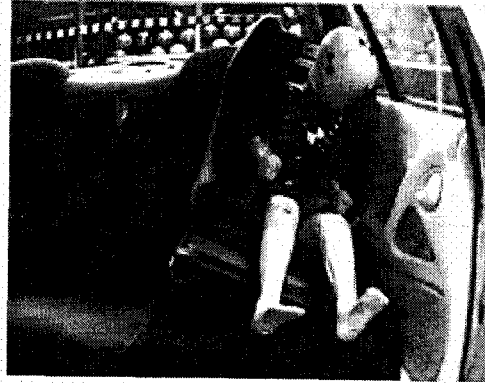
Figure 39. Visual observations from 4585 side impact test [105].

2.8.3.3 Side impact testing to evaluate different anchorage systems

Side impact tests of 50 kph (near and far-side) were conducted by Charlton et al. [106] using a Holden Commodore sedan buck with a peak acceleration of approximately 15 g's. New seat belts, CRS, and top tether anchors were used in each test and the rear seat belt anchor points were reinforced to withstand numerous tests. The front seats of the test bucks were positioned mid-way between full forward and the 95th percentile positions and the seatback angle was 25 degrees from vertical. For the side impact tests, CRABI 6-month dummy in a rearward facing CRS and a TNO P3 dummy positioned in forward facing CRS were used. Three different anchoring methods were investigated that include seatbelt, flexible and rigid anchorage systems. Test configurations are illustrated in Figure 40. The test results showed superior side impact test performance of a rigid anchorage system over a seatbelt anchorage system. The findings of Charlton's research have important implications for the proposed introduction of changes to Australian Standards for CRS to permit both flexible and rigid systems to co-exist with conventional seatbelt anchorage systems.



Seatbelt anchorage at impact



Seatbelt anchorage at rebound



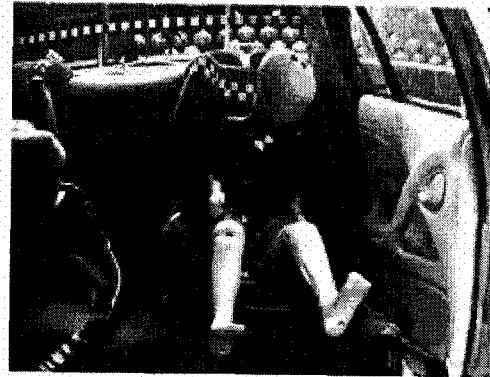
Flexible anchorage at impact



Flexible anchorage at rebound



Rigid anchorage at impact



Rigid anchorage at rebound

Figure 40. Side impact tests (far-side) for forward facing with seatbelt, flexible and rigid anchorages showing maximum lateral head displacement during impact and rebound

[106].

In Comité de Liaison de la Construction d'Equipements et de Pièces d'Automobiles (CLEPA's) side impact tests [107], the ECE R44 sled bench was rotated 80 degrees to obtain lateral as well as forward motion of the dummy so that the test situation was considered to be more severe than a 90 degree bench set up. A rigid fixed door panel with a height of 500 mm above the CRS and 300 mm from the centreline of the ISOFIX anchorage bars was used in the tests. There was no padding on the door during the tests. The sled velocity was prescribed as 40 kph (25 mph), and the peak deceleration was approximately 15.25 g's. TNO P3 dummies, which were accepted for relative comparison but not biofidelic in side impact, were used in the tests. The test configuration is illustrated in Figure 41. The findings of CLEPA's side impact tests also showed the rigid ISOFIX results were superior to LATCH, and that the rigid ISOFIX was easier to use.



Figure 41. CLEPA side impact test configuration [107].

A series of sled tests was performed by Klinich et al. [108] at UMTRI using the Q3s ATD and the ECE R44 sled buck to study CRS and pediatric occupant kinematics in far-side impacts. Using one model of CRS, tests were performed using a 24 kph, 20 g pulse to compare ATD and CRS response to lateral loading in both forward-facing and rearward-facing configurations. For both the forward facing and rearward facing configurations, five different methods for anchoring the CRS were used, which are: lap

belt only, flexible LATCH attachments, flexible LATCH with a left-point belt and a rigid LATCH. Figure 42 shows the peak lateral head excursions observed for the sled tests for the forward facing configuration. Rigid ISOFIX retained the head of the dummy within the CRS and eliminated rotation of the CRS for the forward facing CRS configuration. It was observed that relative to the baseline test with CRS secured by only lap belts, rigid LATCH attachments were more effective in the rear-facing configuration than the forward-facing configuration at reducing ATD head excursion, although rigid LATCH attachments still exhibited good performance in the forward-facing test. Figure 43 shows the peak lateral head excursions for the rearward facing configuration.

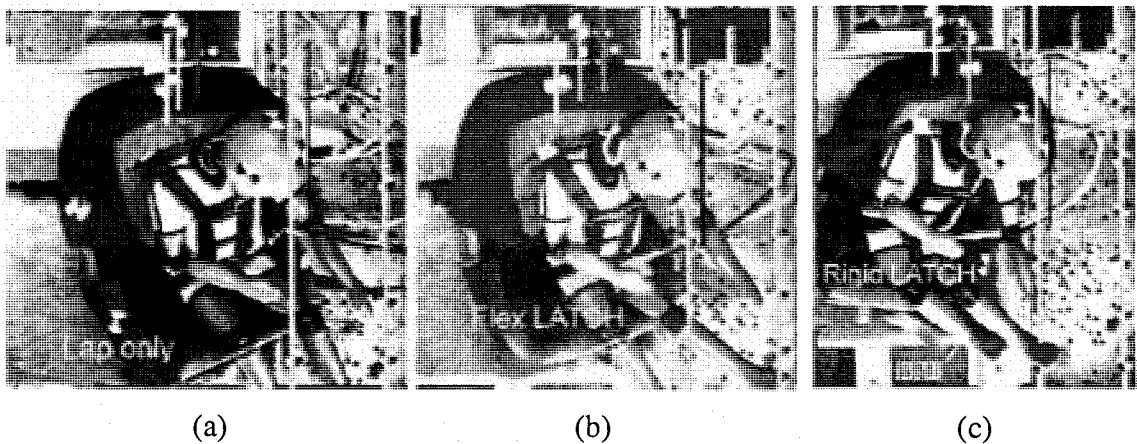


Figure 42. Peak lateral head excursions for (a) lap belt, (b) flexible LATCH, and (c) rigid ISOFIX anchorages in forward facing configurations [108].

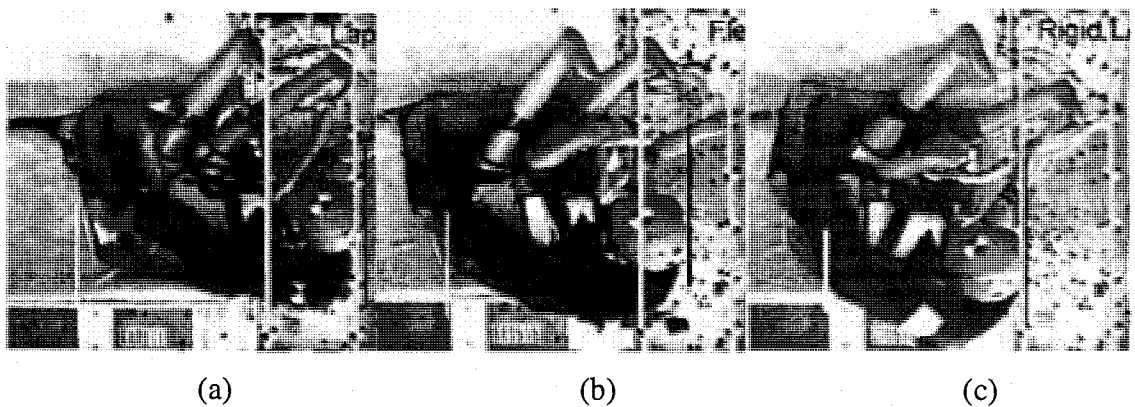


Figure 43. Peak lateral head excursions for (a) lap belt, (b) flexible LATCH, and (c) rigid ISOFIX anchorages in rearward facing configurations [108].

2.8.4 Head and neck safety device

The HANS device (Head And Neck Safety device) is a safety item compulsory in many car racing sports. It reduces the chances of head and/or neck injuries, such as a basilar skull fracture, in the event of a crash [109]. The device was designed in the early 1980s by Dr. Robert Hubbard, a professor of biomechanical engineering at Michigan State University. Figure 44 shows the HANS device used by most of the race-car drivers.

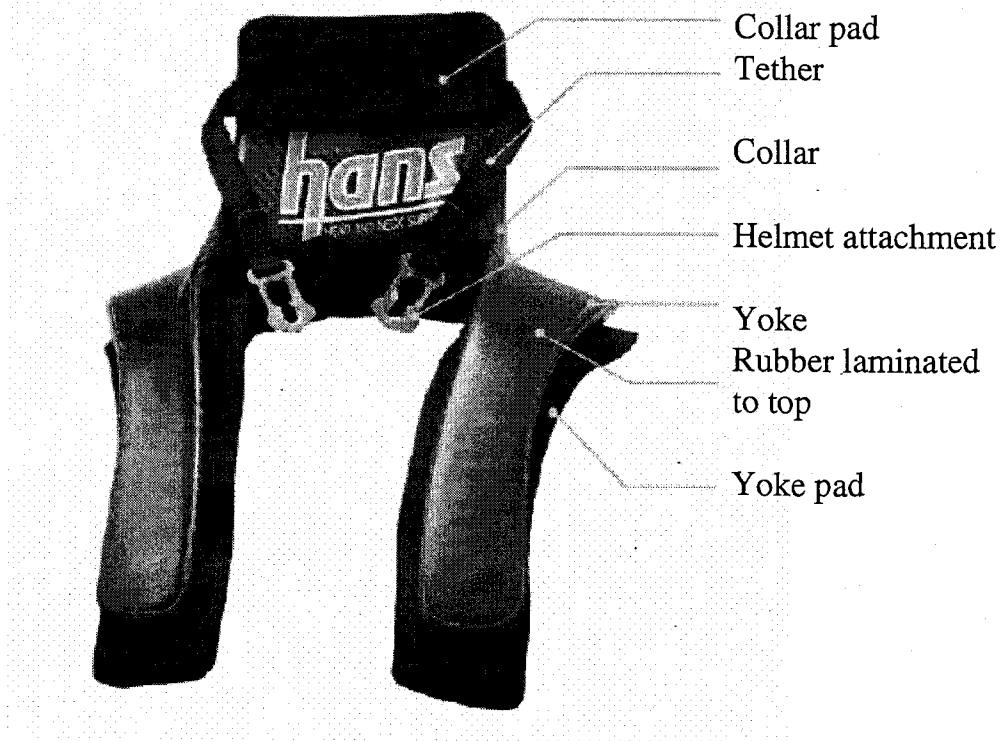


Figure 44. HANS device anatomy [109].

In a crash, the shoulder harness and the seatbelt restrain the driver's torso, but only the neck restrains the head and the helmet. The HANS device reduces the whipping action of the head, keeping the driver's head from being pulled away from the torso [109]. In a frontal impact, the forward head movements are restrained by tethers while the torso and the HANS device are restrained by the shoulder harnesses [109].

Experimental crash tests were conducted at DaimlerChrysler, utilizing an adult male dummy, in order to analyze the effectiveness of using a HANS device and to develop the prototype. Figure 45 illustrates the maximum excursion of the head observed for the testing dummy in the absence and presence of a HANS device. A HANS device is effective in reducing the resultant neck forces by approximately 80 percent, and the *HIC* by approximately 70 percent in the event of a frontal collision [110].

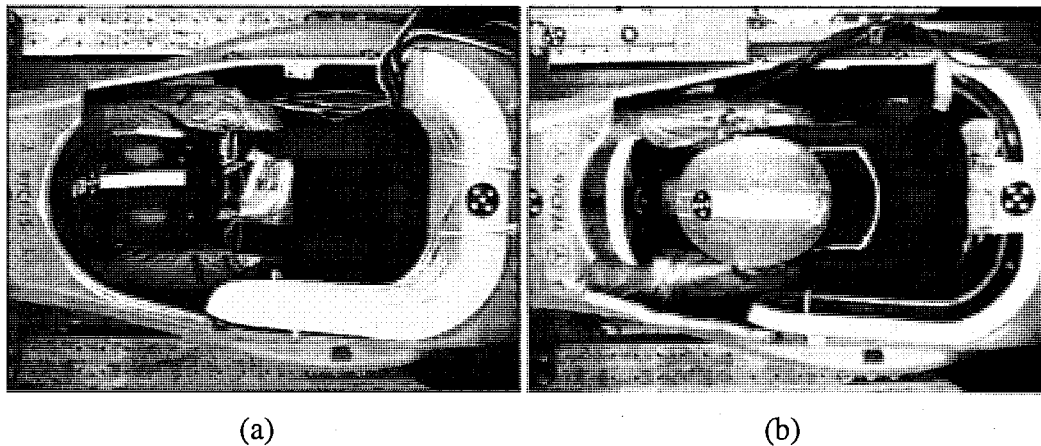


Figure 45. The maximum forward head excursion in the crash test dummy for (a) without HANS device and (b) with HANS device [110].

2.9 Numerical studies applicable to this research

2.9.1 Modeling techniques

Computational modeling continues to play an increasingly significant role in the design of more effective vehicle crash safety systems. Models configured with sophisticated computer analyses permit researchers to perform extensive studies at a fraction of the cost and time that would be required by physical testing alone. Different mathematical models have been used by researchers to simulate the behaviour of a child passenger restrained in a protective device in the case of a vehicle crash. The earliest numerical models of the vehicle safety crashes have been based on multi-body techniques [88]. In a multi-body model rigid bodies are connected by various joint types through which the number of degrees of freedom between the elements can be

constrained. More recently, finite element (FE) techniques have been used for this purpose. In a FE model, the system to be modeled is divided into a number of finite volumes, surfaces or lines representing an assembly of finite elements. These elements are assumed to be interconnected at a discrete number of points: the nodes. In the displacement-based FE formulation, which is applied in practically all major finite element software packages, the motion of the points within each finite element is defined as a function of the motion of the nodes. The state of stress follows from the deformations and the constitutive properties of the material modeled.

A major advantage of the multi-body approach is its capability to simulate, in an efficient way, spatial motions of mechanical systems with complex kinematic connections as present in the human body and in parts of the vehicle structure [88]. The advantage of the FE method is the capability of describing local structural deformations and stresses in a realistic way. However, the creation of a FE model is time-consuming, and the availability of realistic material data is limited, particularly in the case of biological tissue response. Furthermore, relatively large amounts of computer time are required to perform a FE crash simulation, making the method less attractive for complex optimization studies involving many design parameters.

2.9.2 Frontal impact testing

2.9.2.1 Forward/rearward facing CRS configuration

A multi-body dynamic model was developed by Emam [111] for a rearward and forward facing 3-year-old child dummy. Numerical simulation was completed for the 3-year-old P3 dummy in a four-point convertible child safety seat using MADYMO. Numerical simulations were conducted using a moderate acceleration pulse acquired from the National Transportation Biomechanics Research Centre database with a closing speed of 41 kph. This study indicated that the upper neck forces and the neck injury criteria can be greatly reduced by keeping the child in the rearward facing position.

Figure 46 exhibits the numerical set-up for both the forward and rearward facing CRS configurations.

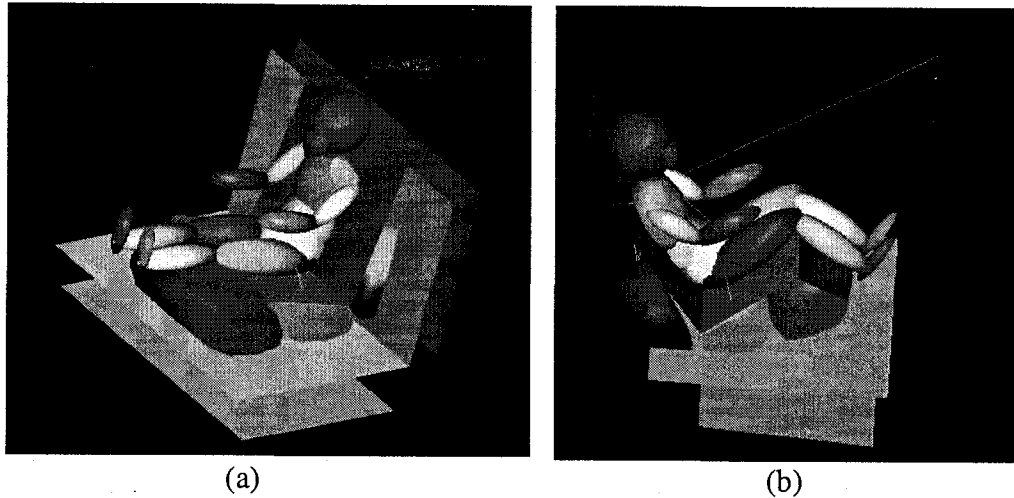


Figure 46. 3-year-old TNO P3 child dummy restrained in a four point safety seat in (a) forward facing, and (b) rearward facing configuration [111].

The FE model developed by Turchi [100 and 101] was used to investigate the head and neck injury potential of toddlers in forward and rearward facing child restraint seats in frontal collisions. Experimental sled tests were completed (Section 2.8.2.2) following the guidelines outlined in the FMVSS 213 using a Hybrid III 3-year-old dummy in a convertible forward/rearward facing child restraint seat. The seat was equipped with a five point child safety belt and the experimental test was completed in the forward facing configuration. The finite element model of the child safety seat only had the pertinent surfaces of the CRS which might have contact with the dummy. The numerical model was validated through a comparison of the head and chest accelerations to the experimental findings. Through an analysis of injury criteria, using neck loads and head accelerations, it was also observed that the rearward facing child dummy sustained significantly lower levels of neck injury criteria while exhibiting similar levels of the head injury criteria as the forward facing child dummy. Figure 47 illustrates the FE model containing the Hybrid III dummy in the CRS.

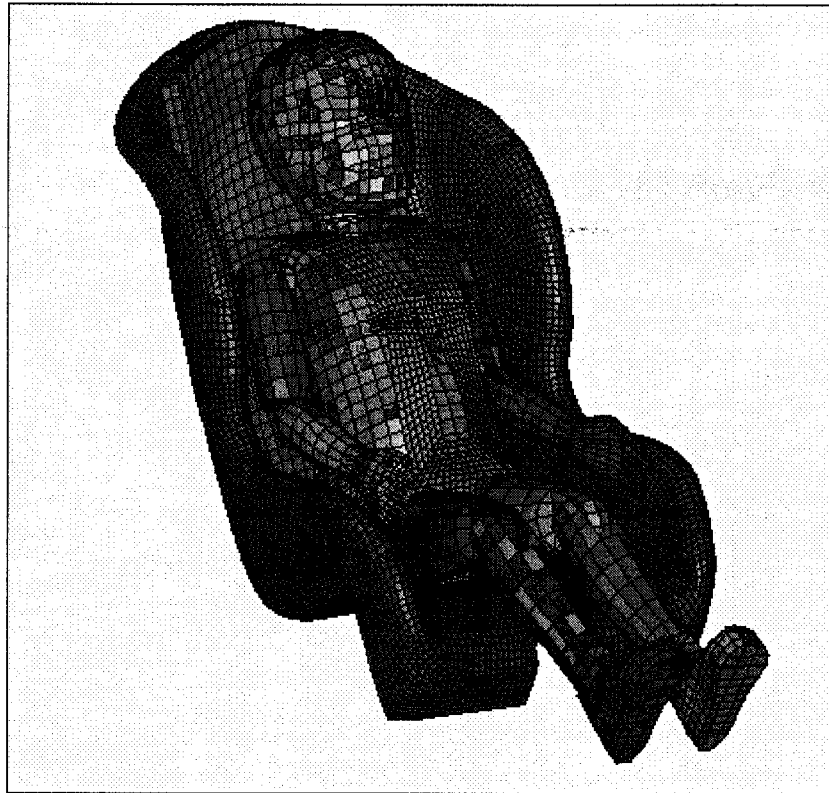


Figure 47. Hybrid III 3-year-old dummy model restrained in a five-point restraint in forward facing CRS configuration [101].

2.9.2.2 Finite element model of a 3-year-old child

The 3-year-old child numerical model presented by Mizuno et al. [112 - 114] was developed to investigate injuries to various body regions of a child and to provide information that can be difficult to obtain from crash test dummies. This FE child model was developed from the AM50 Total Human Model for Safety (THUMS) model by using the model-based scaling method. Responses of this child FE model were also compared to the response-based scaling corridor of a 3-year-old. The mass of the 3-year-old child model is 16.6 kg and the stature height is approximately 99.5 cm. The dimensions of each body region were based upon the anthropometry data of children from the United States and material properties of child bone were defined based on available data. The response-based corridors and impact tests on the Hybrid III 3-year-old child dummy were used to validate the impact responses of the neck, thorax, torso and abdomen of the 3-year-old child FE model which is presented in Figure 48. The model is comprised of

65,947 nodes and 102,661 elements. The skull and the brain were modeled using a rigid material definition, which was only available based upon the current phase of the model development.

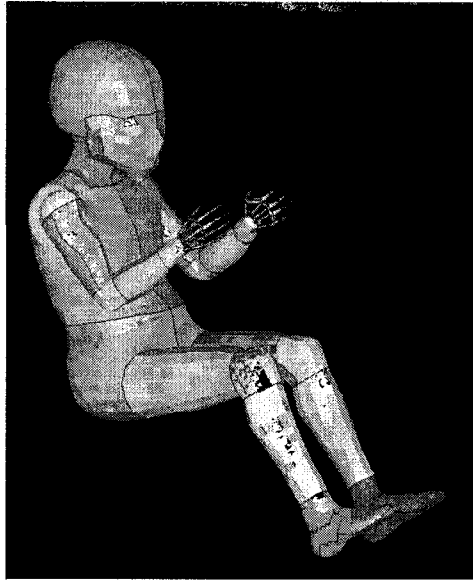


Figure 48. Finite element model of a 3-year-old child [113].

Using this child FE model and Hybrid III FE model, the ECE R44 sled impact test simulations were conducted for three different types of CRS such as a 5-point harness, an impact shield and an ISOFIX CRS [114]. In experimental testing methods a five-point harness child restraint system was utilized [113]. The characteristics of the child FE model were observed to be comparable to the Hybrid III child dummy. The downward displacement of the head and the head rotation were found to be greater for the child model compared to the Hybrid III child dummy. Flexion of the entire segment of the spine was observed for the child FE model while limited rotation of the back was observed for the Hybrid III child dummy as a result of the stiff thoracic spine. Only significant flexion for the cervical spine was observed for the Hybrid III 3-year-old dummy. In the impact shield CRS, the chest deflection was large. The head excursion was particularly small for the ISOFIX CRS. It was concluded that the child FE model could be a useful tool to examine the behaviour of a child in impact, which may be difficult to predict by using the Hybrid III dummy with its stiff thoracic spine region.

Figure 49 illustrates the kinematic comparison between the Hybrid III 3-year-old dummy and the FE child model in a five-point restraining system.

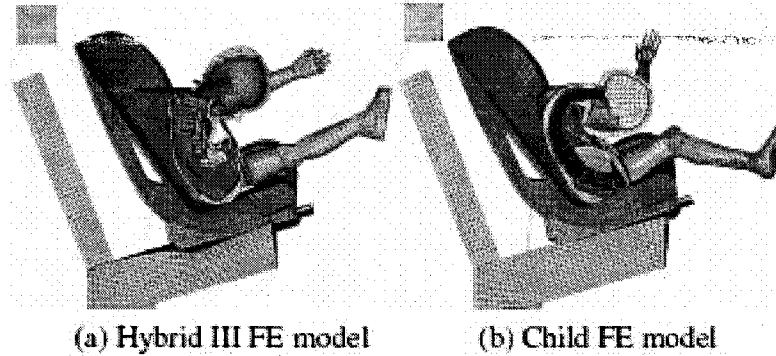


Figure 49. Child occupant kinematics in five-point harness CRS [114].

Zhang et al [115] carried out a comparison between the kinematics of the child FE model and a HYRID III 3-year-old child dummy under a simulated CMVSS 208 frontal crash. A full frontal vehicle crash test was completed in accordance with CMVSS 208 norms, which is detailed in Chapter 4. Both the child models were positioned in a fully deformable CRS model. The development of the deformable numerical model of the CRS will be discussed in Chapter 5. Through a quantitative analysis of the head accelerations, it was observed that the 3-year-old child FE model experienced greater magnitudes of head accelerations in the local x -direction as compared to the Hybrid III 3-year-old child dummy. In addition, the child model exhibited an increased flexibility of the neck and a greater degree of deformation in the thorax. Figure 50 illustrates the sectional comparison of the behaviour of the head, neck and thorax of the Hybrid III 3-year-old dummy and the 3-year-old child FE model at different intervals of time. The child model exhibited an 18 percent greater magnitude of head rotation about the y -axis compared to the Hybrid III child dummy. By comparing the head trajectories of the two FE models with an experimentally completed crash test using a child cadaver (Section 2.8.2.1) it was observed that the child model is more capable of predicting the kinematics believed to be experienced by a child body.

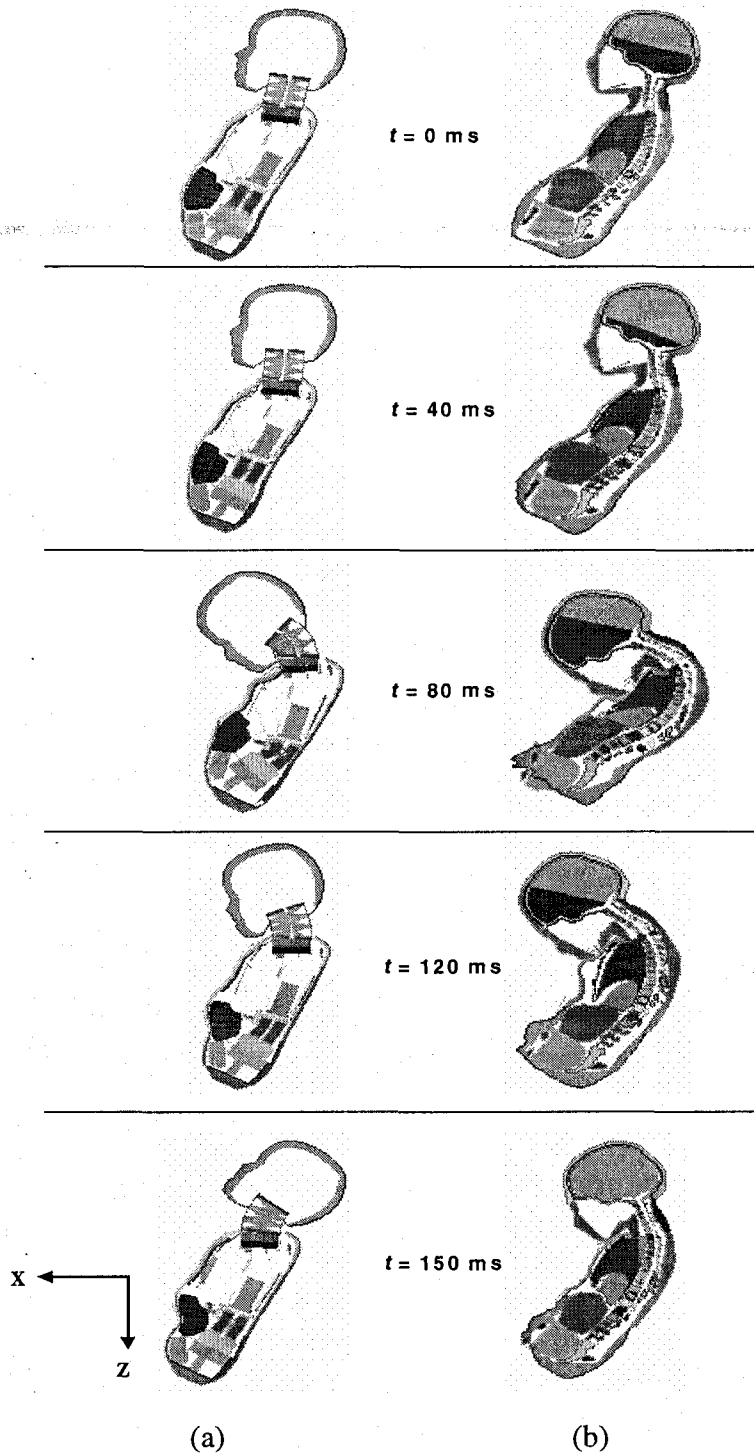


Figure 50. Sectional comparison of the behaviour of the head, neck and thorax of the (a) Hybrid III 3-year-old dummy and the (b) 3-year-old child FE model at different intervals of time [115].

2.9.3 Side impact testing

2.9.3.1 Side impact multi-body simulations

The effectiveness of child restraint systems has been very well proven in the case of a frontal collision, but the performance of the protective devices in a side impact situation have not been clearly demonstrated. Surcel et al. [116] developed a numerical method to simulate the behaviour of a child passenger restrained in a protective device in the case of a vehicle side impact, considering vehicle body deformation.

The side wings of the child restraint system and the vehicle body were modeled by the FE technique, to allow for better representation of the contacts and to allow for simulation of the vehicle body deformation. To reduce the costs and analysis time, the model was mainly based on a multi-body method, which allows the use of already validated dummy models from the MADYMO library and makes possible the comparison with other simulations created with the same software. To simulate the side impact, both a lateral acceleration field and the gravity field were applied to the child dummy and to the CRS. The lateral acceleration field, which had an impact velocity of 33.8 kph with a peak acceleration of 26 g's, complied with the side NCAP specifications. The vehicle model of a 1999 Pontiac Grand Am was chosen for the simulation. This model was validated against similar test data from NHTSA. The simulation results were generally very close to experimental data but differences could be observed for some injury criteria, probably caused by a slightly different child dummy initial position or some differences between real tested belt and belt model characteristics or both. Specifically, head injury criteria and thorax acceleration obtained through the simulation were higher than the reference values but thorax deflection and neck forces were less than the related reference values. Figure 51 shows the model set-up used for this study.

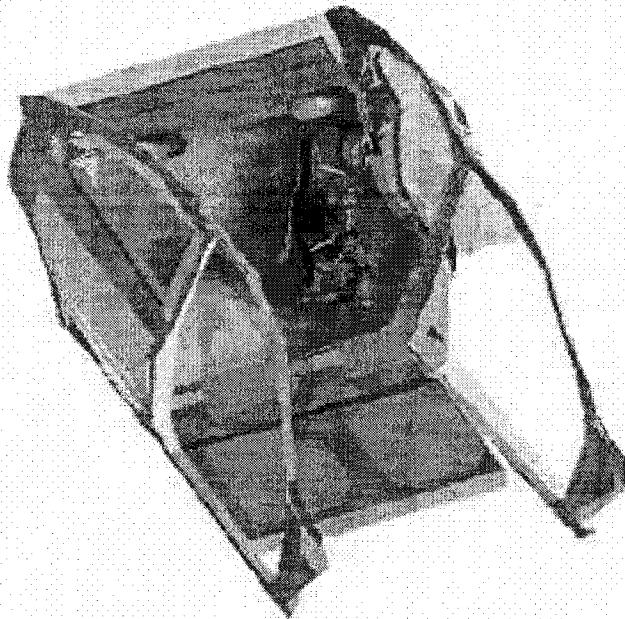


Figure 51. Child restraint system and vehicle body model with intrusion [116].

2.9.3.2 Countermeasure development for far-side impact situations

Wang [117] investigated the injury potential of children seated in forward facing child safety seats during side impact crashes in a far side seated position. Side impact dynamic sled tests were conducted by TRC using two Hybrid III 3-year-old child dummies in convertible forward/rearward child safety seats [118]. The seats were equipped with a LATCH system and a top tether, and the dummies were positioned in a forward-facing/far-side configuration. The tests were completed using an acceleration pulse with a closing speed of 32.8 kph, and the seat fixture with vehicle body oriented at 270 degrees relative to the motion of the sled. A fully deformable CRS model, detailed in Chapter 5, employing a similar set-up as the experimental sled test was generated and simulated using LS DYNA. The simulation results were observed to be in good agreement to the experimental observations. Further studies were conducted to confine lateral movement of the dummy's head by adding energy absorbing foam on the side wings in the vicinity of the contact region of the CRS. It was observed from the simulation results that the addition of foam padding and foam blocks was effective in reducing the head injury criteria of the Hybrid III 3-year-old dummy by approximately

30 percent; and the upper neck lateral shear and lateral bending by approximately 45 percent.

3. FOCUS OF RESEARCH

The literature shows that motor vehicle crashes are the leading cause of death for children under the age of 14 years in North America. Anatomical, physiological and developmental differences between children and adults place children at an increased risk of head and neck injury as compared to adults. The disproportionate size of the child's head relative to the rest of the body increases the relative moment of inertia per unit of acceleration for children as compared to adults. This, in combination with the under developed musculoskeletal paediatric cervical spine put children at an increased risk for cervical injuries in MVC's. The literature also indicates that seating position relative to the point of impact is one of the major factors in side impact crash fatalities. The main cause of injuries during a side impact is contact between the child and the vehicle interior, and between the child and intruding vehicle surfaces. The severity of the injury is correlated to the relative velocity between the child occupant and the vehicle structure.

Extensive experimental work has been completed by various researchers for frontal impacts utilizing state-of-the-art child dummies. The research on child safety in side impacts is very limited because of the uncertainties in many areas. These areas include crash characteristics associated with serious and fatal injuries to children in child restraints and the child injury mechanisms in side impacts, development of test procedures, and a suitable instrumented side impact dummy and appropriate injury criteria. A very small number of numerical models have been developed to investigate the injury potential for children in frontal and side impact tests. More specifically, none of the CRS finite element models in the literature incorporated the nonlinear material properties of all components of a CRS. Furthermore, no models developed were applicable to both frontal and side impact (both near side and far side) events. The deformability of the child restraint is especially significant in side impacts. Finally, there is a lack of research dealing with countermeasures for the child restraint system in frontal and near-side impacts at present.

This research utilizes experimental and numerical methods with a focus to reduce injuries, specifically in the head and neck region, sustained by children seated in a forward facing child restraint system during a vehicle crash.

Based on the various limitations pertaining to child safety observed from the literature, this research focuses on the following areas:

- (i) To develop a completely deformable child seat model to simulate frontal and side crash events. The deformable child seat model will represent an improvement over the previous simplified rigid model developed by Turchi [100 and 101]. Experimental sled testing has been completed by Turchi [100 and 101] in accordance with FMVSS 213 norms. Experimental near-side impact sled testing has been completed by NHTSA [105] incorporating a Hybrid III 3-year-old dummy. In addition, a full vehicle crash test will be completed in accordance to CMVSS 208 crash testing standards. The data obtained from the experimental tests will be utilized for the numerical model validation in both frontal and side impact situations.
- (ii) To investigate the head and neck injury potential of the Hybrid III 3-year-old dummy in both frontal and side impacts. The Hybrid III 3-year-old dummy is applicable to FMVSS 213 and FMVSS 208 norms. In addition, a prototype of Q3/Q3s child dummies and a numerical model of a 3-year-old child will also be investigated. The kinematic response of all the child dummies and the child FE model in a simulated crash will be examined.
- (iii) To develop countermeasures for child restraint systems in both frontal and side impact situations in order to attenuate head and neck injuries. These countermeasures are as follows:
 - a. The amount of head excursion observed in the experimental testing completed by Turchi [100 and 101] was observed to be less than the recommended value by NHTSA. Therefore implementation of load limiting behaviour into the

upper tether and lower LATCH anchors of the CRS will be investigated in order to reduce the injuries by increasing forward head excursion.

- b. The torso of the child is constrained using the seatbelt but the head is free to move. Therefore in a frontal crash severe flexion of the neck occurs due to inertial loading. A head and neck restraining device will be modeled which would limit the forward movement of the head of the child away from the torso.
- c. Literature illustrates the limitations of using a flexible LATCH in case of a side-impact situation. Use of the rigid ISOFIX system outlined in UNECE [83] will be investigated in near-side impacts. The current rigid ISOFIX system limits the lateral movement of the CRS compared to the flexible LATCH. A design modification in the ISOFIX system will be considered to further limit the lateral displacement of the CRS.
- d. The major cause of injury in a near-side impact is due to contact with the vehicle interiors. Use of energy absorbing foam blocks on the side wings of the CRS, in the vicinity of the child's head will be examined in order to reduce the lateral displacement of the head.

These countermeasures will be developed based on experimental and numerical investigations. Experimental sled testing has been completed in accordance with FMVSS 213 norms. In addition, a full frontal vehicle crash test will be conducted in accordance with the CMVSS 208 standards. A fully deformable FE model of the CRS will be developed incorporating the material non-linearities. Standardized testing will be performed to obtain the material properties of the CRS polypropylene, child seatbelt webbing, and polymeric foams. Numerical simulations in both frontal and side impact configurations will be conducted incorporating a Hybrid III 3-year-old dummy using LS-DYNA for the purpose of model validation. In addition, a compressive test of the CRS will also be completed as well as numerically simulated for further model validation purposes.

4. EXPERIMENTAL TESTING

Experimental testing and numerical methods were utilized in this research to investigate the injury potential of 3-year-old children in frontal and side impact situations. This Chapter outlines different experimental methods applicable to this research.

4.1 Sled testing: FMVSS 213

Sled testing was completed by Turchi [100 and 101] at Graco Corporation's sled testing facilities in accordance with FMVSS 213 and has been described in Section 2.8.2.2. It incorporated a Hybrid III 3-year-old dummy, seated in a forward facing CRS configuration, and anchored with the LATCH system and a top tether. Sled impact testing was completed at a speed of 11.6 m/s and the magnitude of the acceleration pulse which the sled experienced in a direction opposite to the impact velocity is illustrated in Figure 33. The acceleration pulse obtained from the sled test was utilized for numerical simulations. The dummy was equipped with tri-axial accelerometers in the head and chest that acquired acceleration data. These results were utilized for the purpose of model validation (Chapter 6).

4.2 Sled testing: ANPRM 213 (Test No. 4585)

Side impact testing has been done by NHTSA in accordance with ANPRM (FMVSS 213) [105] and is detailed in section 2.8.3.2. An acceleration pulse with a closing speed of 24.1 kph was used in the tests and is illustrated in Figure 37. The test incorporated a Hybrid III 3-year-old child dummy restrained in a forward facing child safety seat, and anchored with the LATCH system and a top tether. The dummy was equipped with accelerometers in the head and the chest, and load cells were located in the dummy's upper and lower neck region. Data obtained from the instrumentation was used for numerical model validation presented in Chapter 6.

4.3 Full vehicle crash test: CMVSS 208

Experimental testing was completed with two Hybrid III 3-year-old dummies seated in a forward facing CRS configuration in accordance with CMVSS 208 norms. The experimental data obtained from these tests was used to validate the numerical models. The details of the experimental testing are as follows:

4.3.1 Experimental set-up

The experimental vehicle crash test was carried out by Transport Canada at PMG Technologies vehicle crash testing and research centre in Quebec. A full width, rigid barrier, frontal crash test was completed in accordance to CMVSS 208 [119]. The vehicle used for the crash test was a 2004 Mitsubishi Lancer, four-door sedan having a test mass of 1532 kg. Three accelerometers were mounted to the vehicle, the first one was positioned at the centre of gravity of the vehicle and the other two were fixed at the base of the left and right B-Pillars respectively. Two Hybrid III 3-year-old dummies were used for the experimental crash test. Both of the child dummies were seated inside the vehicle on a convertible forward/rearward facing CRS, acquired from Graco Corporation. For the crash test, both of the CRS were configured for the forward facing orientation and the child dummies were restrained using a five-point restraint system. The first child dummy, labeled P1, was seated behind the driver and was secured to the car seat using the seat lap belt. The second child dummy, labeled P2, was seated behind the passenger and was attached to the car seat using the LATCH system. In both of the configurations a top tether was used as it provides better protection by limiting the child seat's motion in a severe crash. High-speed digital cameras were fastened to the right side and the centre of the CRS in the vehicle and photographs were acquired at a rate of 1000 frames per second. The frontal and side view of the CRS positioning in the vehicle is as illustrated in Figure 52 (a) and (b). Shoulder seat belt loads were acquired by positioning two deflection transducers on the seat belt of the two dummies. The crash test was completed at an impact velocity of 54 kph, in accordance with CMVSS 208 and the magnitude of

the acceleration pulse, as measured by the three accelerometers mounted in the vehicle was as depicted in Figure 53.

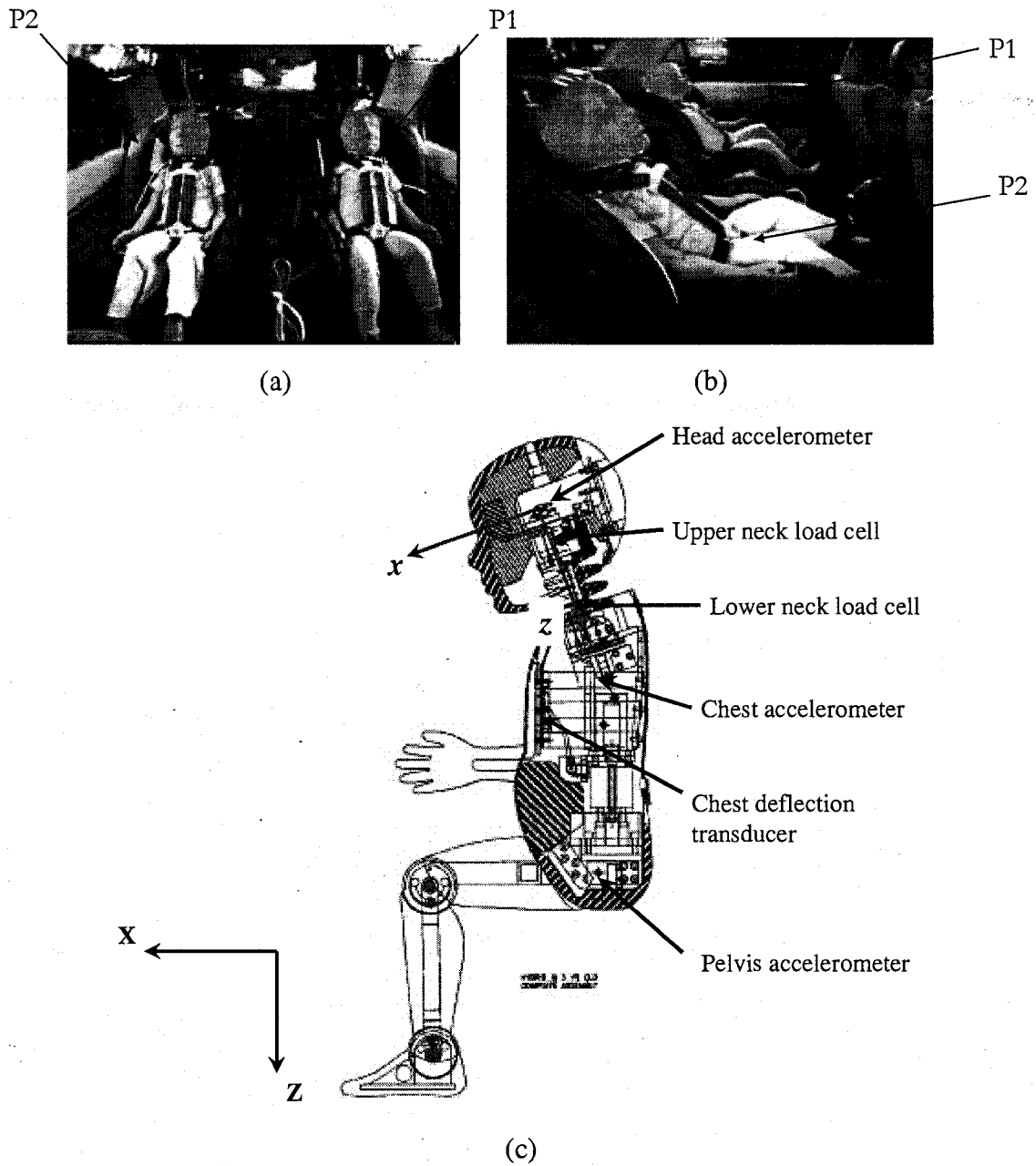


Figure 52. (a) Front and (b) side view of the two Hybrid III 3-year-old child dummies restrained in the five-point restrained child seat in the vehicle, and (c) location of different instrumentation in a Hybrid III 3-year-old dummy.

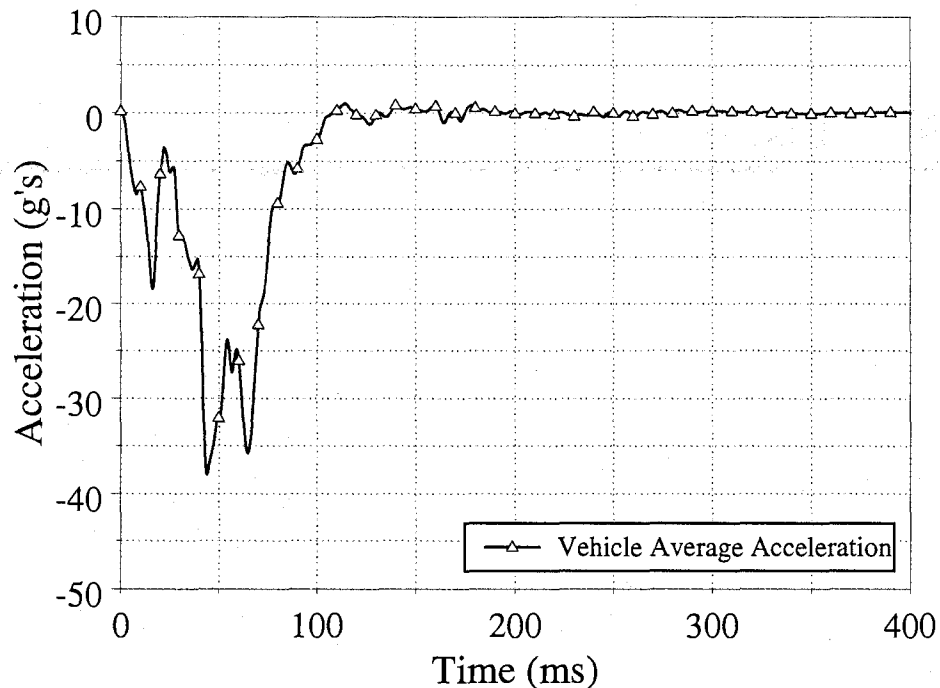


Figure 53. Average vehicle acceleration in local x -direction.

4.3.2 Extraction of data

The dummies were equipped with three tri-axial accelerometers sited in the head and the spinal region and three uni-axial accelerometers in the chest and the sternum. The instrumentation provided in the 3-year-old Hybrid III crash test dummy is tabulated in Table 3. These accelerometers were set-up in such a way that they acquired data in the local x , y and z coordinate systems for the head, chest, upper and lower sternum, and the upper and lower spinal region. The coordinate systems follow the convention outlined in SAE J211 [120]. The accelerometers were rated for a capacity of 2000 g's. In addition to these accelerometers, the dummy contained two multi-axial load cells within the neck and two bi-axial load cells within the shoulders. The load cells in the upper and lower neck region allowed data acquisition through six data channels to measure forces and moments in the local x , y and z directions. The load cells positioned in the left and the right shoulder were used to measure loads in the local x and z coordinate system. A potentiometer was also positioned in the sternum to measure the chest deflection.

Figure 52 (c) illustrates the location of different instrumentation in the Hybrid III 3-year-old dummy [32].

Table 3. Instrumentation provided in 3-year-old Hybrid III child dummies and the SAE-J211 filters used

Type of Instrument	Location	Parameters Measured	Number of data Channels	Direction	Units	Filter
Accelerometer	Head	Head Acceleration	3	Local x, y and z	g	1000
Accelerometer	Upper Spine	Spine Acceleration	3	Local x, y and z	g	180
Accelerometer	Lower Spine	Spine Acceleration	3	Local x, y and z	g	180
Accelerometer	Upper Sternum	Sternum Acceleration	1	Local x	g	1000
Accelerometer	Lower Sternum	Sternum Acceleration	1	Local x	g	1000
Accelerometer	Lower Chest	Chest Acceleration	1	Local x	g	180
Load Cell	Upper Neck	Upper Neck Forces	3	Local x, y and z	N	1000
Load Cell	Upper Neck	Upper Neck Moments	3	Local x, y and z	N-m	600
Load Cell	Lower Neck	Lower Neck Forces	3	Local x, y and z	N	1000
Load Cell	Lower Neck	Lower Neck Moments	3	Local x, y and z	N-m	600
Load Cell	Left Shoulder	Shoulder Forces	2	Local x and z	N	1000
Load Cell	Right Shoulder	Shoulder Forces	2	Local x and z	N	1000
Deflection Transducer	Sternum	Chest Deflection	1	Local x	mm	600

All the data was measured with respect to the dummy's local coordinate system as previously indicated and was sampled at rate of 10 kHz. Figure 52 (c) also illustrates the global and the local coordinate system in the dummy's head for a Hybrid III 3-year-old dummy. The experimental results were filtered in accordance to SAE J211 [120]. Table 3 also summarizes the channel frequency class used during the filtering process for each measurement. Filtering was conducting using a Butterworth 4-pole phase less filter as described in reference [120]. Data filtering was completed prior to any data analysis. Details of the numerical algorithms used to incorporate these filters are shown in Appendix C.

4.3.3 Data analysis/injury parameters

The resultant head and spinal accelerations were computed using equation 2 where the x, y and z-axes are the local coordinate system located at the head and spine locations respectively. The resultant neck forces and moments were computed using

equation 4 and equation 5 respectively where the x , y , and z -axes are the local coordinate systems located at each neck location.

$$a_{\text{resultant}} = \sqrt{a_x^2 + a_y^2 + a_z^2} \quad (2) - \text{repeated}$$

$$F_{\text{resultant}} = \sqrt{F_x^2 + F_y^2 + F_z^2} \quad (4)$$

$$M_{\text{resultant}} = \sqrt{M_x^2 + M_y^2 + M_z^2} \quad (5)$$

4.3.3.1 Head injury criteria

The resultant head acceleration (Equation 2) was used in calculating HIC using the Equation 1. Here the resultant acceleration is expressed as a multiple of the local acceleration due to gravity (g units) calculated at the centre of gravity of the dummy's head and the time is measured in seconds. The HIC was analyzed using both 15 ms and 36 ms time intervals. Appendix C shows the algorithm used to calculate HIC as a function of time.

$$HIC_{t_2-t_1} = \left[\frac{1}{t_2 - t_1} \int_{t_1}^{t_2} a_{\text{resultant}} \cdot dt \right]^{2.5} \cdot (t_2 - t_1) \quad (1) - \text{repeated}$$

4.3.3.2 Neck injury criteria

The Neck Injury Criteria (N_{ij}) was determined using Equation 3. The current FMVSS 208 includes injury criteria of individual tolerance limits for tension and shear of the neck in the local z -axis direction and for the extension and the flexion moment of the neck about the local y -axis. A critical value of 2120 N was used for F_{ZC} in both tension and compression and 68 N·m and 27 N·m in flexion and extension respectively in order to determine the N_{ij} [73]. Appendix C shows the algorithm used to calculate N_{ij} as a function of time. N_{ij} should be evaluated from data acquired from the upper neck load cell [73].

$$N_{ij} = \left(\frac{F_z}{F_{ZC}} \right) + \left(\frac{M_y}{M_{YC}} \right) \quad (3) - \text{repeated}$$

4.3.3.3 Protection reference values

The Hybrid III child PRV's, developed by DeSantis-Klinich et al. [32] using existing observations from various child dummy tests are tabulated in Table 1. These outline limiting values for the various injury parameters and thus provide a method of assessing the level of injury incurred during a crash. These have been described in details in Section 2.4.3.

4.3.3.4 Injury risk analysis

Prasad and Mertz have proposed probability curves that help assess the severity of injury to an occupant during a frontal vehicle crash [73]. The injury risk curves obtained from the test dummy in the crash demonstrate the probability of injury to a real person in that crash. Appendix B provides the injury risk curves used to calculate the probability of head, neck and chest injuries incurred to a 3-year-old dummy.

4.3.4 Experimental observations

Data comparison was carried out for the experimental dummy results in terms of head and chest accelerations, and neck forces and moments in order to investigate the effect of using universal anchorages on the injury potential of children.

4.3.4.1 Qualitative comparison

Figure 54 provides the side and the front view of the two child dummies in the vehicle crash at different time durations. This provides a visual comparison of the behaviour of the two dummies during the crash. At $t = 0$ ms, the vehicle was just about to collide with the rigid barrier. The two dummies were seated in the CRS, anchored to the vehicle seat. At $t = 60$ ms, the dummies started moving forward due to the vehicle crashing into the rigid barrier. At this time, it can be seen that the top tethers started stretching; hence a motion was imparted to the child seat. After this instant, extension of

the hands and legs of both the Hybrid III child dummies was observed. At $t = 90$ ms, the limbs appeared to be in similar position for P1 and P2, and a high degree of neck extension was also seen. The maximum neck extension was observed at $t = 127$ ms, after which the dummies started settling back into their respective CRS. It is apparent that the neck of the P2 dummy, seated behind the passenger seat, extended slightly more than P1. This difference is clearly visible at $t = 160$ ms, where P1 seems to be settling back quicker than P2. This could be because the CRS of the P1 dummy was fixed to the vehicle seat with the car seat belt which is stiff, bearing more loads and thus limiting the motion of the CRS. The lower anchorages of the LATCH system are meant to limit the CRS pitch rotation. Since a top tether is used with both of the configurations, it provides a rigid attachment at the top part of the restraint. This reduces the head excursion of the child, and hence reduces the chances of injury [14].

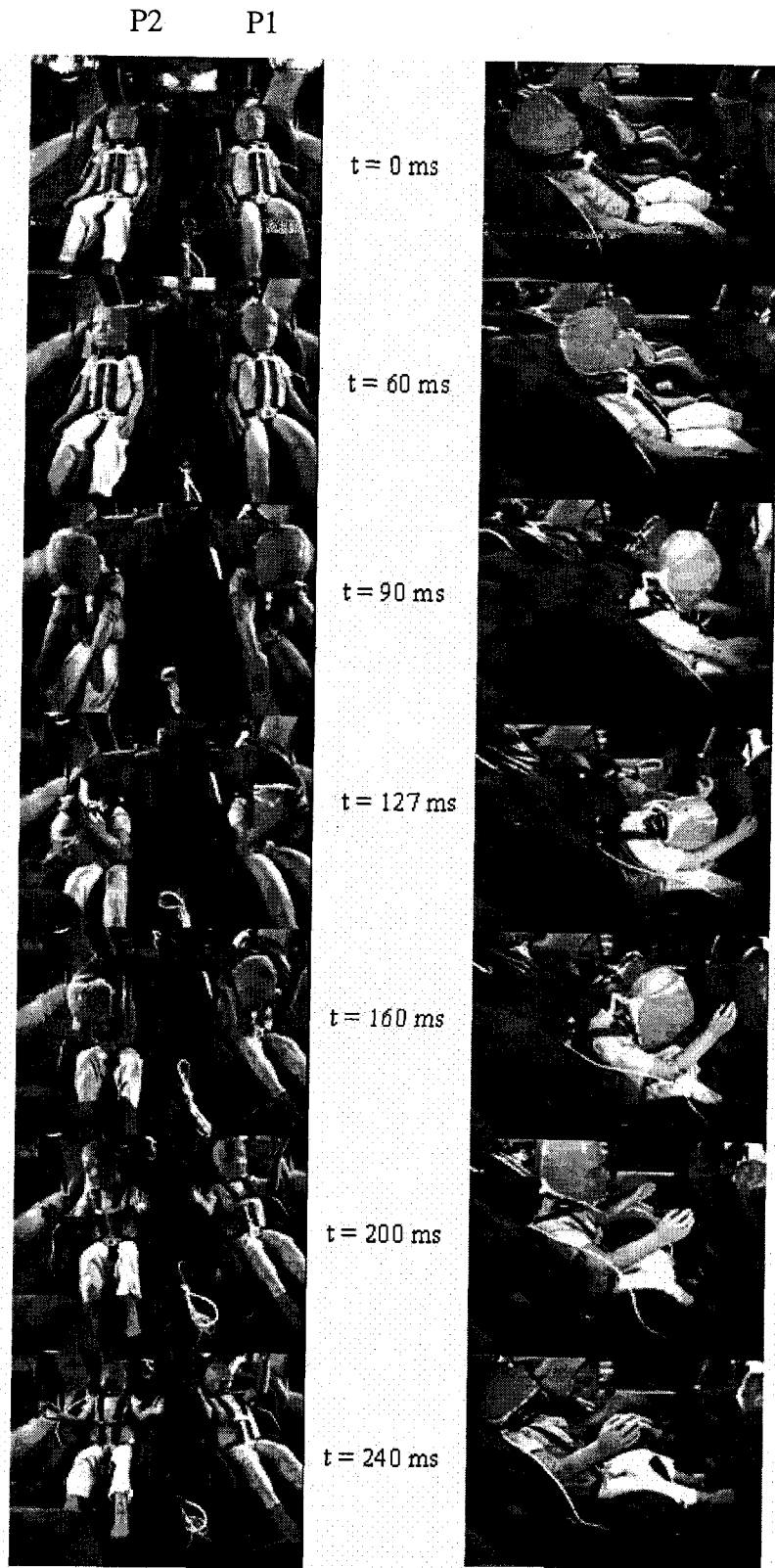


Figure 54. Experimental observations (frontal and side view) at different time intervals.

4.3.4.2 Quantitative comparison

4.3.4.2.1 Head accelerations

Figure 55 illustrates the values of the local x -component of the head acceleration for the two dummies as a function of time. Similar acceleration profiles were observed for both the Hybrid III child dummies. The minimum local x -axis head acceleration for the P1 child dummy and the P2 child dummy were -43 g's and -50 g's respectively. The time required to reach the minimum local x -axis head acceleration for the P1 and P2 child dummies were 113 ms and 110 ms respectively. This is the time when the head experienced the greatest extension as shown in Figure 54. The duration of these peaks was observed to be less than 3 ms and they were followed by an upward ramp to values of -14 g's at 127 ms. The maximum values for local x -axis head acceleration for P1 and P2 were 23.4 g's and 20.4 g's that occurring at 230 ms and 262 ms respectively.

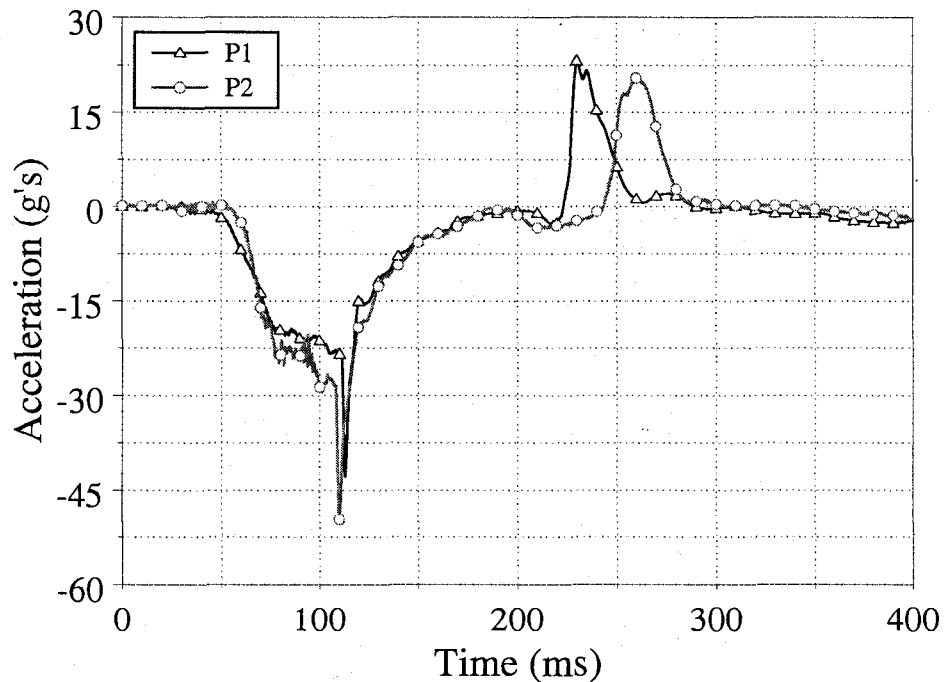


Figure 55. Experimental head acceleration in local x -axis direction as a function of time.

The values of the local z -component of head acceleration for P1 and P2 as a function of time are illustrated in Figure 56. The time profiles illustrate similarities for the local z -axis head acceleration, though they exhibit differences in the peak values. The maximum values for the local z -axis head acceleration for the P1 child dummy and the P2 child dummy were observed to be 47 g's and 56 g's respectively. These peak values for the z -axis head acceleration occurred at 90 ms and 92 ms respectively for both the dummies due to severe bending of the neck. These peaks were followed by a downward ramp to 7.47 g's (at 116 ms) for P1 and 10.57 g's (at 115.6 ms) for P2 respectively.

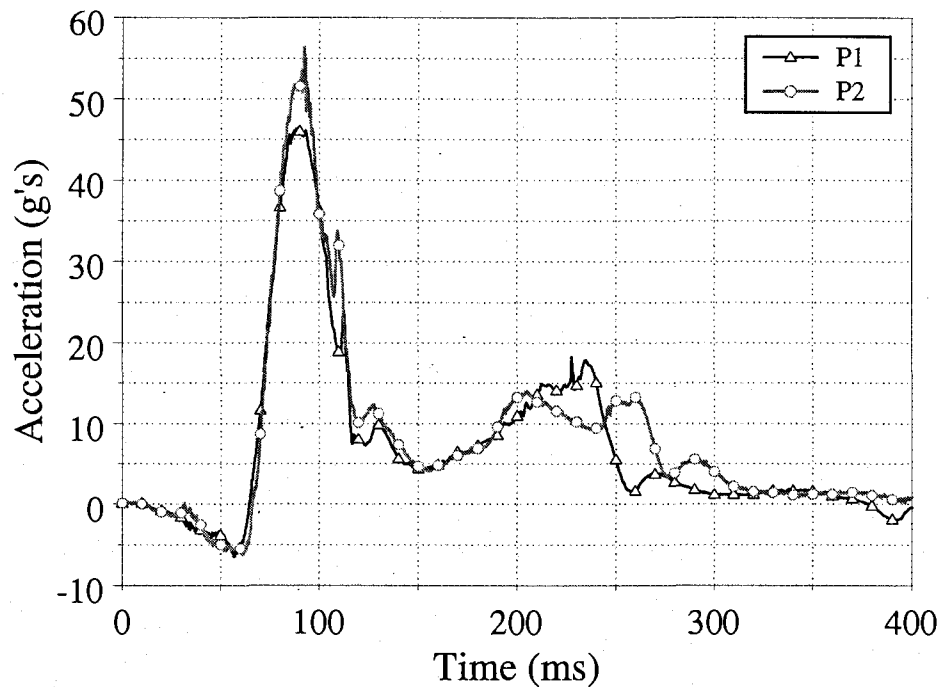


Figure 56. Experimental head acceleration in local z -axis direction as a function of time.

4.3.4.2.2 Chest accelerations and deflection

Figure 57 illustrates the local x -component of the chest acceleration for the P1 and P2 child dummies as a function of time. The two profiles were very similar with the minimum x -axis chest acceleration being approximately 40 g's. The minimum x -axis chest acceleration for the P1 and P2 child dummies occurred at 77 ms and 90 ms respectively. The recommended critical value for a 3-year-old Hybrid III child dummy

chest acceleration is 55 g's [73] which exceed the observed chest acceleration values. These peaks were followed by an ascent and reached 3.83 g's (at 103 ms) for the P1 child dummy and 13.2 g's (at 108 ms) for P2.

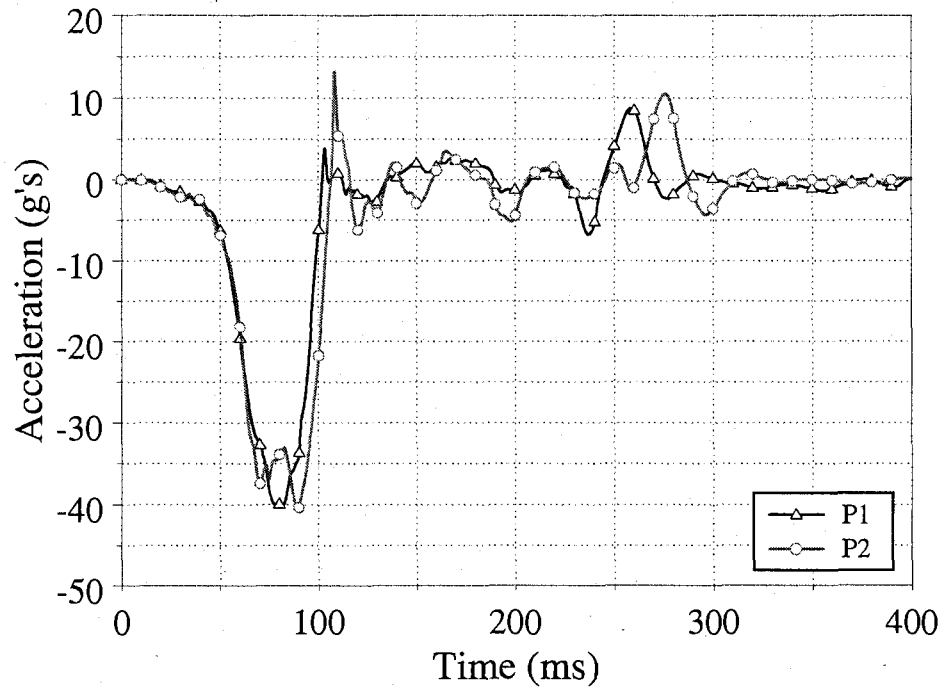


Figure 57. Experimental chest acceleration in local x -axis direction as a function of time.

The chest deflection for the two child dummies is illustrated in Figure 58 as a function of time. Both of the dummies exhibited comparable chest deflection profiles with a different maximum values. The peak values for the chest deflection were observed to be 14.5 mm for P1 and 17.5 mm for the P2 Hybrid III child dummy. The maximum chest deflection occurred at 116 ms due to the maximum extension of the seat belt. Both of the chest deflection values did not exceed the critical value of 35 mm, recommended for a 3-year-old Hybrid III child dummy [73].

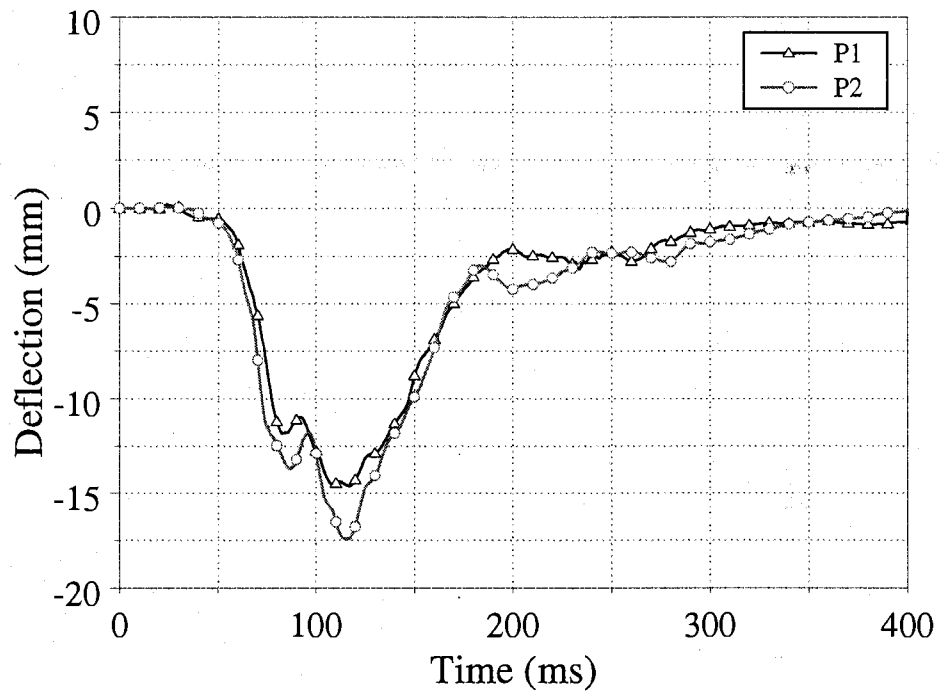


Figure 58. Experimental chest deflection in local x -axis direction as a function of time.

4.3.4.2.3 Seatbelt loads

Figure 59 presents loads sustained by the CRS seat belts of P1 and P2 child dummies. The load profiles are similar to each other with a maximum load of 1795 N (at $t = 84$ ms) and 1760 N (at $t = 90$ ms) sustained by P1 and P2 CRS seat belts respectively. This is the time at which the dummies experienced the maximum chest accelerations. The seatbelt load profiles indicate that irrespective of the type of anchorage device used, the loading of the CRS tethers is consistent.

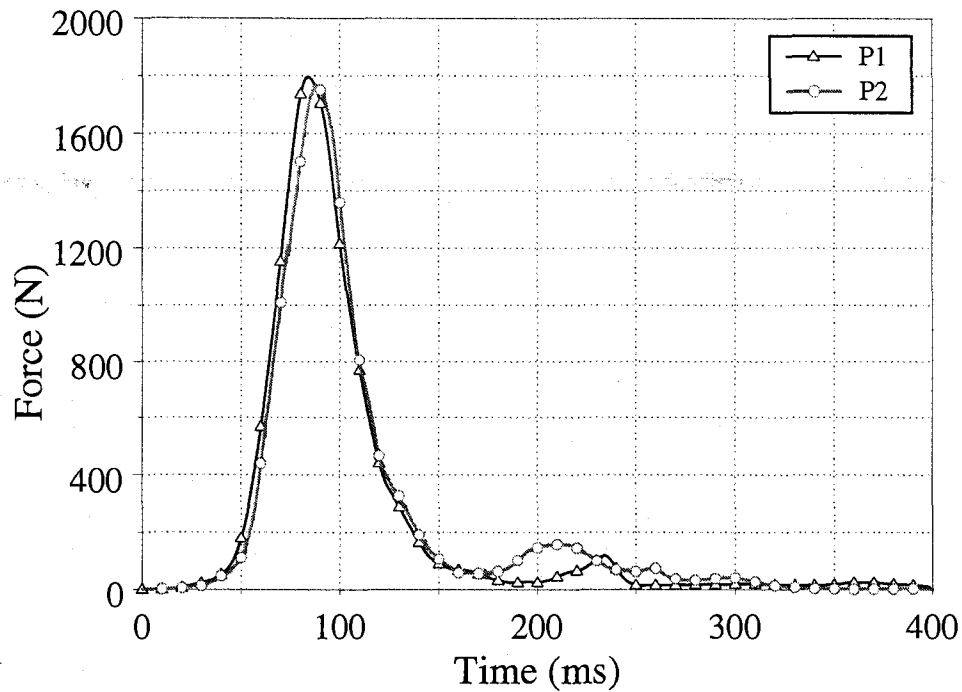


Figure 59. Experimental seatbelt loads as a function of time.

4.3.4.2.4 Resultant upper and lower neck forces

Figure 60 and 61 demonstrate the resultant upper and lower neck forces as function of time for the P1 and P2 child dummies respectively. The maximum values for the resultant lower neck forces vary between 920 N for the dummy using the seat belt and 1020 N for the dummy using LATCH as the anchorage device. Similar maximum values for the resultant upper neck forces (approximately 1680 N) were observed for both the dummies in the forward facing configuration. It should be noted that these high forces are sustained by the dummy's neck for approximately 40 to 50 ms.

4.3.4.2.5 Resultant upper and lower neck moments

Resultant upper and lower neck moments are presented in Figure 62 and 63 respectively. Both of the dummies exhibited similar time profiles with differences in the peak values. From the upper neck load cell a peak value of approximately 16 N·m was

observed for the P1 child dummy and approximately 9 N·m for the P2 child dummy. In comparison, much higher values were observed for the resultant lower neck moments. This difference is due to considerable extension of the neck during the crash. The peak values ranged from 95 N·m for the P1 dummy to 122 N·m for the P2 child dummy.

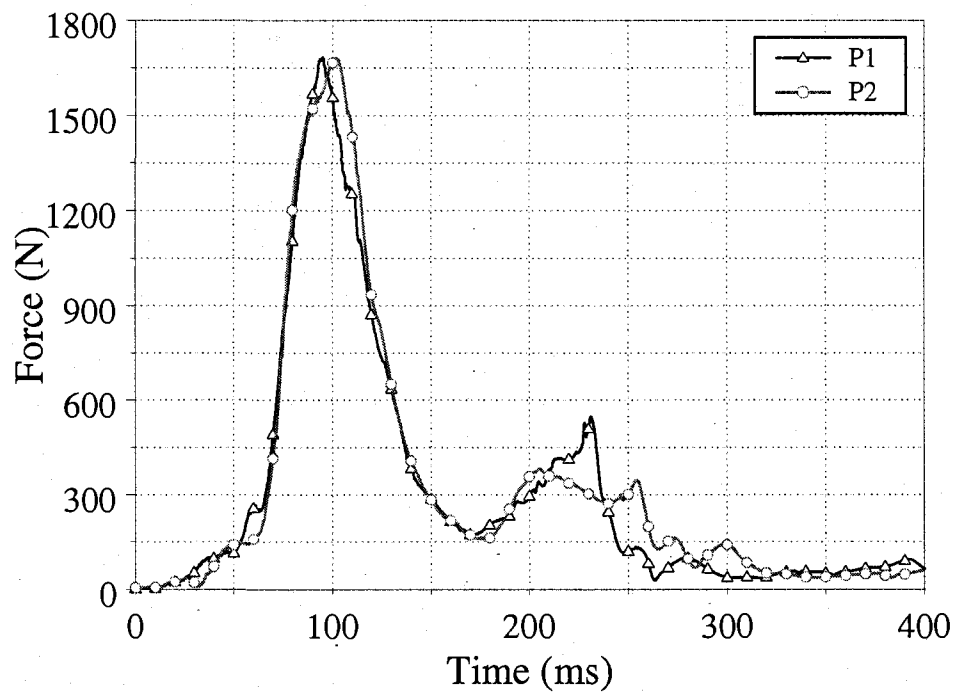


Figure 60. Experimental upper neck resultant force as a function of time.

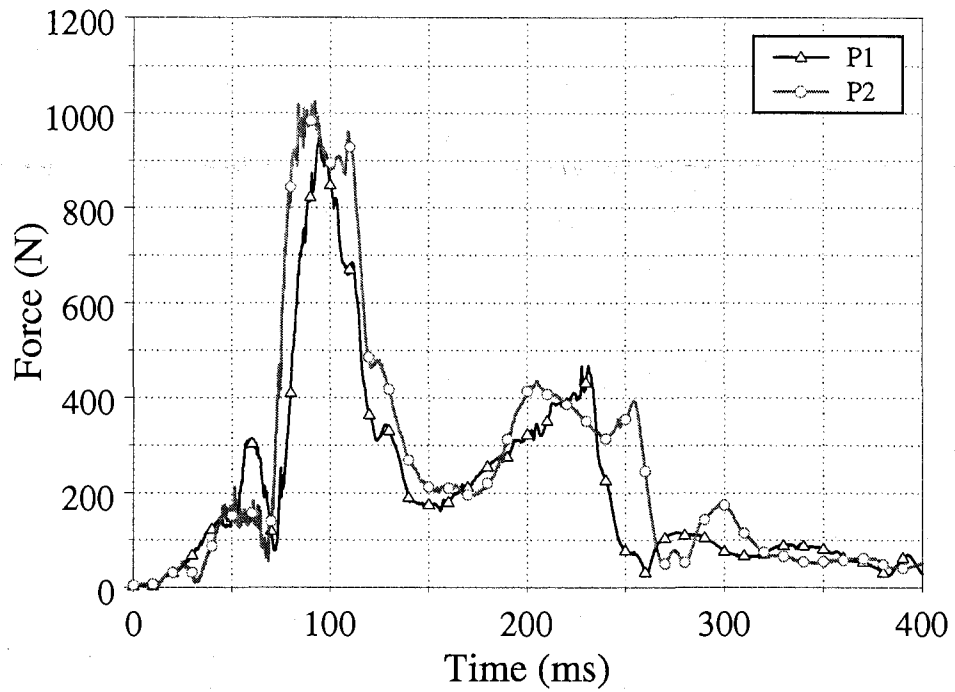


Figure 61. Experimental lower neck resultant force as a function of time.

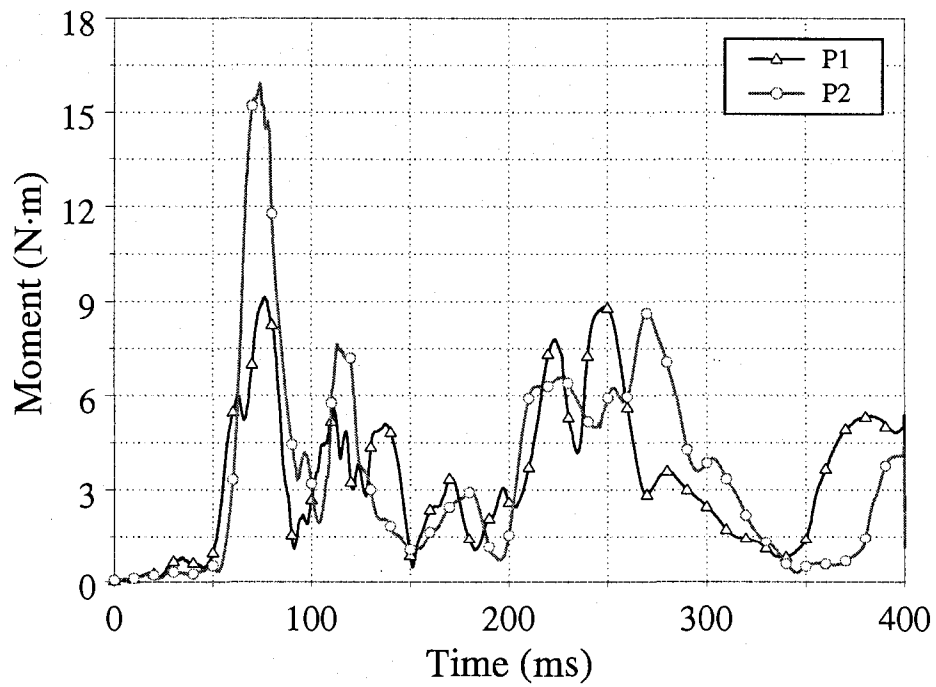


Figure 62. Experimental upper neck resultant moment as a function of time.

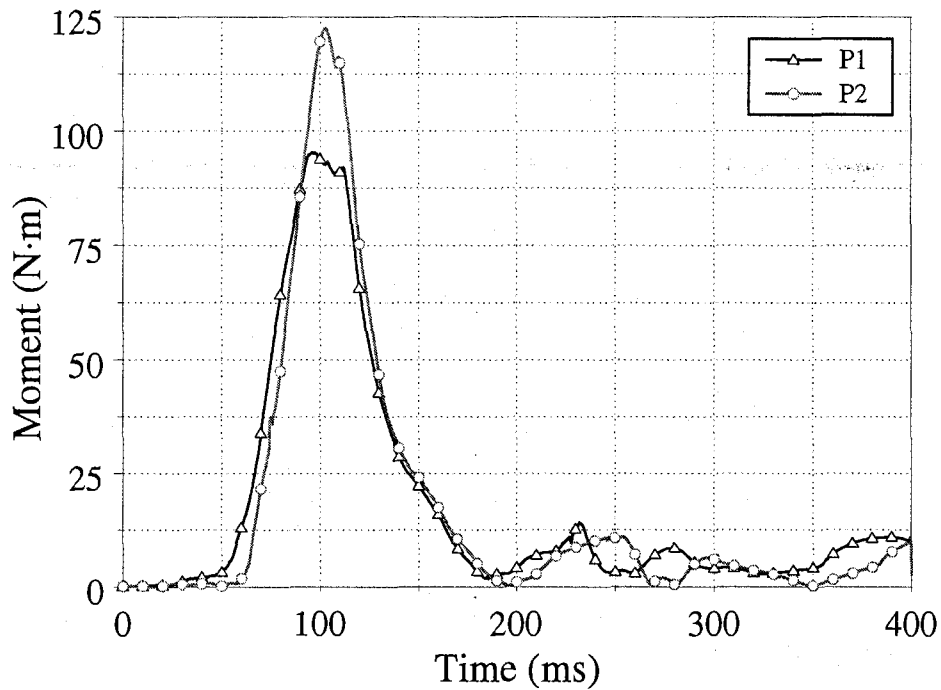


Figure 63. Experimental lower neck resultant moment as a function of time.

4.3.4.2.6 Head injury criteria

HIC was calculated over a 15 ms and 36 ms evaluation period for both P1 and P2 in the forward facing configuration of the CRS during the frontal vehicle crash. Figure 64 illustrates the values of HIC_{36} which are presented as these values were greater than HIC_{15} . The peak values of HIC_{15} for P1 and P2 were observed to be 255 and 337 respectively. Likewise, maximum values for HIC_{36} were 450 for P1 and 615 for the P2 child dummy. The limiting values recommended for HIC_{15} and HIC_{36} by NHTSA are 570 and 1000 respectively [73], and the *HIC* values for both of the dummies were considerably lower than these limiting values.

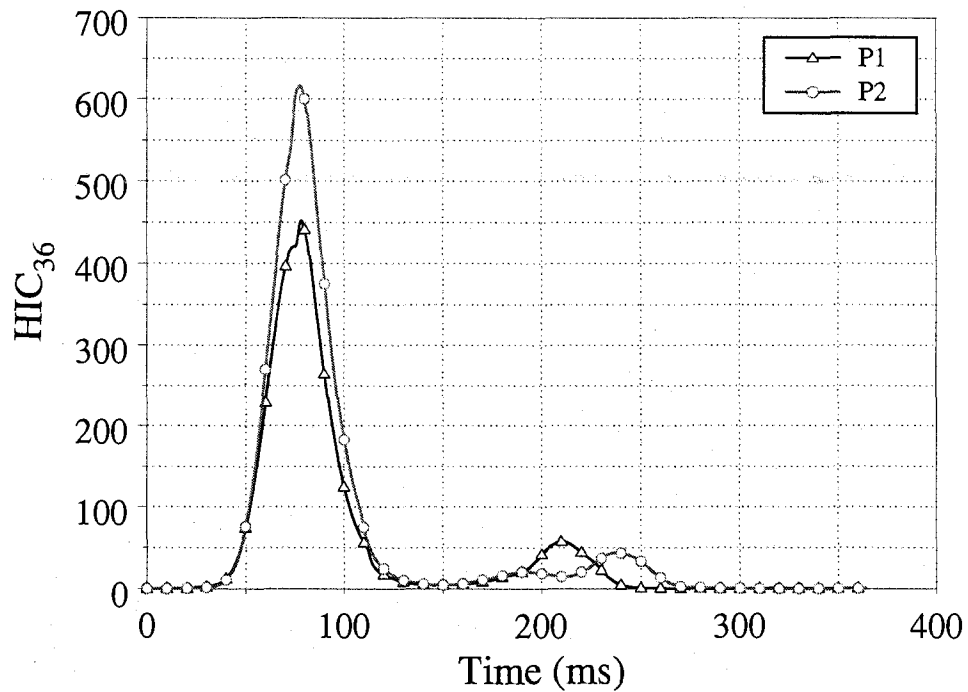


Figure 64. Experimental HIC_{36} as a function of time.

4.3.4.2.7 Neck injury criteria

Figure 65 presents the N_{ij} as a function of time for the 3-year-old child dummies with the CRS anchored to the vehicle seat with car seat belt and with LATCH respectively. Figure 65 illustrates the N_{ij} computed from the values obtained from the upper neck load cell. Maximum values for the seat belt anchorage and the ISOFIX configurations were observed to be 0.8 and 1 respectively.

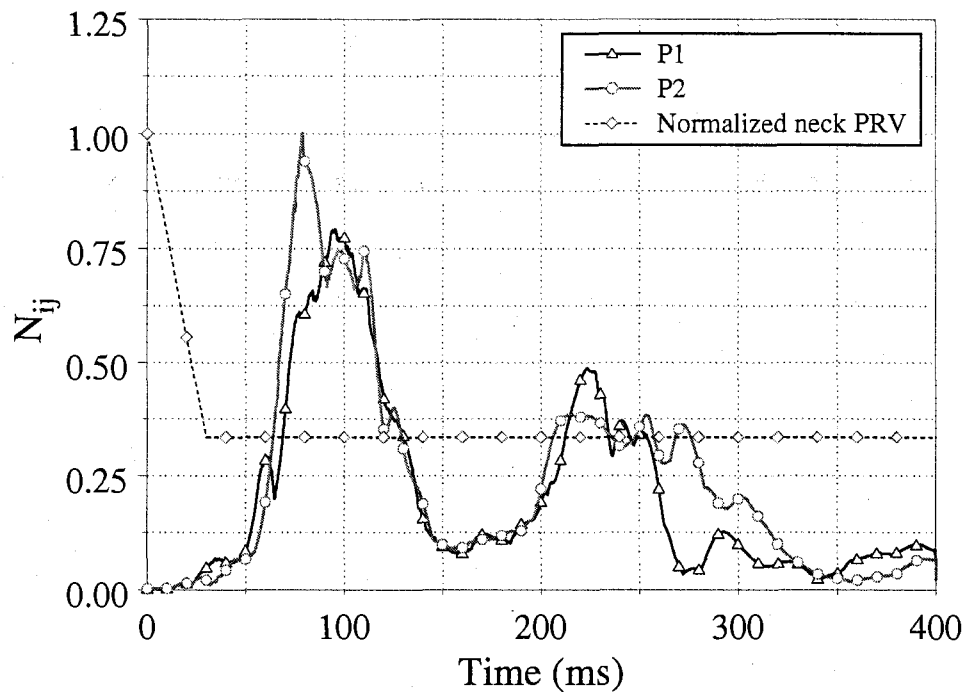


Figure 65. Experimental N_{ij} as a function of time.

4.3.4.3 Discussion

4.3.4.3.1 Injury risk analysis

Table 4 summarizes the probability of severe head, neck and chest injuries to the two dummies. These values have been evaluated using Prasad and Mertz injury risk probability curves (Appendix B) for the maximum values of HIC , N_{ij} , and chest accelerations. There is a high risk of sustaining severe chest injuries for both the child dummies. There is a moderate risk of severe neck injuries for both the dummies and severe head injuries for P2 dummy. Whereas, there is a low risk of sustaining severe head injuries for P1 dummy. The injury severity has been defined by the author as low risk for AIS 3+ probability of 0 to 15 percent, moderate risk for 15 to 30 percent and high risk for a probability of sustaining injury above 30 percent.

Table 4. Probability of severe injuries (AIS 3+) to both the dummies using Prasad and Mertz injury risk analysis

Type of Injury	Parameter used	AIS 3+ probability for P1 (%)	AIS 3+ probability for P2 (%)
Head injuries	<i>HIC-15</i>	11.18	19.34
Neck injuries	N_{ij}	16	22
Chest injuries	Chest acceleration	40	40

4.4.3.2 Protection reference values

According to the PRV's the critical value for head acceleration is 80 g's. For both the dummies, the maximum resultant head acceleration is approximately 62 g's, which is less than the critical value. The recommended critical value for chest and spinal acceleration for a 3-year-old Hybrid III child dummy is 60 g's. The maximum values for chest acceleration for both the methods of anchoring the CRS to the vehicle seat varied between 35 g's and 40 g's. Figure 65 also illustrates the PRV for the N_{ij} . It can be seen that both the dummies exhibited neck injury criteria higher than the critical curve, for a long duration of time. This implies that both of the dummies would sustain severe neck injuries.

The qualitative and quantitative analysis indicates that anchoring the CRS to the vehicle seat using a seatbelt is slightly better than using a flexible LATCH system. A greater amount of injury was sustained by the dummy anchored using the flexible LATCH system compared to the dummy anchored using the seat lap belt. Greater head accelerations, chest deflections and neck forces and moments were observed for the P2 dummy compared to the P1 dummy. The two point ISOFIX does not eliminate the CRS rotation because of the presence of upper tethers, which leads to a rotation in the child's upper body part segments. Therefore the P2 dummy was observed to settle down into the CRS later than the P1 dummy. The other reasons for the difference in various injury parameters could be the difference in seatbelt length of both the CRS, or presence of slack in the seatbelt for the P2 dummy. Based on the observations from this work,

mounting of the CRS using flexible LATCH does not provide any significant safety improvements over the use of seat lap belts as an anchorage device in a frontal impact, and in fact may increase the risk of injury.

These experimental findings are consistent with the observations by Belcher et al. Belcher et al. [103] performed a series of frontal impact sled tests incorporating a Hybrid III 3-year-old dummy with different anchoring devices. The experimental tests are detailed in Section 2.8.2.4. In most cases, results obtained for flexible LATCH anchorage indicate a head injury risk approximately equal to or greater than that of 3-point seatbelt mounting. In addition, for each child restraint model tested; flexible lower anchorage and 3-point seatbelt mounting produced similar maximum resultant chest accelerations.

5. NUMERICAL MODEL DEVELOPMENT

The child safety seat, and all other components of the numerical model including the seat buck, the CRS webbing and the CRS foam pad, was meshed using Finite Element Model Builder (FEMB). This Chapter details the modeling of the numerical models involved in this research.

5.1 Simplified rigid model

The CRS model developed by Turchi [100 and 101] incorporated only the relevant surfaces of the CRS that might have contact with the child dummy as it did not incorporate material deformability and was modeled rigid. The seat was equipped with a five point child safety belt. Some of the rearward facing preliminary simulations involved in this research were conducted using a simplified rigid model of the CRS. The following section outlines the basic details of this model.

5.1.1 Modeling of the rigid CRS

The child safety seat was modeled using a rigid material model assuming negligible deformation of the CRS. For the purposes of this research, only the pertinent surfaces of the CRS which may come into contact with the dummy were considered when meshing the seat since it was modeled rigid. The seat belt travels through eight slots which were also incorporated into the FE model. Values for the density, elastic modulus, and Poisson's ratio were 900 kg/m^3 , 1.2 GPa, and 0.3 respectively, which are typical of the polypropylene CRS material. These values are required for various contact algorithms between the seat and the dummy. The mesh of the CRS was comprised of 12002 nodes and 11990 Belytschko-Tsay shell elements, 11500 of which were quadrilateral shaped while 490 were triangular. Belytschko-Tsay shell element is based on combined co-rotational and velocity-strain formulation [121]. The efficiency of the element is obtained from the mathematical simplifications that result from these two

kinematical assumptions. The co-rotational portion of the formulation avoids the complexities of non-linear mechanics by embedding a coordinate system in the element. The choice of velocity strain or rate of deformation, in the formulation facilitates the constitutive evaluation, since the conjugate stress is Cauchy stress. The element size varied from 2.80 mm to 10.60 mm and the largest aspect ratio of the CRS finite element mesh was 2.82. Figure 66 (a) provides an isometric view of the meshed portion of the CRS.

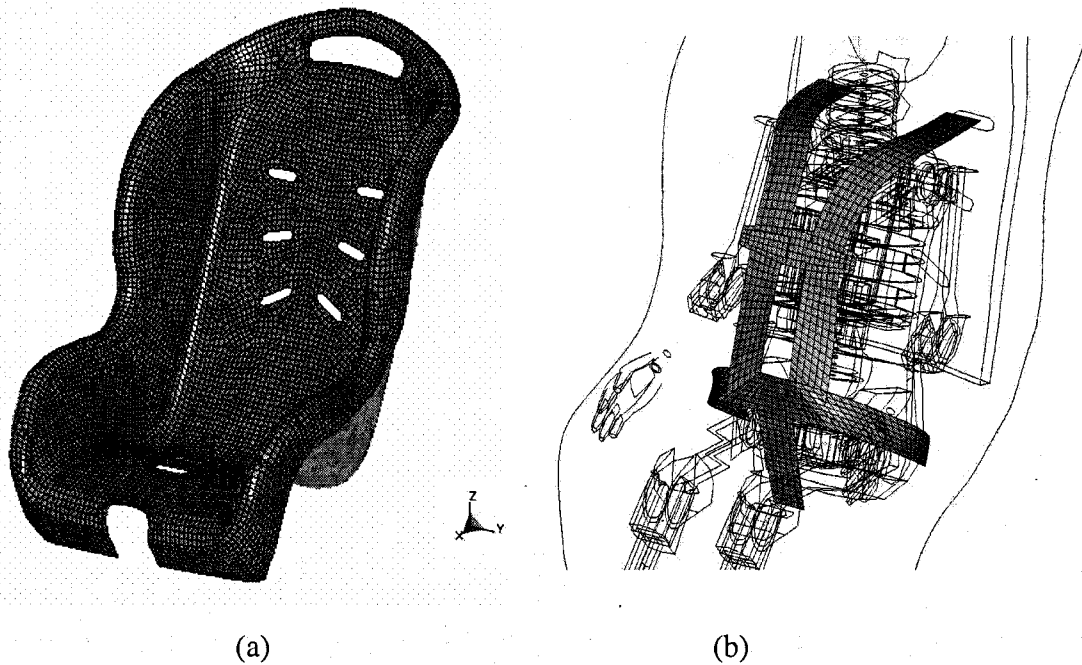


Figure 66. (a) Meshed portion of the simplified rigid CRS model, and (b) numerical model of the seatbelt and clasps for the simplified rigid CRS model.

5.1.2 Modeling of the seatbelt restraints

The seat belt was modeled to fit around the Hybrid III 3-year-old dummy. Figure 66 (b) illustrates the meshed region of the five point restraint seat belt with the torso and waist clasps. A fabric material model specifically designed for seatbelts was used to simulate the material characteristics of the seat belt webbing. Isotropic material behaviour was assumed and the density, elastic modulus, and Poisson's ratio was specified as 911.8 kg/m^3 , 6.27 GPa , and 0.3 respectively. Values for the density and

elastic modulus were experimentally determined from testing completed on sections of the seat belt webbing from the CRS [100 and 101]. This model invokes a special membrane element formulation that is better suited to the large deformations experienced by fabrics. A fully integrated Belytschko-Tsay membrane element was utilized for all elements of the seat belt. Element edge lengths associated with the seat belt varied from 4.8 mm and 8.9 mm. The top two ends of the seat belt near the shoulders of the child dummy were positioned to fit through the top slots of the CRS. The upper two restraint points of the seat belt within the model terminated at the upper slots. Furthermore, the bottom end of the seat belt, which passed in between the dummy's legs, was positioned to fit through the slot closest to the seat backing and terminated at the lower slot. The two ends of the seat belt that passed beside the hips of the child dummy were positioned such that they followed the contour of the dummy's hip side and terminated rear of the child dummy. Modeling the length of the seat belt only up to the mesh of the CRS was made to simplify the difficulties associated with belt wrap and motion through seat belt slots and passageways of the CRS. The seat belt was meshed as closely as possible to the FE mesh of the child dummy in regions where initial contact existed. No preload within the model of the seat belt webbing was specified. The last two rows of nodes at the end of the five seat belt lengths, which terminated near the CRS, were constrained to follow the prescribed motion of the seat.

The torso clasp was modeled to allow travel of the seat belt through it. This sliding contact between the belt and the clasp was modeled using an automatic surface to surface contact algorithm. Values for the coefficients of static and dynamic friction were 0.3 and 0.2 respectively. The torso clasp was positioned such that the horizontal centre line of the clasp was just below the armpits of the child dummy. Due to the complex contact and wrapping of the seat belt around the waist clasp, the numerical model of this clasp contained merged nodes in between itself and the belt lengths leading into the clasp. This was achieved with an assumption that no travel of the belt occurred through the waist clasp during the impact. Both the waist and torso clasps were modeled using a rigid material definition with density, elastic modulus, and Poisson's ratio identical to the CRS. The mesh density of both clasps was similar to the seat belt.

5.1.3 Modeling of the foam insert

A foam pad, which was inserted in between the polypropylene shell and the seat fabric of the CRS, was also incorporated into the FE model of the CRS. The foam was modeled using a selectively reduced solid element formulation. A highly compressible low-density foam material model was selected to model the material behaviour of the solid elements representing the foam pad. This material model is commonly used to simulate polymeric foams. Density and the stress/strain relationship for the foam were experimentally determined from compressive foam specimens used in automotive seats. Values for the density and elastic modulus of the material were defined as 50.2 kg/m^3 and 5.463 MPa respectively. The stress/strain relationship (for loading only) was also incorporated into the material model for the foam. The details of the material model are presented in Appendix D. This material model was obtained from Turchi et al. [100 and 101] and the mesh of the foam pad is shown in Figure 67.

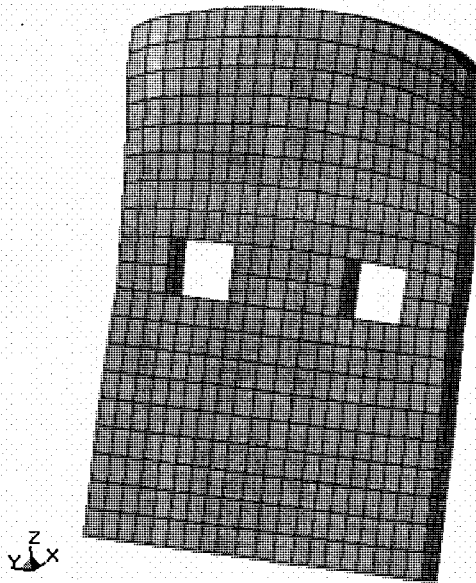


Figure 67. The FE mesh of the foam insert.

5.1.4 Contact definitions

Figure 68 illustrates the complete FE model containing the child dummy, CRS, seat belt webbing, and both the waist and torso clasps. An automatic surface to surface penalty contact algorithm was used to model the contact between the child dummy and the CRS seat. The identical algorithm was used to simulate contact between the child dummy and both the seat belt webbing and clasps. Finally, an automatic surface to surface definition was used to simulate sliding contact in between the child dummy and the foam insert. In this case a nodal-based option was used, however, the penalty scale factors of the slave segments, which contained the segments defined by the foam pad was increased from the default value of unity to one hundred.

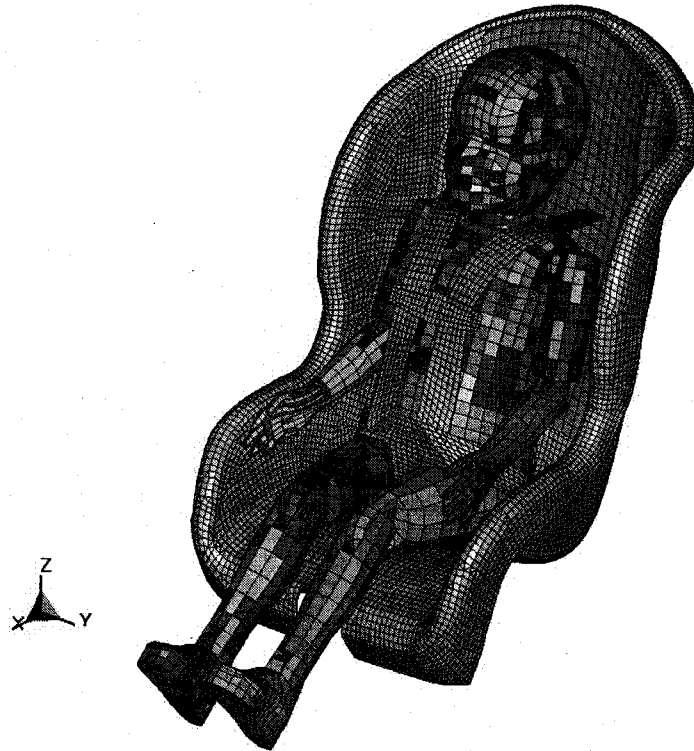


Figure 68. Hybrid III 3-year-old dummy model restrained in the simplified rigid CRS model using a five-point restraint in a forward facing position.

5.2 Deformable CRS model

The simplified CRS model did not incorporate material deformability of the CRS. This model has been successfully validated in frontal impact situations detailed in Chapter 6. In the case of other impact situations such as side impacts that involve the dummy and CRS interactions amongst themselves and with the vehicle interior, this model could not be used. Higher contact forces were observed between the CRS and the child dummy during a simulated side impact using the simplified rigid model. In addition, the simplified rigid model did not incorporate a seat buck to which the CRS could be anchored using a top tether and the LATCH system. The seatbelt webbing had a limited length and therefore the tightening of the harness strap could not be completed. Therefore a more complex model that incorporates complete deformability of the CRS including material non-linearities and contact definitions amongst different components of the CRS was developed. A seat buck was also modeled, and the CRS was anchored to the seat buck using the LATCH system and a top tether. The following sections outline the development of the deformable CRS model.

5.2.1 Modeling of the deformable child seat

The child seat was modeled using Computer Aided Design (CAD) surfaces provided by Century/Graco Corp. To appropriately model the elastic/plastic behaviour of the CRS, tensile testing was completed in accordance with American Society for Testing and Materials (ASTM) D638M [122] on a total of five specimens. These specimens were extracted from side rib regions of the CRS to determine mechanical characteristics of the CRS polypropylene material. The change in length was measured using an extensometer of 25.4 mm gauge length. Figure 69 illustrates the engineering stress versus engineering strain curve obtained for all the five tensile tests. Table 5 tabulates the yield stress and the ultimate tensile stress obtained from the tensile testing of the polypropylene specimens. The tests were stopped after 25 percent of strain and no failure of specimens was observed for all the five tensile tests. Experimental results were observed to be consistent with each other in terms of the stress/strain behaviour.

Changes in the thickness of panel sections from the CRS were investigated and measured with a Vernier caliper. It was observed that the various panel sections had thickness of 3.5 mm and 4.5 mm. Two different section properties were generated for the CRS, both incorporating the Belytschko-Tsay shell elements which were assigned thickness of 3.5 mm and 4.5 mm for both regions of the CRS. Fully integrated shell elements were also used to investigate the influence of different element formulations on mechanical behaviour of the numerical model. No obvious differences were observed from the simulation results, although the use of element formulation number 2 saved considerable CPU time.

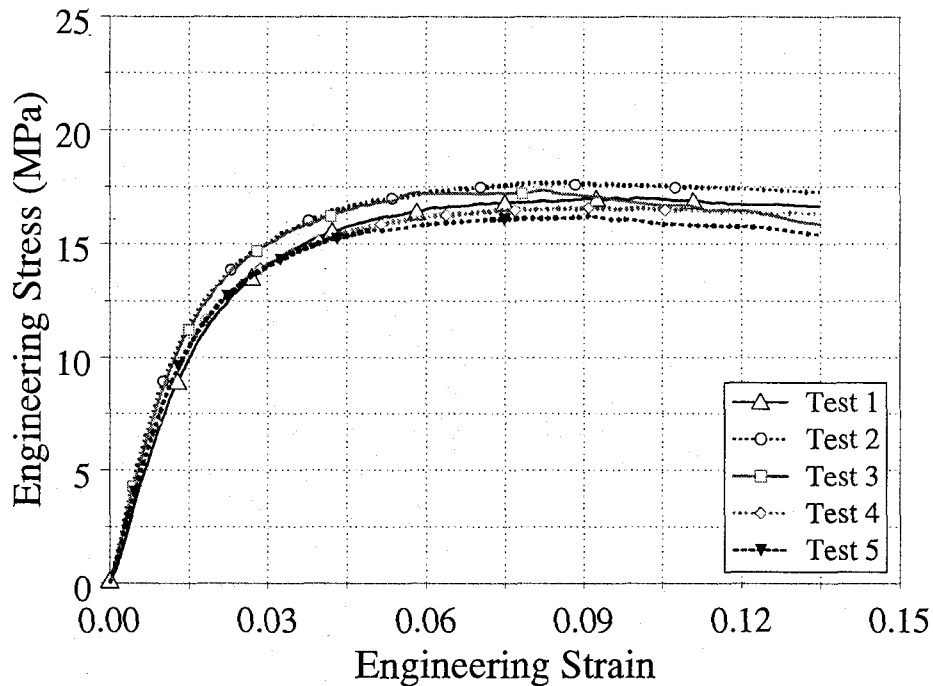


Figure 69. Engineering stress/strain curve for CRS polypropylene tensile tests.

Table 5. Yield stress and ultimate tensile stress for the polypropylene tensile testing.

Test No.	Yield Stress (MPa)	Ultimate Tensile Stress (MPa)
1	9.347	18.8
2	9.02	19.6
3	8.897	17.91
4	8.76	18.7
5	8.577	17.48

An isotropic elastic-plastic material model within LS-DYNA which utilizes the von Mises yield criterion was selected to model the material behaviour of the polypropylene. This material model requires the density, Young's modulus, Poisson's ratio and a stress versus effective plastic strain relation through a series of data points, was used for the CRS polypropylene. Values for the density, Young's modulus, and Poisson's ratio were 800 kg/m^3 , 0.842 GPa , and 0.3 respectively. The yield and ultimate tensile strengths of the CRS polypropylene were found to be 8.76 MPa and 18.7 MPa respectively. As well a stress versus effective plastic strain curve obtained from the tensile testing results and illustrated in Figure 70 was assigned to the CRS material card. The details of the material model are presented in Appendix D. The mesh of the child seat was comprised of 12,728 nodes and 13,379 shell elements, among which 11935 elements were quadrilateral elements and 1444 elements were triangular elements. The final mesh of the deformable child safety seat is illustrated in Figure 71.

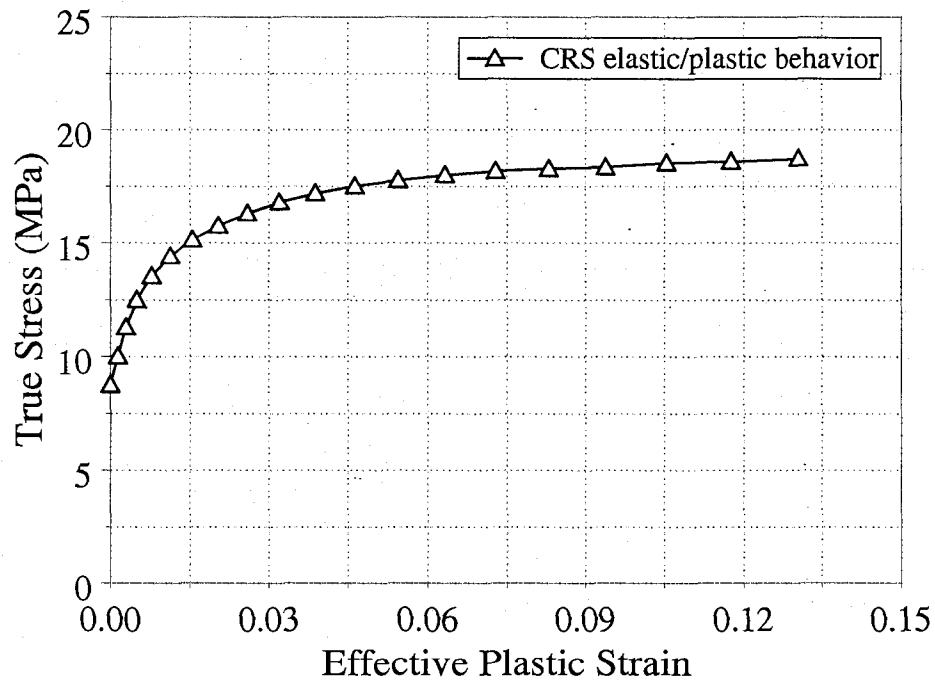
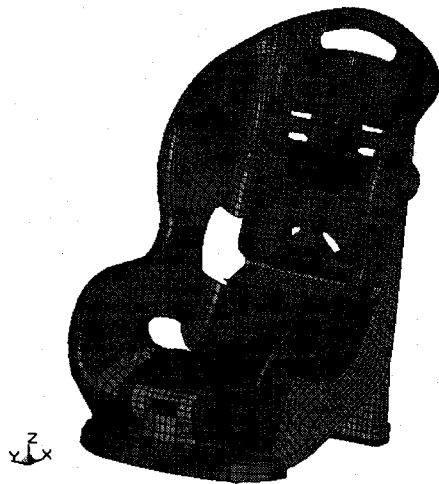


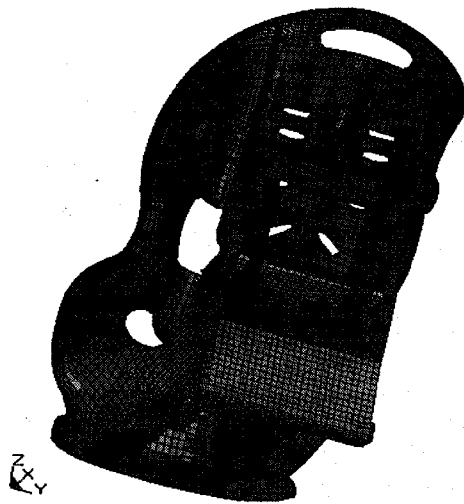
Figure 70. Elastic/Plastic behaviour of the CRS polypropylene.



(a)



(b)



(c)



(d)

Figure 71. Front (a) numerical and (b) actual; Rear (c) numerical and (d) actual view of the deformable Child Restraint System (CRS).

5.2.2 Modeling of the seatbelt restraints

The seatbelt was modeled to pass through a series of openings and channels of the CRS and to fit around the Hybrid III 3-year-old dummy, which had the same configuration as all experimental tests. Figure 72 illustrates the finite element model of the seatbelt, LATCH, top tether, and the five-point restraint system. To reduce the computational time, a portion of the seatbelt which generally contacts the back of the CRS was modeled using one-dimensional seatbelt elements. The seatbelt webbing that came into contact with the dummy was modeled using two-dimensional shell elements. Connectivity to the one-dimensional seatbelt elements and the two-dimensional shell elements, used for modeling contact between the seatbelt and dummy, was completed through the use of nodal rigid bodies. For appropriate modeling of contact between the one-dimensional seatbelt elements and the CRS, an offset of the seatbelt elements equal to half of the shell thickness of the CRS was necessary. The lower ends of the three portions of the seatbelt that passed through the child dummy's crotch and wrapped around the child dummy's legs were connected directly to the child safety seat as in the actual CRS.

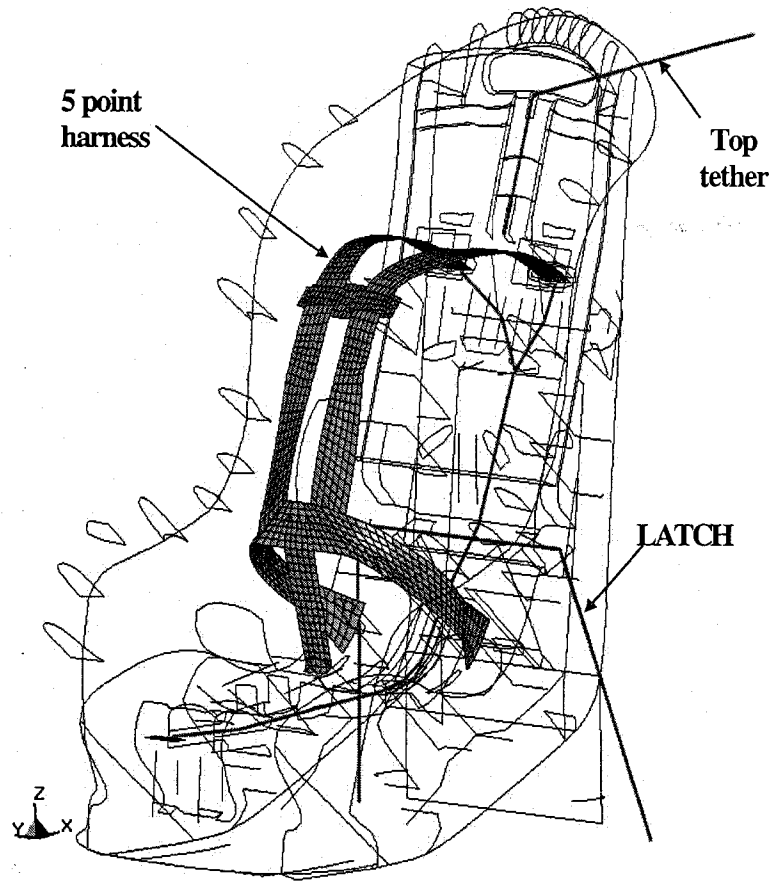


Figure 72. The seatbelt, LATCH, top tether, and the five point restraint system.

To assess the mechanical characteristics of the seatbelt webbing, tensile testing was completed on specimens extracted from the CRS. Testing was completed under a loading/unloading condition in order to obtain information on the behaviour of the seatbelt. These tests were completed on a hydraulic Tinius-Olsen testing machine at room temperature at a nominal crosshead speed of approximately 25 mm/min. Mechanical behaviour of the seatbelt was also obtained from Narricot Industries, a CRS webbing supplier in North America. The experimental results were observed to be consistent with the loading/unloading information obtained from the supplier. The loading/unloading behaviour of the seat belt webbing as extracted from the tensile specimens is illustrated in Figure 73 and was incorporated into the material model for the CRS webbing.

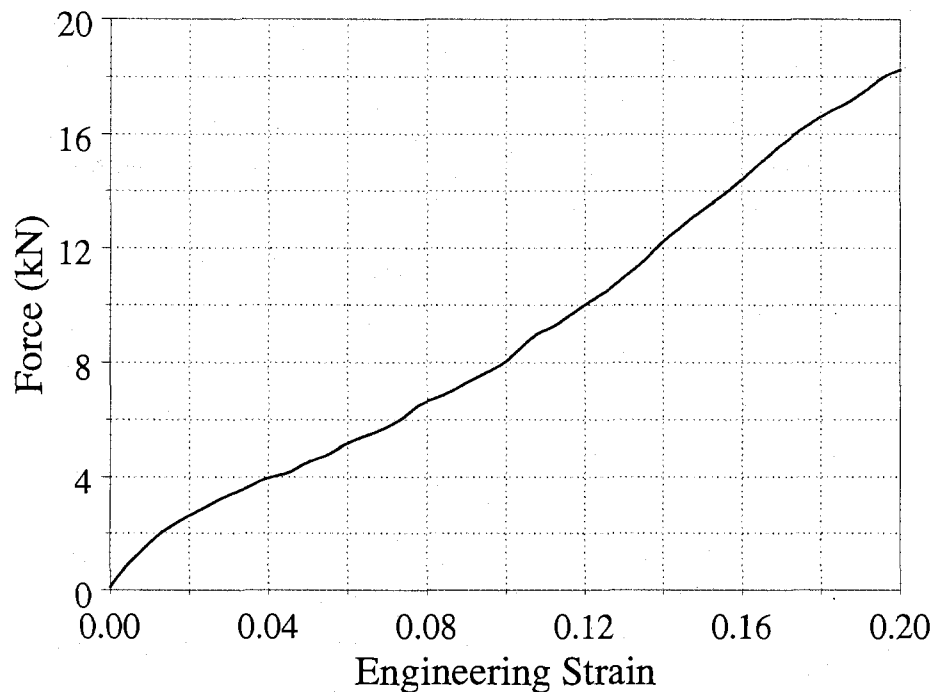


Figure 73. Force versus engineering strain response of the CRS webbing.

A fabric material model was selected to model the material behaviour of the two-dimensional seatbelt finite elements. Isotropic material behaviour was assumed. The density, elastic modulus, and Poisson's ratio was specified as 890.6 kg/m^3 , 2.068 GPa and 0.3 respectively. In addition, a force versus engineering strain relationship for the material was generated from experimental observations and implemented into the material model. For the one-dimensional seatbelt finite elements a material model specifically developed for this element formulation was utilized. The experimental loading/unloading behaviour was incorporated in the material model for the one-dimensional seatbelt elements. A fully integrated Belytschko-Tsay membrane element formulation was utilized for the two-dimensional shell elements of the seatbelt. An element formulation specifically developed for one-dimensional seatbelt elements was used for the top tether, LATCH, and portion of the CRS seatbelt. Appendix D details the material models incorporated for both the two-dimensional and one-dimensional seatbelt elements.

The buckle in front of the dummy's chest was modeled to permit sliding motion of the webbing. The horizontal centre line of the buckle was aligned slightly below the armpits of the child dummy. The buckle at the waist of the dummy was modeled on the assumption that there was no relative movement between the waist buckle and the seatbelt, thus the nodes at the ends of the waist buckle were merged with the nodes in the seatbelt. The material model and element formulation of the buckles were identical to the CRS.

5.2.3 Modeling of the foam insert

A foam pad, which was inserted in between the polypropylene shell and the seat fabric of the CRS, as described in Section 5.1.3 was also incorporated into the FE model of the CRS.

5.2.4 Modeling of the seat buck

Two parts, namely a rigid car seat frame and a deformable seat pad, were created in order to model the vehicle seat. The rigid car seat was modeled using shell elements, and the deformable seat pad was modeled using solid elements. An under-integrated solid element formulation was specified for the solid elements of the seat pad. The identical material model used for modeling the foam pad the CRS was also used for the seat padding. Values for the density, and elastic modulus were specified as 50.2 kg/m^3 , and 5.463 MPa . The hysteretic unloading factor and shape factor required for this material model were specified as 0.1 and 5 respectively. The uniform thickness of the seat pad was specified as 120 mm. A rigid material definition was selected to model the seat frame. The seat foam and frame were connected by constraining the outermost nodes of the seat pad to the frame. The kinematics of only these nodes on the seat pad will be identical to the seat frame.

The seat buck was developed following the FMVSS 213 norms [78]. A node was created defining the point Z in the system. Point Z (Figure 20) defines the location from

where the dummy excursions are measured [82]. The seat buck was meshed with an inclination of 15 degrees to the horizontal and 22 degrees to the vertical axis, in line with the standard 213 seat bench. Figure 74 illustrates the side view of the deformable CRS model including a Hybrid III 3-year-old dummy exhibiting the location of the point Z in the model as well as the inclination angles of the seat buck.

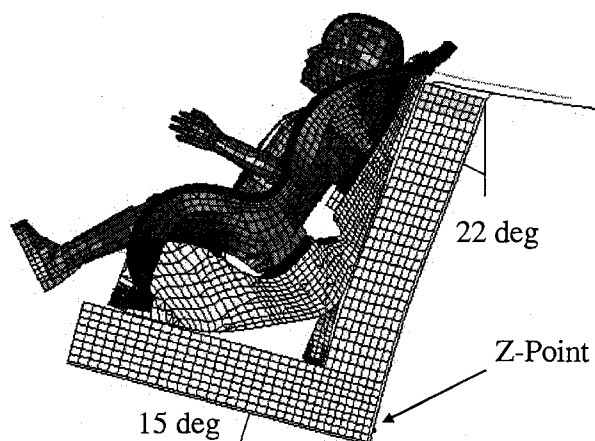


Figure 74. Side view of the deformable CRS model including the seat buck and the Hybrid III 3-year-old dummy.

Towards the end of this child safety research, foam compressive specimens from a 213 seat bench were made available to the author by Magna International. A parametric study was completed on a numerical model incorporating a Hybrid III 3-year-old dummy, which incorporated the foam mechanical characteristics acquired from automotive seats [100] and from foam specimens acquired from a 213 seat bench. The comparison between the two models is detailed in Section 5.2.4.1.

5.2.4.1 Parametric Study on Seat Buck Foam

As mentioned above, a parametric study was completed on the described numerical models which have incorporated the foam mechanical characteristics acquired from automotive seats [100] and from foam specimens acquired from a 213 seat bench. The 213 seat bench consisted of two different densities of foam material. Both the foam

specimens were acquired from a 213 seat bench. Compressive testing was completed on both the foam specimens and corresponding material models were developed. The thickness of the low density foam was 100 mm, and for the high density foam was 50 mm respectively. Values for the density of the material were defined as 23.2 kg/m^3 for the low density foam and 40.1 kg/m^3 for the high density foam respectively. Figure 75 illustrates the stress versus strain behaviour of both the foam specimens. These curves (loading only) were incorporated in the input file to define the material model.

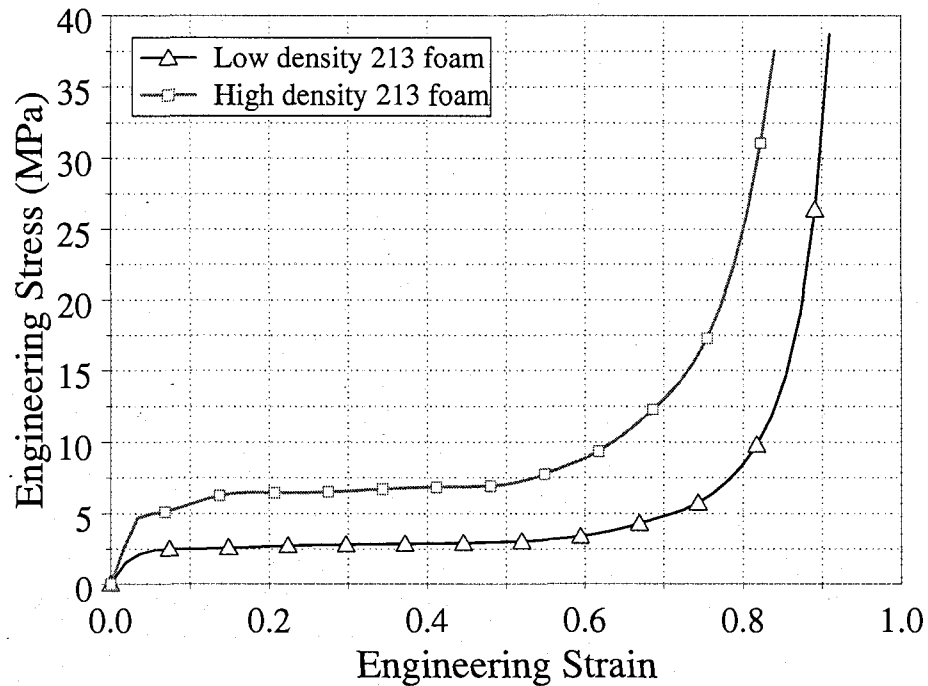


Figure 75. Engineering stress versus engineering strain response for the 213 seat bench foam.

Under the FMVSS 213 testing procedure (utilizing a Hybrid III 3-year-old dummy) it was observed that incorporation of the mechanical characteristics from a 213 seat bench resulted in approximately 55 mm and 60 mm of increased head and knee excursions respectively. Numerical simulation results indicated that the deformation behaviour of the 213 seat bench (for both types of foam) was significant and typically localized to the contact region between the CRS and 213 seat bench. The model which

incorporated mechanical behaviour from the 213 seat bench foam resulted in an additional compression, near the base of the CRS, of approximately 17 mm. Figure 76 illustrates the maximum local x direction displacement of the head as well as the maximum local z direction displacement of the CRS bottom for both the cases.

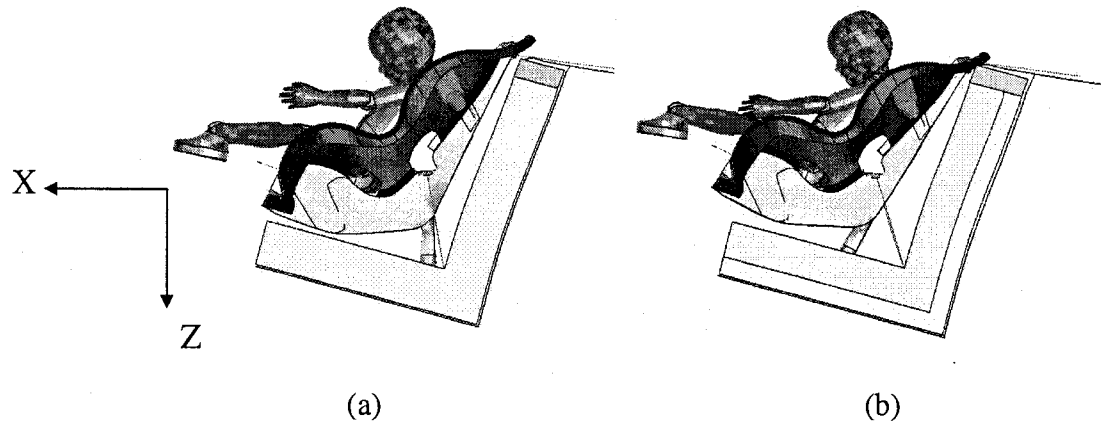


Figure 76. Maximum head excursion observed for the Hybrid III 3-year-old dummy for seat buck with material properties of (a) automotive seat, and (b) 213 seat bench.

Additionally, observations from the Hybrid III dummy indicated that accelerations in the local x direction, which were most significant, did not significantly vary. Accelerations in the local z direction did illustrate a variation in the peak value of approximately 15 percent. The general time domain response of both acceleration profiles (in the local x and z directions) did not significantly change. A minor degree of variation (approximately 10 percent) in the resultant neck force was also observed. The peak values of various injury parameters for both the foam models are tabulated in Table 6.

Table 6. Peak values for different injury parameters for the simulated FMVSS 213 crash involving a Hybrid III 3-year-old dummy for different material properties of the seat buck.

	Seat buck foam	
	Automotive seat	213 seat bench
Resultant head acceleration (g's)	50.3	59
Resultant chest acceleration (g's)	44	56
Head injury criteria (HIC-15)	203.5	270
Head injury criteria (HIC-36)	258.6	284
Resultant upper neck force (N)	1841.6	2078
Resultant upper neck moment (N.m)	39.86	35.2
Neck injury criteria (Nij)	0.95	1.1
Head Excursion (mm)	259.8	315
Knee Excursion (mm)	493.5	555

A minor degree of variation was observed between the FMVSS 213 seat bench foam and the foam from the automotive seats. It is an accepted fact that the 213 sled bench foams exhibit lower strength characteristics compared to the actual foam in the automotive vehicles. The model validation detailed in Chapter 6 illustrates that the numerical model that incorporates the material properties from an automotive seat predicts CMVSS 208 experimental tests with a better degree of accuracy. The parametric study illustrated that the foam mechanical response from the specimens extracted from automotive seats best represents the mechanical behaviour of foam from seats within vehicles of the current fleet.

5.3 Anthropomorphic testing devices

5.3.1 Hybrid III 3-year-old dummy

The numerical model of the Hybrid III 3-year-old dummy (version 2.3-2), illustrated in Figure 77 (a), was provided by FTSS. The mass of the Hybrid III 3-year-old child dummy is 15.4 kg and the stature height is 94.5 cm. The dummy model contains 12,172 elements and 11,698 nodes. The Hybrid III 3-year-old dummy model is a completely deformable finite element model and detailed information of the child dummy can be found in reference [123]. No alterations of the FE model obtained from FTSS

were applied and the default values for the materials, joints and element formulations were utilized. The upper and lower arms of the child dummy were rotated upwards 15 degrees corresponding to the positioning of the arms in the full vehicle test configuration. The positioning of the child dummy model in the CRS was completed using FEMB by a combination of nodal translations and nodal rotations until the child dummy was in a position as close as possible to what was believed to be the experimental position of the Hybrid III dummy in the CRS. Figure 77 (b) illustrates the isometric view of the complete FE model of the Hybrid III 3-year-old child dummy seated in the CRS.

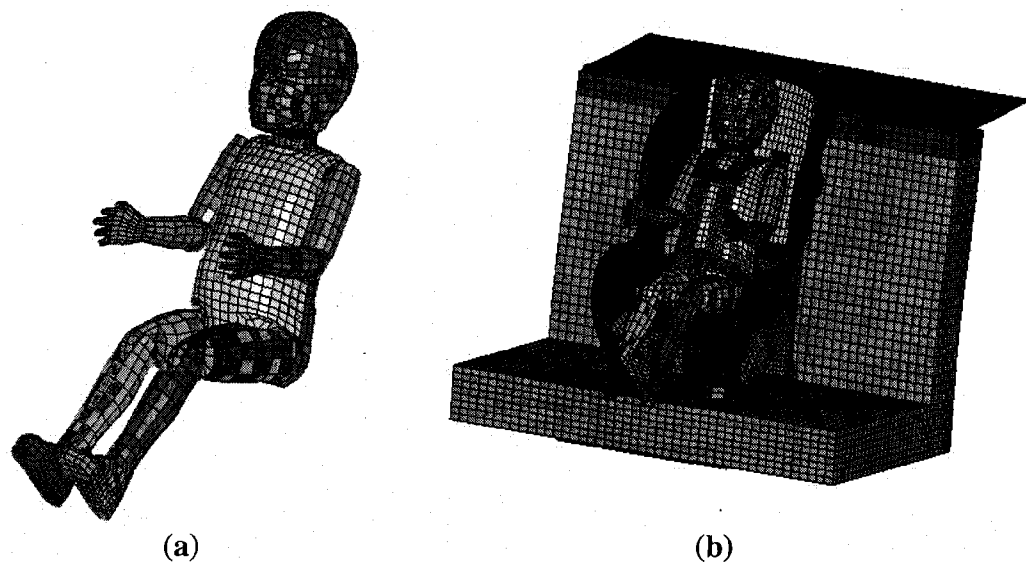


Figure 77. (a) Finite element model of the Hybrid III 3-year-old dummy, and (b) the complete FE model of the dummy seated in the CRS.

5.3.2 Q3 3-year-old child dummy

The Q3 3-year-old finite element child dummy model used for this research was developed by FTSS. The Q3 dummy, developed in 1998, is advanced in terms of its biomechanical and anthropometric basis compared to other child dummies. Specific design features of the Q-dummies are the anatomical representation of body regions, use of advanced materials, dummy-interchangeable instrumentation, multi-directional use (frontal & side impact) and easy handling properties (limited components, easy

assembly/disassembly, and simple calibration) [92]. Section 2.7.3.2 details the material and geometrical aspects of the physical Q3 dummy. The FE model was created based on physical Q3 dummy version August 2005 [124].

The FE model of the Q3 dummy (Q3 v1.0 beta) is comprised of 36,051 nodes and 70,895 elements. The mass of the Q3 child dummy is 14.45 kg. Details of the Q3 finite element model beta version can be found in the user's manual [125]. No alterations of the FE model obtained from FTSS were applied and the default values for the materials, joints and element formulations were utilized. Positioning of the Q3 dummy in the completely deformable CRS model was attained using FEMB. The seatbelt around the dummy's groin was slightly modified to fit properly around the dummy's legs as the crotch region of the Q3 is slightly narrower than the Hybrid III dummy. Figures 78 (a) and 78 (b) illustrate respectively the FE mesh of the Q3 dummy and the complete CRS model including the Q3 dummy used for this research.

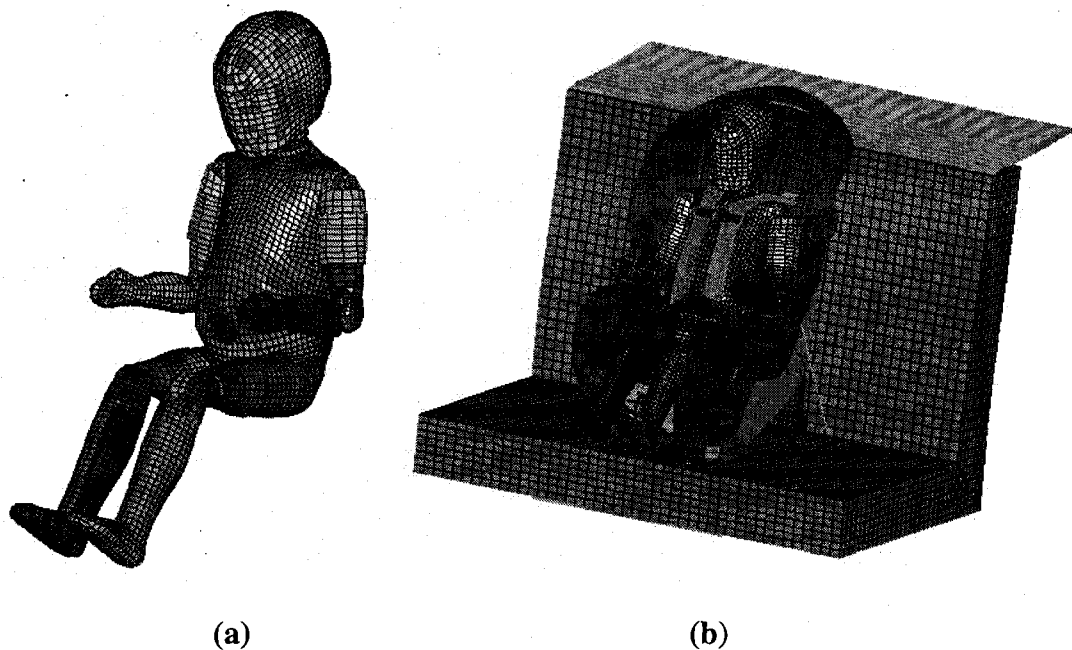


Figure 78. (a) Finite element model of the Q3 3-year-old dummy, and (b) the complete FE model of the Q3 dummy seated in the CRS.

5.3.3 Q3s 3-year-old child dummy

Q3s is a 3-year-old child dummy (detailed in section 2.7.3.3) specifically designed for side impact. The new Q3s dummy incorporates improved lateral impact performance and enhanced instrumentation for side impact testing [94]. The Q3s has shown improved biofidelity in the lateral direction compared to the Hybrid III 3-year-old and Q3 child dummies [94].

The FE model of the Q3s dummy (Q3s v1.0 beta) is comprised of 39,400 nodes and 82,550 elements. The mass of the Q3s child dummy is 14.54 kg. Details of the Q3s finite element model beta version can be found in the user's manual [126]. Positioning of the Q3s dummy in the completely deformable CRS model was attained using FEMB. The seatbelt around the dummy's groin was slightly modified to fit properly around the dummy's legs as the crotch region of the Q3s is slightly narrower than the Hybrid III dummy.

5.3.4 Child FE model

The 3-year-old child FE model was developed at Nagoya University by model-based scaling from the AM50 THUMS finite element model. The 3-year-old child numerical model presented by Mizuno et al. (Section 2.9.2.2) was developed to investigate injuries to various body regions of a child and to provide information that can be difficult to obtain from crash test dummies. This FE child model was developed from the AM50 THUMS model by using the model-based scaling method. The mass of the 3-year-old child model is 16.6 kg and the stature height is approximately 99.5 cm. The model is comprised of 65,947 nodes and 102,661 elements.

The child FE model differs from the Hybrid III 3-year-old dummy in terms of material properties and geometrical differences [112]. Material properties of some parts of the upper torso and abdomen of the child FE model were adjusted in order to overcome numerical instabilities resulting from large mesh deformation, such that at

large strains (approximately 80 percent) the material begins to significantly harden. This technique is often applied to FE models where large mesh deformation results in an element having a negative volume (or negative Jacobian). Use of this technique permits the specific finite element of concern to behave somewhat stiffer than may be expected at large values of strain but will allow for a more realistic distribution of loading to neighbouring finite elements. The positioning of the child FE model was attained using Hypermesh. Figure 79 (a) illustrates the child FE model and Figure 79 (b) shows the isometric view of the child FE model seated in the CRS.

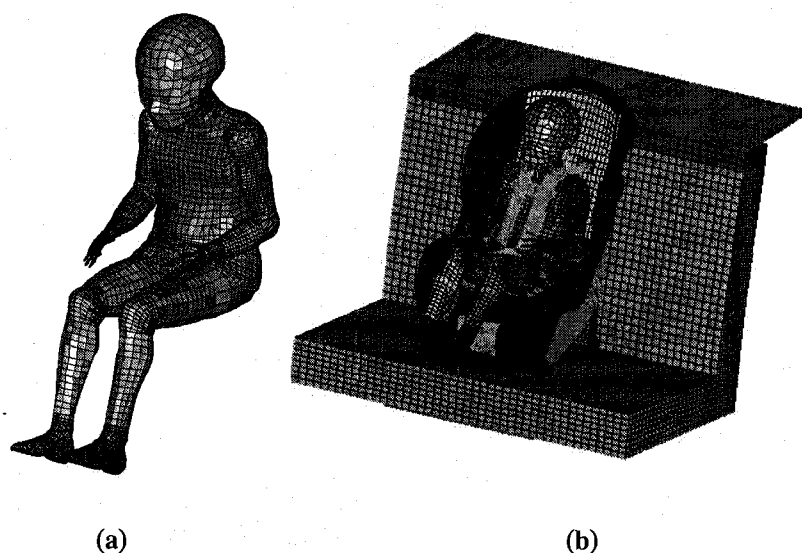


Figure 79. (a) The child FE model, and (b) the child FE model seated in the CRS.

5.4 Simulation procedure

Tightening of the front-adjusting harness strap was simulated quasi-statically to properly position the child dummy into the CRS. This process was achieved prior to the application of the acceleration pulse to the seat buck through dynamic relaxation. The number of iterations between the convergence checks and the convergence tolerance for dynamic relaxation were specified as 1000 and 0.0001 respectively. In this stage, the front-adjusting harness strap as well as the upper tether and lower LATCH anchor were

preloaded. Loads assigned to the LATCH and the top tether in the dynamic relaxation phase were of a magnitude of 60 N [78 and 82] respectively in the direction of the tethers.

An acceleration pulse with the magnitude/time history as observed from the experimental tests was prescribed to the rigid car seat in the global positive X-direction (frontal impacts) and global positive Y-direction (side impacts) after the dynamic relaxation was completed. No other motion of the rigid car seat in the remaining two axes directions was permitted. The ends of the top tether and LATCH were constrained to the rigid car seat. In addition, a gravity force was applied to the whole system for the entire simulation.

A rigid entity was modeled on the portion of the seat buck that came into contact with the one-dimensional seatbelt elements of the top tether. This was an approximation to ensure appropriate connection between the top tether, the CRS and the seat buck. The penalty method, which consists of placing normal interface springs between all penetrating nodes and the contact surface, was used for all the contact algorithms. Five types of contact algorithms, which were most important to the numerical model, are described below. Input for the contact definitions of all the contact algorithms are shown in Appendix E.

The automatic nodes to surface contact algorithm was used for the contact between the one dimensional seatbelt elements and shell elements of the CRS. The tied nodes to surface contact algorithm was used to simulate the contact between the foam pad and the CRS. The Hybrid III dummy was constrained to the CRS through contact between the dummy and the two-dimensional seatbelt elements. To appropriately model contact between these entities, an initial separation distance equal to one half of the thickness of the seatbelt was necessary. The automatic surface to surface contact algorithm was used to simulate contact between the child dummy, CRS and the foam padding. The soft constraint option (pinball segment-based contact) was also utilized in this contact definition. The automatic single surface contact algorithm was used for the sliding contact between the buckles and the seatbelt, and the automatic surface to surface

contact algorithm was used for the contact between the buckles and the child dummy. The values for static and dynamic frictional coefficient were specified as 0.25 and 0.2 respectively for all contact algorithms involving the dummy, the CRS and seatbelt webbing. Due to the complexity of the child model discretization, significant alterations to the penalty scale factors in the contact interfaces between the child model and the CRS were necessary.

All the computer simulations were conducted using LS-DYNA on a personal computer with a dual 2.6 GHz AMD Athlon processor with 2 gigabytes of random access memory (RAM). The double precision version of LS-DYNA version 970 revision 5434a was used. The computational time for simulations involving the Hybrid III dummy was approximately 16 hours, whereas the numerical simulations involving the Q3/Q3s child dummies' and the child FE model took approximately 35 to 40 hours for completion.

5.5 Data extraction

Child occupant injury data was extracted from the instrumentation, including accelerometers and load cells, equipped within the dummy model. Tri-axial accelerometers were mounted in the head, chest and pelvis of the Hybrid III 3-year-old and Q3/Q3s dummy models which provided acceleration data in the local x , y and z -directions. Three nodes were defined as accelerometers, and nodal acceleration data were stored in the "nodout" American Standard Code for Information Interchange (ASCII) time history file. Figure 80 illustrates the location of the head and chest accelerometers in a Hybrid III 3-year-old dummy.

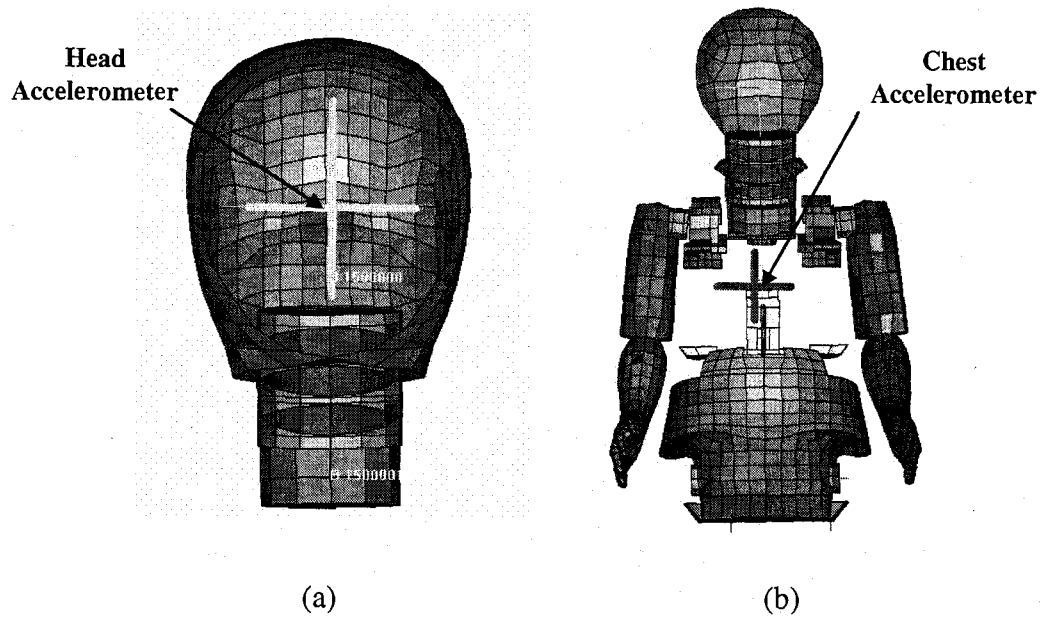


Figure 80. Accelerometer locations in the (a) head and (b) chest of the Hybrid III 3-year-old dummy model.

Load cells were defined using beam elements and were assigned material Type 66 (linear elastic discrete beam) in LS-DYNA. They acted as stiff translational and rotational springs (an accurate representation of reality). Each load cell beam had a unique part, material and section ID. Each beam was located at the intersection of the load cell's neutral axes. The numerical load cells provided all six output channels consisting of three forces and three moments for the upper and lower neck of the dummy in the local x , y and z directions. Figure 81 illustrates the location of the upper and lower neck load cells in a Hybrid III 3-year-old dummy.

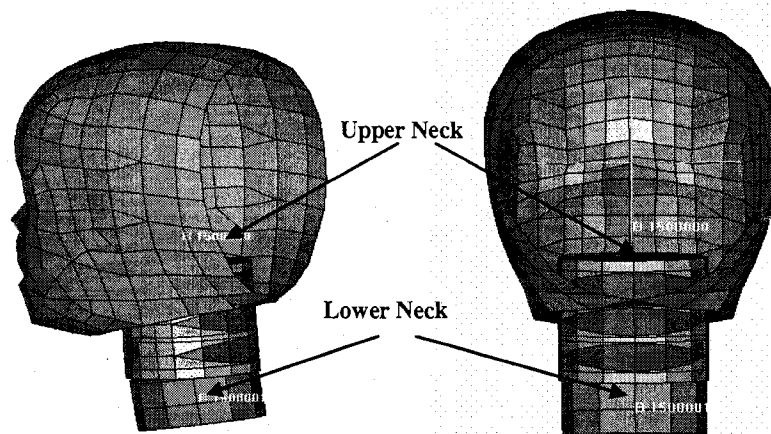


Figure 81. Upper and lower neck areas of the Hybrid III 3-year-old finite element dummy model.

The child FE model is not equipped with any instrumentation. Two nodes, specifically in the head and the chest of the child model were included in the nodal data output file to track the head and chest accelerations. The positioning of these nodes (Figure 82) was selected similar to the head and chest accelerometers in the Hybrid III and Q3/Q3s dummies. Two section planes were created in the upper neck portion of the child FE model in order to evaluate the upper neck cross-section forces. The first section plane passed through the C2-C3 region of the neck, perpendicular to the cervical vertebrae. The second section plane passed through the annulus fibrosis around C2. The location of both the section planes is illustrated in Figure 83. The cross-section plane LS-DYNA input data is presented in Appendix D.

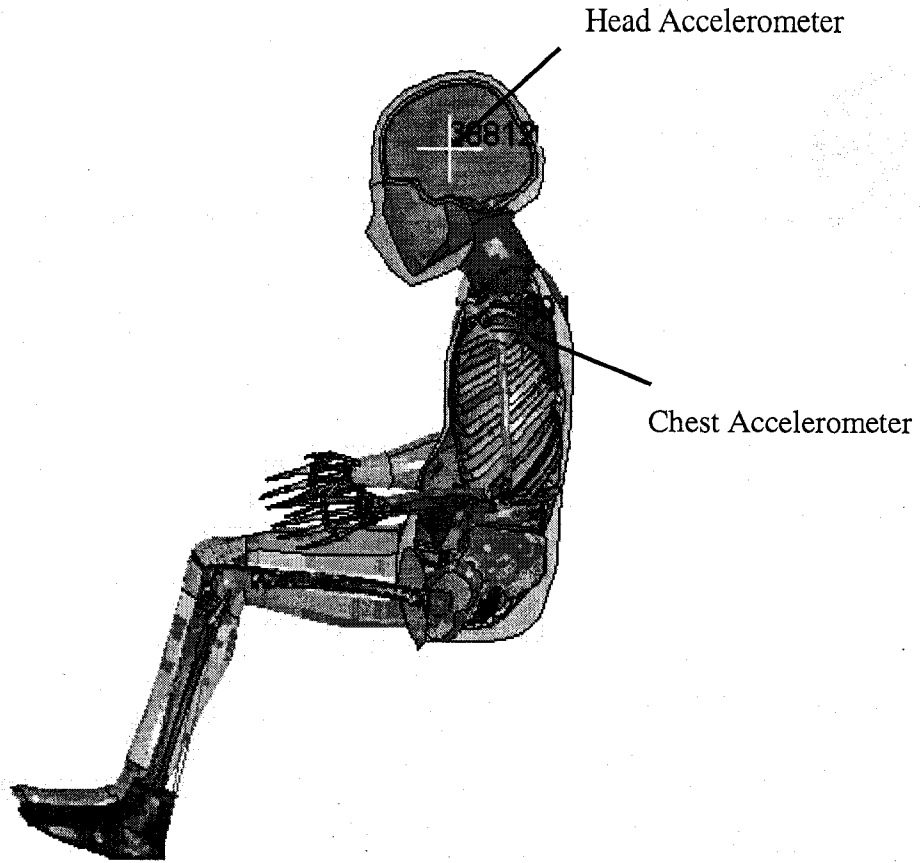


Figure 82. Location of the nodes in the head and chest of the Child FE model used to track accelerations.

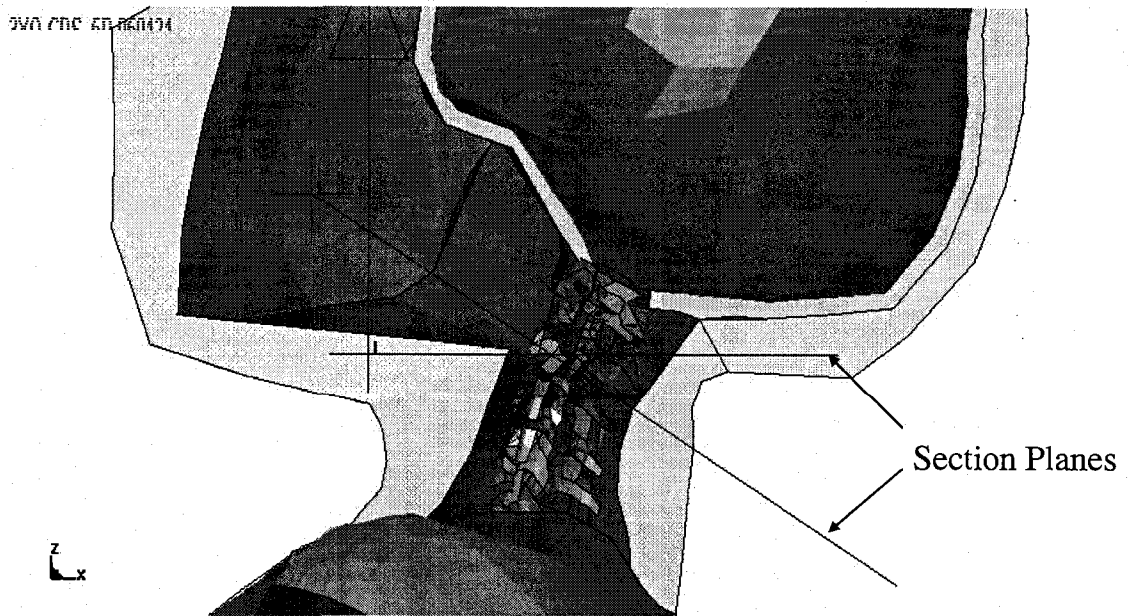


Figure 83. Location of the section planes in the neck of the Child FE model.

Due to the fact that human body parts respond to certain frequencies, standard SAE J211 was utilized to filter all the experimental and numerical data. All the data was measured with respect to the dummy's local coordinate system as outlined in SAE J211 [120] and was sampled at a rate of 10 kHz. The numerical results were filtered in accordance to SAE J211 [120]. Filtering was conducted using a Butterworth 4-pole phaseless filter as described in reference [120]. Data filtering was completed prior to any data analysis. Details of the numerical algorithms used to incorporate these filters are shown in Appendix C. Table 3 tabulates the filters for dummy data channels prescribed by SAE J211. After the extraction of data from the dummy, the injury parameters presented in Section 4.1.3 were calculated.

6. NUMERICAL MODEL VALIDATION

6.1 Validation technique utilized in this research

A number of techniques have been established by researchers for the purpose of numerical model validation. For example, Rebba et al. [127] utilize Bayesian methodology for assessing the confidence in model prediction by comparing the model output with numerical data when both are stochastic. Many other metrics have been developed to calculate the correlation between the experimental and numerical data. However, the method proposed by Oberkamp et al. [128] appears to be quite thorough and provides a validation metric as a function of relative error. The validation metric (V) is calculated as presented in Equation 6.

$$V = 1 - \frac{1}{L} \int_0^L \tanh \left| \frac{y(x) - Y(x)}{Y(x)} \right| dx \quad (6)$$

Where $y(x)$ is the measured value, $Y(x)$ is the expected value and L is the range of the independent variable. The advantages of using the Oberkamf and Trucano's scheme [128] are as follows. This validation metric normalizes the difference between the computational results and the experimental data. Secondly, the absolute value of the relative error only permits the difference between the computational results and the experimental data to accumulate, therefore positive and negative differences cannot offset one another. Thirdly, when the difference between the computational results and the experimental data is zero at all measurement locations, then the validation metric is unity, therefore perfect agreement between the computational results and the experimental data. In addition, when the summation of the relative error becomes large, the validation metric approaches zero. Figure 84 illustrates the validation metric (V) proposed by Oberkamf et al. [128] as a function of relative error.

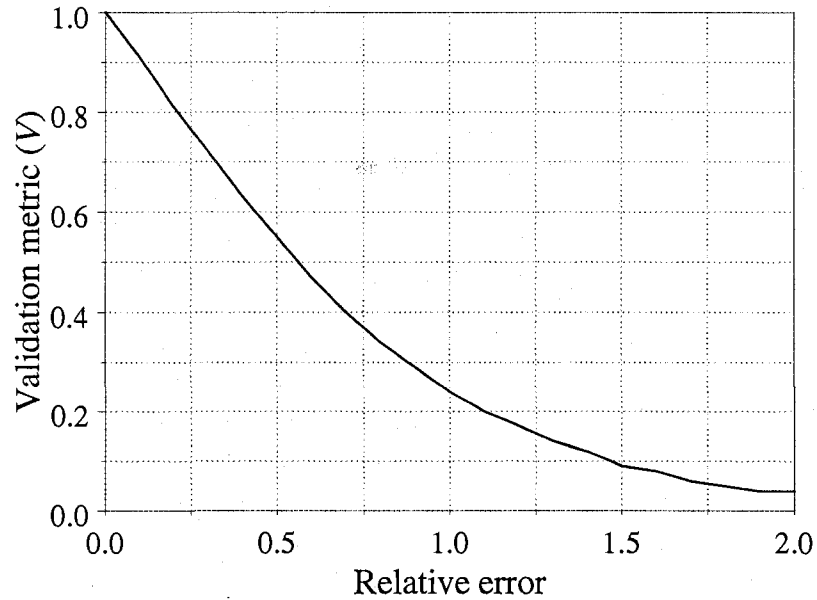


Figure 84. Validation metric as a function of relative error.

In order to maintain a consistent value between both the expected and measured functions, cubic spline curve fitting was completed utilizing 5000 data points prior to the error analysis. The main disadvantage of using this technique is that the normalization is inappropriate when $Y(x)$ is closer to zero. This was overcome by introducing an error criterion. An upper and lower bound were specified as ± 10 percent of the maximum absolute expected value. The error was calculated as presented in Equation 7:

$$\begin{aligned} &\text{For } \text{lower} \leq Y(x) \leq \text{upper}, \text{error}(x) = 0 \\ &\text{else } \text{error}(x) = \frac{y(x) - Y(x)}{Y(x)} \end{aligned} \quad (7)$$

Therefore, within the window of the upper and lower bounds, the error was evaluated as zero; otherwise the error was evaluated as the relative error between the measured and expected values. The average error (E) was calculated by integrating the error in the range of the independent variable. The validation metric (V) was also computed using equation 6. This technique has been utilized in this research for the purpose of numerical model validation.

The completely deformable finite element model was validated by comparing the numerical simulation results with experimental findings in frontal and side impact tests. Experimental frontal impact sled tests were completed in accordance to the FMVSS 213 using a Hybrid III 3-year-old dummy in a five point child restraint system. A full vehicle crash test was completed in accordance to the CMVSS 208 with the addition of a 3-year-old Hybrid III crash test dummy, seated behind the passenger seat, restrained in the identical five-point child safety seat. For the sled tests, the comparison was based on head and chest accelerations as no load cells were incorporated into the experimental dummy. The numerical model was validated in accordance with the full vehicle crash test in terms of head and chest accelerations; and upper and lower neck forces and moments. The data comparison for the CMVSS 208 tests was carried out with the experimental dummy labeled P2 in Chapter 4, which was anchored to the vehicle seat using the LATCH system. The acceleration pulse obtained from the experimental tests was applied to the rigid portion of the sled buck in the global positive X-direction. Numerical simulations were also completed with the previously developed simple child seat model [100] for both the acceleration pulses. The deformable model of the CRS is labeled “complex model” and the simplified model of the CRS has been labeled “simple model” respectively.

Zhang et al. [115] carried out a comparison between the kinematics of the child FE model and the Hybrid III 3-year-old dummy under a simulated CMVSS 208 crash which is detailed in Section 2.9.2.2. Further parametric studies were completed employing the FMVSS 213 testing conditions for the Q3 child dummy and the child FE model. A data comparison was carried out between the three numerical models (Hybrid III 3-year-old, Q3 and child FE model) in order to compare the kinematic response of the three child models under similar crash conditions.

The completely deformable model of the CRS has been validated in the far-side impact configuration (section 2.9.3.2) by Wang et al. [117]. Sled tests were conducted by NHTSA in 2001 at TRC. This test, labeled 4585, was a sled test without a vehicle body and in the presence of a side rigid wall [105]. A numerical model incorporating a

Hybrid III 3-year-old dummy with a side rigid wall was developed and simulated under similar testing conditions. A data comparison was carried out in terms of head and chest accelerations; and upper and lower neck forces and moments.

A compressive test on the side wings of the CRS was performed to further verify the child seat finite element model. The force versus displacement curve was obtained from the test and was compared with the numerical results.

6.2 Finite element model validation – CMVSS 208 vehicle crash test

6.2.1 Qualitative Comparison

Figure 85 provides the side view of the child dummies relative to the CRS at specific intervals of time through the simulations of the prescribed acceleration pulse. This provides a visual comparison of the behaviour of the specimens during the crash. For convenience, the whole simulated event has been divided into five phases. There appeared to be a slight shift in time between the experimental and numerical acceleration pulses for the vehicle crash test. This was due to the fact that the acceleration pulse recorded in the vehicle was applied to the seat in the numerical test. The time difference between these two testing methods was estimated to be no greater than 30 ms. The time shifts have been adjusted in the quantitative analysis.

Phase I depicts the state of rest. At this time, the experimental and the numerical dummies are seated in their original configuration. Phase II marks the onset of head rotation. At this time the dummies start moving forward. This was observed to occur at approximately $t = 30$ ms for the numerical dummies and $t = 60$ ms for the experimental dummy. Phase III marks the maximum extension in the neck which was observed at $t = 85$ ms for both the numerical models and $t = 127$ ms for the experimental dummy. Differences were observed in the positions of the dummies' heads and limbs at that moment. In the experimental test, the neck and spine of the dummy rotated a significant amount and momentarily stayed in between the arms. In both of the numerical

simulations, there was not as much bending and neck rotation predicted as was observed in the experimental test. This may be due to differences in stiffness of the necks of the experimental and numerical dummies. Also, positioning of the seatbelt used to restrain the dummy in the CRS could be different in the vicinity of the neck region. Phase IV marks the rebound phase which occurred at approximately $t = 110$ ms for the numerical models and $t = 160$ ms for the experimental dummy. At this time the dummy started to settle back into the CRS. The numerical dummy in the complex model was observed to settle quicker in the CRS. Phase V is the stage when a contact between the dummy's head and the CRS was observed. It should be noted that the times corresponding to the experimental dummy are the actual time durations and the time shifts have not been incorporated for the qualitative analysis.

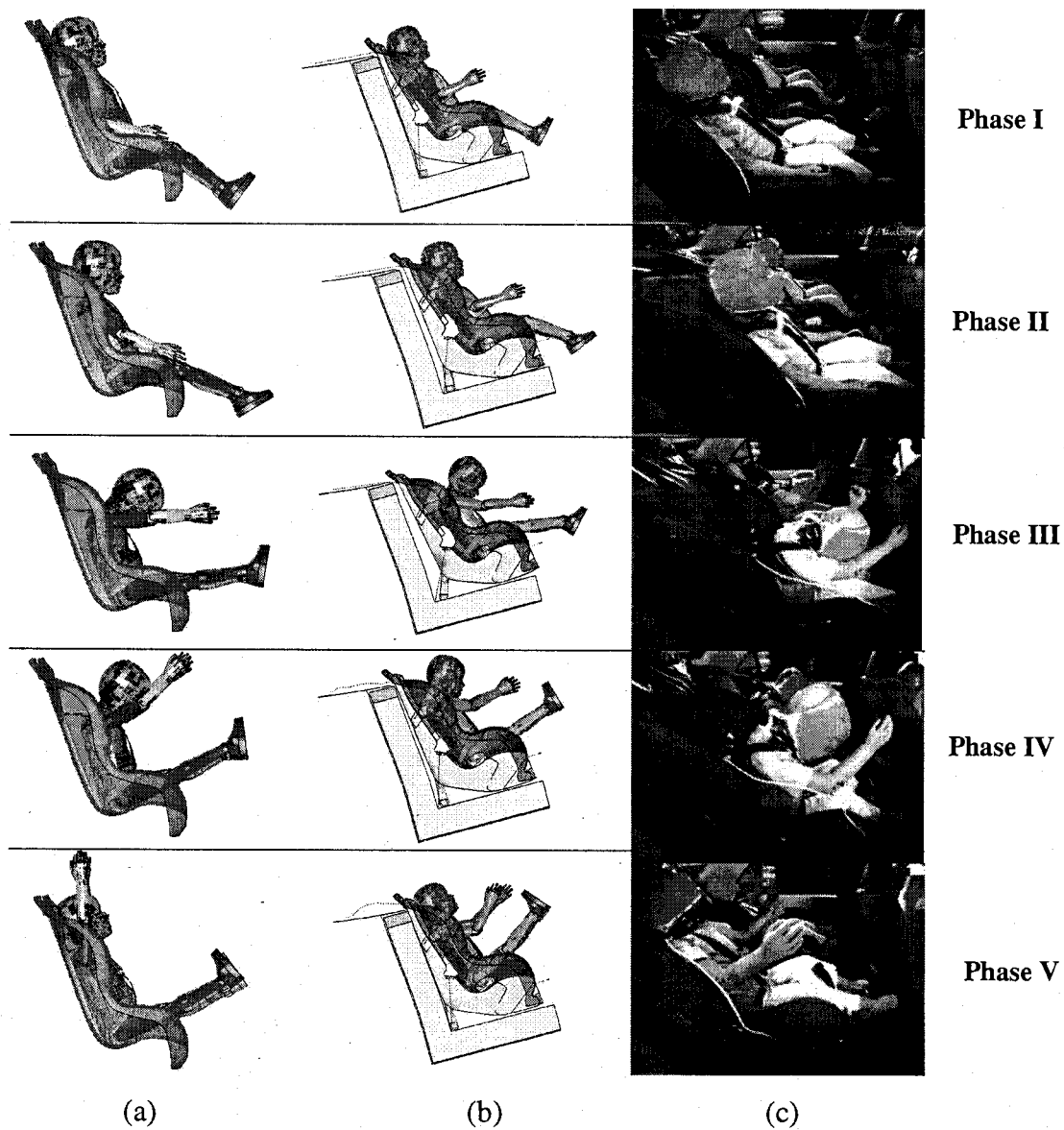


Figure 85. (a) Simplified rigid model, (b) complex model and (c) experimental observations for the full vehicle crash test in accordance with CMVSS 208.

6.2.2 Quantitative comparison

6.2.2.1 Head accelerations

Figure 86 illustrates the values of the local x -component of the head acceleration for the three dummies as a function of time. Similar acceleration profiles were observed for the numerical and experimental Hybrid III child dummies. The minimum local x -axis head acceleration for the simple model was -37 g's, for the complex model was -51 g's and for the experimental dummy was approximately -49 g's. Table 7 tabulates the peak values observed for all the three child dummies for the CMVSS 208 test. The time required to reach the minimum local x -axis head acceleration for the child dummies was approximately 80 ms. This is the time when the head experienced the greatest extension as shown in Figure 85. The duration of these peaks was observed to be less than 3 ms and they were followed by an upward ramp and returned to zero at approximately 140 ms.

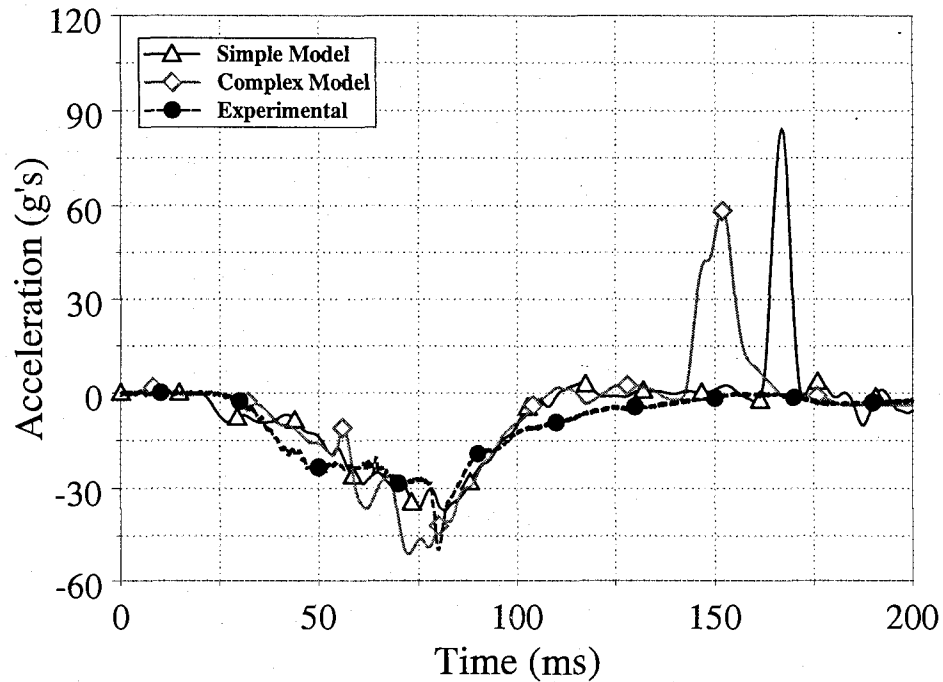


Figure 86. Experimental and numerical head accelerations in the local x -axis direction.

After 140 ms, a spike was observed in the acceleration response of all the dummies. The spikes for the simple model were generated as a result of the child dummy falling back into the seat and the head contacting the back of the rigid CRS. For the complex model, these spikes were due to the interaction between the CRS and the rigid entity on the seat buck that was created to ensure appropriate connection between the one-dimensional seatbelt elements of the top tether and the seat buck. However, the spikes of the numerical models occurred earlier than the spike in the experimental test. The slippage of the seatbelt and the unknown damping factors, for example the friction within the joints and the viscous characteristics, which were not included in the model might have contributed to the time difference.

It was also observed that after 140 ms, the spike of the simple model occurred later than the spike of the complex model. The seatbelt tightening was not incorporated into the simple model, which resulted in more slack between the seatbelt and the child dummy in the simulation. Therefore, the incident of the child dummy' head contacting the back of the CRS was delayed by the slack in the simple model. Based on the fact that children are most likely injured in frontal crashes by excessive accelerations and forces generated when their heads move forward relative to the CRS, and the fact that the spike caused by the head contacting the back of the CRS are normally not an important factor to child occupant injuries, these spikes can be neglected for the data analysis.

The values of the local z -component of head acceleration for experimental and numerical dummies as a function of time are illustrated in Figure 87. The time profiles illustrate similarities for the local z -axis head acceleration, though they exhibit differences in the peak values. The peak values are tabulated in Table 7. The maximum values for the local z -axis head acceleration for the simple model and complex model were observed to be approximately 41 g's, whereas the peak values observed for the experimental dummy was observed to be 56 g's. These peak values for the z -axis head acceleration occurred at approximately 62 ms for all the child dummies due to severe bending of the neck.

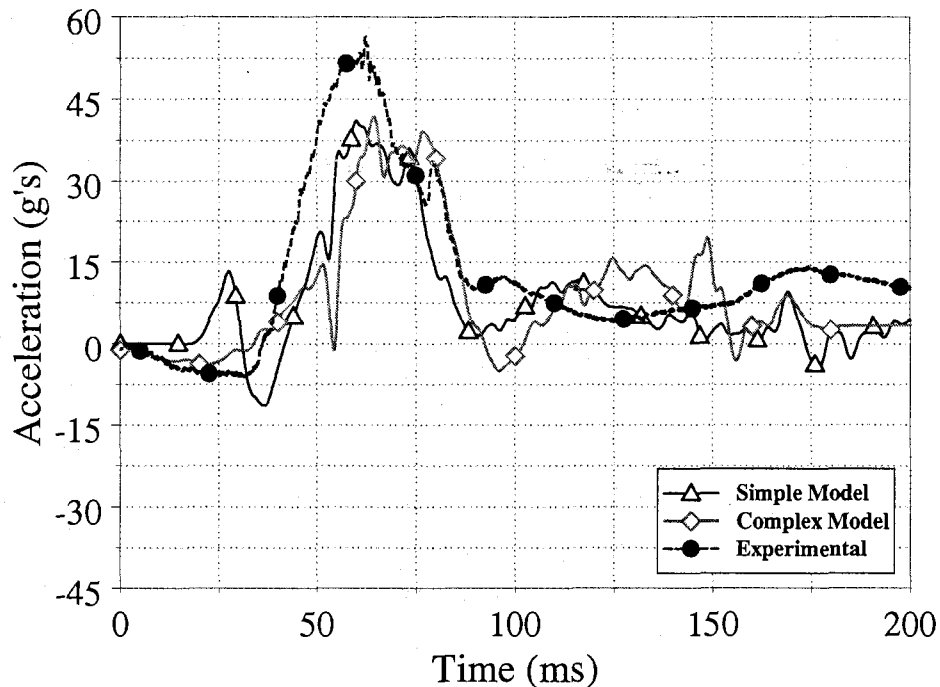


Figure 87. Experimental and numerical head accelerations in the local z -axis direction.

6.2.2.2 Chest accelerations

Figure 88 illustrates the local x -component of the chest acceleration for the numerical and experimental child dummies as a function of time. The time profiles were very similar with the minimum x -axis chest acceleration being approximately 40 g's for the simple model and the experimental dummy, and 50 g's for complex model. The time duration of the peak for the complex model was observed to be less than 3 ms. The minimum x -axis chest acceleration for the child dummies occurred at approximately 60 ms, which is the time when each dummies' chests come in contact with the seat belt. After this the seat belt starts stretching and hence takes up load, further attenuating the high accelerations experienced by the chest of the child dummy. After approximately 150 ms, both models and experimental test illustrated the torso of the dummy returning to the CRS, which had an effect on the chest acceleration responses in the local x -axis direction.

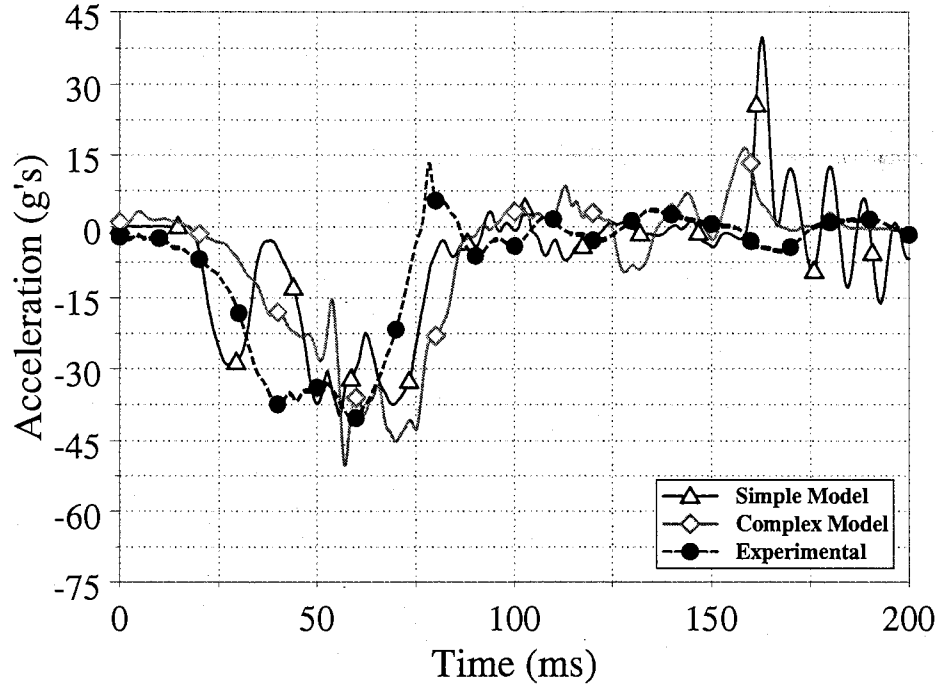


Figure 88. Experimental and numerical chest accelerations in the local x -axis direction.

6.2.2.3 Resultant upper and lower neck forces

Figures 89 and 90; demonstrate the resultant upper and lower neck forces as a function of time for the numerical and experimental child dummies respectively. All the child dummies exhibited similar time profiles for the neck forces. The peak values for the resultant upper and lower neck forces are tabulated in Table 7. It should be noted that the high values of neck forces are sustained by the dummy's neck for times greater than 50 ms.

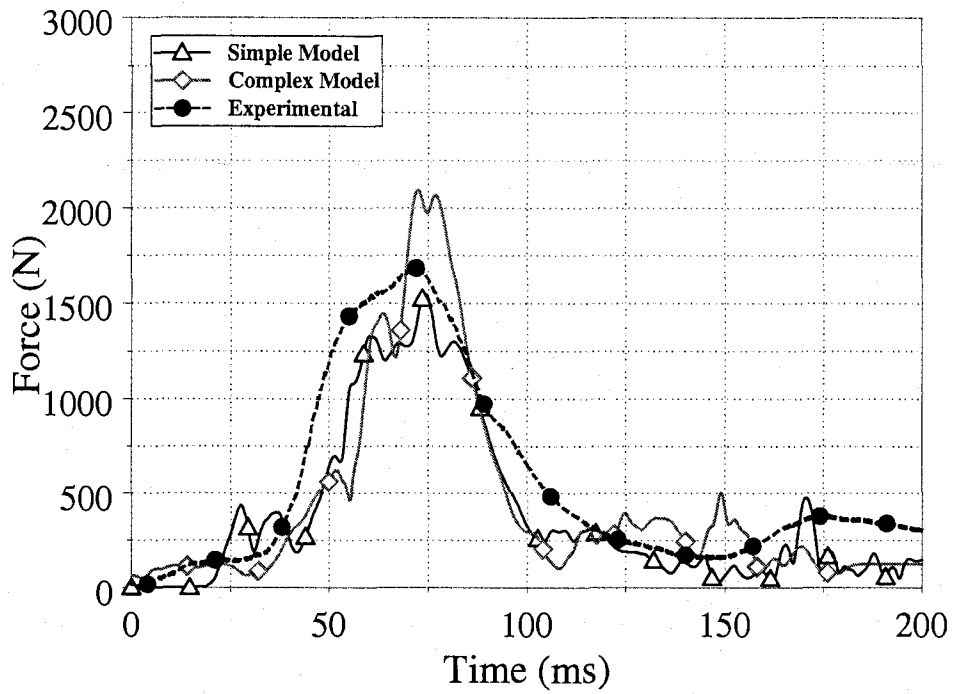


Figure 89. Experimental and numerical upper neck resultant forces.

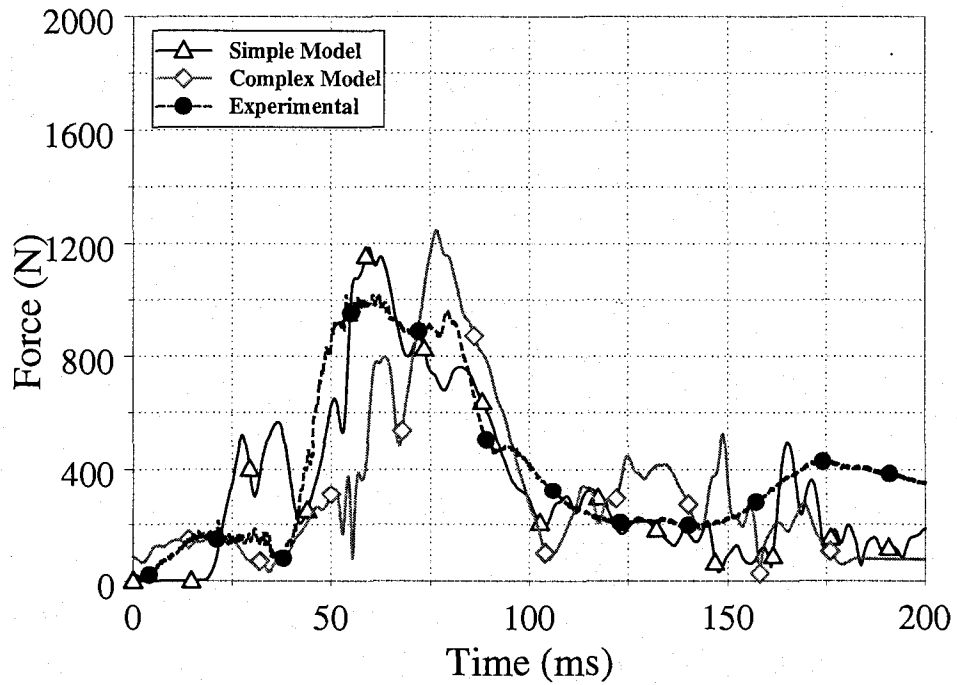


Figure 90. Experimental and numerical lower neck resultant forces.

6.2.2.4 Resultant upper and lower neck moments

Resultant upper and lower neck moments are presented in Figures 91 and 92 respectively. All the dummies exhibited similar time profiles with differences in the peak values. From the upper neck load cell peak values of approximately 23 N·m and 36 N·m were predicted for the complex and simple models, while a value of approximately 16 N·m was observed for the experimental child dummy. In comparison, much higher values were observed for the resultant lower neck moments. The peak values ranged from 122 N·m for the experimental dummy to 140 N·m for the simple model and 160 N·m for the complex model respectively. This difference is due to considerable extension of the neck during the crash. The numerical models over-predicted the resultant neck moments compared to the experimental results, which can be attributed to the difference in the stiffness of the neck of the experimental and the numerical dummies.

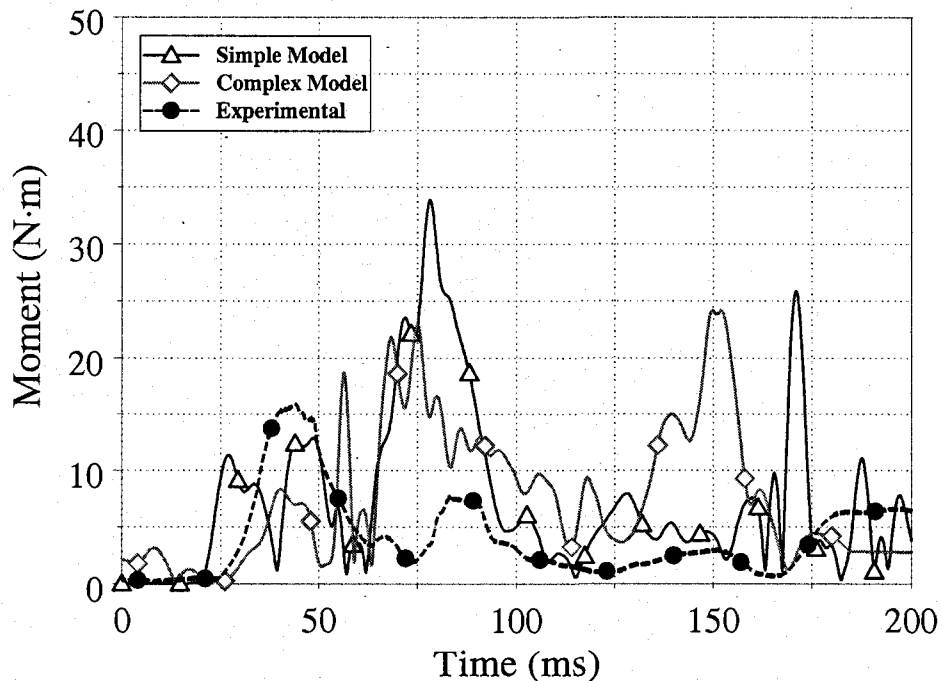


Figure 91. Experimental and numerical upper neck resultant moments.

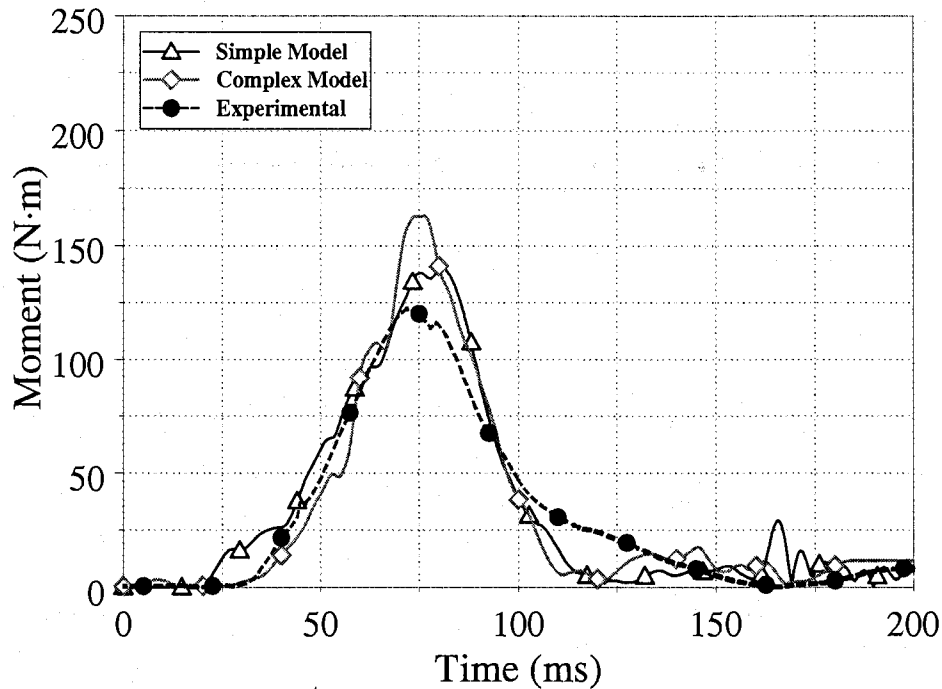


Figure 92. Experimental and numerical lower neck resultant moments.

Table 7. Summary of the peak values* of experimental and numerical results from CMVSS 208 test.

Injury Parameters	Experimental	Numerical (Simple model)	Error Analysis		Numerical (Complex model)	Error Analysis	
			E	V		E	V
Head accelerations in x direction (g's)	-49.85	-36.86	0.286	0.761	-51.02	0.328	0.715
Head accelerations in z direction (g's)	56.34	41.1	0.353	0.717	41.36	0.345	0.716
Chest accelerations in x direction (g's)	-40.82	-39	0.443	0.7	-50.12	0.593	0.693
Resultant upper neck forces (N)	1681.6	1534	0.221	0.793	1958.4	0.259	0.76
Resultant lower neck forces (N)	1023.7	1230.8	0.41	0.711	1302.3	0.317	0.712
Resultant upper neck moments (N·m)	15.92	33.86	1.308	0.579	22.93	1.317	0.501
Resultant lower neck moments (N·m)	122.41	138.83	0.2	0.819	163.11	0.234	0.788

*Neglecting the later spikes that occur due to the settling back of the child dummy

Table 7 also tabulates the values for the average error (E) and the validation metric (V) obtained for both the simple and complex models. An acceptable correlation in terms of the peak values as well as the dynamic response within the entire time domain between the numerical simulation results and the experimental findings showed the numerical model's ability to predict the kinematics and kinetics which the Hybrid III 3-year-old child dummy experienced in full vehicle crash test. Head and chest accelerations of the child dummy were well predicted by both of the numerical models,

especially in the first 140 ms. Upper and lower neck forces were over-predicted by the complex model by approximately 20 percent. Similarly for the upper and lower neck moments the complex model over-predicted experimental findings by approximately 30 percent. The qualitative and quantitative analysis illustrate that incorporation of the fully deformable CRS model exhibited acceptable predictions of the child dummy kinematic and kinetic responses in a full vehicle crash. Most especially the dummy response in the time interval of zero to 140 ms is well predicted by numerical simulations. It is in this time duration when neck trauma occurs.

6.3 Finite element model validation – FMVSS 213 sled test

6.3.1 Qualitative comparison

Figure 93 provides the side view of the child dummies relative to the CRS at different intervals of time through the simulations of the prescribed acceleration pulse. Phase I depicts the state of rest. At this time, the experimental and the numerical dummies are seated in their original configuration. The positioning of the limbs of the Hybrid III dummy for the complex model was identical to the experimental dummy. Phase II marks the onset of head rotation. At this time the dummies start moving forward. This was observed to occur at approximately $t = 30$ ms for all the three models. Phase III marks the maximum extension in the neck which was observed at $t = 70$ ms for both the numerical models and at $t = 85$ ms for the experimental dummy. Bending of the neck was observed to be slightly greater for the experimental dummy, and compared better with the simple model than to the complex model. The seatbelt tightening effect was not simulated for the simple model, thus a slack in the seatbelt existed in the numerical simulation for the simple model. Therefore, one possible explanation to this situation is the presence of slack in the experimental tests. The positioning of the limbs for the simple model was observed to be slightly different than the complex model and the experimental dummy throughout the simulation. Phase IV marks the rebound phase which occurred at approximately $t = 92$ ms for the numerical models and at $t = 116$ ms for the experimental dummy. At this time the dummy started to settle back into the CRS. The numerical

dummies were predicted to settle quicker in the CRS. The possible explanation for this variation is the absence of slack in the complex model and the limited seatbelt length in the simple model. Due to the presence of slack, the rebound phase was delayed in the experimental tests. Phase V is the stage when a contact between the dummy's head and the CRS was observed.

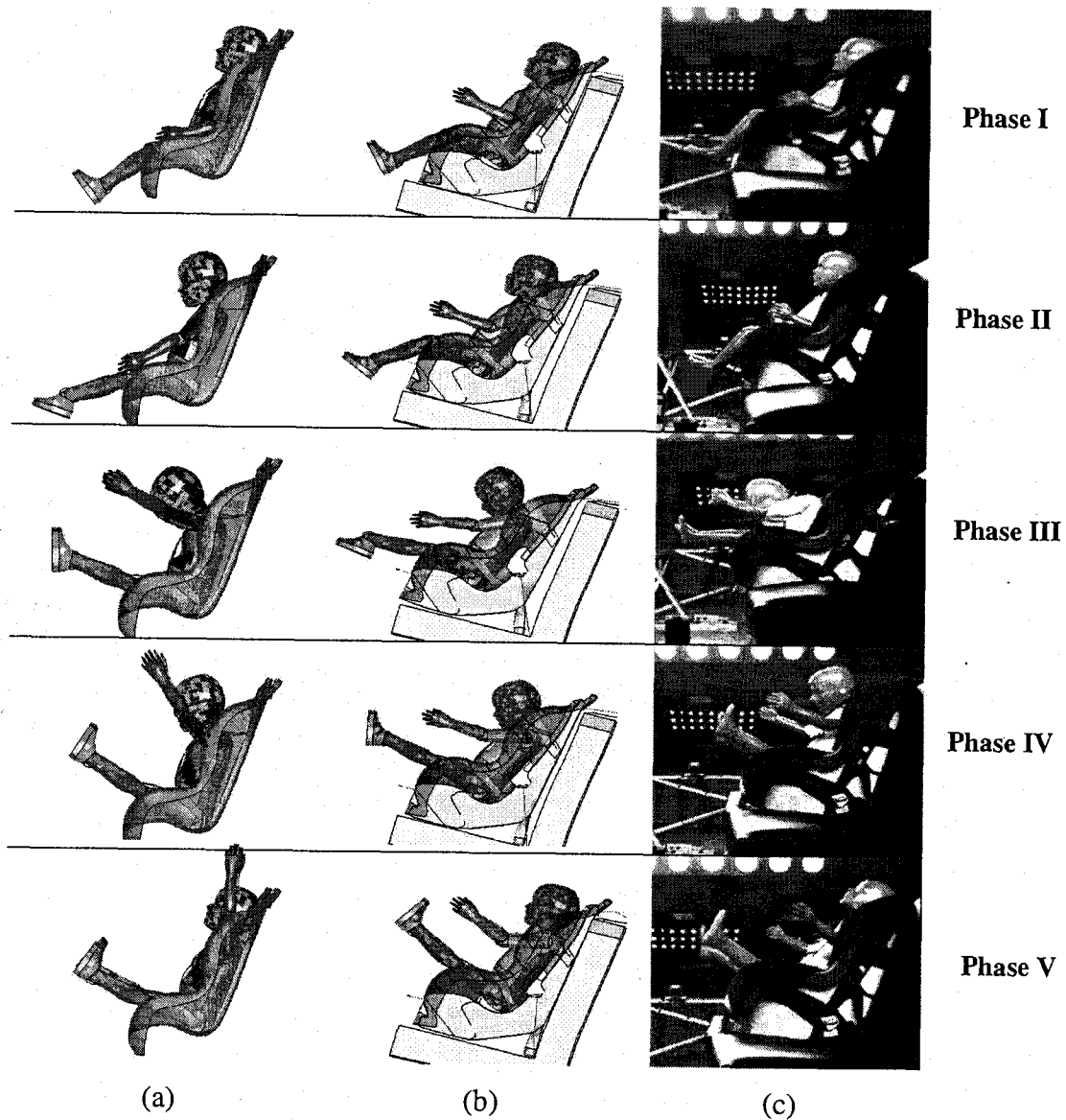


Figure 93. (a) Simplified rigid model, (b) complex model and (c) experimental observations for the full vehicle crash test in accordance with FMVSS 213.

6.3.2 Quantitative comparison

6.3.2.1 Head accelerations

Figure 94 illustrates the values of head accelerations in the local x -axis direction for all the three child models as a function of time. Similar time profiles were observed for all the three FE models with differences in peak values. All the three responses of head accelerations in the x -axis direction reached their lowest values at approximately 60 ms. Head accelerations were over-predicted by the complex model. As it has been previously mentioned, the spikes in the curves of numerical simulations after 130 ms were caused due to the secondary impacts between the dummy's head and the back of the CRS. The minimum values of the head x -accelerations were observed to be -23 g's for the experimental dummy, -30 g's for the simple model and -43 g's for the complex model respectively.

The values of the head accelerations in the local z -axis direction are presented in Figure 95. Numerical predictions of the head accelerations in the local z direction showed good agreement with the experimental findings for the first 120 ms. The complex model and the experimental dummies reached their peak values at roughly 50 ms. For the simple model the peak values were observed at $t = 40$ ms. The peak values are tabulated in Table 8.

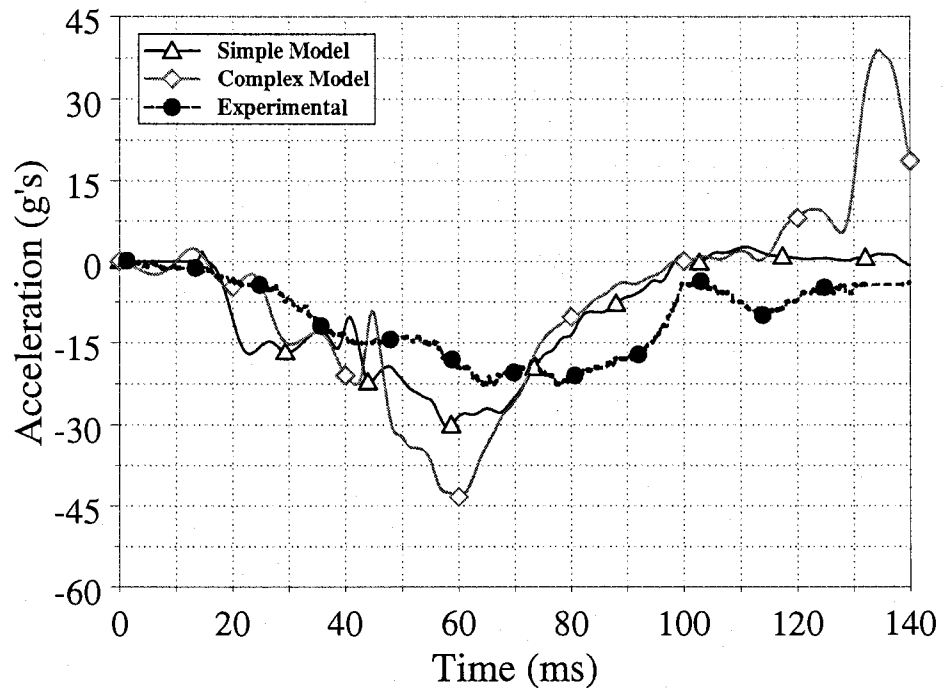


Figure 94. Experimental and numerical head accelerations in the local x -axis direction.

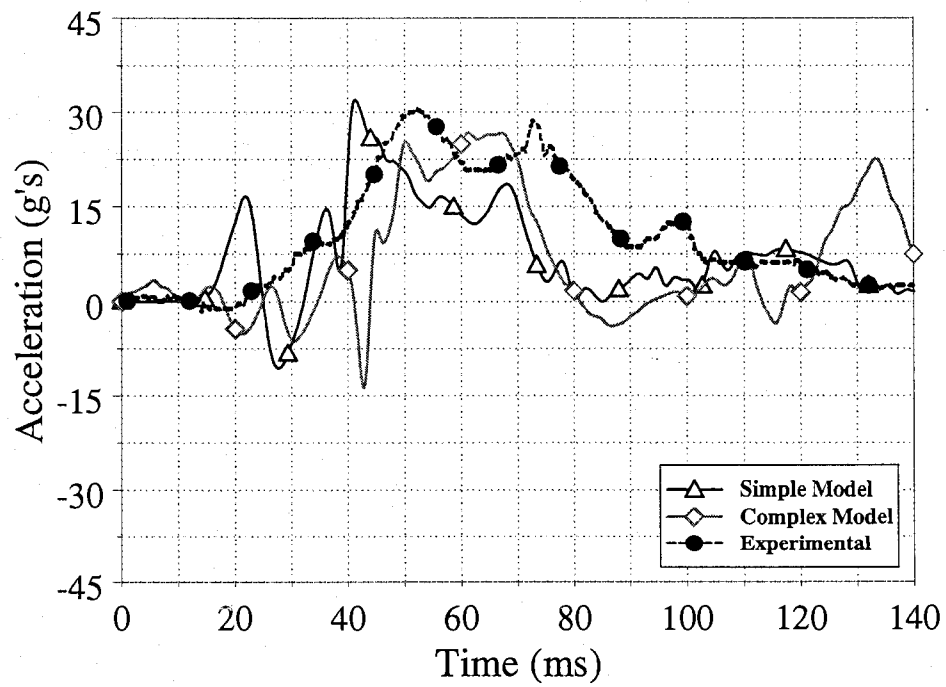


Figure 95. Experimental and numerical head accelerations in the local z -axis direction.

6.3.2.2 Chest accelerations

Figure 96 exhibits the experimental and numerical results of the child dummy's chest accelerations in the local x -axis direction as a function of time. There were two major differences between the results from the complex model and data from the other two tests. Both the experimental test and the simple model reached their peak accelerations at approximately 25 ms, while the complex model predicted the peak chest acceleration in the local x direction at roughly 45 ms. The minimum value of chest x -acceleration was observed to be approximately -35 g's for the complex model, while both the experimental and the simple model reached peak accelerations of -62 g's. It has been stated in the previous sections that there was no seatbelt tightening in the simple model so slack in the seatbelt existed in the numerical simulation. Therefore, one possible explanation to this situation is the presence of slack in the experimental tests. After 40 ms, similar time responses were observed for all the three dummies.

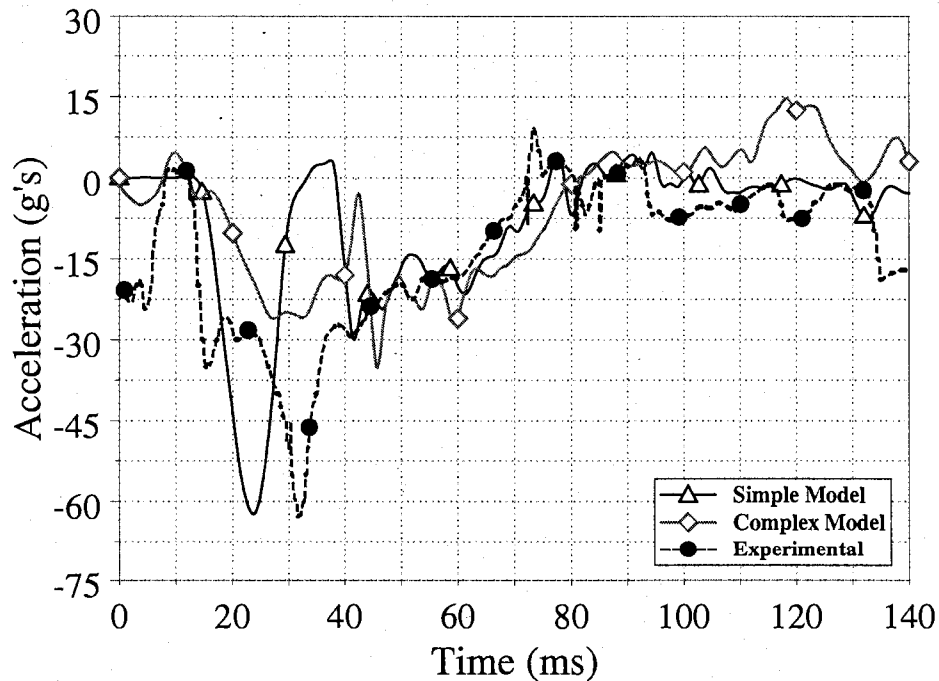


Figure 96. Experimental and numerical chest accelerations in the local x -axis direction.

Experimental and numerical chest accelerations in the local z-axis direction as a function of time are illustrated in Figure 97. The minimum values predicted for the simple model and the complex model were -37 g's and -30 g's. The experimental dummy exhibited a peak value of -40 g's for the chest z-acceleration. These peak values are noted in Table 8.

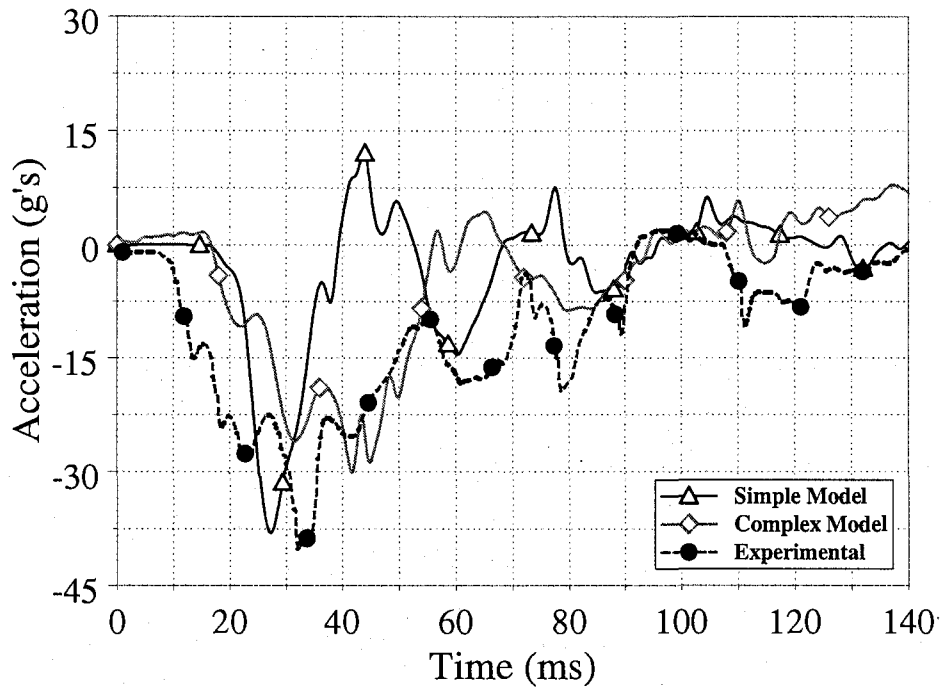


Figure 97. Experimental and numerical chest accelerations in the local z-axis direction.

Table 8. Summary of the peak values of experimental and numerical results from FMVSS 213 test.

Injury Parameters	Experimental	Numerical (Simple model)	Error Analysis		Numerical (Complex model)	Error Analysis	
			E	V		E	V
Head accelerations in x direction (g's)	-22.54	-30.09	0.684	0.523	-43	0.68	0.493
Head accelerations in z direction (g's)	30.45	32.01	0.462	0.64	26.58	0.573	0.572
Chest accelerations in x direction (g's)	-32.74	-32.33	0.373	0.703	-35.12	0.413	0.698
Chest accelerations in z direction (g's)	-40.11	-37.95	0.638	0.528	-30.2	0.471	0.63

Table 8 also tabulates the values for the average error (E) and the validation metric (V) obtained for both the simple and complex models. The data analysis for the

FMVSS 213 sled tests illustrates that the numerical simulation results from the simple model are in a good agreement to the experimental findings but simulation results from the complex model had two notable differences with the test data; peak accelerations and the time to reach the maximum or minimum values. The complex model exhibited similar time response compared to the experimental findings. It has been mentioned earlier that the seatbelt tightening event was not simulated for the simple model, due to which there was a slack in the system. No preloads were utilized for the simple model. Therefore, the similarity of the numerical results from the simple model to the experimental findings could be explained, that there was a similar amount of slack between the seatbelt and the child dummy in the experimental test as well. The slack allowed the dummy's chest to have more forward movement relative to the CRS when the body of the child dummy experienced the acceleration pulse. The fact that the seatbelt failed to hold back the dummy at the beginning of the crash also resulted in the less severe predicted head accelerations of the child dummy.

A parametric study was carried out on the complex model utilizing a Hybrid III 3-year-old dummy in the presence of slack. The seatbelt tightening of the front adjusting harness strap, between the legs of the child, at the far end of the dummy was not simulated. The numerical simulation was completed in accordance with FMVSS 213 norms. This study was performed to validate the above mentioned assumption of the presence of seatbelt slack in the experimental tests.

Similar time profiles with a difference in peak values were observed between the numerical simulations in the presence and absence of seatbelt slack. The peak values for both the simulations are tabulated in Table 9. It can be seen that the simulation results for the seatbelt slack exhibited higher values for the chest acceleration in the local x direction due to forward movement of the dummy. Also, as the slack in the system did not hold back the dummy's head, a reduction in head acceleration in the local x direction and an increase in the head acceleration in the local z direction, compared to the no slack situation was observed. The amount of slack present in the experimental tests was not

measured. The predictions from the parametric study validate the assumption of the presence of slack in the experimental sled tests.

Table 9. Peak values for the parametric study on the seatbelt slack for a simulated FMVSS 213 crash.

Injury Parameters	Experimental results	Numerical results	
		(No Seatbelt Slack)	(Seatbelt Slack)
Head accelerations in x direction (g's)	-22.54	-43	-39
Head accelerations in z direction (g's)	30.45	26.58	34.5
Chest accelerations in x direction (g's)	-62.74	-35.12	-41
Chest accelerations in z direction (g's)	-40.11	-30.2	-27

6.4 Comparison between Hybrid III, Q3 and child FE model

The complex model incorporating the Hybrid III 3-year-old dummy has been validated for FMVSS 213 and CMVSS 208 tests in the previous sections. Zhang et al. [115] have validated the child FE model in accordance with CMVSS 208 conditions. Numerical simulations were completed incorporating Q3 child dummy and the child FE model in accordance with similar FMVSS 213 situations in order to compare the kinematic and kinetic response of the three child models. All the peak values obtained from the data analysis are summarized in Table 10.

6.4.1 Qualitative analysis

Figure 98 provides the side view of the child dummies relative to the CRS at specific intervals of time through the simulations of the prescribed acceleration pulse. This provides a visual comparison of the behaviour of the specimens during the crash. For convenience, the whole simulated event has been divided into five phases.

Phase I depicts the state of rest. At this time both the dummies and the child FE model are seated in their original configuration. Phase II marks the onset of head rotation. At this time both the dummies and the child FE model start moving forward. This was observed to occur at approximately $t = 30$ ms.

The maximum extension in the neck (phase III) was predicted at approximately $t = 65$ ms for all the three FE models. It should also be noted that the maximum neck rotation was predicted to be 77 degrees for the child FE model, 73 degrees for the Q3 dummy and 62 degrees for the Hybrid III 3-year-old dummy. Maximum neck rotation was predicted for the child FE model, which complies with the previous findings by Mizuno et al. [114]. The Q3 dummy exhibited greater neck rotation compared to the Hybrid III dummy which makes it more biofidelic.

Phase IV marks the rebound phase which was observed to occur at approximately $t = 100$ ms (Hybrid III was observed to settled back quicker compared to Q3 and child FE model). The contact between the dummy's head and the CRS (phase V) was observed to occur at $t = 130$ ms for Hybrid III, $t = 138$ ms for Q3 and $t = 147$ ms for the child FE model. This was also noted in the quantitative analysis.

It is evident from Figure 98 that bending of the neck, displacement of the head, and extension of the limbs for the Q3 dummy were similar to those predicted for the child FE model. Thus based upon the kinematic response of the Q3 FE dummy it can be stated that the Q3 dummy more appropriately predicts the response of a child cadaver, as illustrated by the child FE model, (Section 2.9.2.2) [114 and 115] compared to the Hybrid III 3-year-old FE dummy.

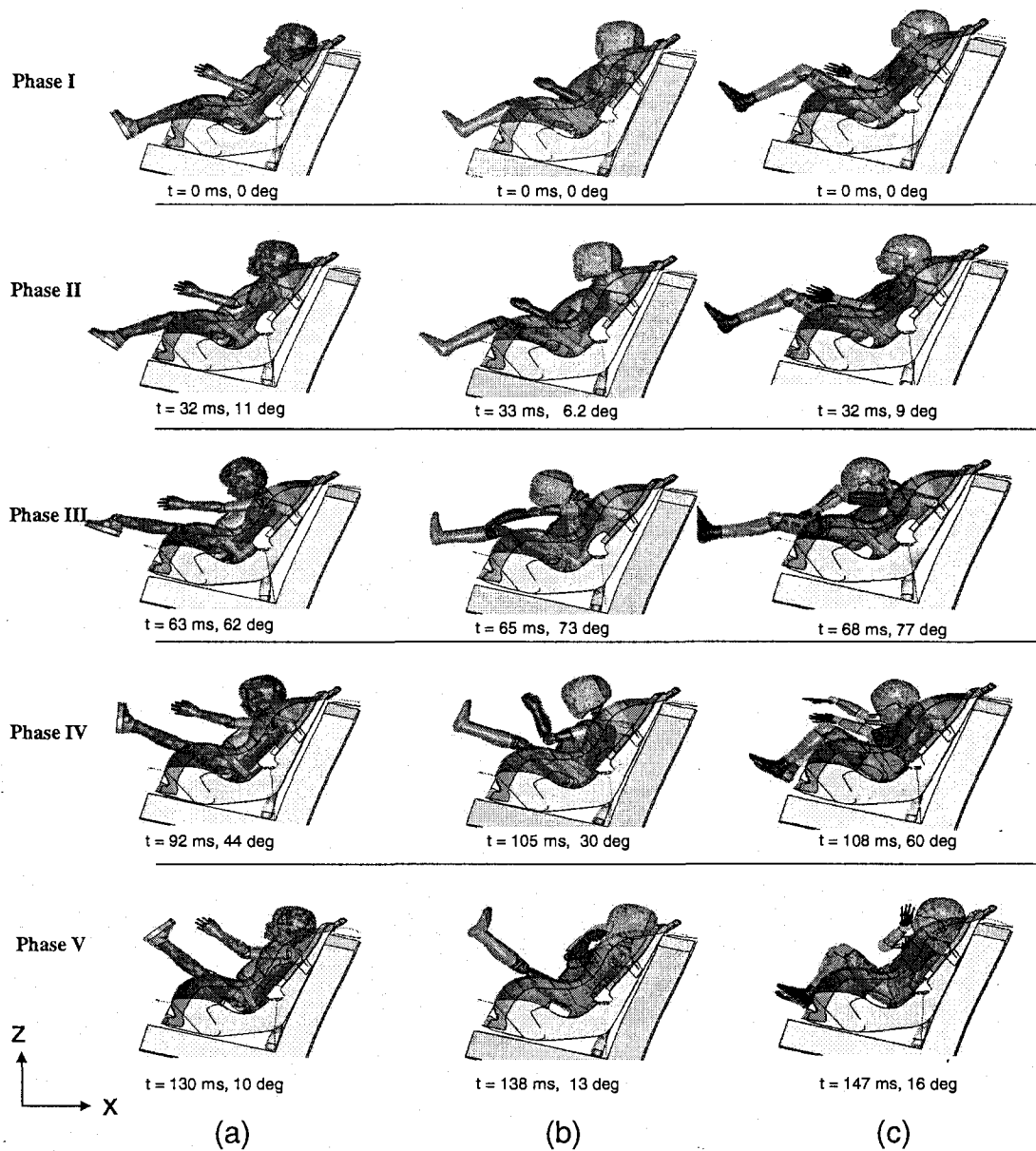


Figure 98. Numerical observations (side view) for the (a) Hybrid III 3-year-old dummy, (b) Q3 child dummy and (c) the child FE model at different durations of time.

6.4.2 Quantitative analysis

6.4.2.1 Resultant head accelerations

Figure 99 illustrates the values of resultant head accelerations for all three child models as a function of time. Similar time profiles were predicted for all three FE models. The maximum resultant head accelerations were predicted to be 50 g's for the Hybrid III 3-year-old child dummy, 57 g's for the Q3 dummy and 45 g's for the child FE model. The time required to reach the maximum resultant head acceleration for all three child models was predicted to be approximately 65 ms. This is the time when the head experienced the greatest extension, as shown in Figure 98. A second peak of approximately 45 g's was predicted for the Hybrid III 3-year-old dummy occurring at 130 ms. This is due to the contact of the dummy's head with the CRS after the rebound phase. These peaks were not predicted for either the Q3 dummy or the child FE model.

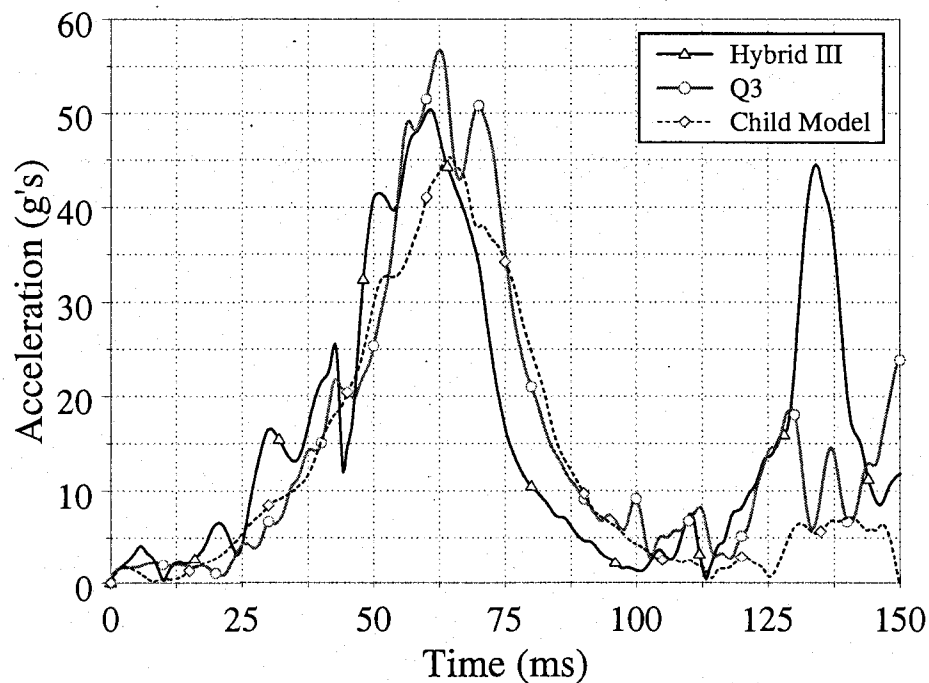


Figure 99. Resultant head acceleration for Hybrid III, Q3 and child FE model as a function of time.

6.4.2.2 Resultant chest accelerations

The resultant chest accelerations for the Hybrid III, Q3 and child FE model as a function of time are exhibited in Figure 100. Similar time profiles were predicted for all the three child models with a difference in peak values. The maximum value for the resultant chest acceleration was predicted to be approximately 44 g's for both the Hybrid III and Q3 child dummies. Comparatively lower values were predicted for the child FE model, the maximum value being 33 g's. The spikes were predicted to occur after 30 ms when the child models start moving forward, up to 70 ms when maximum flexion in the neck is predicted (Figure 98). It should also be noted that after 70 ms, higher peaks were predicted for the Q3 dummy and the child FE model compared to the Hybrid III dummy. This can be attributed to the flexion of the upper torso and the head contact with the sternum in the child FE model and the Q3 dummy.

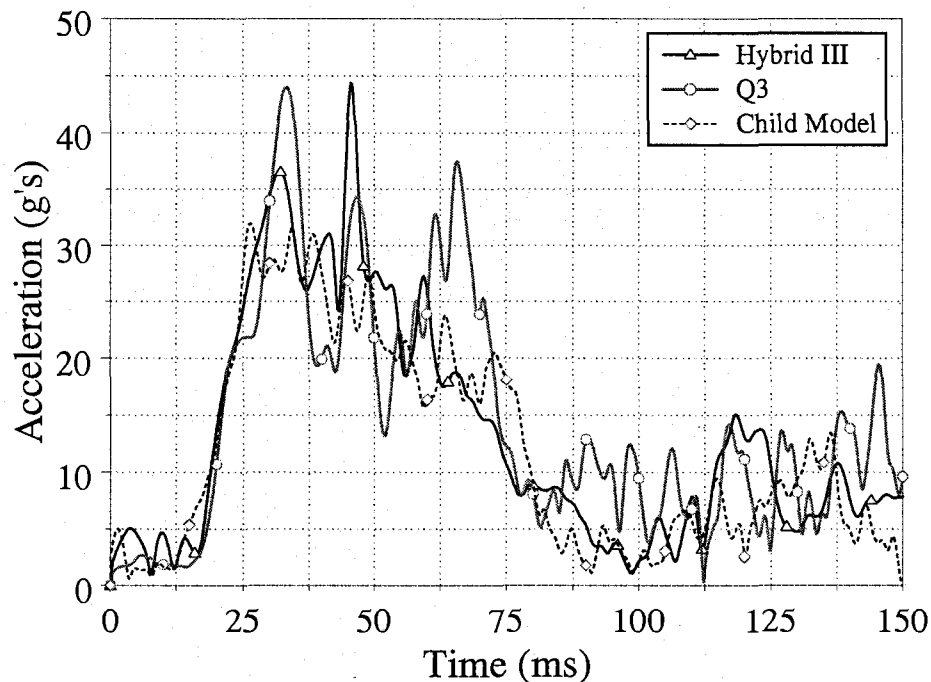


Figure 100. Resultant chest acceleration for Hybrid III, Q3 and child FE model as a function of time.

6.4.2.3 Head injury criteria

HIC was calculated over a 15 ms and 36 ms evaluation period for all three child models using equation 1. Figure 101 illustrates the values of HIC_{36} (as these values were greater than HIC_{15}). All the child dummies exhibited similar maximum values for HIC_{15} . The peak values of HIC_{15} for Hybrid III, Q3 and child FE models were predicted to be 204, 263 and 178 respectively. Likewise, the maximum values for HIC_{36} were similar, which were 260 for Hybrid III, 272 for child FE model and 337 for the Q3 child dummy. It should be noted that Q3 dummy exhibited higher HIC values compared to the Hybrid III dummy and the child FE model. This is due to a higher degree of neck rotation for the Q3 dummy. The limiting values recommended for HIC_{15} and HIC_{36} by NHTSA are 570 and 1000 respectively [73], and the HIC values for both of the dummies and the child FE model were considerably lower than these limiting values.

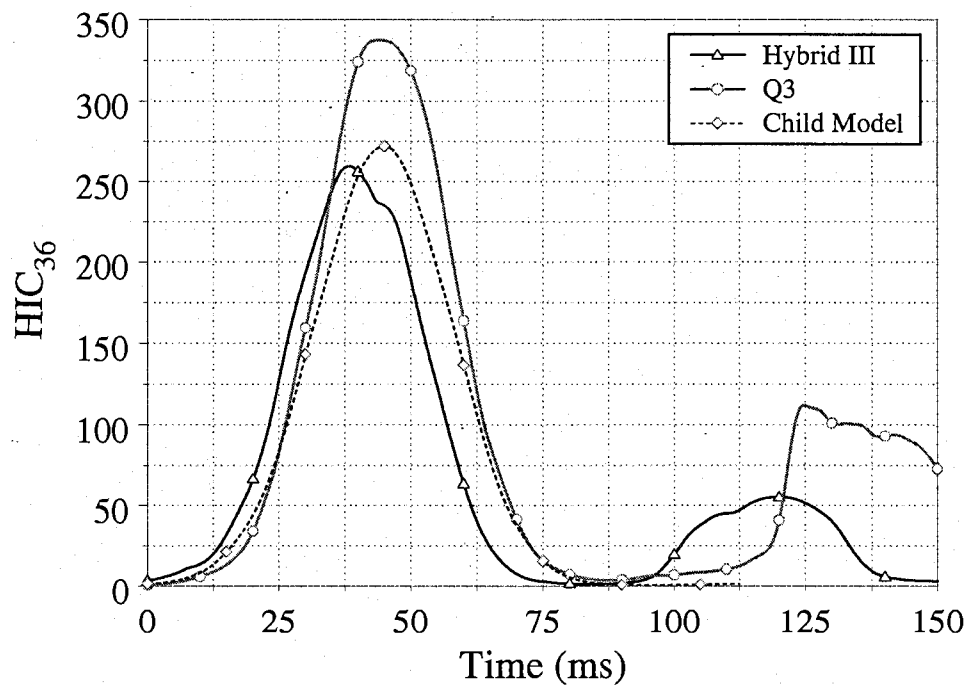


Figure 101. HIC_{36} for Hybrid III, Q3 and child FE model as a function of time.

6.4.2.4 Head trajectories

Figure 102 presents the trajectories of the centre of mass of the head (local z axis displacements as a function of local x axis displacements) for the three dummies. The displacements were measured relative to the rigid portion of the seat buck. Greater head excursions were predicted for the child FE model. These observations can be attributed to the fact that the Hybrid III dummy's neck is stiffer compared to the actual child, which conforms with the findings of Mizuno et al. [114] and Zhang et al. [115]. The Q3 head trajectories were predicted to be similar to the head profiles for the child FE model. Therefore it can be stated that the Q3 neck is more biofidelic compared to the Hybrid III 3-year-old dummy.

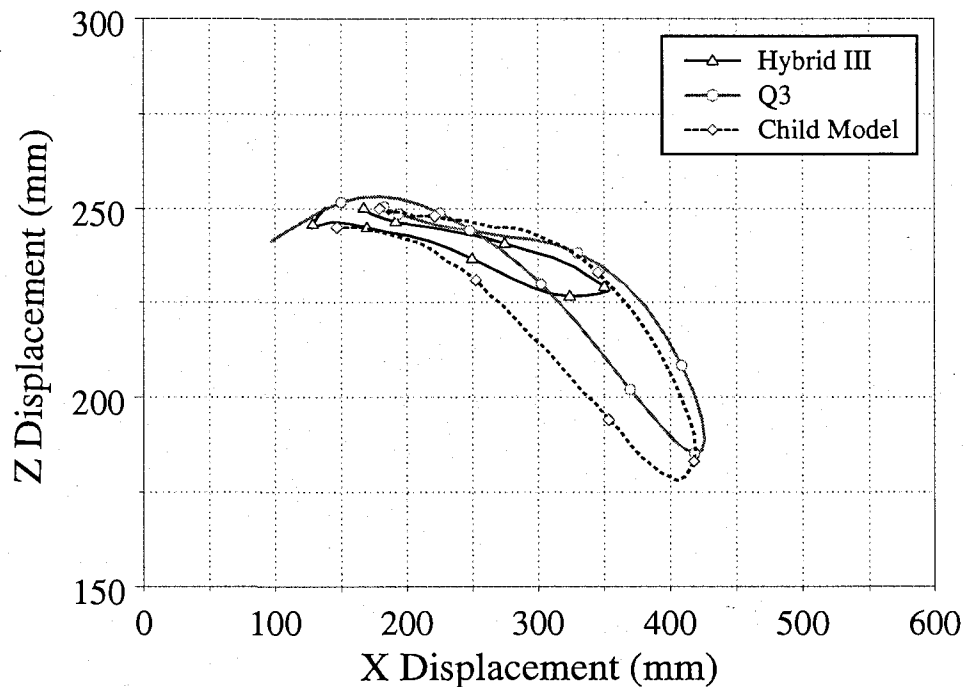


Figure 102. Head trajectories of the centre of mass of the head for the Hybrid III, Q3 and child FE model.

6.4.2.5 Upper neck resultant forces and moments

The child FE model is not equipped with load cells in the neck region. Therefore resultant forces and moments were evaluated for the Hybrid III and the Q3 dummies from the information obtained from the load cell located in the upper neck. Figure 103 illustrates the resultant upper neck forces for the two dummies, and the cross-sectional forces in the upper neck region for the child FE model as a function of time. Both the dummies exhibited similar time profiles. The maximum values of resultant upper neck forces were predicted to be 1835 N for the Hybrid III and 2100 N for the Q3 dummy. The maximum value of the child FE model sectional force was predicted to be 1107 N.

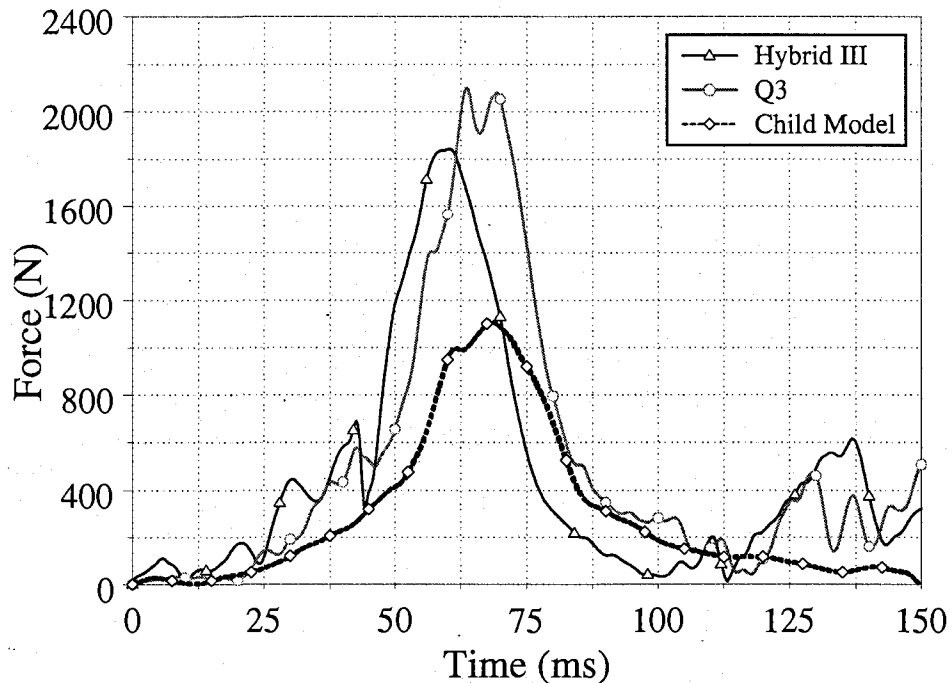


Figure 103. Resultant upper neck forces for the Hybrid III and Q3 dummy, and cross sectional forces for the child FE model as a function of time.

Since the child FE model is not equipped with any instrumentation, cross-sectional forces serve as an appropriate way of accessing neck loads. Neck loads were also calculated based on the resultant head acceleration multiplied by the mass of the head (2.79 kg). It was observed that both the responses (based on cross-sectional

forces and the product of head mass and resultant head accelerations) exhibited similar peak values and magnitudes throughout the time domain. Therefore the force data obtained from the cross-sectional planes in the upper neck region of the child FE model can be appropriately used. The correct moments could not be obtained for the child FE model using the data acquired for the cross-sectional planes. The cross-sectional forces obtained from the child FE model were observed to be less than the forces obtained from the upper neck load cells in both the Hybrid III and the Q3 child dummies. This can be attributed to the fact that the cross-sectional data does not take into account the force data obtained from the discrete elements passing through the cross-sectional plane. Therefore, throughout this dissertation, the forces obtained from the child FE model's neck have been labeled as cross-sectional forces instead of upper neck forces.

The resultant upper neck moments for Hybrid III and Q3 dummies are exhibited in Figure 104 as a function of time. Neck moment data could not be obtained from the cross sectional planes for the child FE model. Both the dummies illustrated similar time profiles with a difference in peak values. The maximum value of resultant upper neck moment was observed to be 31 N·m for the Hybrid III dummy at 45 ms, whereas the maximum value of resultant upper neck moment for the Q3 dummy was noted to be 18.5 N·m at 67 ms. Higher values of neck moment were observed for the Q3 dummy compared to the Hybrid III dummy after 60 ms. This is due to greater flexion and neck rotation in the Q3 neck compared to the Hybrid III dummy. Also a second peak of 40 N·m was observed for the Hybrid III dummy at approximately 137 ms. This is due to the contact of the dummy's head with the CRS. This contact between the dummy head and the CRS was not observed for the Q3 dummy. Table 10 tabulates the peak values observed for all the three child models.

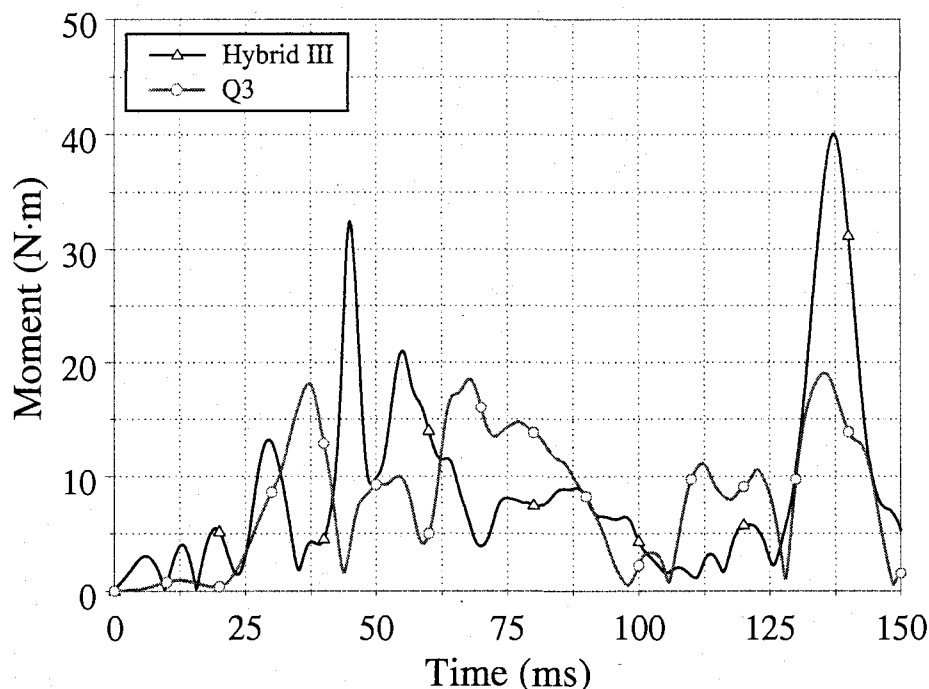


Figure 104. Resultant upper neck moments for the Hybrid III and Q3 dummy as a function of time.

6.4.2.6 Neck injury criteria

Figure 105 illustrates the N_{ij} as a function of time for both the Hybrid III and the Q3 child dummies. The critical intercept values for the Q3 dummy have not been established; therefore the values outlined for the Hybrid III crash test dummy were used to evaluate the neck injury criteria for the Q3 dummy. The neck injury criteria could not be evaluated for the child FE model due to the lack of upper neck moment data. The N_{ij} presented in Figure 105 was evaluated using Equation 3 based upon the information acquired from the upper neck load cell. Maximum values of the N_{ij} for both the Hybrid III and Q3 dummies were 0.96 and 1.21 respectively.

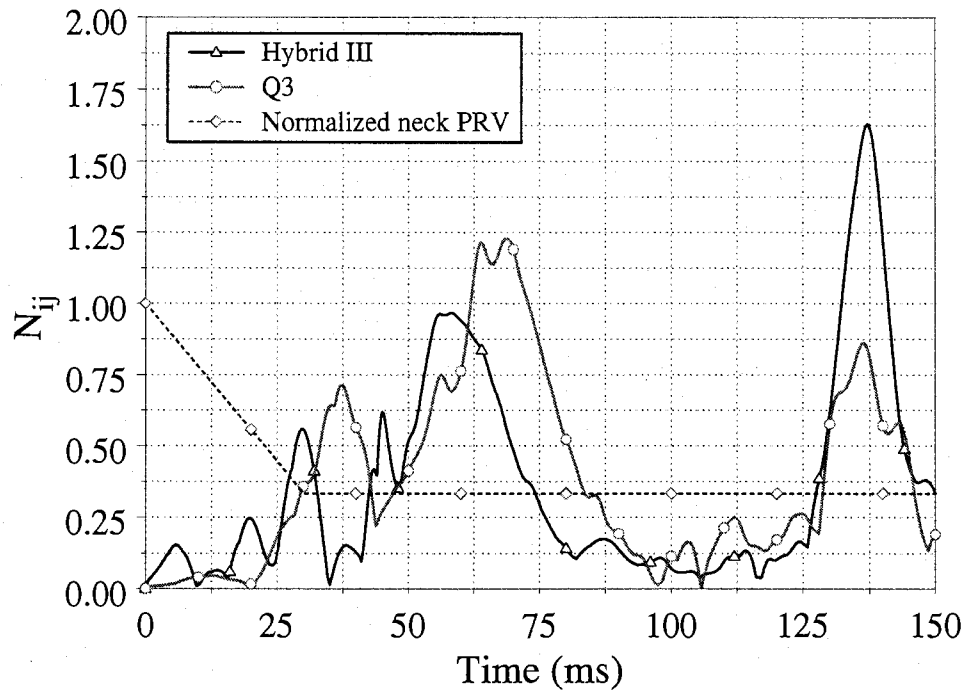


Figure 105. N_{ij} for the Hybrid III and Q3 as a function of time.

Table 10. Summary of peak values of all injury parameters for the Hybrid III, Q3 and child FE model for the simulated 213 test.

Injury Parameter	Hybrid III	Q3	Child FE Model
Resultant head acceleration (g's)	49.6	56.2	45.4
Resultant chest acceleration (g's)	44	43.7	31
HIC-15	204	263	178
HIC-36	260	337	272
Resultant upper neck force (N)	1835	2100	1107
Resultant lower neck force (N)	780	562	n/a
Resultant upper neck moment (N.m)	31	18.5	n/a
Resultant lower neck moment (N.m)	147	115	n/a
Upper neck injury criteria (N_{ij})	0.96	1.21	n/a
Probability of AIS 3+ head injuries (%)	6.7	10.8	5.4
Probability of AIS 3+ neck injuries (%)	20.48	30.47	n/a
Probability of AIS 3+ chest injuries (%)	46.87	46.87	24.3

6.4.3 Discussion

Similar acceleration/time profiles were observed for resultant head and chest accelerations for all the three finite element models. Through the qualitative comparison it was observed that the child model and the Q3 dummy exhibited a higher magnitude of head rotation about the global y-axis compared to the Hybrid III child dummy. The maximum values were observed to be 77 degrees for child model, 73 degrees for the Q3 child dummy and 62 degrees for the Hybrid III 3-year-old child dummy. The child FE model and the Q3 dummy exhibited greater head excursions compared to the Hybrid III 3-year-old child dummy. Thus based upon the kinematic response of the Q3 dummy it can be stated that the Q3 dummy more appropriately predicts the response of a child cadaver as illustrated by the child FE model, (Section 2.9.2.2) [114 and 115] compared to the Hybrid III 3-year-old dummy.

6.5 Finite element model validation - CRS compressive test

During side impact crashes there exists a contact between the CRS and the vehicle interior. Also, there exists a direct contact between the child and the side structures of the CRS. The main cause of injuries in side impact crashes is contact between the child and vehicle interior or the CRS [54, 63 and 64]. A compressive test was conducted on the side-wings of an actual CRS obtained from Graco Corporation to obtain its mechanical behaviour.

6.5.1 Experimental CRS compressive test

The compressive test was completed on a hydraulic Tinius-Olsen testing machine at room temperature. The CRS was placed on a translating crosshead of the compression testing machine such that the lateral direction of the CRS was parallel to the direction of translation of the moving crosshead. The testing configuration is illustrated in Figure 106 and Figure 107. An extra wood block was placed under the CRS in order to maintain the CRS balance during the test and so the forces could evenly pass through the wood block

to the moving crosshead. A fixed crosshead was located above the CRS to the extent that the fixed crosshead contacted one side wing of the CRS without generating any initial forces or any deformation from the seat. The load cell used to measure the compressive force had a range of 150 kN. Displacement was measured using a linear voltage differential transformer (LVDT) with a range of 150 mm. A personal computer equipped with data acquisition software was used to record the measurements from the load cell and the LVDT at a sampling rate of 60 Hz. The nominal speed of the translating crosshead was approximately 15 mm/min. At this testing speed, it was considered acceptable to evaluate the crush behaviour as quasi-static deformation. In the loading phase of the test, the side wings of the CRS deformed gradually as the translating crosshead traveled approximately 140 mm vertically. The side wing contacting the fixed crosshead had more local deformation than the other side wing due to reduced contact areas of the rigid testing platform. In the unloading phase of the test, the CRS returned to its former shape and no significant permanent deformation was observed from the seat after the test. A force versus displacement curve with both loading and unloading phases of the CRS was obtained from the compressive test.

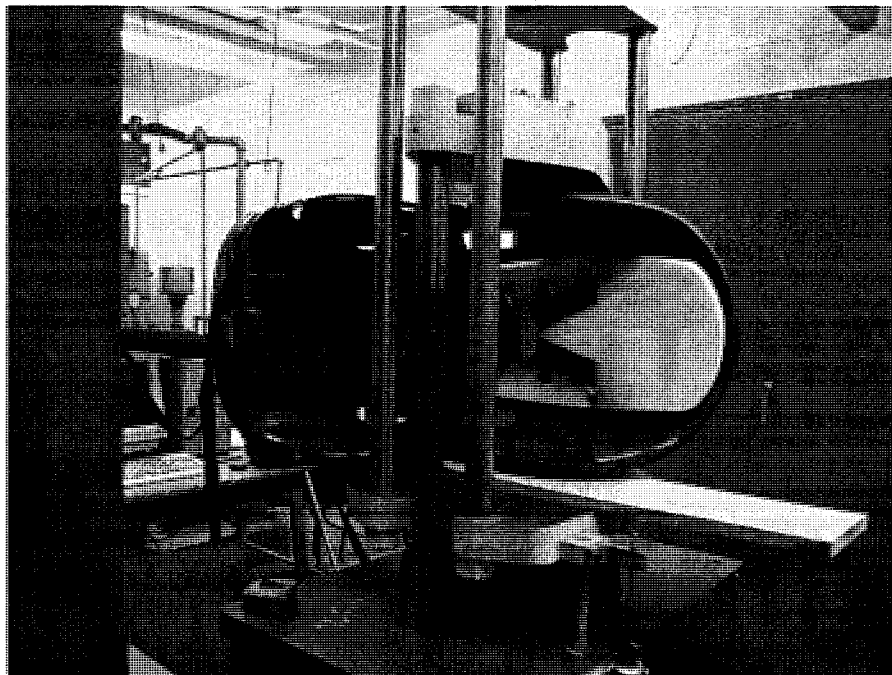


Figure 106. Isometric view of the testing configuration of the CRS compressive test.

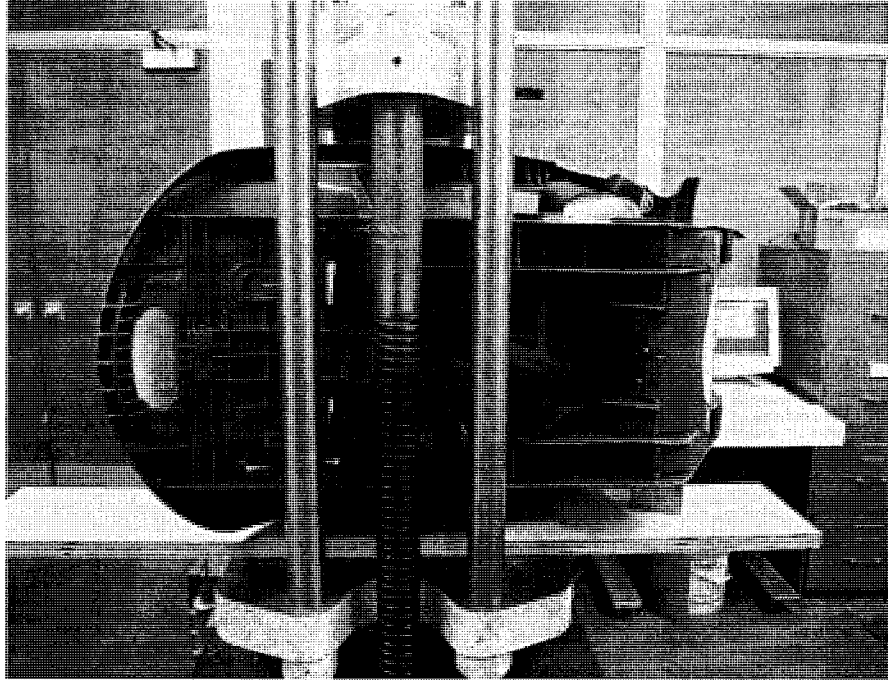


Figure 107. Rear view of the testing configuration of the CRS compressive test.

6.5.2 Simulation procedure

A numerical model was developed of the experimental compressive test. The geometry of the Tinius-Olsen testing machine was measured and used in the finite element model construction. Rigid material definition was used for all the components of Tinius-Olsen testing machine. Figure 108 illustrates all entities associated with the numerical model of the compressive test. Numerical simulation was completed under similar test conditions and the numerical model validation was based on the data comparison of the force versus displacement responses from the experimental and numerical tests.

LS-DYNA USER INPUT
Time = 0

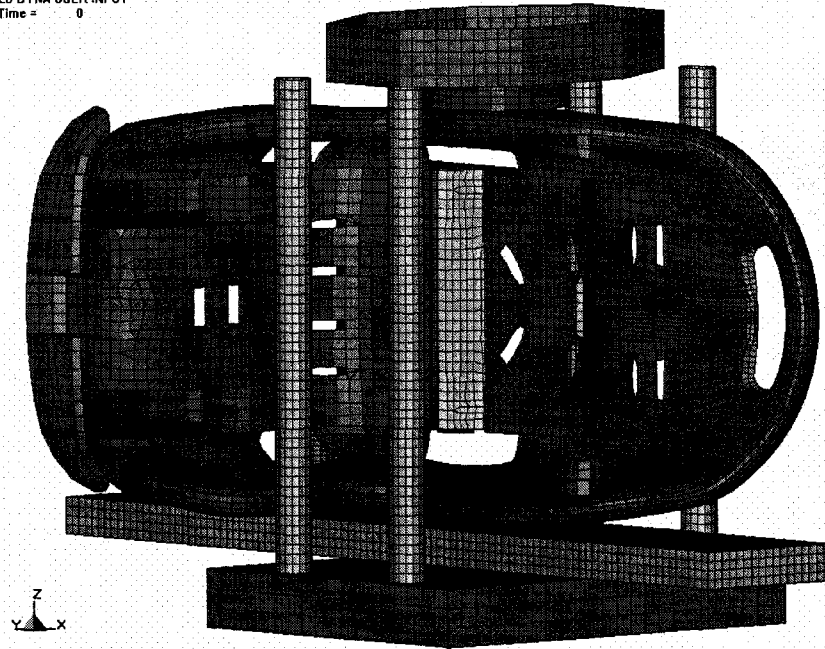


Figure 108. Isometric view of the numerical model of the CRS compressive test.

A prescribed displacement of 140 mm was assigned to the fixed crosshead, which could translate in global Z-direction. The other parts of the testing machine were constrained in all directions. An automatic surface to surface contact algorithm was used to model contact between the CRS and all parts of the testing machine.

The termination time of the simulation was 20 minutes. Given that the test was considered to be a quasi-static process, a static analysis was completed. The numerical simulations were completed using an implicit solver in LS-DYNA. Values for the displacement convergence tolerance and energy convergence tolerance were 0.010 and 0.15 respectively. Approximate 400 steps were utilized in the side crushing simulation of the CRS.

6.5.3 Numerical model validation - CRS compressive test

The numerical simulations exhibited a greater amount of permanent deformation in the CRS compared to the experimental tests. This can be attributed to different material properties as well as differences in testing methodology. Also, the configurations

of the two tests were not exactly the same, especially the location of the fixed crosshead where the compressive force was applied, which could significantly affect the way the CRS deformed.

Figure 109 illustrates the force versus displacement curves obtained from the experimental and numerical tests. The testing apparatus utilized in the numerical simulations was not identical to the experimental compressive test. In general, the maximum relative movement of the two side wings of the CRS in the lateral directions for most side impact simulations was observed to be no greater than 60 mm. In fact, in most side impact cases only one side wing would have a large amount of deformation. Model validation technique noted in Section 6.1 was utilized to validate the numerical simulation predictions with the experimental testing results for the first 100 mm of displacement. The values for the average relative error (E) and the validation metric (V) were calculated as 0.254 and 0.756 respectively. Therefore an acceptable correlation was obtained between the experimental and the numerical CRS compressive tests.

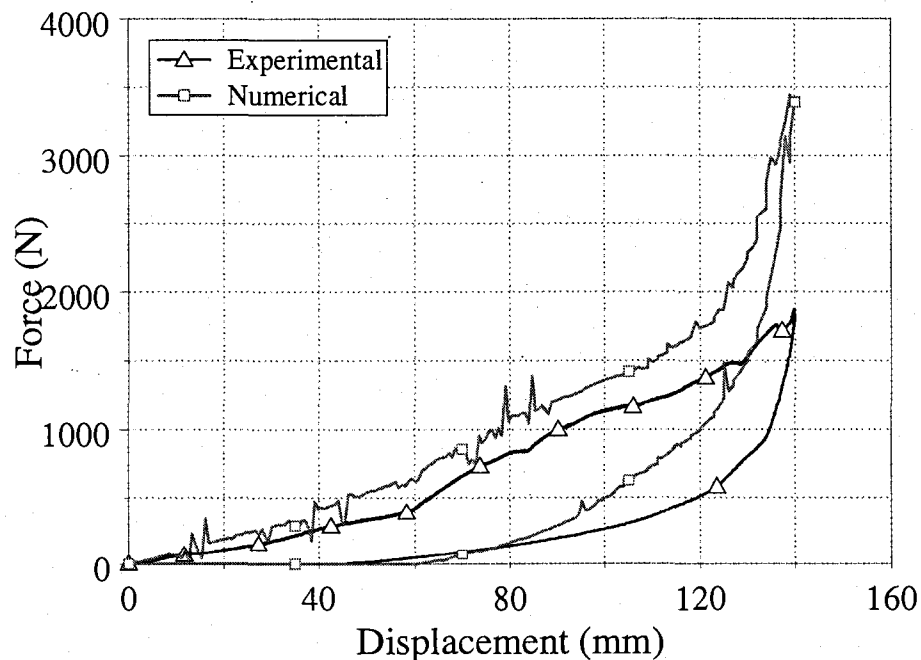


Figure 109. Force versus displacement curves of the compressive test.

6.6 Finite element model validation – 4585 near-side impact sled test

The complex model has previously been validated by Wang et al. in far-side crash situations in accordance with ANPRM FMVSS (213) norms [117]. Side impact dynamic sled tests were conducted by NHTSA at TRC using a Hybrid III 3-year-old child dummy seated in a convertible forward/rearward child safety seat [105]. The seat was equipped with a LATCH and a top tether and the dummy was positioned in a forward-facing/near-side configuration. The test was completed using an acceleration pulse with a closing speed of 24.1 kph, in the presence of a rigid wall and in the absence of a vehicle body.

The numerical model utilizing a Hybrid III 3-year-old dummy, employing a similar set-up as the experimental sled test was generated and simulated using LS DYNA. A rigid wall was meshed using shell elements on the seat buck which represents the location of a vehicle's side structure, positioned 508 mm from the point Z1, adjacent to the CRS [15]. The rigid wall was meshed extending from the seat cushion to a height of approximately 762 mm. The wall extended forward a distance of approximately 690 mm, to ensure that head contact would only be with a flat surface. The wall was modeled using a rigid material definition in LS-DYNA. The acceleration pulse obtained from the experimental sled test is presented in Figure 37. Finite element model validation was completed by comparing the numerical simulation results with the experimental findings from the side impact tests which involved the Hybrid III dummy only. For all tests, the comparison was based on the lateral head and chest accelerations as well as the resultant upper and lower neck forces and moments. Figure 110 illustrates the isometric view of the complete FE model of the Hybrid III 3-year-old child dummy seated in the CRS and the initial configuration of the numerical model in accordance to FMVSS 213 norms.

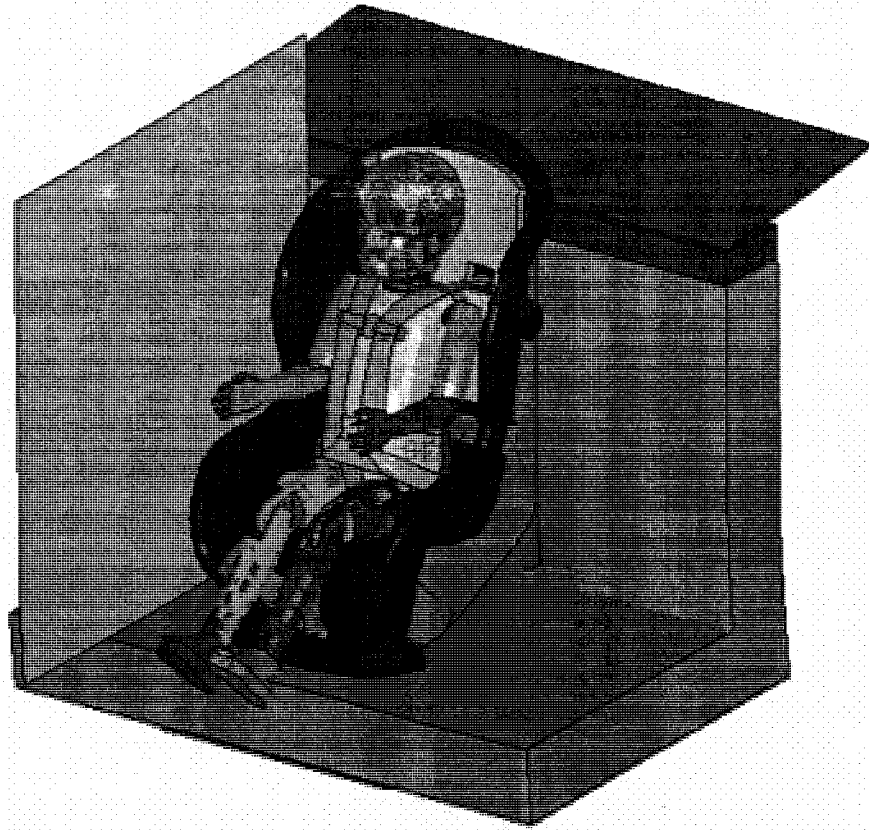
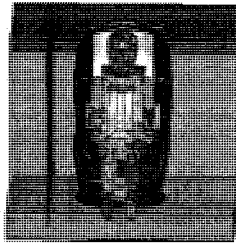


Figure 110. Hybrid III 3-year-old child dummy seated in the CRS for the rigid-wall near-side impact test.

6.6.1 Qualitative analysis

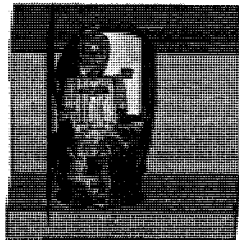
The videos of the experimental sled test were not available to the author. Figure 39 illustrates the experimental sled test results obtained from NHTSA [105]. The test results exhibit a contact between the dummy's head and the side wings of the CRS. Also, a minor contact between the dummy's head and the rigid wall was observed. Figure 111 illustrates the front view of the numerical simulation at different time durations. The simulation event has been divided into five phases. Phase I depicts the original configuration of the dummy at the time of application of the acceleration pulse. Phase II occurs when the dummy and the CRS start moving laterally towards the rigid wall. This was observed at $t = 44$ ms.

The maximum CRS and head lateral displacement (Phase III) for the numerical simulations was observed to occur at approximately $t = 66$ ms. At this time the CRS and foot contact with the rigid wall was observed. In addition a contact between the dummy's head and the side wings of the CRS occurred. This contact is consistent with the experimental observations. No head contact of the Hybrid III dummy was observed with the rigid wall. This can be attributed to difference in the CRS used for both the tests. Also, there could be a difference in the neck stiffness of the experimental and the numerical dummies. After this time the dummy and the CRS started rebounding back (Phase IV) at approximately $t = 80$ ms. Phase V is the stage when the dummy settles laterally back into the CRS.



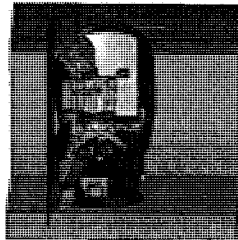
t = 0 ms

Phase I



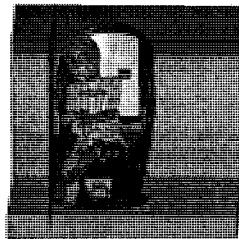
t = 44 ms

Phase II



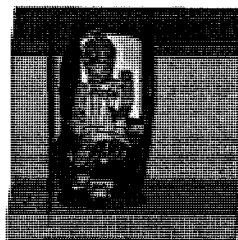
t = 66 ms

Phase III



t = 80 ms

Phase IV



t = 120 ms

Phase V

Figure 111. Numerical observations for the 4585 near-side impact test.

6.6.2 Quantitative analysis

Data comparison was carried out based on head and chest accelerations in the local y-axis direction, and resultant upper and lower neck forces and moments. There appeared to be a slight shift in time between the experimental and numerical acceleration pulses for the near-side impact sled tests. The CRS used in the experimental test was a Cosco Forerunner, and the CRS used for the numerical simulations was Graco forward/rearward convertible. This time shift can be due to the difference in the CRS's used for the experimental and numerical investigations. The time difference between these two testing methods was estimated to be no greater than 15 ms. The time shifts have been adjusted in the quantitative analysis.

6.6.2.1 Head acceleration in the local y-direction

Figure 112 shows the experimental and numerical results of the child dummy's head accelerations in the local y-direction as a function of time. Head accelerations in the local y-direction were the result of the dummy's head experiencing the acceleration pulse in the lateral direction resulting in contact with the side wing of the child safety seat. The acceleration response of the Hybrid III dummy from the numerical simulation showed similarities to the experimental results. The minimum values for y-axis head acceleration were observed to be -45 g's for the numerical simulations and -51 g's for the experimental dummy respectively. The time to reach the peaks was approximately 60 ms for both the tests. This is the time when the contact between the head of the dummy and the CRS side wings occurs (Figure 111).

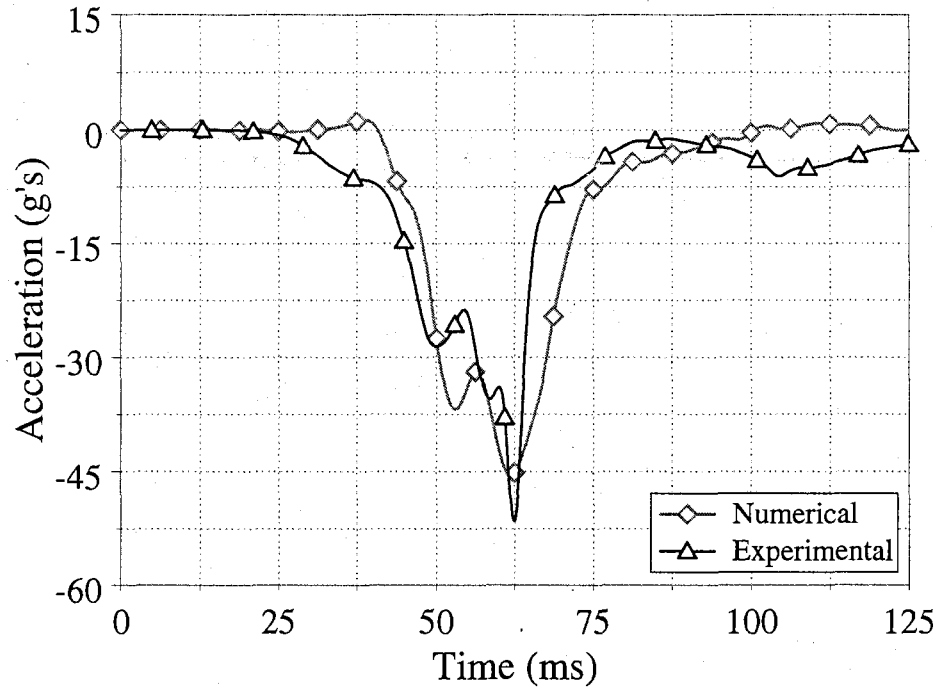


Figure 112. Experimental and numerical head acceleration in local y-axis direction as a function of time.

6.6.2.2 Chest acceleration in the local y-direction

The chest accelerations in local y-direction as a function of time are presented in Figure 113. Similar time profiles were observed for both the experimental results and numerical predictions. The peak values for the chest acceleration in local y-axis direction were observed to be approximately -69 g's for both the numerical and experimental tests. The time to reach the peaks was approximately 50 ms for both the cases.

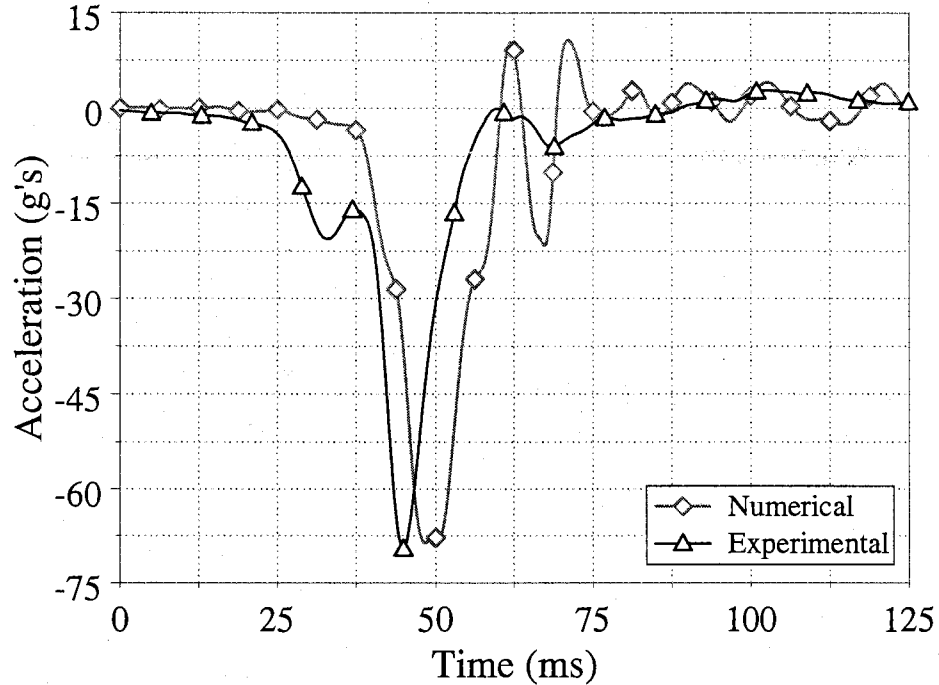


Figure 113. Experimental and numerical chest acceleration in local y-axis direction as a function of time.

6.6.2.3 Resultant upper and lower neck forces

Figure 114 and Figure 115 respectively demonstrate the resultant upper and lower neck forces experienced by the child dummy. Numerical simulations exhibited similar time profiles for the resultant neck loads with a difference in peak values. The maximum values for the resultant upper neck forces were 965 N and 1177 N for experimental and numerical tests respectively. The maximum values for the resultant lower neck forces were observed to be 1021 N for the experimental child dummy, and 1288 N for the numerical child dummy respectively. The numerical model over-predicted the resultant peak neck forces from experimental tests by approximately 20 percent.

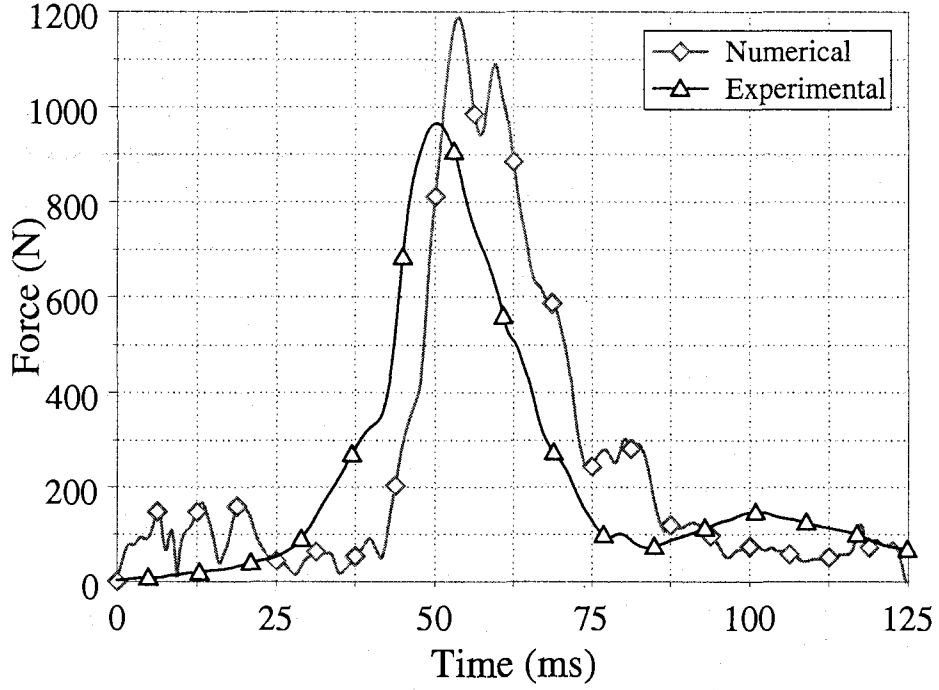


Figure 114. Experimental and numerical resultant upper neck force as a function of time.

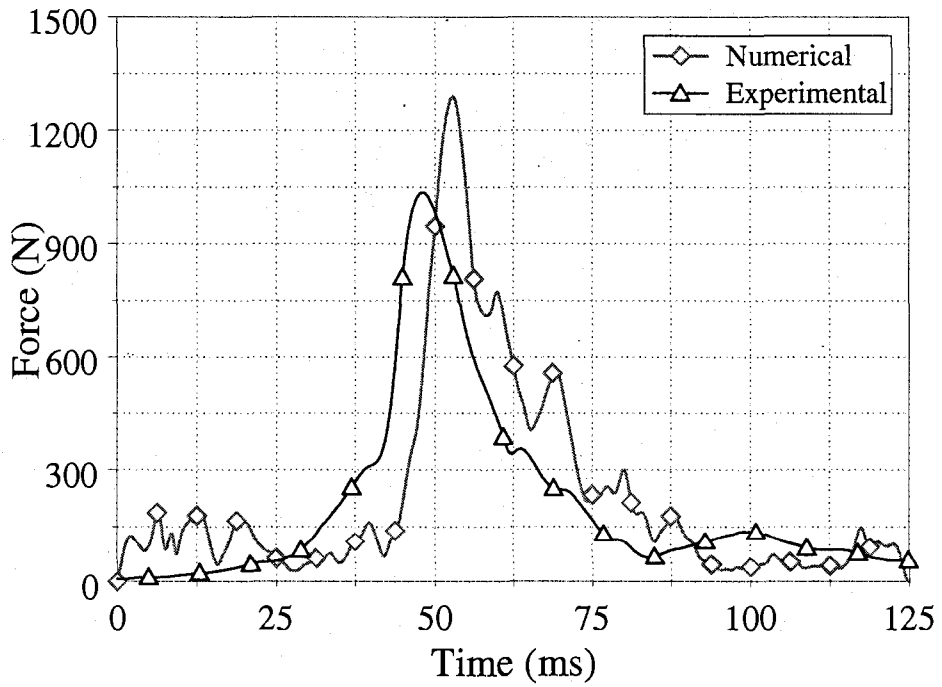


Figure 115. Experimental and numerical resultant lower neck force as a function of time.

6.6.2.4 Resultant upper and lower neck moments

The time profiles for the resultant upper and lower neck moments of the child dummy are illustrated in Figure 116 and Figure 117 respectively. The resultant upper and lower neck moments of the child dummy were over-predicted by the numerical model. Variation in the peak values for the resultant upper and lower neck moments may be due to the use of different child restraining systems. The peak resultant upper neck moments were 45 N·m and 75 N·m for experimental and numerical tests respectively. The respective peak resultant lower neck moments were 105 N·m for the experimental child dummy and 165 N·m for the numerical child dummy. It should be noted that the maximum moments were observed at approximately 60 ms for the numerical dummy. At this time the maximum lateral displacement of the dummy's head was observed (Figure 111).

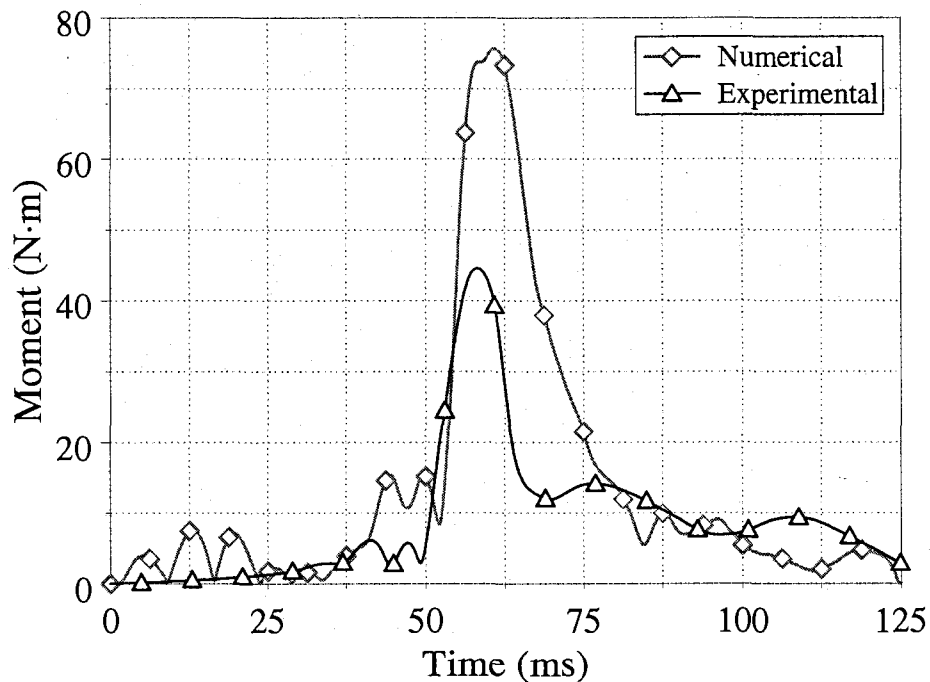


Figure 116. Experimental and numerical resultant upper neck moment as a function of time.

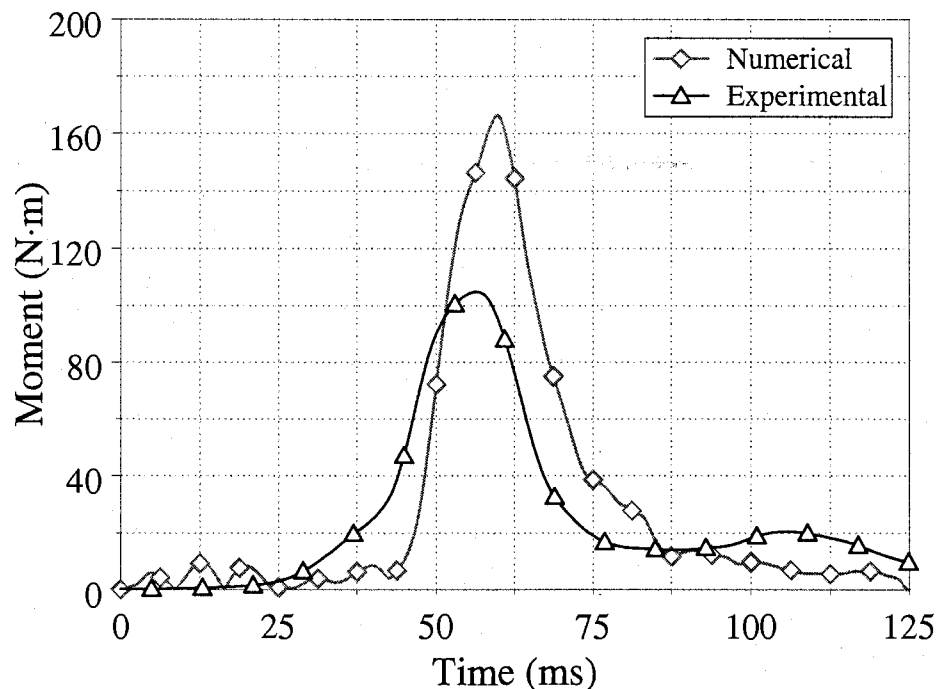


Figure 117. Experimental and numerical resultant lower neck moment as a function of time.

Table 11 summarizes the peak values of all the injury parameters for the experimental and numerical results. Table 11 also tabulates the values for the average error (E) and the validation metric (V).

Table 11. Summary of peak values of all injury parameters for experimental and numerical sled tests (Test No. 4585) incorporating Hybrid III 3-year-old dummy.

Injury Parameters	Experimental	Numerical	Error Analysis	
			E	V
Head y-axis acceleration (g's)	-51.4	-45.5	0.27	0.804
Chest y-axis acceleration (g's)	-69.5	-68.2	0.225	0.848
Resultant upper neck forces (N)	963.45	1186.4	0.404	0.665
Resultant lower neck forces (N)	1021	1288	0.337	0.715
Resultant upper neck moments (N·m)	44.5	75.5	0.432	0.707
Resultant lower neck moments (N·m)	105	165	0.469	0.612

Numerical simulations were observed to be in a good agreement with the experimental findings in terms of head and chest local y-axis accelerations, and upper and

lower neck forces. The resultant upper and lower neck moments of the child dummy were over-predicted by the numerical model. This can be attributed to the difference in the CRS's used for the experimental and the numerical tests. In addition, there could be a difference in the contact frictional behaviour between the CRS and the dummy's head; and the CRS and the rigid wall. Also, there could be a difference between the neck stiffness of the experimental and the numerical dummies. An acceptable correlation between the numerical simulation results and the experimental findings shows the numerical model's ability to predict the kinetic response, which the Hybrid III 3-year-old child dummy experienced in near-side impact sled tests. This model has previously been validated for far-side crash conditions [117]. The simple model was not incorporated for side impact situation as it involves contact between the dummy and the CRS. Since the simple model was modeled rigid, it could not be appropriately used for side impact simulations.

7. FRONTAL IMPACT PROTECTION - REARWARD-FACING

7.1 Simulation procedure

Numerical simulations have been completed by Turchi et al. [100 and 101] that illustrate a reduction in injury parameters for the Hybrid III 3-year-old dummy in the rearward-facing configuration compared to the forward-facing CRS configuration in accordance to FMVSS 213 norms. The simplified rigid model (Section 5.1) was simulated in both forward and rearward-facing CRS configurations utilizing the CMVSS 208 acceleration pulse acquired from the accelerometers mounted in the vehicle during the experimental vehicle crash test (Figure 53), in order to test the efficacy of the simplified CRS model under a more aggressive acceleration pulse. The numerical simulations were completed using the explicit finite element code LS-DYNA version 970 revision 3711 on a personal computer with dual 2.0 GHz AMD Athlon processors with 1 gigabyte of random access memory. The time taken to complete one numerical simulation was approximately 8 hours.

The acceleration pulse was prescribed to the child safety seat in the negative X-direction, restricting the motion of the seat in the Y or Z-directions. This X-axis direction as illustrated in Figure 118 represents a global coordinate system that does not translate or rotate during the impact event. Figure 118 illustrates the configurations of both the forward and rearward-facing configurations at decline angles of 20 degrees and 45 degrees respectively.

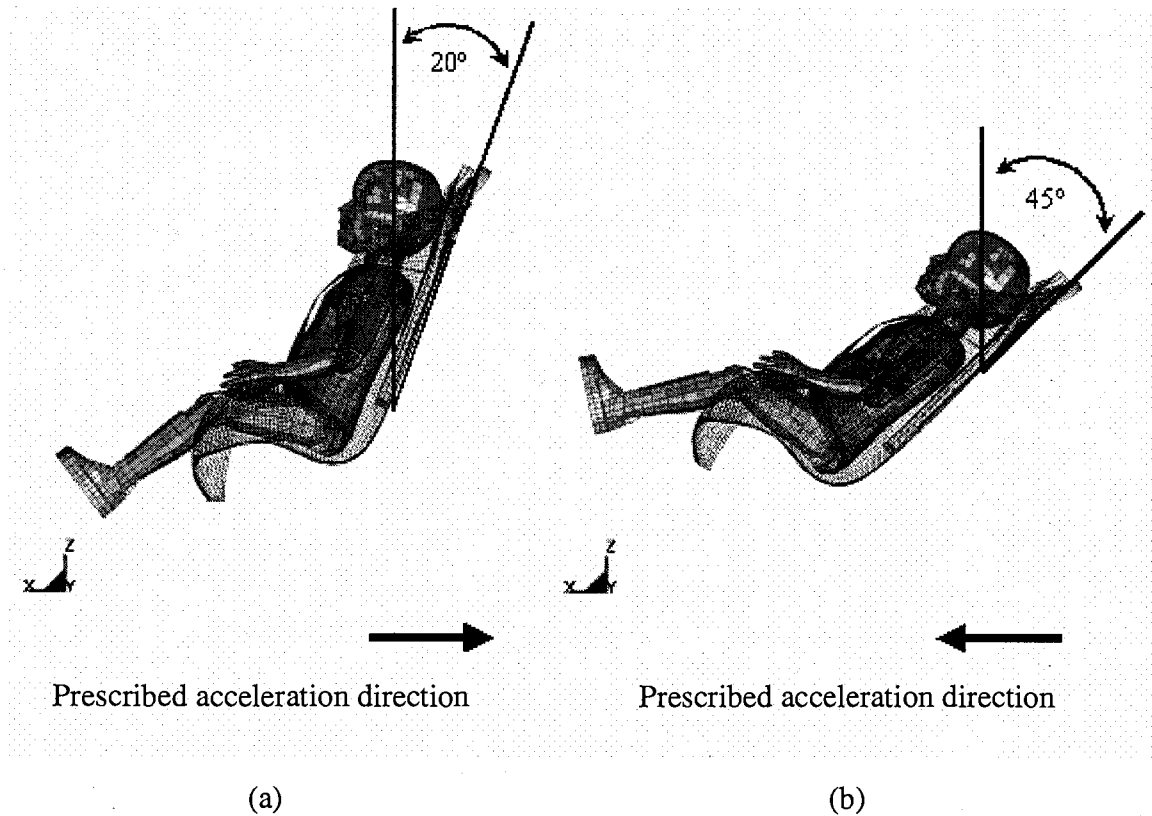


Figure 118. Hybrid III 3-year-old dummy model in (a) forward and (b) rearward-facing configurations.

Numerical simulations were used to compare the head and neck injury potential for the Hybrid III 3-year old child dummy in both forward and rearward-facing CRS configurations which were subjected to the same acceleration pulse (Figure 53). The Hybrid III dummy was designed for frontal impact situations and technically is not acceptable to be used in the simulation of the rearward-facing condition. However, Lau et al. [129] found that regardless of the intended application of the dummy, it has been utilized in a variety of impact environments due to the lack of viable alternatives. The frontal crash simulation of the rearward-facing CRS and child dummy was completed by reversing the direction of application of the acceleration pulse and declining the CRS to an angle of 45 degrees to the vertical.

7.2 Qualitative analysis

Illustrated in Figure 119 is the positioning of the child dummy, relative to the CRS, at specific instants of time through the simulations of the prescribed acceleration pulse to the CRS in both forward and rearward-facing configurations. The entire simulation period has been divided into five phases. Phase I occurs at $t = 0$ ms, when both the dummies are seated in their original configurations. At $t = 30$ ms (Phase II), the dummy seated in the forward-facing configurations started moving forward, whereas the rearward-facing dummy moved into the back of the child safety seat.

For the forward-facing configuration the maximum head excursion, bending in the neck and extension of the limbs, that marks Phase III, was predicted at approximately $t = 85$ ms. It is evident from Figure 119 that bending of the neck, displacement of the head, and extension of the limbs were typically much more severe for the child dummy in the forward-facing configuration.

Phase IV was predicted to occur at $t = 110$ ms, when the forward-facing dummy started to rebound back into the CRS. The rearward-facing dummy was predicted to settle back into the CRS. The head of the rearward-facing dummy was supported by the back of the CRS throughout the simulation. Finally, Phase V is the stage when the forward-facing dummy's head made contact with the back of the CRS. Qualitatively, the images project the rearward-facing configuration to be safer than the forward-facing.

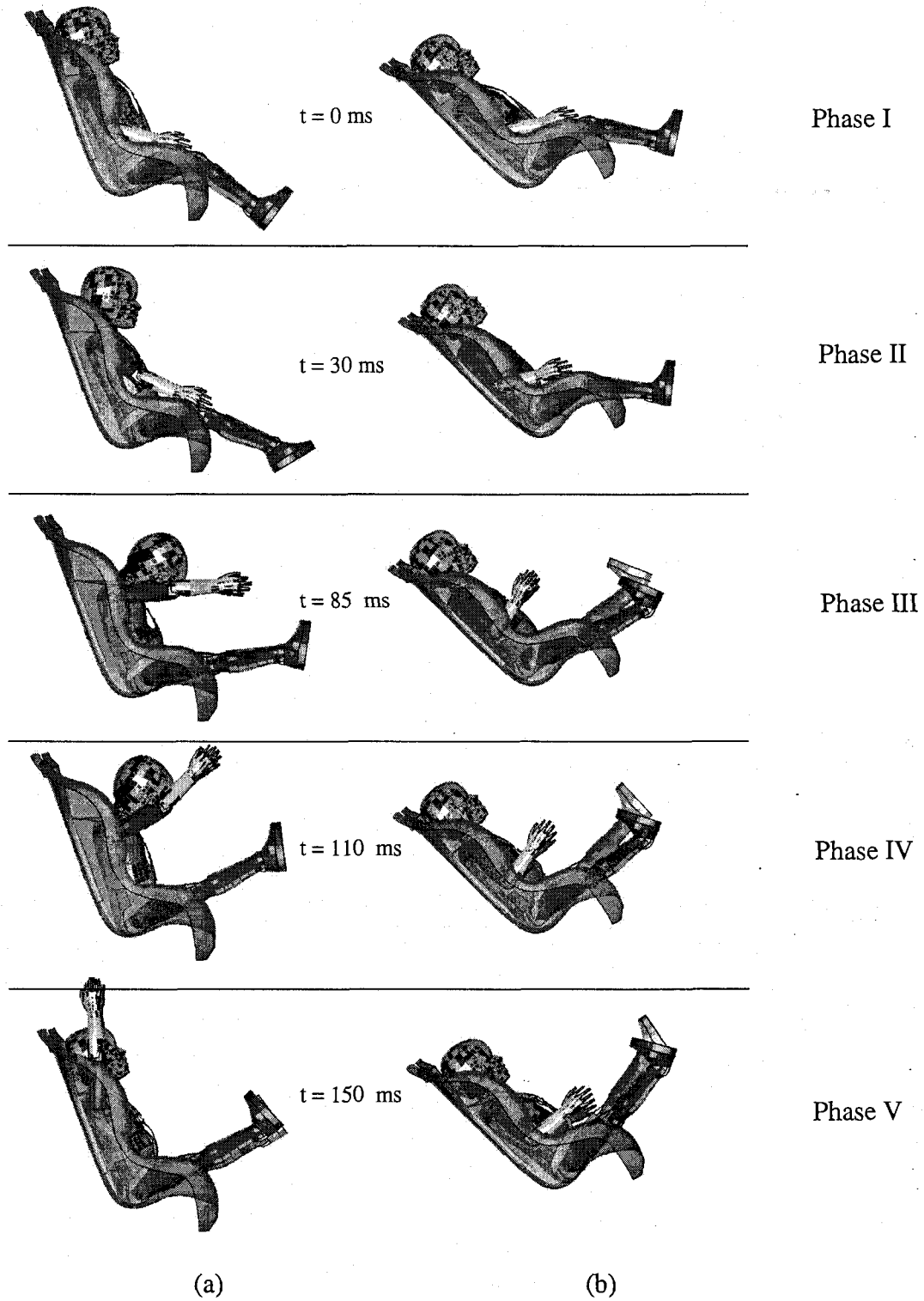


Figure 119. Numerical observations (side view) for the (a) forward-facing and (b) rearward-facing CRS configuration under a simulated CMVSS 208 crash.

7.3 Quantitative analysis

7.3.1 Resultant head and chest accelerations

Figures 120 and 121 illustrate respectively the resultant head and chest acceleration profiles for the forward and rearward-facing simulations as a function of time. The maximum values for the resultant head accelerations were predicted to be 50 g's and 63 g's for the forward and rearward-facing CRS orientation. Higher peaks were predicted for the rearward-facing configurations for the head accelerations which can be attributed to the contact made by the dummy's head with the rigid CRS. It should be noted that these peak values were predicted to occur for approximately 25 ms for the rearward-facing configuration and 50 ms or greater for the forward-facing configuration. After $t = 50$ ms, greater head accelerations were predicted for the forward-facing CRS configuration. Similar time profiles were predicted for the resultant chest accelerations with the maximum value being approximately 40 g's for both the configurations.

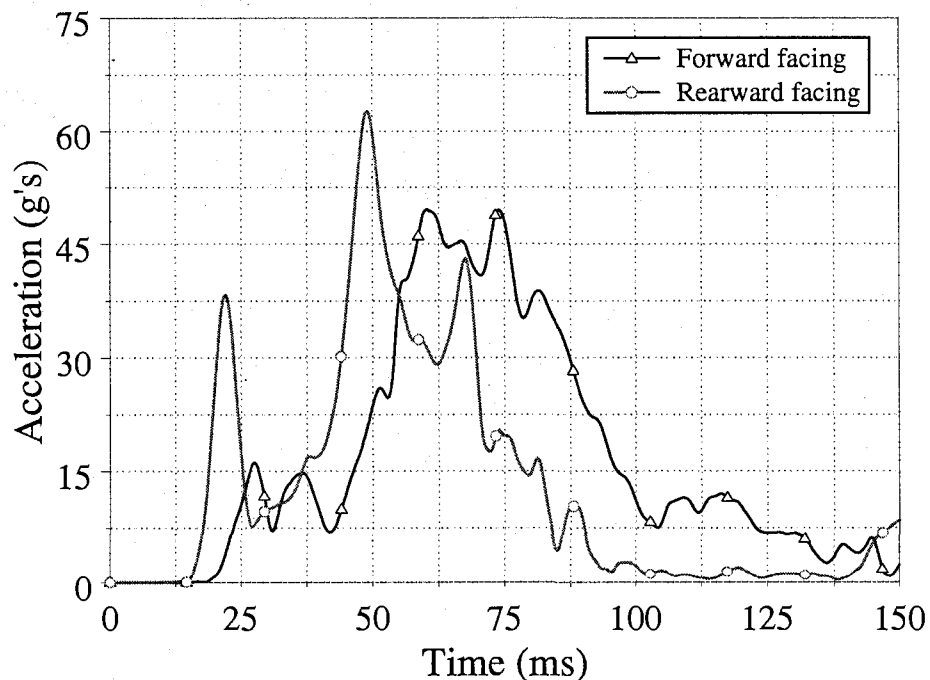


Figure 120. Forward and rearward resultant head accelerations as a function of time.

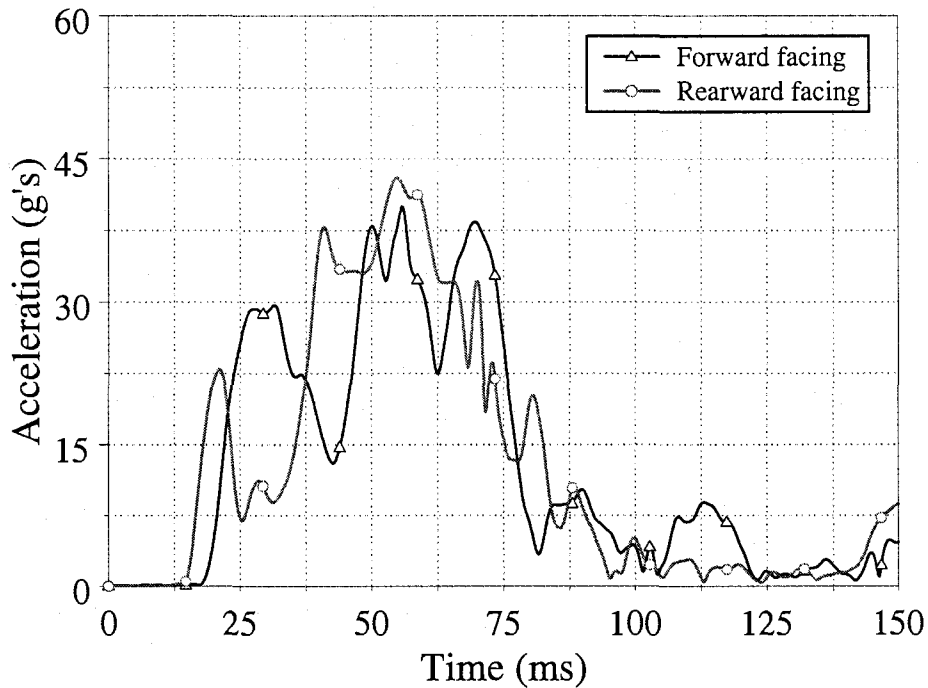


Figure 121. Forward and rearward resultant chest accelerations as a function of time.

7.3.2 Resultant neck forces and moments

Figure 122 illustrates the resultant upper neck forces as functions of time for the forward and rearward-facing crash simulations. Maximum values of the resultant forces predicted by the upper neck load cell were 1545 N and 1050 N for the forward and rearward-facing configurations respectively. Similar values (approximately 1400 N) were predicted by the lower neck load cell in both forward and rearward configurations.

Resultant upper neck moments for both forward and rearward-facing CRS configurations are presented in Figure 123. From the upper neck load cell in the forward-facing configuration a peak resultant moment of slightly over 34 N·m was predicted whereas in the rearward-facing configuration a peak resultant moment of 17 N·m was noted. Observations from the lower neck load cell indicated a much greater resultant moment in forward-facing configuration than in the rearward-facing configuration. This

is due to the significant extension which the neck is subjected to during the crash. Peak values noted from the lower load cell were 19.5 N·m and 142 N·m for the rearward and forward CRS configurations. For both the upper and lower neck load cells, the higher magnitudes of the resultant moments for the forward-facing configuration were predicted for approximately 50 ms.

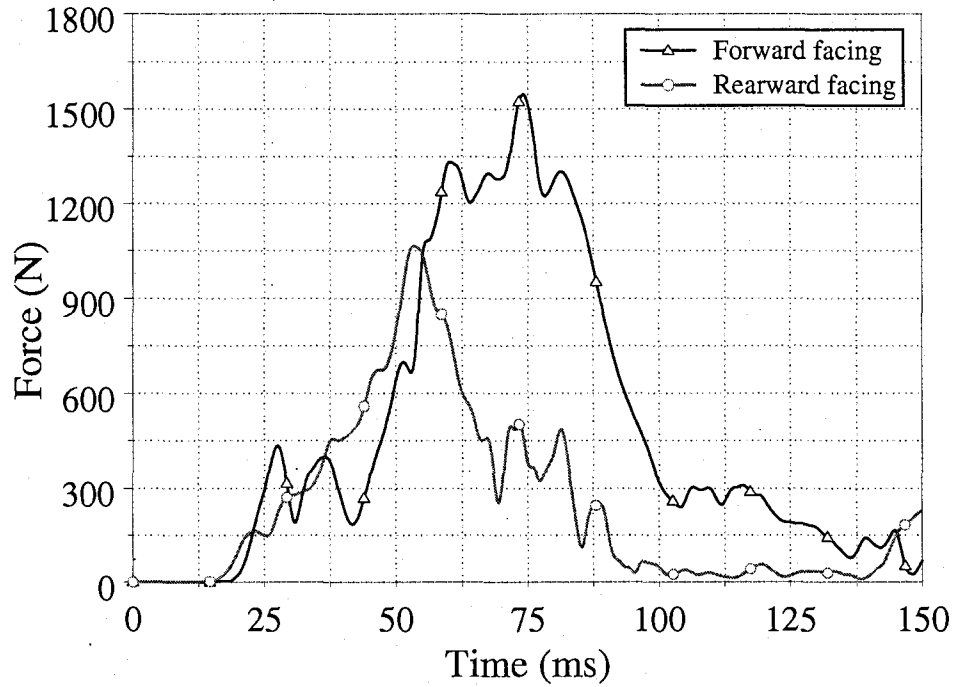


Figure 122. Forward and rearward resultant upper neck forces as a function of time.

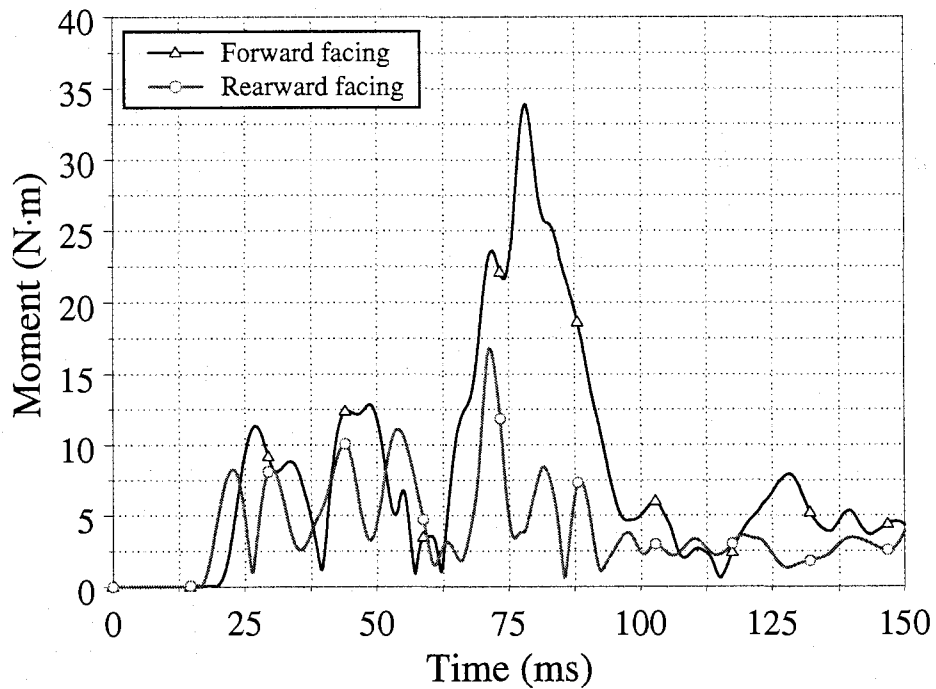


Figure 123. Forward and rearward resultant upper neck moments as a function of time.

7.3.3 Head injury criteria

HIC was calculated for both forward and rearward-facing configurations of the CRS, using a 15 ms and 36 ms sampling window. The HIC_{36} (Figure 124) was, for both CRS configuration positions, greater than the HIC_{15} . Slightly higher values of the *HIC* were predicted for the forward-facing configurations for each evaluation time period. The maximum values of the HIC_{15} for the forward and rearward-facing CRS configurations were 212 and 200 respectively. Maximum values of the HIC_{36} for the forward and rearward-facing CRS configurations were 390 and 265 respectively.

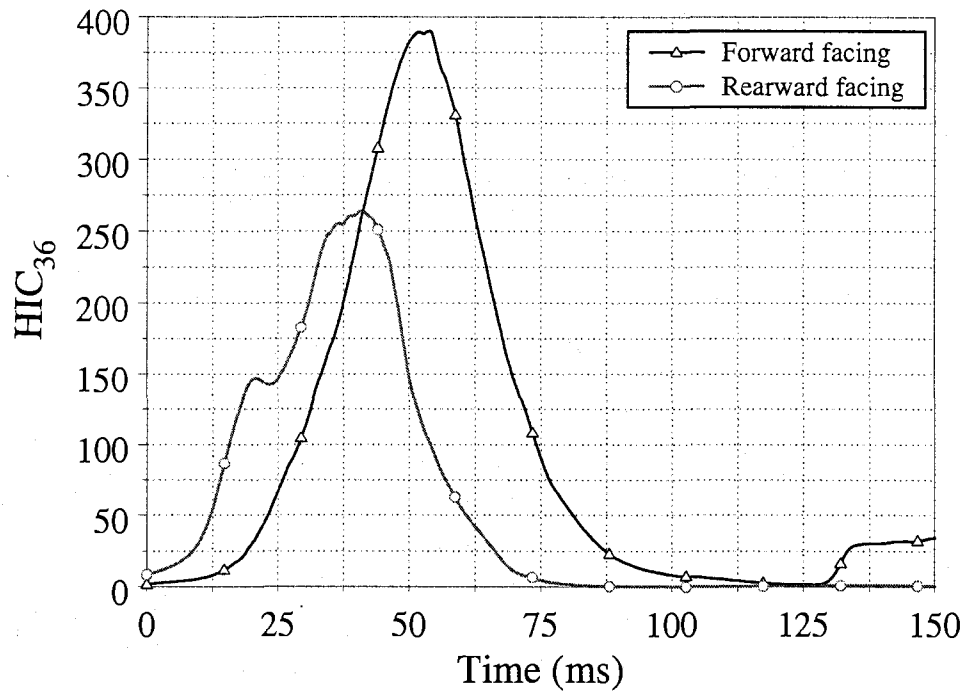


Figure 124. Forward and rearward HIC_{36} as a function of time.

7.3.4 Neck injury criteria

Figure 125 illustrates the N_{ij} as a function of time for both the rearward and forward-facing CRS configurations. The N_{ij} presented in Figure 125 was evaluated based upon the information acquired from the upper neck load cell. Maximum values of the N_{ij} for both forward and rearward-facing CRS configurations were 0.91 and 0.87 respectively. Values for the N_{ij} from the rearward CRS configuration illustrate lower values than the N_{ij} for the forward-facing CRS in the entire time domain.

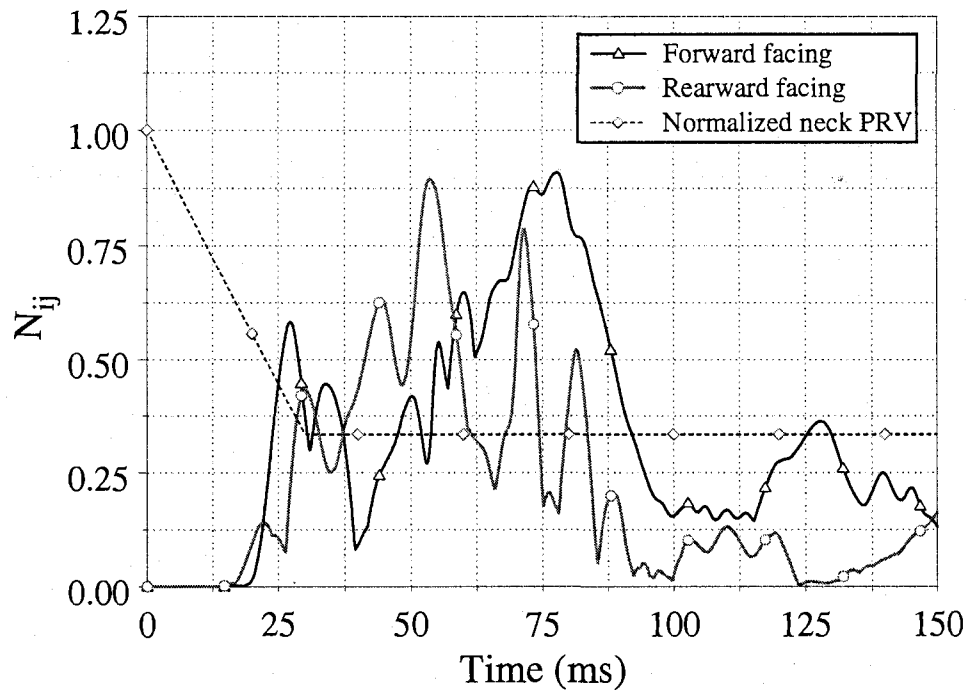


Figure 125. Forward and rearward (upper neck) N_{ij} as a function of time.

Table 12 tabulates the peak values for various injury parameters for both the forward and rearward-facing CRS orientations. Considerable amount of reduction in the neck forces and moments was predicted for the rearward-facing CRS configuration under the CMVSS 208 simulated crash.

Table 12. Peak values predicted by the Hybrid III 3-year-old dummy in both forward and rearward-facing CRS configurations.

Injury Parameter	Forward facing	Rearward facing
Resultant head acceleration (g's)	50	63
Resultant chest acceleration (g's)	40	42
Head injury criteria (HIC-15)	212	200
Head injury criteria (HIC-36)	390	265
Resultant upper neck force (N)	1545	1050
Resultant lower neck force (N)	1400	1400
Resultant upper neck moment (N.m)	34	17
Resultant lower neck moment (N.m)	142	19.5
Upper Neck Injury criteria (Nij)	0.91	0.87
Lower Neck Injury Criteria (NIJ)	2.25	0.97
Probability of AIS 3+ head injuries (%)	4.8	4.2
Probability of AIS 3+ neck injuries (%)	19.2	18
Probability of AIS 3+ chest injuries (%)	40.13	43.47

7.4 Discussion

7.4.1 Injury risk analysis

Table 12 also tabulates the probability of severe head, neck and chest injuries to the two dummies. These values have been evaluated using Prasad and Mertz injury risk probability curves (Appendix B) for the maximum values of *HIC*, *N_{ij}*, and chest accelerations. There is a high risk of sustaining severe chest injuries for both the child dummies. There is a moderate risk of severe neck injuries and a low risk of sustaining severe head injuries for both the dummies.

7.4.2 Protection reference values

According to the PRV's the critical value for head acceleration is 80 g's. The maximum values for the resultant head accelerations were predicted to be 50 g's and 63 g's for the forward and rearward-facing configurations respectively. Both these values are less than the critical head PRV. The recommended critical value for chest and spinal acceleration for a 3-year-old Hybrid III child dummy is 60 g's. For both the

dummies the maximum values of chest acceleration were predicted to be approximately 40 g's which is less than the critical value. Figure 125 also illustrates the normalized neck PRV curve proposed by Klinich et al. [32]. Higher values for the N_{ij} from the rearward CRS configuration were observed to occur for a shorter duration of time compared to the forward-facing configuration. Therefore there is a greater probability of sustaining severe neck injuries in a forward-facing configuration compared to the rearward-facing CRS orientation.

The data analysis illustrates similar peak values for the head accelerations and the N_{ij} for both the forward and rearward-facing CRS configurations. These maximum values for the rearward-facing configuration were observed to occur for a shorter duration of time compared to the forward-facing configuration. Generally higher values were predicted for the forward-facing configuration in the entire time domain. The Prasad and Mertz injury risk analysis is solely based on the peak values of the HIC , N_{ij} and the chest accelerations. Therefore similar injury risk probabilities were obtained for both the forward and rearward-facing configurations.

The study conducted by Skold [13] states that the development of the rearward-facing child safety seat for toddlers reduces the risk of serious injuries. In a study conducted by Howard [56], he suggested that "raising the age at which children are turned from rear to forward-facing might prevent catastrophic neck injuries among North American toddlers". Arbogast et al. [66] also suggested that parents should be encouraged to keep their children facing the rear of the vehicle for as long as possible while following the manufacturer's instructions for their child safety seat. In a study by Weber [16] dealing with rear facing restraint systems for children, it was stated that child safety seats that face the rear of the vehicle are very effective in preventing serious and fatal injuries to small children. They are especially effective in preventing injuries to the upper spinal cord that typically occur in children in forward-facing child restraint systems due to inertial loading. Weber [16] has found that tensile forces acting on the neck can be reduced by half when forward-facing child dummies are turned to face the rear.

The numerical findings illustrate a reduction of approximately 33 percent in the upper neck resultant forces for the rearward-facing configuration compared to the forward-facing CRS orientation. The qualitative and quantitative analysis depicts a greater amount of resultant neck moments for a forward-facing dummy. Extreme hyper-flexion leads to rupture of the tectorial membrane and separation of vertebrae which leads to AOD [40]. In the case of a rearward-facing configuration the dummy falls back into the CRS, thus bending in the neck is not predicted. Therefore there is a higher probability for a child to acquire an AOD in the case of a frontal impact. There is an inversely proportional relationship between the duration of time a load was applied and the critical load to cause injury [32]. After 30 ms of the crash, the critical load that can be sustained without causing injury is approximately 1,000 N. The maximum values of resultant forces predicted by the upper neck load cell for the forward-facing CRS configuration were predicted to be approximately 1500 N. These high forces were predicted for approximately 50 ms. This implies that there are greater chances of sustaining neck injuries in case of a forward-facing configuration compared to the rearward-facing configuration. These simulation results support the hypothesis that a rearward-facing configuration is safer for children older than one year old compared to the forward-facing configuration. These observations are consistent with the observations of Turchi et al. [100 and 101].

8. FRONTAL IMPACT PROTECTION - LOAD LIMITING OF TETHERS

8.1 Load limit evaluation

The main objective of this research was to implement load limiting behaviour into the upper tether and lower LATCH anchors of the CRS in order to reduce the neck injury criteria by increasing forward head excursion. Values of the load limits for both upper tether and lower LATCH anchors were calculated based on two approaches, namely, the injury based approach and the energy based approach.

8.1.1 Injury based approach

DeSantis-Klinich et al. have developed the Hybrid III child PRV's, detailed in Section 2.4.3, using existing observations from various child dummy tests [32]. According to these values the neck injury criteria (N_{ij}) evaluated at the upper neck load cell should be less than 0.33 beyond the first 30 ms of the crash. Observations from our previous work of model validation, shown in Chapter 6, have illustrated that values of the neck injury criteria exceeded the protection reference values. The axial load within the one-dimensional seatbelt elements in the upper tether and lower LATCH anchors were plotted as a function of time and are illustrated in Figure 126. The maximum values of these axial loads were predicted to be higher than the values occurring at 30 ms. In order to reduce the neck injury criteria, it was necessary to load limit the tethers to the values predicted at 30 ms. The axial loads predicted by the one-dimensional elements in the upper tether and lower LATCH anchors after the first 30 ms of the numerical simulations were predicted to be 2.6 kN and 0.85 kN respectively for the FMVSS 213 crash condition (Figure 126). For more appropriate calculations, a similar analysis was conducted on numerical simulations in accordance with CMVSS 208. The axial loads predicted by the one-dimensional elements in the upper tether and lower LATCH anchors after the first 30 ms of the simulation in accordance with CMVSS 208 crash conditions were predicted to be 1.25 kN and 0.73 kN respectively. Table 13 tabulates the load limit values obtained for the injury based approach.

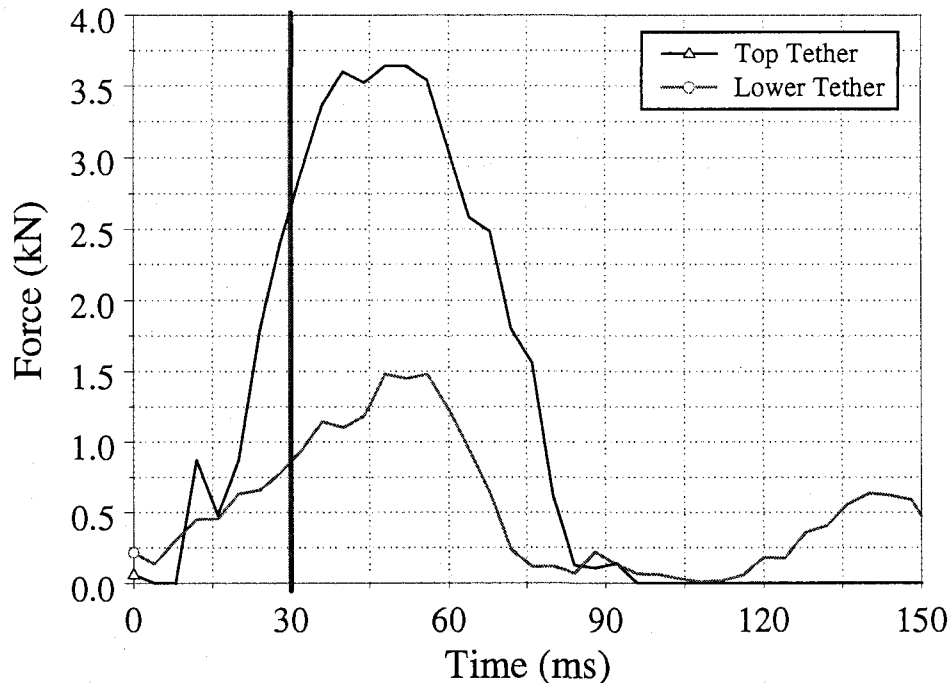


Figure 126. Loads predicted in top tether and LATCH anchors for FMVSS 213 simulations as a function of time.

8.1.2 Energy based approach

FMVSS 213 requires child restraints to meet certain performance specifications when subjected to frontal sled tests simulating a 48 kph (30 mph) crash. Limits are placed on head and knee excursions to limit forward movement in the event of a frontal crash, and the risk of injury to the head and chest also are measured [78]. The Z-point (Figure 127) is the reference location that defines the SORL. According to the FMVSS 213 norms, no portion of the dummy's head should pass through a vertical transverse plane that is 720 mm forward of the Z-point on the standard seat assembly along the center SORL. Also, neither knee pivot point should pass through a vertical transverse plane that is 915 mm forward of the Z-point on the standard seat assembly along the center SORL [78]. From our previous work the maximum head excursion was

predicted to be 259.8 mm and 290 mm for the FMVSS 213 and CMVSS 208 crash conditions respectively.

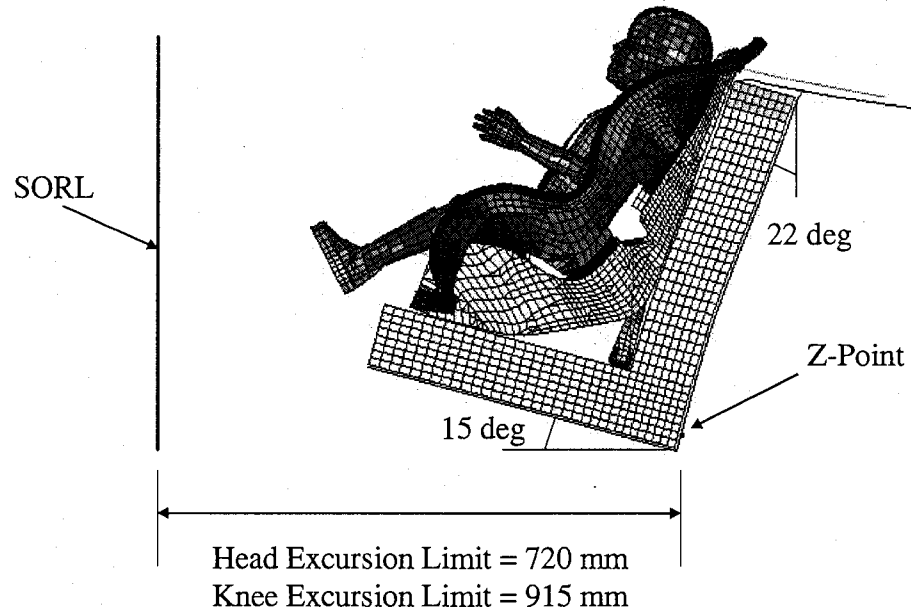


Figure 127. Side view of the CRS illustrating the Z-point, SORL and the head/knee excursion limits.

The maximum internal energy based on the maximum loads predicted by the upper tether and lower LATCH anchors was calculated and was used to evaluate the load limit values utilizing the maximum permissible head excursion limit. A factor of safety of 0.9 was incorporated into the excursion limits; consequently, all load limiting calculations were based on an excursion limit of 650 mm. The safety factor used in the present research of 90 percent is an appropriate assessment for typical engineering design for a preliminary analysis purposes. The critical load limit values evaluated based on this criterion were 1.4 kN (FMVSS 213) and 2.2 kN (CMVSS 208) for the upper tethers, and 0.6 kN and 0.76 kN for the lower LATCH anchors. Table 13 tabulates the load limit values obtained for the energy based approach.

Table 13. Load limit values obtained for the top tether and the lower LATCH anchor.

	Preliminary Simulations				Final Values
	Injury based approach		Energy based approach		
	FMVSS 213	CMVSS 208	FMVSS 213	CMVSS 208	
Top tether load limit (kN)	2.6	1.25	1.4	2.2	1.22
Lower LATCH anchors load limit (kN)	0.85	0.73	0.6	0.76	0.8

Preliminary simulations incorporating various combinations of the above mentioned load limit values were conducted. Finally based on the preliminary simulation results, both of the aforementioned approaches were combined and the final load limit values for the upper tether and lower LATCH anchors were evaluated as 1.22 kN and 0.8 kN respectively. The load limit curve for the upper tether varied linearly from zero load corresponding to zero strain, to 1.22 kN corresponding to 0.013 strain and was limited to 1.22 kN for strains onward. Similarly, the load limit curve for the lower LATCH anchors varied linearly from zero load corresponding to zero strain, to 0.8 kN corresponding to 0.0086 strain and was limited to 0.8 kN for strains onward. Figure 128 illustrates the final load limit curves obtained from the two approaches for the top tether and the lower LATCH anchors. These curves were incorporated in the material properties for the one-dimensional seatbelt elements. Numerical simulations were completed to investigate the neck loads and head and chest accelerations associated with the impact conditions of FMVSS 213 for all the three FE models. The numerical models were simulated under similar conditions that provided a method to compare head and chest accelerations as well as neck loads and moments with the previously validated simulation results incorporating no load limiting behaviour in the tethers.

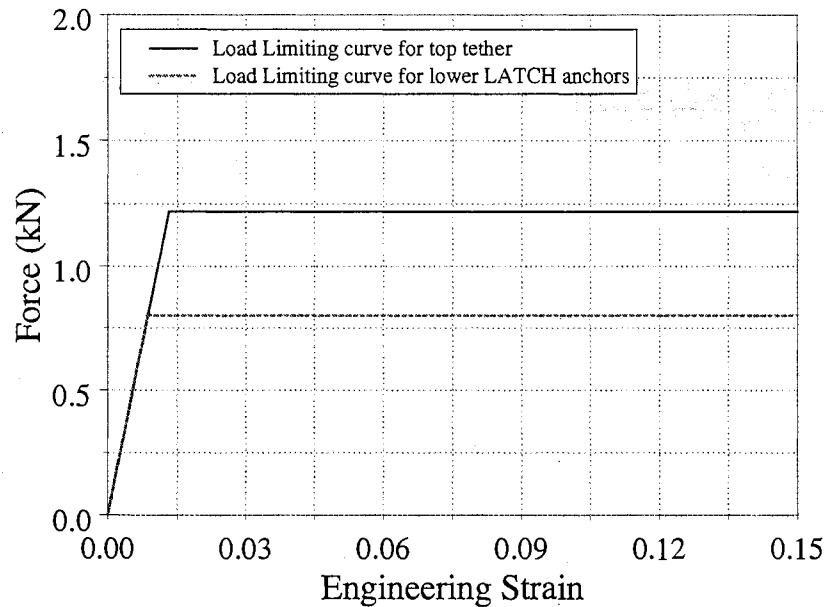


Figure 128. Load limiting curves for the upper tether and lower LATCH anchors.

Numerical simulations, utilizing the identical 213 testing conditions were completed incorporating both no load limiting and load limiting capabilities of the upper tether and the lower LATCH anchors; for Hybrid III 3-year old dummy, Q3 dummy and the child FE model. The simulation results for both conditions were compared in terms of resultant head and chest accelerations as well as neck loads and moments. Cross-sectional forces were evaluated at the upper neck region of the child FE model for both the load limiting and no load limiting case. Finally, head and neck injury potential was calculated for both the Hybrid III and Q3 child dummies. Tables 14 and 15 (Page no. 222) tabulate the peak values predicted for all the injury parameters for the Hybrid III 3-year-old dummy, Q3 dummy and the child FE model.

8.2 Qualitative analysis

Figures 129, 130 and 131 provide the side view of the child dummies relative to the CRS at specific intervals of time through the simulations of the prescribed acceleration pulse in both no load limiting and load limiting configurations. This provides

a visual comparison of the behaviour of the specimens during the crash. For convenience, the whole simulated event has been divided into five phases.

Phase I depicts the state of rest. At this time both the dummies and the child FE model are seated in their original configuration. Phase II marks the onset of head rotation. At this time both the dummies and the child FE model start moving forward. This was predicted to occur at approximately $t = 30$ ms.

The maximum extension in the neck (Phase III) was predicted at approximately $t = 70$ ms for all the three FE models in the no load limiting conditions. This phase was delayed by approximately 15 – 20 ms in all the three FE models simulated with load limiting characteristics in the tethers. It should also be noted that the maximum neck rotation was predicted to be 77 degrees for the child FE model, 73 degrees for the Q3 dummy and 62 degrees for the Hybrid III 3-year-old dummy for the no load limiting configuration. Also, due to load limiting of the tethers the maximum neck rotation was predicted to be less than the values predicted in the no load limiting case.

Phase IV marks the rebound phase which was predicted to occur at approximately $t = 100$ ms (the Hybrid III settled back quicker compared to Q3 and child FE model) for the no load limiting condition. It was apparent that the numerical model of the child dummy in the no load limiting situation settled back into the CRS quicker than the dummy in the load limiting configuration. The contact between the dummy's head and the CRS (Phase V) was predicted to occur at $t = 130$ ms for Hybrid III, $t = 138$ ms for Q3 and $t = 147$ ms for the child FE model in the no load limiting configuration. Due to implementation of load limiting behaviour there was a delay in the rebound phase, due to which the dummies were predicted to settle back slowly and hence no contact between the head and CRS was predicted during the whole simulated period. It is evident from Figures 129 to 131 that the bending of the neck, displacement of the head, and the extension of the limbs were typically much greater for the child dummies and the child FE model in the no load limiting configuration.

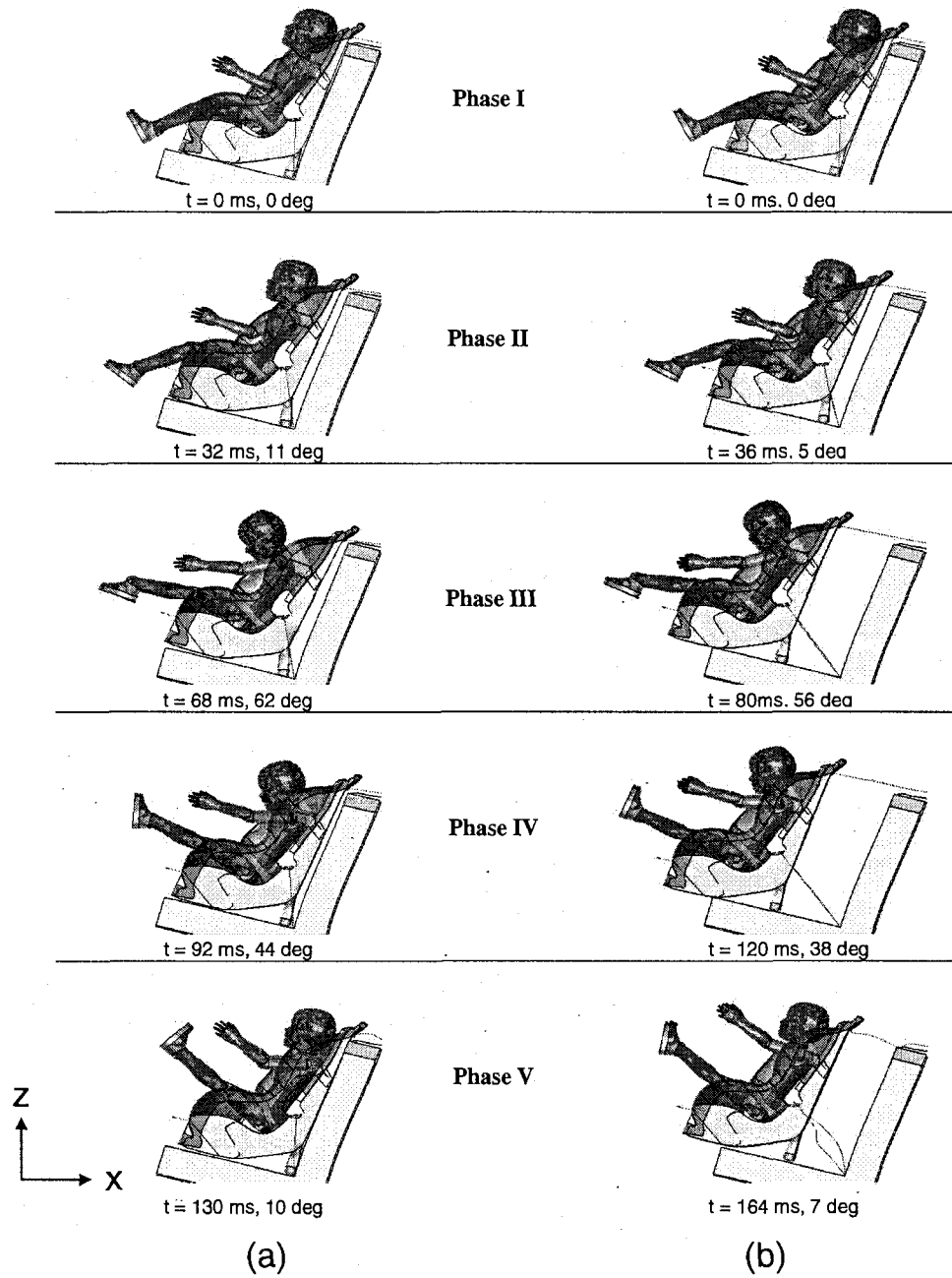


Figure 129. Numerical observation (side view) of Hybrid III 3-year-old dummy for (a) No load limiting and (b) Load limiting conditions.

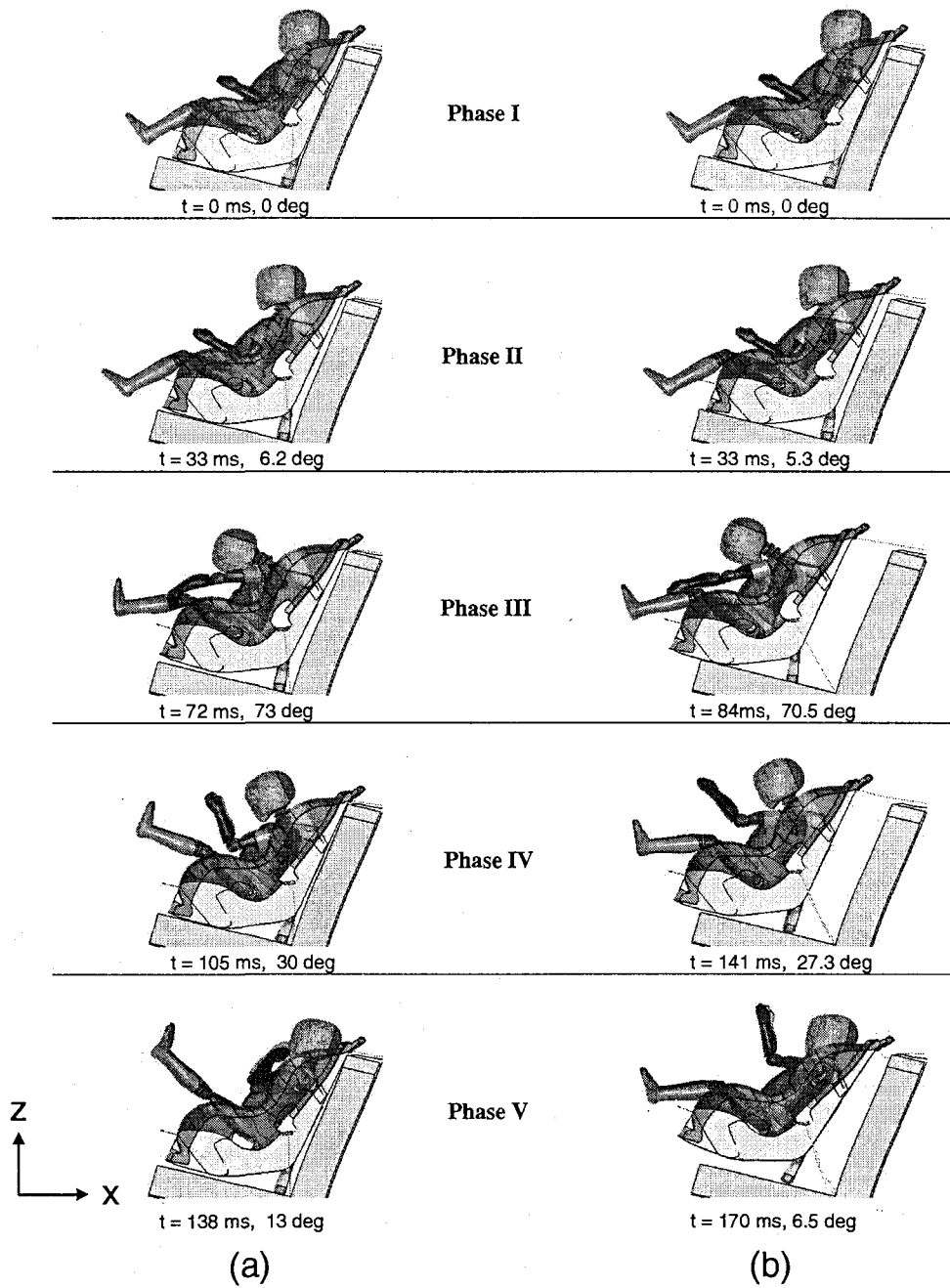


Figure 130. Numerical observation (side view) of Q3 dummy for (a) No load limiting and (b) Load limiting conditions.

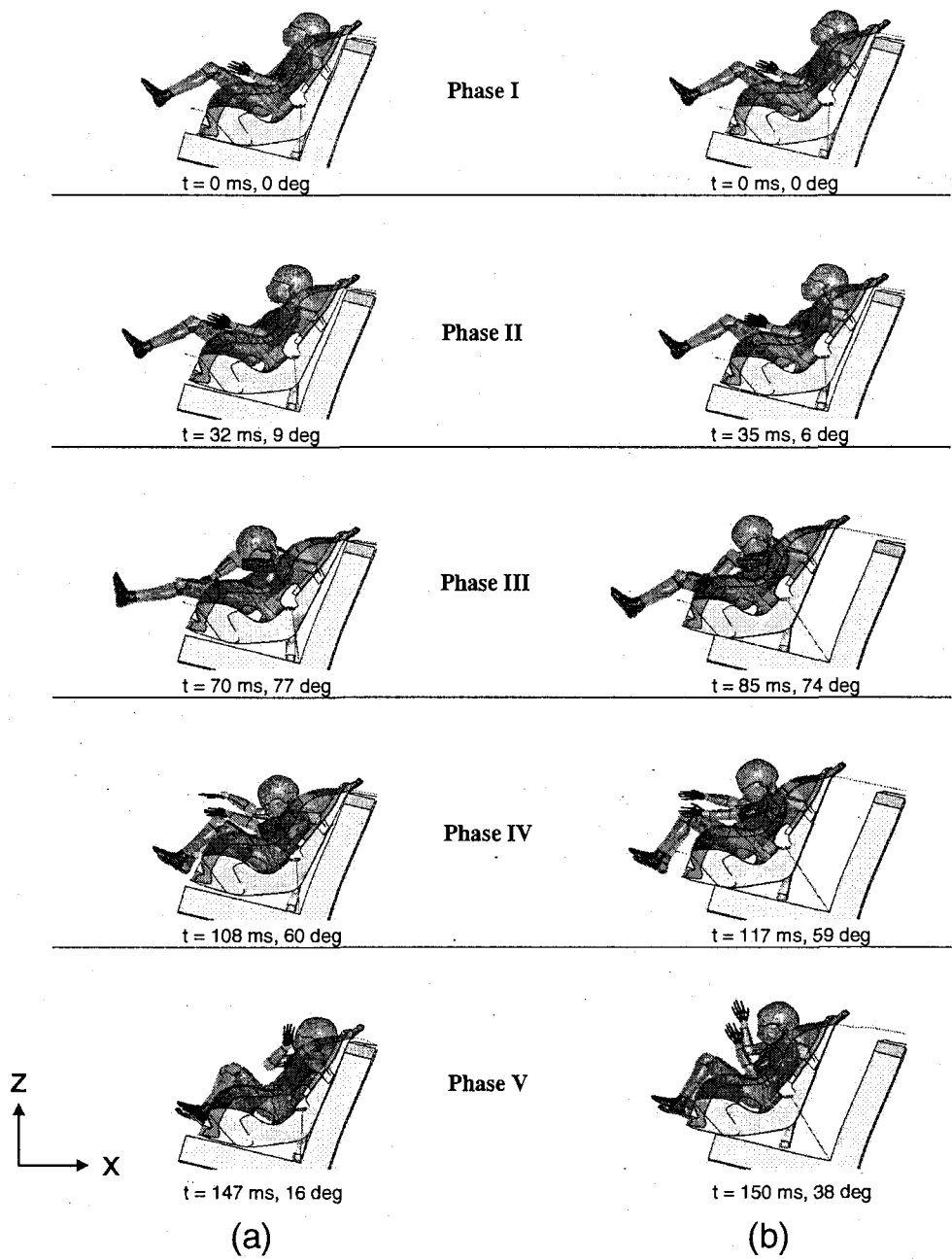


Figure 131. Numerical observation (side view) of child FE model for (a) No load limiting and (b) Load limiting conditions.

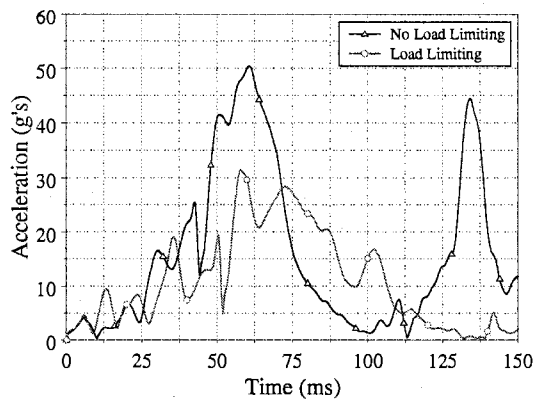
8.3 Quantitative analysis

8.3.1 Resultant head accelerations

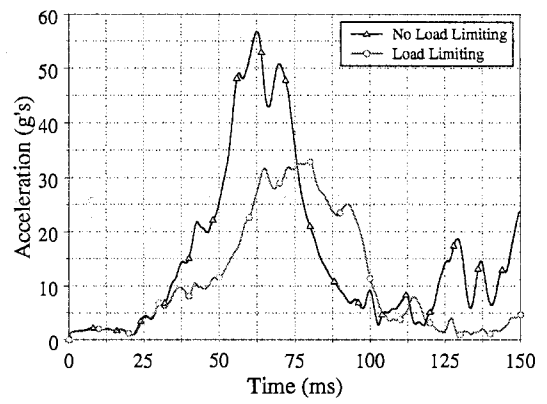
Figures 132 (a), (b), and (c) illustrate the resultant head accelerations for the Hybrid III, Q3 and child FE model respectively as a function of time. The peak values of head accelerations were predicted to be reduced by approximately 40 percent for the Hybrid III and Q3 child dummies, and 34 percent for the child FE model. For the no load limiting condition, a second head acceleration peak was predicted for the Hybrid III dummy at $t = 135$ ms due to the contact of the dummy's head with the CRS. This was also predicted in the qualitative analysis. These peaks were delayed and were noted to be of a lower magnitude for the Q3 dummy, whereas they were not predicted for the child FE model. Also, in the load limiting simulations the second peak for the resultant head accelerations were not apparent.

8.3.2 Resultant chest accelerations

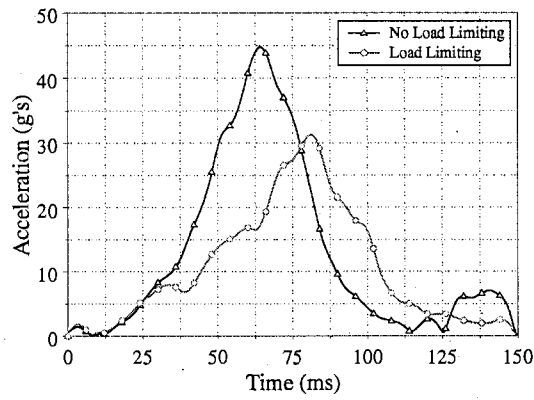
Resultant chest acceleration profiles as a function of time are exhibited in Figures 133 (a), (b), and (c). Similar time profiles were predicted for all the three FE models with a difference in peak values. The maximum values of the resultant chest accelerations were predicted to decrease by approximately 20 percent for the Hybrid III dummy and the child FE model, and 40 percent for the Q3 dummy respectively due to load limiting of the upper tether and lower LATCH anchors.



(a)



(b)



(c)

Figure 132. Resultant head accelerations for load limiting and no load limiting conditions for (a) Hybrid III dummy, (b) Q3 dummy and (c) Child FE model as a function of time.

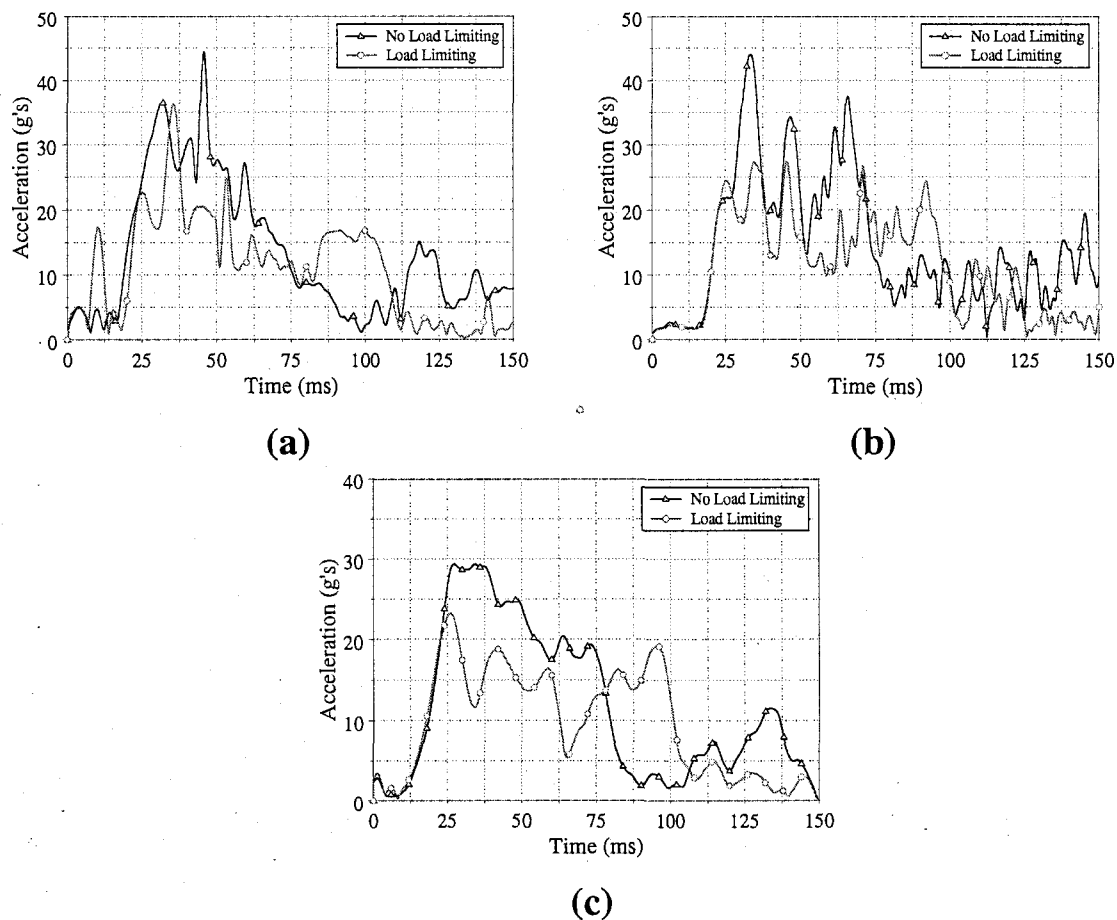


Figure 133. Resultant chest accelerations for load limiting and no load limiting conditions for (a) Hybrid III dummy, (b) Q3 dummy and (c) Child FE model as a function of time.

8.3.3 Resultant upper neck forces and cross-sectional forces

Figures 134 (a) and (b) illustrate respectively the resultant upper neck forces for the Hybrid III 3-year-old dummy and the Q3 dummy as a function of time, for no load limiting and load limiting conditions. A reduction of approximately 45 percent was predicted for the Hybrid III dummy in the upper neck resultant forces due to load limiting of tethers. The resultant upper neck forces were predicted to be reduced by approximately 35 percent for the Q3 child dummy. Figure 134 (c) illustrates the cross-sectional forces evaluated at the upper neck portion of the child FE model as a function of time. The

maximum values for the cross-sectional forces were predicted to be 1110 N for the no load limiting condition and 740 N for the load limiting condition respectively. Therefore a reduction of approximately 35 percent was predicted in the cross-sectional forces for the child FE model due to load limiting of tethers.

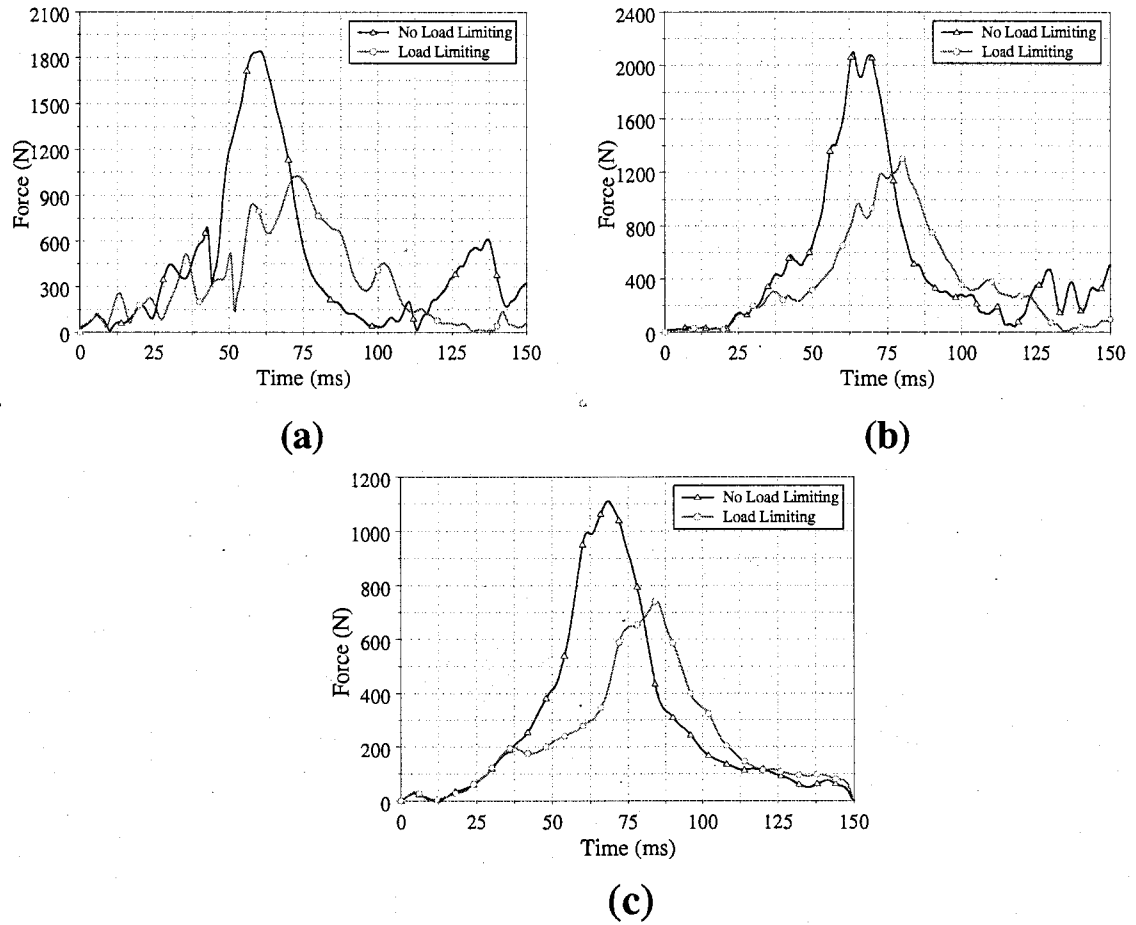


Figure 134. Resultant upper neck forces for load limiting and no load limiting conditions for (a) Hybrid III dummy and (b) Q3 dummy and (c) resultant cross-sectional force for the child FE model as a function of time.

8.3.4 Head injury criteria

The head injury criteria were evaluated over a 15 ms and 36 ms time interval using equation 1. The maximum values obtained from equation 1 for both no load limiting and load limiting situations are presented in Tables 14 and 15, and illustrated in Figure 135. For the Hybrid III 3-year-old child dummy the HIC_{15} and HIC_{36} were predicted to be reduced by approximately 75 and 60 percent respectively. It should be noted that the head injury criteria depends on the acceleration observed at the center of mass of the head. By limiting loads in the upper tether and the lower LATCH anchors, the head accelerations are also limited. Therefore due to load limiting of tethers, a reduction in the HIC values was observed. The implementation of load limiting behaviour in the upper tether and lower LATCH anchors resulted in a reduction of approximately 70 percent in HIC_{15} and 55 percent in HIC_{36} for the Q3 child dummy. For the child FE model a reduction of approximately 60 percent in the head injury criteria was predicted due to load limiting of tethers.

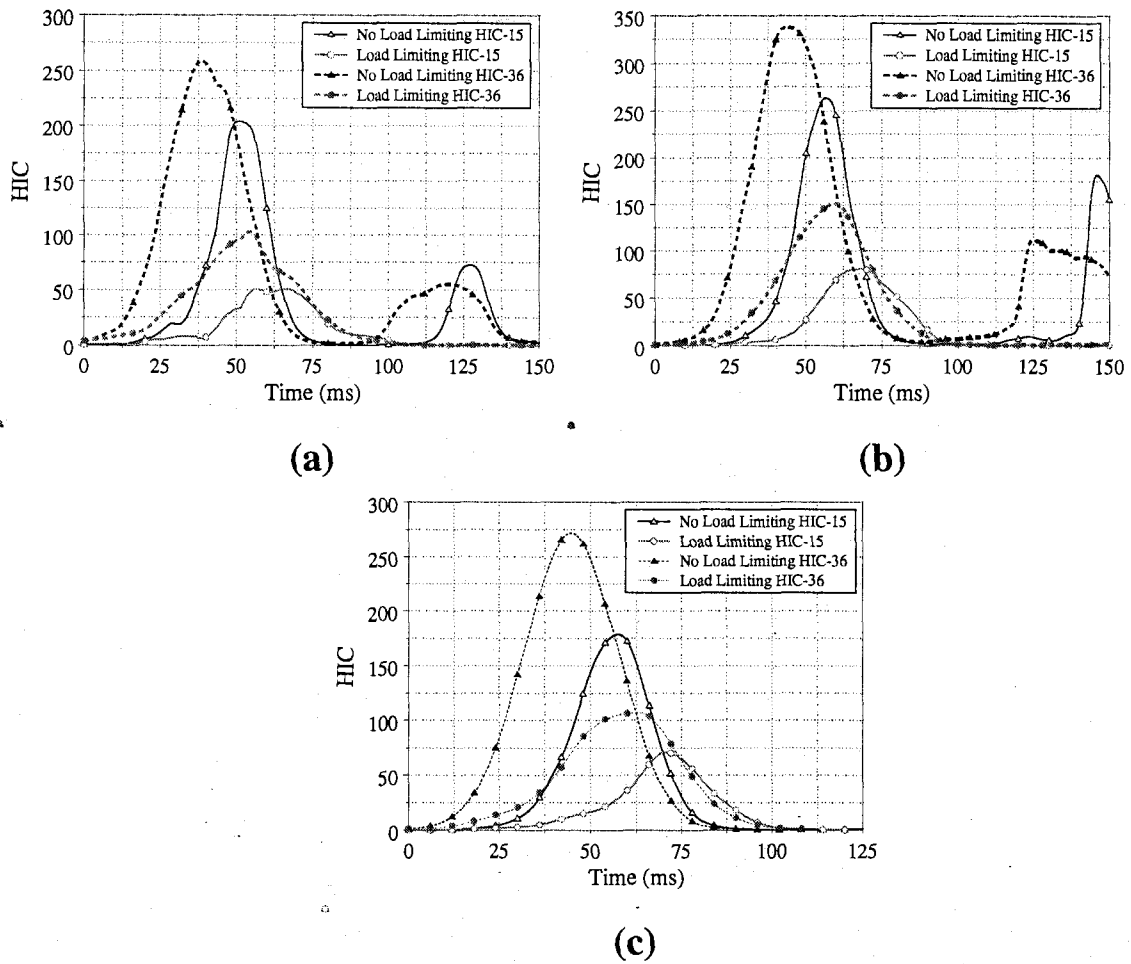


Figure 135. Head Injury Criteria (HIC_{15} and HIC_{36}) for load limiting and no load limiting conditions for (a) Hybrid III dummy, (b) Q3 dummy and (c) child FE model as a function of time.

8.3.5 Neck injury criteria

Figures 136 (a) and (b) illustrate respectively the N_{ij} as a function of time for both the Hybrid III and the Q3 child dummies for no load limiting and the load limiting crash conditions. As it has been mentioned previously in Section 6.3.2.6, the critical intercept values for the Q3 dummy have not been established; therefore the values outlined for the Hybrid III crash test dummy were used to evaluate the neck injury criteria for the Q3 dummy. Also, the neck injury criteria could not be evaluated for the child FE model due to lack of upper neck moment data. The N_{ij} presented in Figure 136 was evaluated based

upon the information acquired from the upper neck load cell. Values for the N_{ij} from the load limiting simulations illustrate significantly lower values than the N_{ij} for the no load limiting condition in the entire time domain. A reduction of approximately 35 percent was predicted for both the Hybrid III dummy the Q3 dummy, in the peak values for the neck injury criteria for the first 100 ms of the numerical simulations. Although the N_{ij} is not applicable to US FMVSS 213, the use of load limiting tethers in CRS does indicate a significant reduction in this injury parameter.

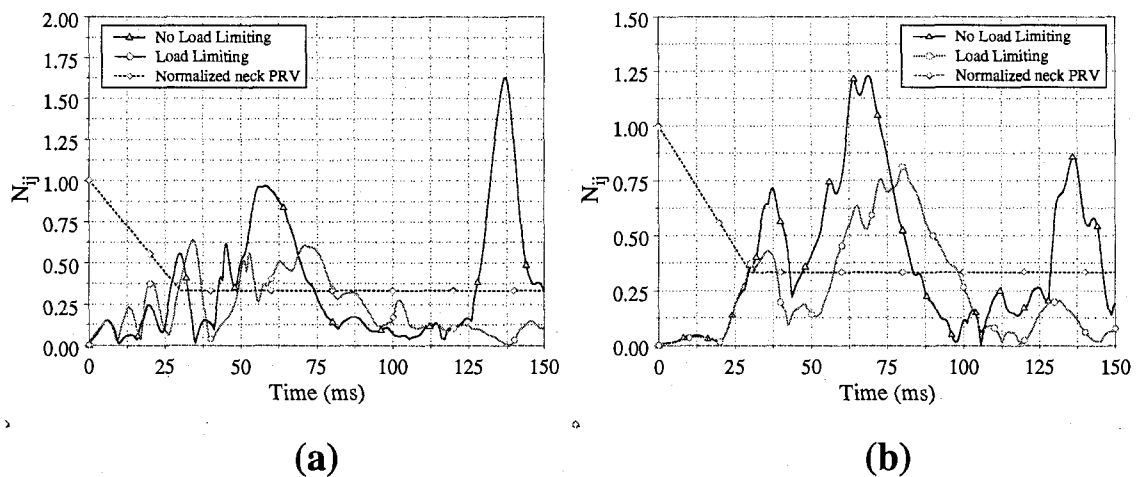


Figure 136. Neck Injury Criteria (N_{ij}) for load limiting and no load limiting conditions for (a) Hybrid III dummy and (b) Q3 dummy as a function of time.

Tables 14 and 15 summarize the peak values predicted for both the load limiting and no load limiting simulations. The maximum head excursion calculated from the Z-point was predicted to be 437.7 mm for Hybrid III 3-year-old dummy, 473 mm for the child FE model and 512 mm for the Q3 dummy respectively due to load limiting of tethers. All these values were found to be less than the proposed value of 720 mm by NHTSA [78]. Also the maximum values for knee excursion were predicted to be 655 mm (Hybrid III), 740 mm (child FE model), and 590 mm (Q3 dummy) which are less than the limiting value of 915 mm.

Table 14. Summary of peak values of various injury parameters predicted for the Hybrid III and the Q3 child dummies for load limiting and no load limiting situations.

	Hybrid III 3-year-old		Q3	
	No Load Limiting	Load Limiting	No Load Limiting	Load Limiting
Resultant head acceleration (g's)	50.3	31	62.8	32.8
Resultant chest acceleration (g's)	44	36	44	26.7
Head injury criteria (HIC-15)	203.5	50	263	80
Head injury criteria (HIC-36)	258.6	102.5	337	150
Resultant upper neck force (N)	1841.6	1005.5	2100	1303
Resultant lower neck force (N)	790.9	641.4	563	540
Resultant upper neck moment (N.m)	39.86	31.6	18.4	15
Resultant lower neck moment (N.m)	146.7	88.8	115	77
Neck injury criteria (NI)	0.95	0.64	1.22	0.8
Head Excursion (mm)	259.8	437.7	376.7	512
Knee Excursion (mm)	493.5	655	515	590
Probability of AIS 3+ head injuries (%)	6.7	0.47	10.8	1.3
Probability of AIS 3+ neck injuries (%)	20.48	12.27	30.47	16
Probability of AIS 3+ chest injuries (%)	46.87	33.7	46.87	21.2

Table 15. Summary of peak values of various injury parameters predicted for the child FE model for load limiting and no load limiting situations.

	Child FE Model	
	No Load Limiting	Load Limiting
Resultant head acceleration (g's)	44.6	31.2
Resultant chest acceleration (g's)	29.3	23
Head injury criteria (HIC-15)	178	71
Head injury criteria (HIC-36)	271.5	106.5
Cross-sectional force (N)	1110	740.4
Head Excursion (mm)	318.22	473
Knee Excursion (mm)	614	740
Probability of AIS 3+ head injuries (%)	5.4	1.1
Probability of AIS 3+ chest injuries (%)	24.3	17.24

8.3.6 Head trajectories

Figure 137 presents the trajectories of the centre of mass of the head (local z axis displacements as a function of local x axis displacements) for the three dummies for both the no load limiting and load limiting situations. The displacements were measured relative to the rigid portion of the seat buck. Greater excursions in both local x and z directions were found for all the three FE models due to implementation of load limiting behaviour. Increase in head excursions along the x -axis was a result of the load limit behaviour of the tether anchors. Since the seat buck is inclined at 15 degrees to the horizontal, displacement in x -direction makes the CRS slide over this ramp. This leads to an increase in the z -direction head trajectories for the dummies. When the CRS reaches

the end of the seat buck, it was predicted to bounce back. This further increases the z-trajectory of the head, as illustrated in Figure 137.

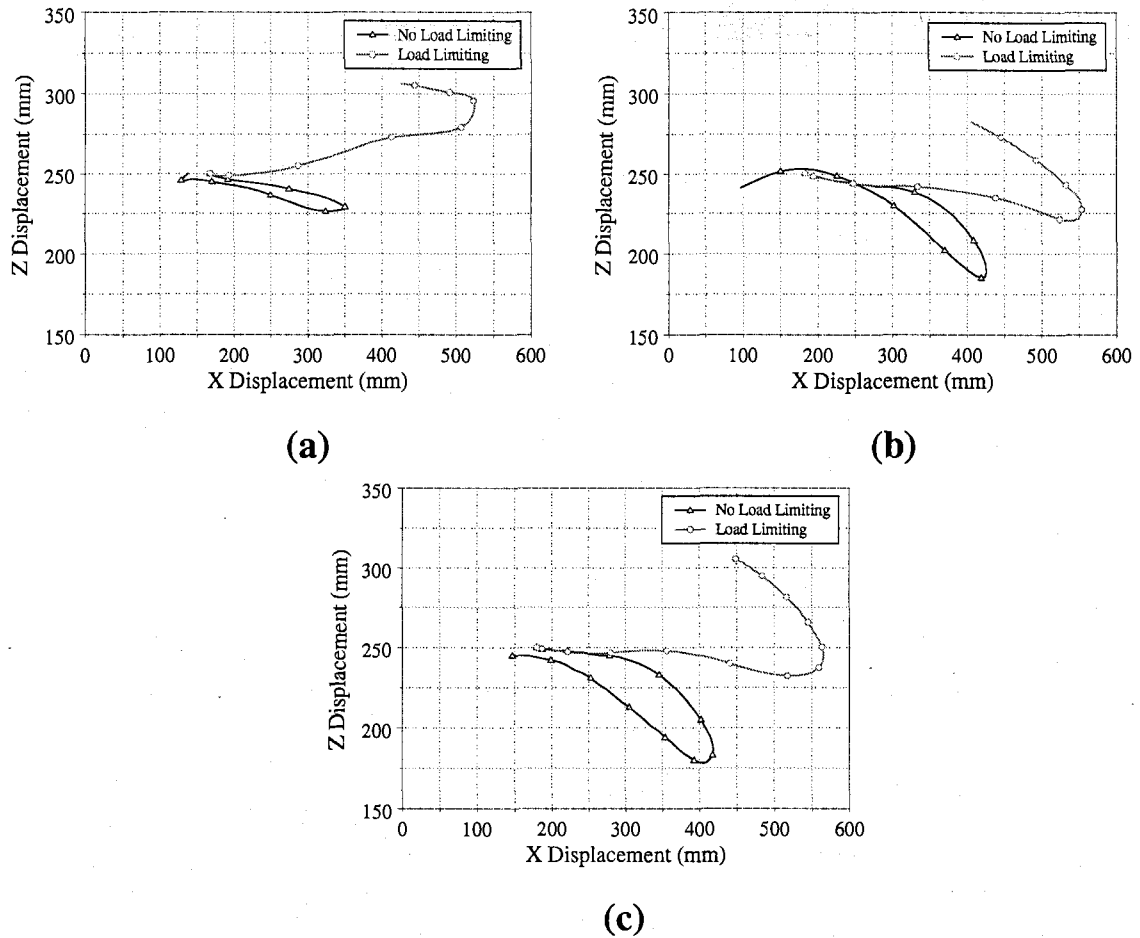


Figure 137. Head trajectories of the center of mass for load limiting and no load limiting conditions for (a) Hybrid III dummy, (b) Q3 dummy and (c) Child FE model.

It should be noted that the Hybrid III head trajectories were different compared to the child FE model. For the load limiting condition, the Hybrid III dummy illustrated greater z-displacement for the first 60 ms of the simulation. The child FE model exhibited greater head x-displacement compared to the Hybrid III child dummy. For the no load limiting configuration, greater head excursions were predicted for the child FE model. These predictions can be attributed to the fact that the Hybrid III dummy's neck is stiffer compared to the actual child, which conforms to the findings of Mizuno et al. [114] and

Zhang et al. [115]. The Q3 head trajectories were predicted to be similar to the head profiles for the child FE model, for both the load limiting and no load limiting conditions.

8.4 Discussion

8.4.1 Injury risk analysis

Tables 14 and 15 also tabulate the probability of severe head, neck and chest injuries to the two dummies and the child FE model. These values have been evaluated using the Prasad and Mertz injury risk probability curves (Appendix B) for the maximum values of HIC , N_{ij} , and chest accelerations. There is a high risk of sustaining severe chest injuries as predicted by the Hybrid III and the Q3 dummies for the no load limiting condition and the Hybrid III dummy for the load limiting condition. Also, there is a high risk of sustaining severe neck injuries for the Q3 dummy for the no load limiting condition. There is a moderate risk of severe neck injuries for the Hybrid III dummy for the no load limiting case and for the Q3 dummy under the load limiting condition. In addition a moderate risk of severe chest injuries was predicted for the child model for both no load limiting and load limiting situations, and for the Q3 dummy due to incorporation of the load limiting behaviour in the tethers. A low risk of sustaining severe neck injuries was predicted for the Hybrid III dummy due to load limiting of tethers. The probability of severe head injuries was predicted to be low for all the child models for both the cases. The implementation of load limiting of tethers illustrated a reduction in the probability of severe head, neck and chest injuries.

8.4.2 Protection reference values

The PRV's proposed by Klinich et al. [32] are applicable to the Hybrid III 3-year-old dummies. The PRV's and critical intercepts have not yet been established for a Q3 dummy and the child FE model. Therefore the PRV values outlined for the Hybrid III 3-year-old dummy have been used for all the child models for the purpose of data comparison. The maximum values for the resultant head accelerations were predicted to

lie in the range of 45 – 63 g's for the no load limiting case and approximately 30 g's for the no load limiting condition. All these values are less than the critical head PRV of 80 g's. The recommended critical value for chest acceleration for a 3-year-old child dummy is 60 g's. For all the child models the maximum values of chest acceleration were predicted to be less than the critical value for both load limiting and no load limiting conditions. Figure 136 also presents the normalized neck PRV proposed by Klinich et al. [32]. It is worth noting that the neck injury criteria curves obtained from the load limiting simulations were observed to be lower than the neck PRV for a longer duration of time, when compared to the no load limiting situation.

Implementation of load limiting behaviour in the upper and lower tethers of the CRS was found to be effective in reducing the probability of severe head, neck and chest injuries. At present the load limits have been calculated using the neck PRV and the head and knee excursions proposed by NHTSA. When the load limit is reached, the increased stretchiness of the belt permits the vehicle occupant to move forward during a crash as crash energy is absorbed by the belt. Therefore, the crash energy is dissipated through limiting of loads, leading to a reduction in neck loads and moments, which reduces the neck injuries. According to Klinich et al. [32], there is an inversely proportional relationship between the duration of time a load was applied for and the critical load to cause injury. After 30 ms of the crash, the critical load that can be sustained without causing injury is approximately 1,000 N for a 3-year-old child dummy. The maximum values of resultant forces observed by the upper neck load cell for the Hybrid III and the Q3 dummies were observed to be greater than 1800 N for the no load limiting condition. These high forces were observed for approximately 40 ms. This implies that the chance of sustaining neck injuries is reduced with the implementation of load limiting behaviour in the tethers.

The severity of head injury depends on head acceleration. By increasing head excursions, the head accelerations are decreased which reduces the potential for accelerations/inertial based head injuries. The current research tested excursion limits based upon FMVSS 213 norms. In some situations the dummy excursions may seem

large for small passenger cars. Increasing head excursion to mitigate the risk of acceleration induced injury to the head may increase the likelihood of excursion related contact injuries. In a frontal crash, for properly restrained children positioned in a CRS seating in the rear seat of the vehicle, acceleration based head injuries do occur and the proposed implementation of load limiting behaviour into the upper tether and lower anchors does illustrate benefits. Load limiting of tethers was observed to be effective in reducing head and neck injury criteria by approximately 70 percent and 35 percent respectively. To the best of the authors' knowledge, incorporation of the load limiting behaviour in upper tethers and lower LATCH anchors has not been applied to the CRS, and this work is the first study of this kind. With further research and design, an appropriate balance between load limitation for the CRS tethers and child excursion may be achievable.

9. FRONTAL IMPACT PROTECTION - HEAD AND NECK RESTRAINING DEVICE

9.1 Model development

In a frontal crash, the torso of the child is restrained by the seatbelt, whereas the head of the child is restrained only by the neck. Due to heavy heads and weak neck musculature in children, there is a greater chance of sustaining severe head and neck injuries [56]. The objective of this study was to develop a head and neck restraining device for children in order to limit the forward movement/rotation of the head of the child. The device was similar in design to the HANS device used by various race car drivers (Section 2.8.4). The HANS device was modeled into two parts: The HANS collar and the HANS tether. The HANS collar would be restrained by the shoulder harness and the HANS tethers would be constrained to the dummy's head, thereby providing a leverage mechanism between the head and the torso of the child. The geometry of the HANS collar was based on the geometry of the torso of the Hybrid III FE model. The FE mesh of the HANS device is illustrated in Figure 138.

Preliminary simulations were completed incorporating a rigid material definition as well as deformability by considering different materials for the HANS collar. Through an exhaustive data analysis of the preliminary simulations it was concluded that the material definition for the HANS collar should exhibit high strength and ductility for up to 10 percent elongation. In addition the material selected to model the HANS collar should be polymeric for the ease of injection molding. Therefore Acrylonitrile Butadiene Styrene (ABS), 20 percent glass fiber filled was selected. Values for the density, Young's modulus, and Poisson's ratio for ABS, 20 percent glass fiber filled are 1200 kg/m^3 , 6 GPa, and 0.3 respectively [130]. The yield and ultimate tensile strengths of the selected material are 81 MPa and 96.6 MPa respectively. An isotropic elastic-plastic material model was used to model the material property of the HANS collar. The material properties of ABS, 20 percent glass fiber filled were assigned to the material card (Appendix D). The HANS collar was modeled using fully integrated shell elements. The

portion of the collar that extended downward from the shoulders to the dummy's torso was assigned a thickness of 4 mm. The rest of the collar (around the dummy's head and neck) was assigned a thickness of 6 mm.

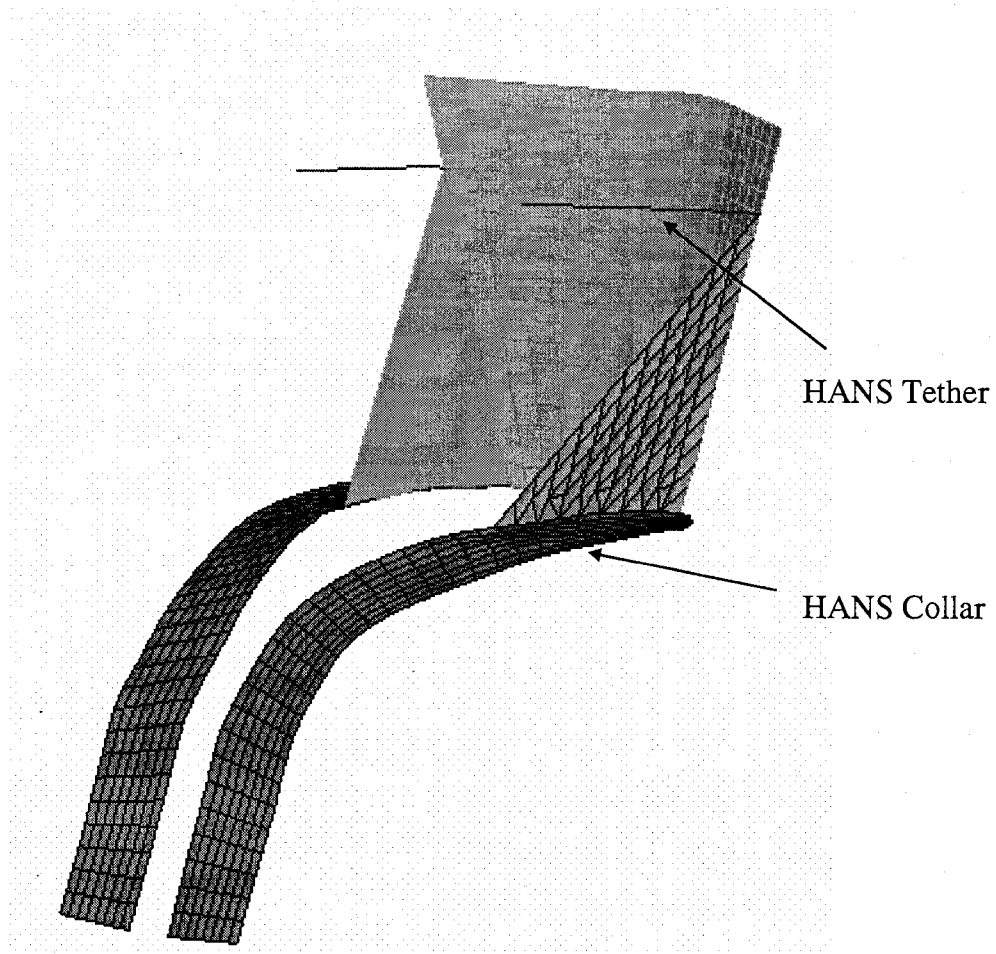


Figure 138. Finite Element mesh of the HANS device.

The HANS tether was modeled using one-dimensional seatbelt elements. The experimental loading/unloading behaviour utilized for the top tether and the lower LATCH anchors was incorporated in the material model for the HANS tether seatbelt elements (Figure 73). An element formulation specifically developed for one-dimensional seatbelt elements was used for the HANS tethers.

9.2 Simulation procedure

Five contact algorithms (Appendix E) were defined for modeling the contact between the HANS device, the seatbelt and the dummy. The HANS collar was restrained around the dummy's torso by the seatbelt webbing, and the HANS tether was constrained to the dummy's head, in the proximity of the center of mass of the dummy's head, using constrained extra nodes. For the preliminary studies, this mechanism has been selected to constrain the HANS tether to the head. Minor modifications to the seatbelt webbing geometry around the torso were necessary for the Q3 dummy and the child FE model in order to properly constrain the HANS collar. Figure 139 illustrates the positioning of the HANS device around a Hybrid III 3-year-old dummy.

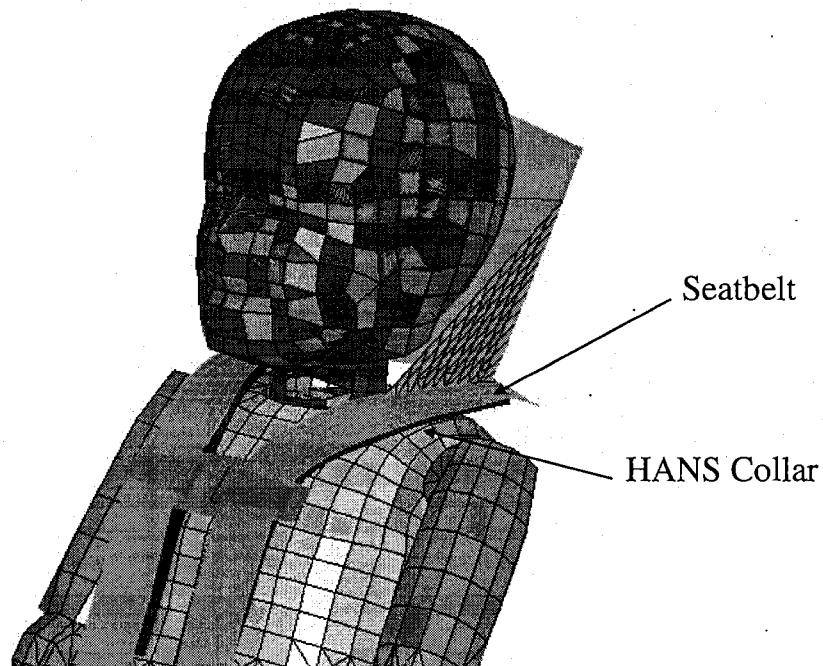


Figure 139. Positioning of the HANS device around the Hybrid III 3-year-old dummy.

Numerical simulations, utilizing the identical FMVSS 213 testing conditions were completed in the absence and presence of the HANS device; for the Hybrid III 3-year-old dummy, the Q3 dummy and the child FE model. The simulation results for both conditions were compared in terms of resultant head and chest accelerations as well as neck loads and moments. Cross-sectional forces were evaluated in the upper neck region

of the child FE model for both the cases. Finally, head and neck injury potentials were calculated for both the Hybrid III and Q3 child dummies. Tables 16 and 17 (Page no. 242) tabulate the peak values predicted for all the injury parameters for the Hybrid III 3-year-old dummy, Q3 dummy and the child FE model.

9.3 Qualitative analysis

Figures 140, 141 and 142 provide the side view of the child dummies relative to the CRS at specific intervals of time through the simulations of the prescribed acceleration pulse in both the absence and presence of the HANS devices. This provides a visual comparison of the behaviour of the specimens during the crash. For convenience, the whole simulated event has been divided into five phases.

Phase I depicts the state of rest. At this time both the dummies and the child FE model are seated in their original configuration. Phase II marks the onset of head rotation. At this time both the dummies and the child FE model start moving forward. This was predicted to occur at approximately $t = 30$ ms.

The maximum extension in the neck (Phase III) was predicted at approximately $t = 70$ ms for all the three FE models in the situation without the HANS device. This phase was predicted approximately 15 – 20 ms earlier in all the three FE models simulated with the addition of the HANS device. It should also be noted that the maximum neck rotation was observed to be 77 degrees for the child FE model, 73 degrees for the Q3 dummy and 62 degrees for the Hybrid III 3-year-old dummy in the absence of the HANS device. Due to the addition of the HANS device, the maximum neck rotation was predicted to be reduced by approximately 50 percent or greater for all the three child models.

Phase IV marks the rebound phase which was predicted to occur at approximately $t = 100$ ms (the Hybrid III was predicted to settled back quicker compared to Q3 and child FE model) for the situation with no HANS device. This phase occurred at

approximately $t = 75$ ms with the addition of the HANS device. The contact between the dummy's head and the CRS (Phase V) was predicted to occur at $t = 110$ ms for Hybrid III, and $t = 130$ ms for Q3 and the child FE model in the presence of the HANS device. For the numerical simulations conducted in the absence of the HANS device, there was a delay in the rebound phase. It is evident from Figures 140 to 142 that the addition of the HANS device efficiently reduces the forward head excursion and the neck rotation in the event of a frontal impact.

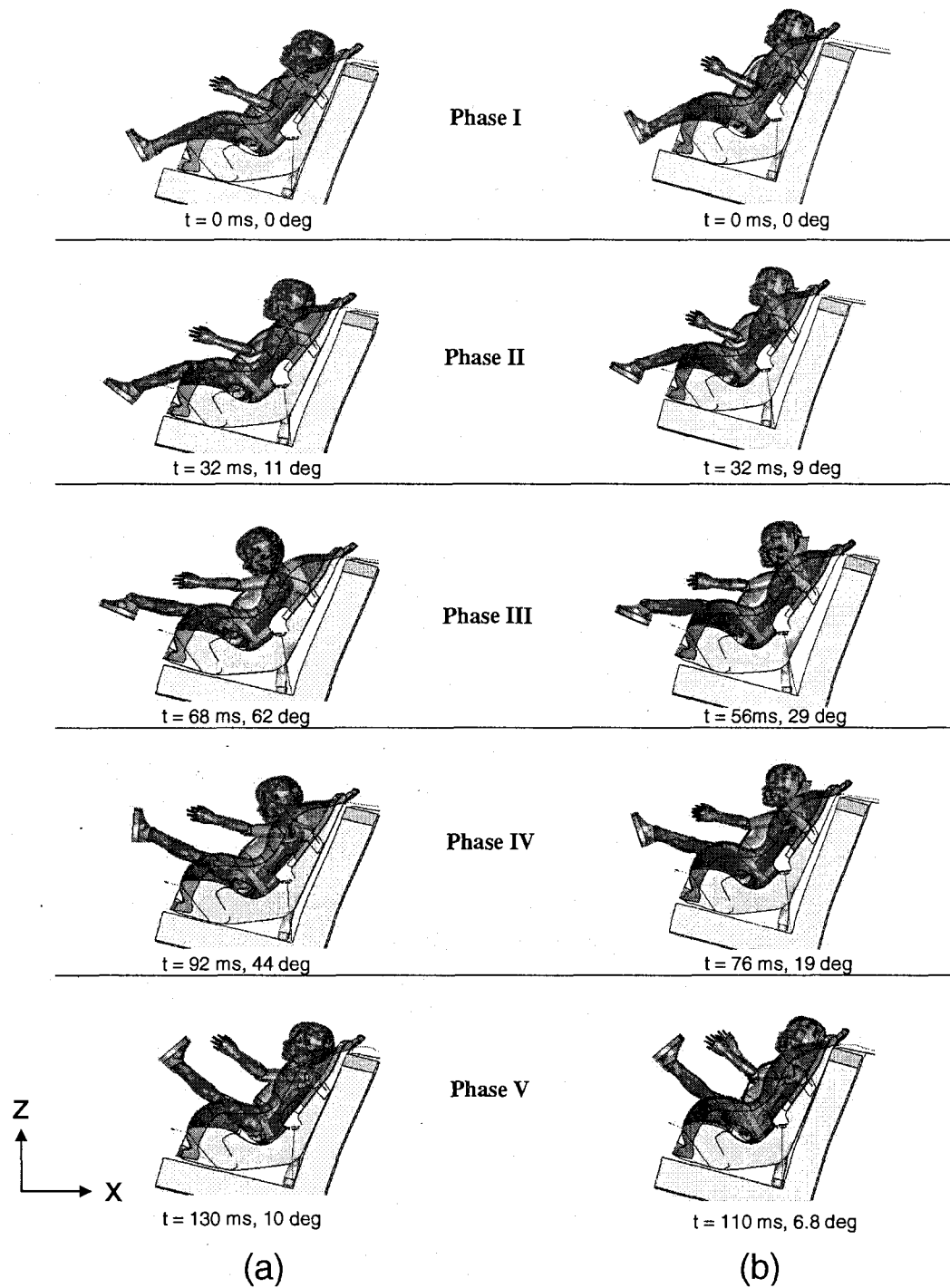


Figure 140. Numerical observation (side view) of Hybrid III 3-year-old dummy in the (a) absence, and (b) presence of the HANS device.

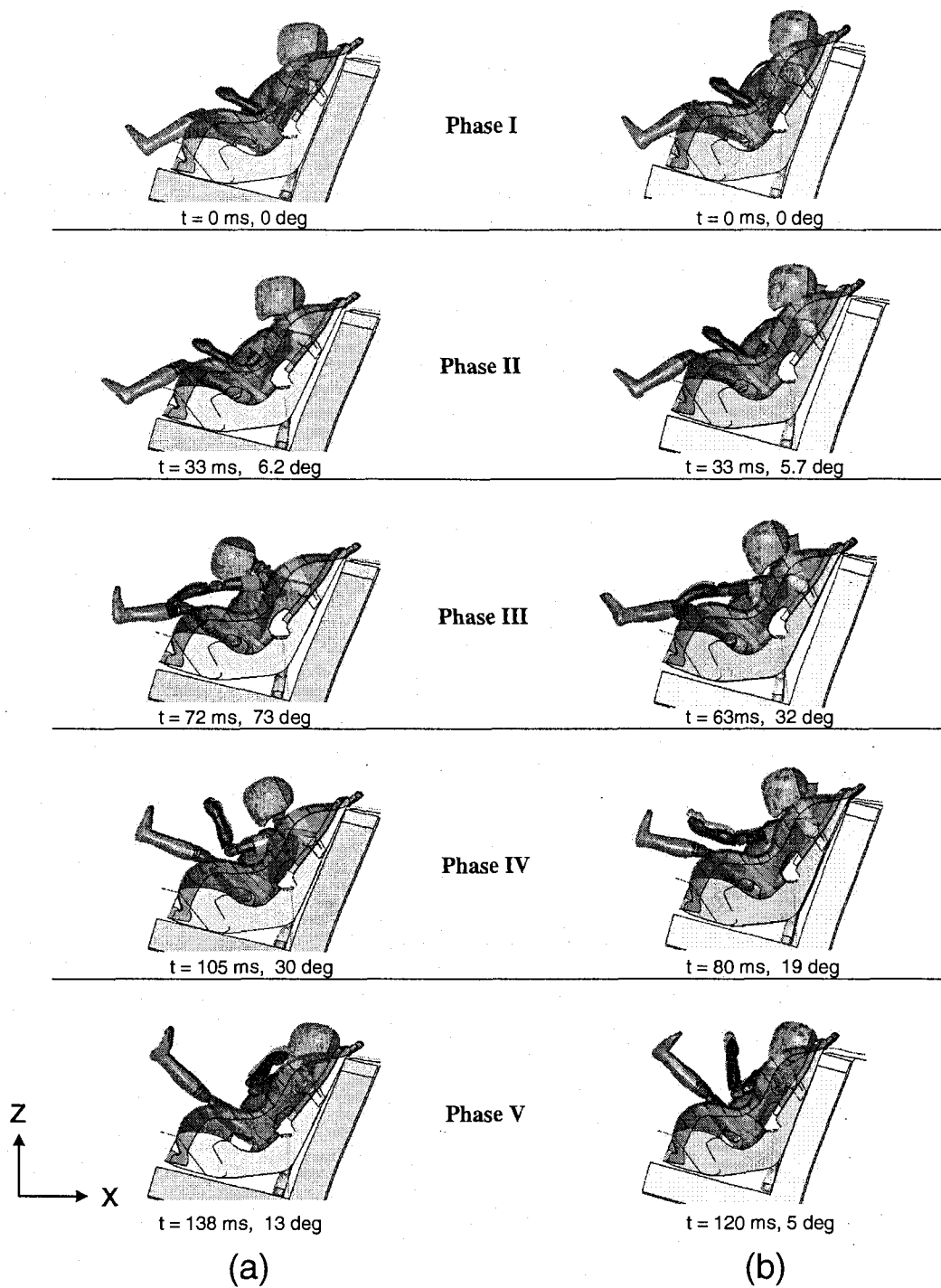


Figure 141. Numerical observation (side view) of Q3 child dummy in the (a) absence, and (b) presence of the HANS device.

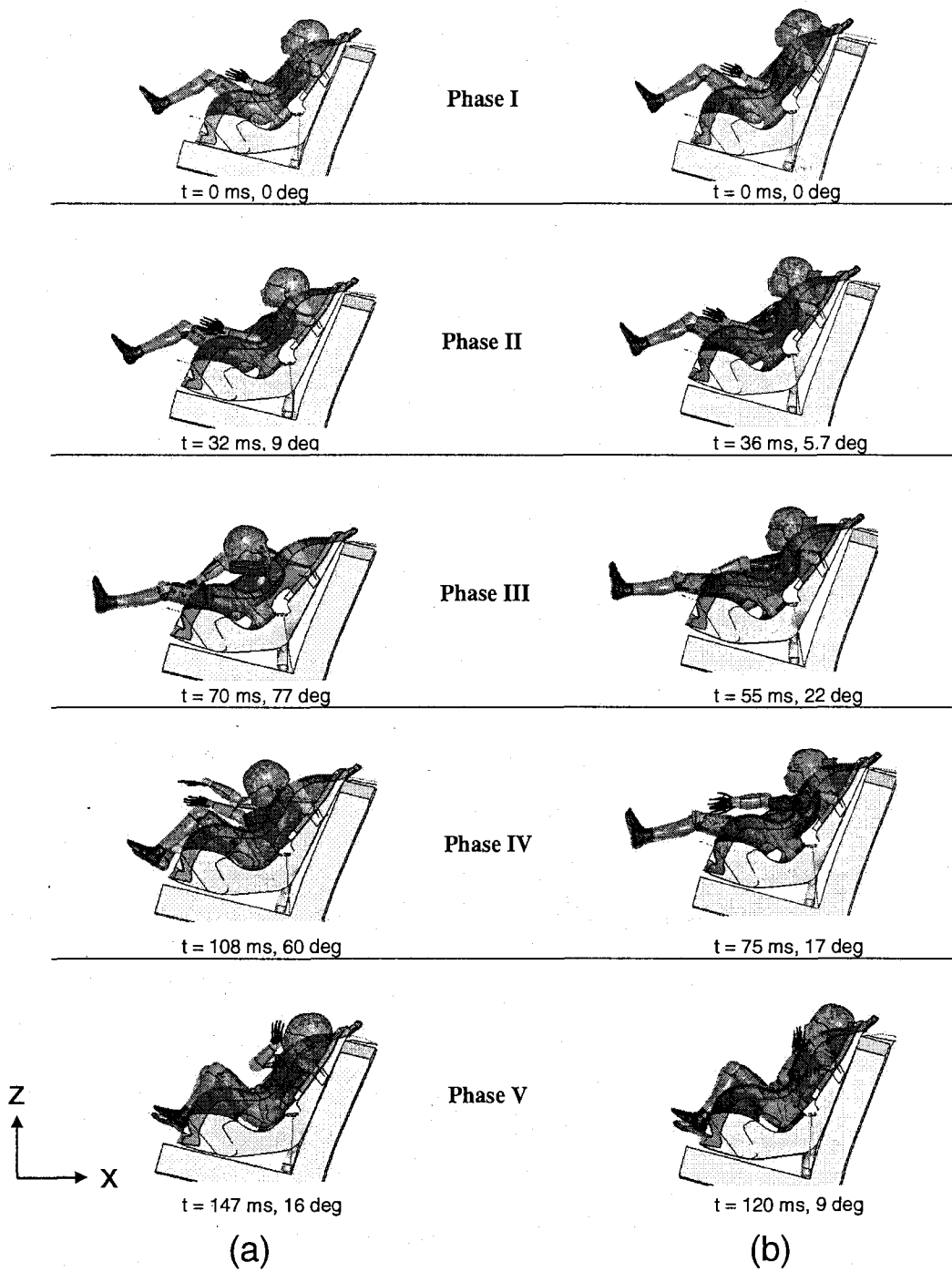


Figure 142. Numerical observation (side view) of child FE model in the (a) absence, and (b) presence of the HANS device.

9.4 Quantitative analysis

9.4.1 Resultant head accelerations

Figures 143 (a), (b), and (c) illustrate the resultant head accelerations for the Hybrid III, Q3 and child FE model respectively as a function of time. Similar time profiles for the head accelerations were predicted for both in the absence and presence of HANS device. The peak values of head accelerations were predicted to be reduced by approximately 40 percent for the Q3 child dummy and 20 percent for the child FE model. In the presence of the HANS device, a second head acceleration peak was predicted for all the child models around approximately $t = 120$ ms due to the contact of the dummy's head with the CRS. In the absence of the HANS device, a second head acceleration peak was predicted for the Hybrid III dummy at $t = 135$ ms. These peaks were delayed and were predicted to be of a lower magnitude for the Q3 dummy, whereas they were not predicted for the child FE model.

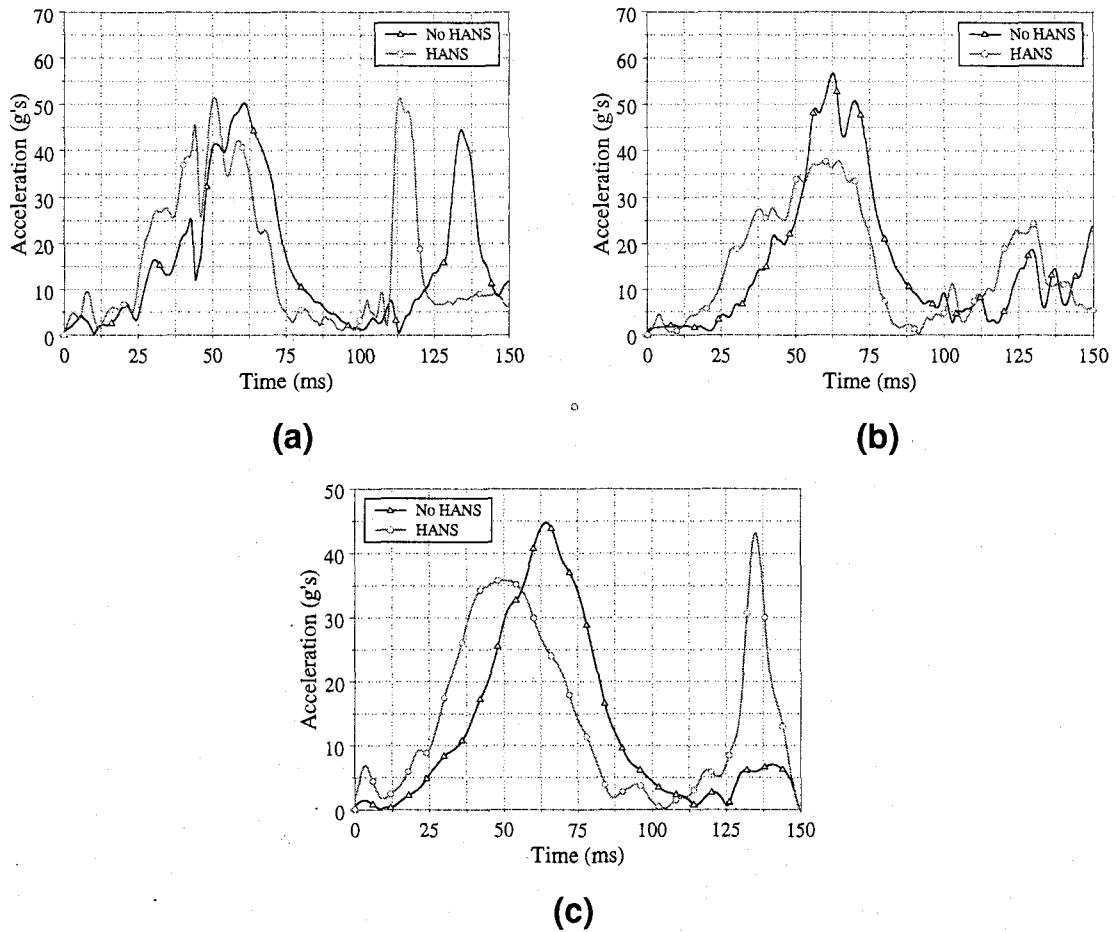


Figure 143. Resultant head accelerations in the presence and absence of the HANS device for (a) Hybrid III dummy, (b) Q3 dummy, and (c) Child FE model as a function of time.

9.4.2 Resultant chest accelerations

Resultant chest acceleration profiles as a function of time are exhibited in Figures 144 (a), (b), and (c). Similar time profiles were predicted for all the three FE models with a minor difference in peak values. The maximum values for the resultant chest accelerations are tabulated in Tables 16 and 17.

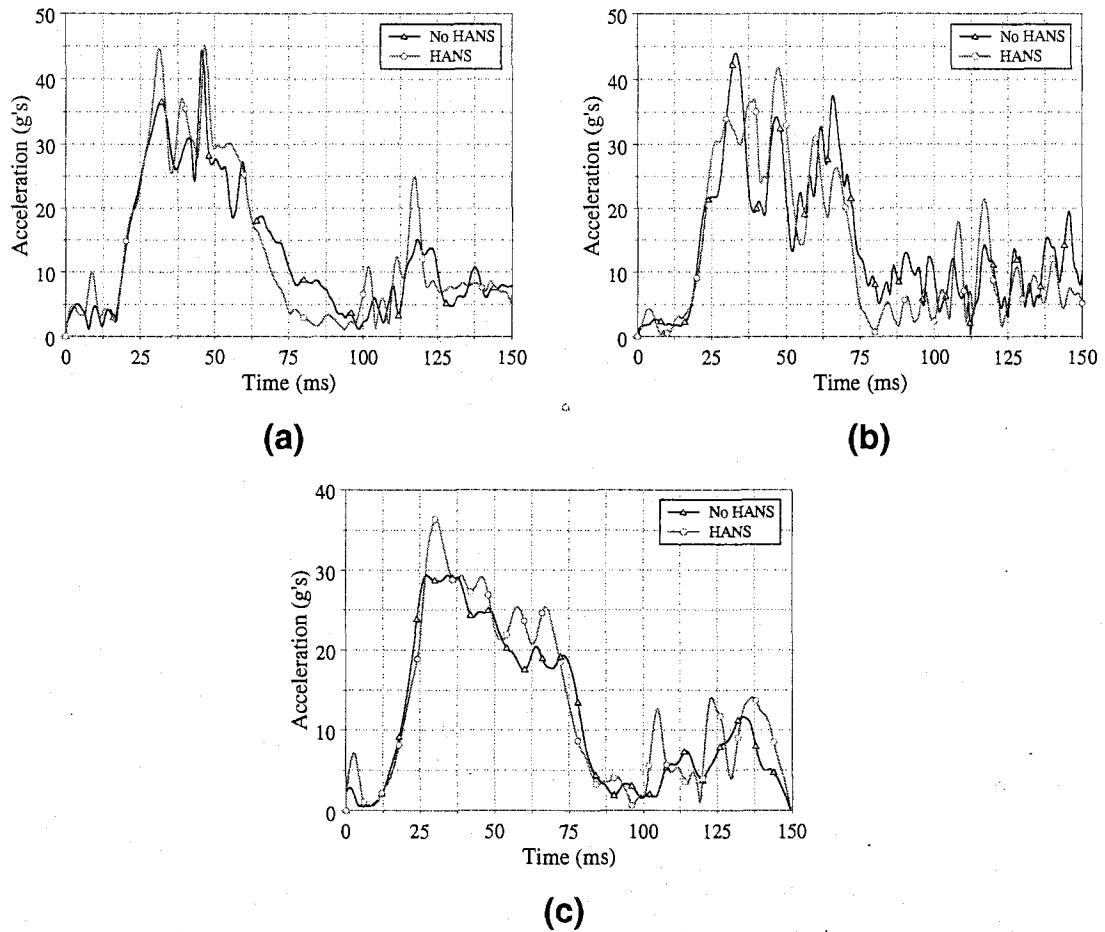


Figure 144. Resultant chest accelerations in the presence and absence of the HANS device for (a) Hybrid III dummy, (b) Q3 dummy, and (c) Child FE model as a function of time.

9.4.3 Resultant upper neck forces and cross-sectional forces

Figures 145 (a) and (b) illustrate respectively the resultant upper neck forces for the Hybrid III 3-year-old dummy and the Q3 dummy as a function of time, in the absence and presence of the HANS device. A reduction of approximately 40 percent was predicted for the Hybrid III dummy in the upper neck resultant forces due to the presence of the HANS device. The resultant upper neck forces were predicted to be reduced by approximately 80 percent for the Q3 child dummy.

Figure 145 (c) illustrates the cross-sectional forces evaluated at the upper neck portion of the child FE model as a function of time. The maximum values for the cross-sectional forces were predicted to be 1110 N for the condition without the HANS device and 546.7 N for the simulation in the presence of the HANS device respectively. Therefore a reduction of approximately 50 percent was predicted in the cross-sectional forces for the child FE model due to the presence of the HANS device.

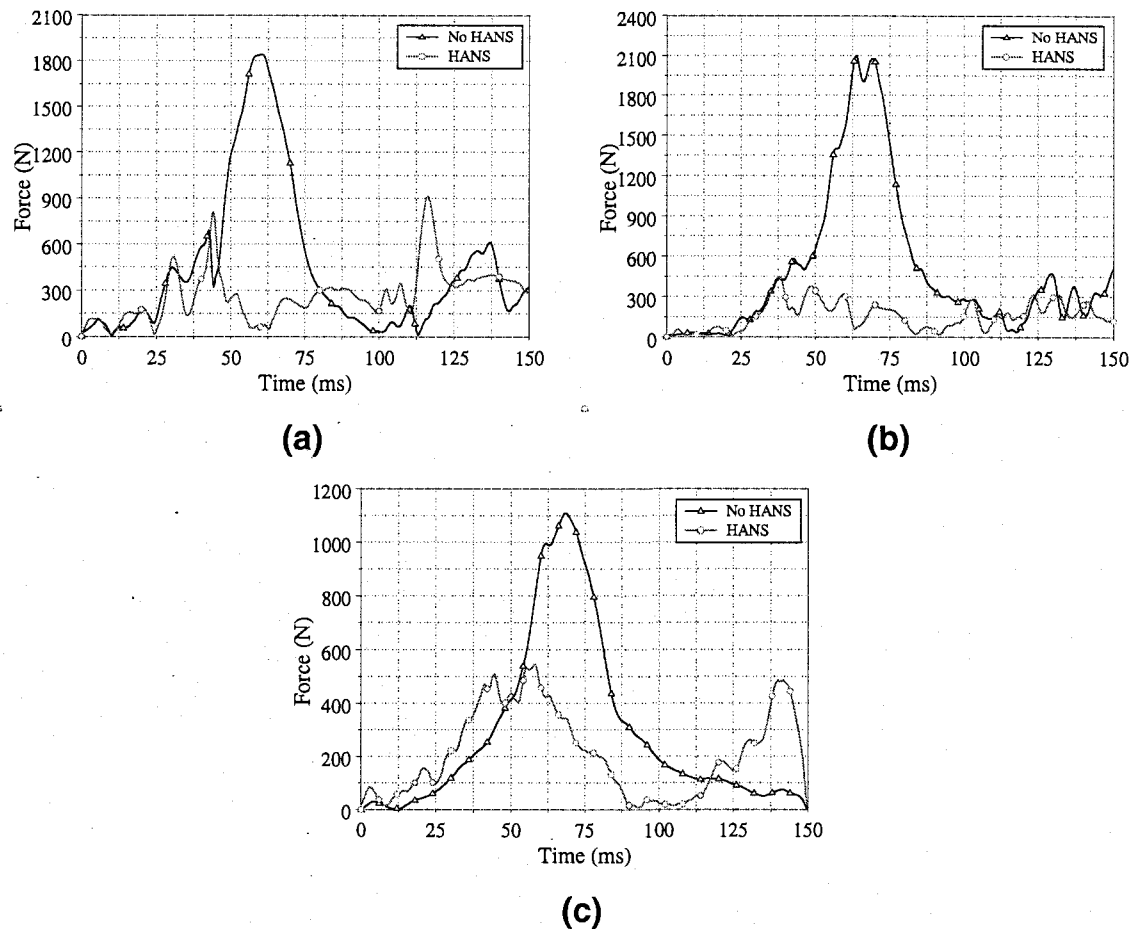


Figure 145. Resultant upper neck forces in the absence and presence of the HANS device for (a) Hybrid III dummy and (b) Q3 dummy, and (c) Resultant cross-sectional forces for child FE model as a function of time.

9.4.4 Resultant upper and lower neck moments

Similar time profiles with similar peak values were predicted for the upper neck moments for the Hybrid III and Q3 child dummies. These values are tabulated in Tables 16 and 17. Resultant lower neck moments are presented in Figure 146 (a) and (b) respectively as a function of time. A reduction of approximately 70 percent was predicted in the resultant lower neck moments with the addition of HANS device for both Hybrid III and Q3 child dummies.

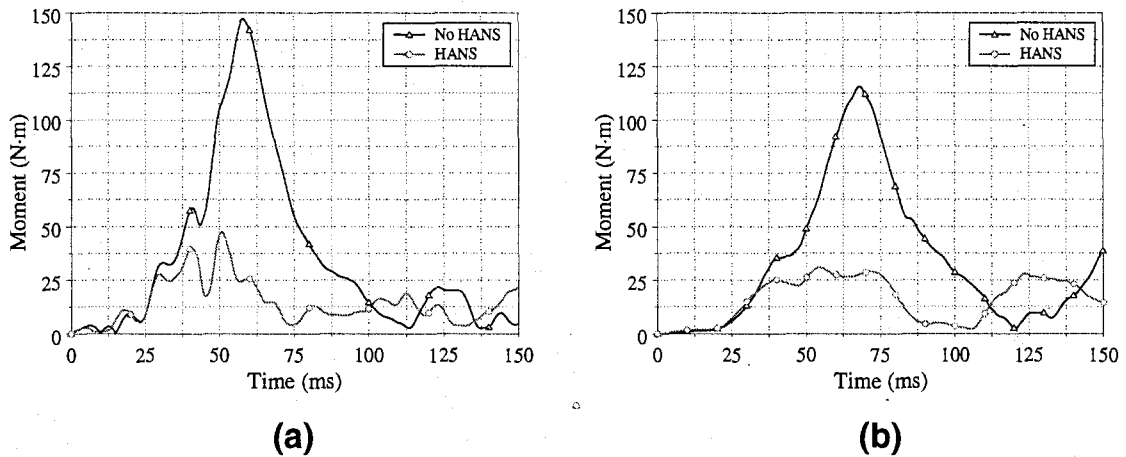


Figure 146. Resultant lower neck moments in the absence and presence of the HANS device for (a) Hybrid III dummy, and (b) Q3 dummy.

9.4.5 Head injury criteria

Head injury criteria were evaluated over a 15 ms and 36 ms time interval using equation 1. The maximum values obtained from equation 1 for both the situations (with and without HANS device) are presented in Tables 16 and 17, and illustrated in Figure 147. For the Hybrid III 3-year-old child dummy the HIC_{15} was predicted to be reduced by approximately 20 percent. The addition of a HANS device resulted in a reduction of approximately 50 percent in HIC_{15} and 40 percent in HIC_{36} for the Q3 child dummy. For the child FE model a reduction of approximately 30 to 40 percent in the head injury criteria was predicted due to addition of the HANS device.

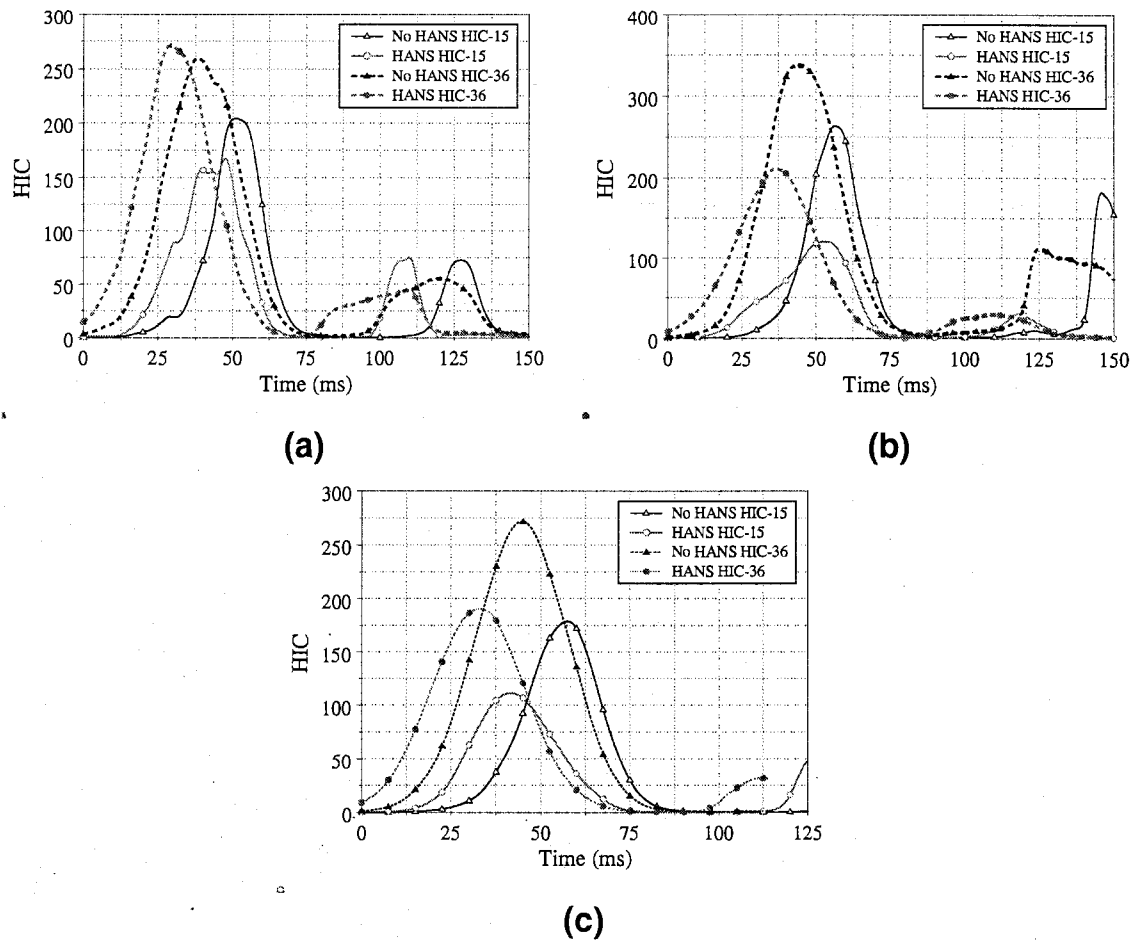


Figure 147. Head Injury Criteria (HIC_{15} and HIC_{36}) in the absence and presence of HANS device for (a) Hybrid III dummy, (b) Q3 dummy and (c) child FE model as a function of time.

9.4.6 Neck injury criteria

Figures 148 (a) and (b) illustrate respectively the N_{ij} as a function of time for both the Hybrid III and the Q3 child dummies in the absence and presence of the HANS device. The N_{ij} presented in Figure 148 was evaluated based upon the information acquired from the upper neck load cell. Values for the N_{ij} due to the addition of the HANS device illustrate significantly lower values than the N_{ij} for the condition in the absence of the HANS device over the entire time domain. A reduction of approximately 25 percent was predicted for the Hybrid III dummy, and 40 percent for the Q3 dummy, in

the peak values for the neck injury criteria for the first 100 ms of the numerical simulations.

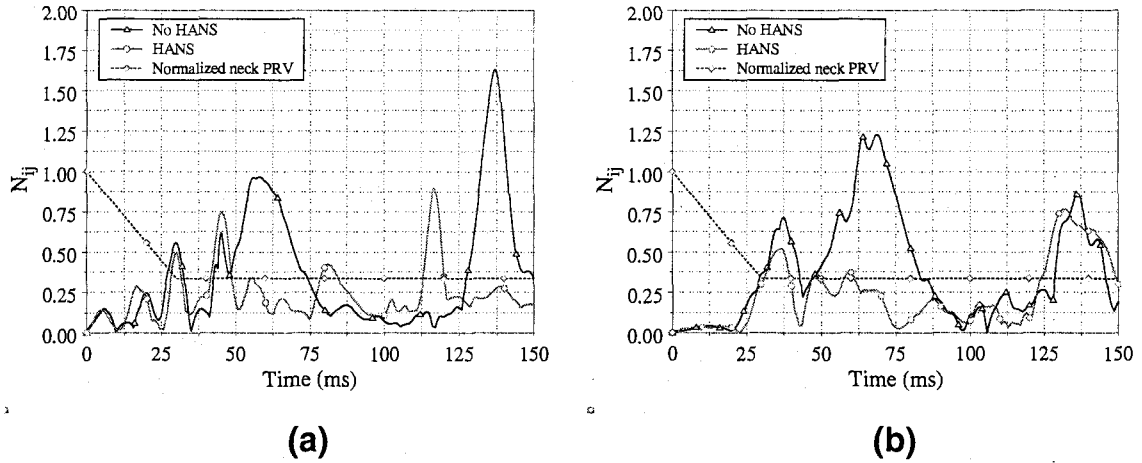


Figure 148. Neck Injury Criteria (N_{ij}) in the absence and presence of the HANS device for (a) Hybrid III dummy and (b) Q3 dummy as a function of time.

Tables 16 and 17 summarize the peak values predicted for the numerical simulations conducted in the absence and presence of the HANS device. The addition of HANS device reduced the head excursion by approximately 25 percent for the Q3 child dummy and the child FE models. Similar values for the head excursion were predicted for the Hybrid III 3-year-old child dummy.

Table 16. Summary of peak values of various injury parameters predicted for the Hybrid III and the Q3 child dummies in the absence and presence of the HANS device.

	Hybrid III 3-year-old		Q3	
	No HANS	HANS	No HANS	HANS
Resultant head acceleration (g's)	50.3	51.4	62.8	37.1
Resultant chest acceleration (g's)	44	44	44	41.7
Head injury criteria (HIC-15)	203.5	163	263	120.4
Head injury criteria (HIC-36)	258.6	270.7	337	211.5
Resultant upper neck force (N)	1841.6	912	2100	443
Resultant lower neck force (N)	790.9	1095	563	610
Resultant upper neck moment (N.m)	39.86	36	18.4	16.2
Resultant lower neck moment (N.m)	146.7	45.6	115	30.8
Neck injury criteria (Nij)	0.95	0.73	1.22	0.75
Head Excursion (mm)	259.8	244	376.7	276
Knee Excursion (mm)	493.5	518	515	527
Probability of AIS 3+ head injuries (%)	6.7	4.6	10.8	2.7
Probability of AIS 3+ neck injuries (%)	20.48	14.3	30.47	14.8
Probability of AIS 3+ chest injuries (%)	46.87	46.87	46.87	42.9

Table 17. Summary of peak values of various injury parameters predicted for the child FE model in the absence and presence of the HANS device.

	Child FE Model	
	No HANS	HANS
Resultant head acceleration (g's)	44.6	35.8
Resultant chest acceleration (g's)	29.3	36.4
Head injury criteria (HIC-15)	176	110
Head injury criteria (HIC-36)	271.5	190.7
Cross-sectional force (N)	1110	546.7
Head Excursion (mm)	318.22	230
Knee Excursion (mm)	614	620
Probability of AIS 3+ head injuries (%)	5.4	2.39
Probability of AIS 3+ chest injuries (%)	24.3	34.36

9.4.7 Head trajectories

Figure 149 presents the trajectories of the centre of mass of the head (local z axis displacements as a function of local x axis displacements) for the three child models for both the no HANS and presence of HANS situations. The displacements were measured relative to the rigid portion of the seat buck. Lower excursions in both local x and z directions were predicted for all the three FE models due to implementation of HANS device. The presence of the HANS device demonstrated a reduction of approximately 27 percent in the head excursions for the Q3 dummy and the child FE model.

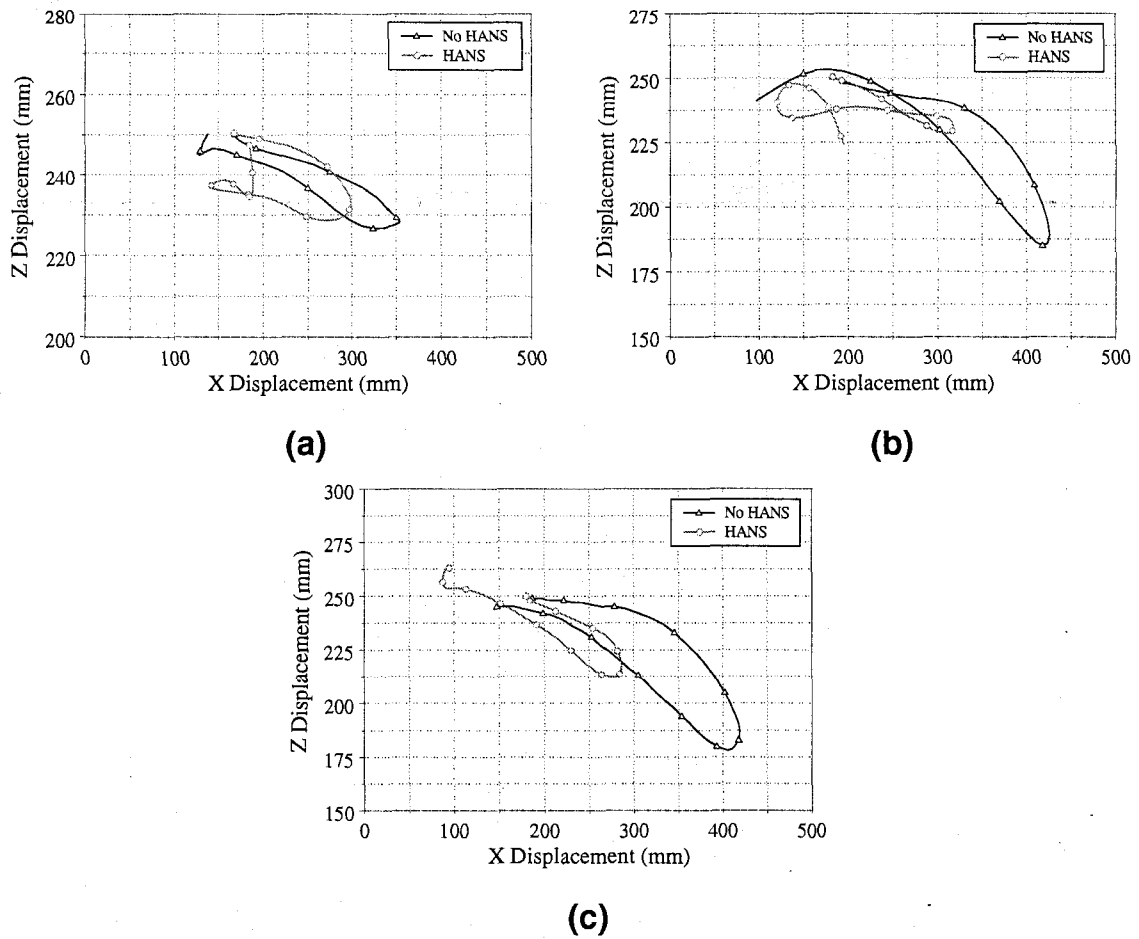


Figure 149. Head trajectories of the center of mass in the absence and presence of a HANS device for (a) Hybrid III dummy, (b) Q3 dummy and (c) Child FE model.

9.5 Discussion

9.5.1 Injury risk analysis

Tables 16 and 17 also summarize the probability of severe head, neck and chest injuries to the child dummies and the child FE model. These values have been evaluated using the Prasad and Mertz injury risk probability curves (Appendix B) for the maximum values of HIC , N_{ij} , and chest accelerations. There is a high risk of sustaining severe chest injuries for both the Hybrid III and the Q3 dummies in the absence and presence of the HANS device. Whereas a moderate risk of chest injuries was calculated for the child FE

model in both the configurations. There is a high risk of sustaining severe neck injuries for the Q3 dummy and a moderate risk of severe neck injuries for the Hybrid III dummy in the presence of the HANS device. It should be noted that the probability of acquiring severe neck injuries was reduced to a low risk for both the dummies due to the presence of the HANS device. The probability of severe head injuries was predicted to be low for all the child models for both the absence and presence of the HANS device.

9.5.2 Protection reference values

The recommended critical values for head and chest accelerations is 80 g's and 60 g's respectively [32]. The peak values for resultant head and chest accelerations noted in Tables 16 and 17 were observed to be less than these critical values for both the absence and the presence of the HANS device. Figure 148 also presents the normalized neck PRV proposed by Klinich et al. [32]. It is worth noting that the neck injury criteria curves obtained with the addition of the HANS device were observed to be lower than the PRV for a longer duration of time.

In a frontal crash, the seatbelt restrains the torso of the child but the head is restrained only by the neck. The HANS device acts like a lever between the head and the torso of the child. This provides a change in loading path; therefore the high forces are transferred from the head to the torso through the HANS device instead of the neck. After 30 ms, to the crash, the critical load that can be sustained without causing injury is approximately 1,000 N for a 3-year-old child dummy [32]. Figure 140 illustrates higher magnitudes (approximately 1800 N and greater) of upper neck resultant force for the child dummies. A reduction in the upper neck resultant forces due to the presence of the HANS device of approximately 40 percent and 80 percent was observed for the Hybrid III and the Q3 dummy respectively. In addition, a reduction of approximately 50 percent was observed in the cross-sectional forces for the child FE model due to the presence of the HANS device. The HANS device produced a reduction in the whipping action of the head that results in a reduction of the inertial loads. A reduction of approximately 30 – 50 percent was observed in the head injury criteria due to the

presence of a HANS device. Therefore the probability of sustaining severe inertia-based head and neck injuries is drastically reduced by using a HANS device.

In crash tests without a HANS device, neck rotation is largest due to the swinging motion of the head. The HANS tethers restrain the head with forces that directly counteract the head's forward excursion while the torso and HANS collar are restrained by the shoulder harness. The qualitative and quantitative analysis illustrates a reduction of approximately 50 percent in the neck rotation and 70 percent in the neck moments due to the presence of a HANS device. Extreme hyper-flexion leads to rupture of the tectorial membrane and separation of vertebrae which leads to AOD [40]. Therefore, there is a higher probability for a child to acquire an AOD in the case of a frontal impact in the absence of a HANS device. The presence of the HANS device demonstrated a reduction of approximately 27 percent in the head excursions for the Q3 dummy and the child FE model. Also, a reduction in the head excursions decreases the probability of the child to acquire excursion based contact injuries.

Frontal impact testing has been completed at DaimlerChrysler in the absence and presence of the HANS device utilizing an adult male dummy [110]. The experimental crash results demonstrated a reduction of approximately 80 percent in the neck forces and 70 percent in the *HIC* for an adult due to the presence of a HANS device. The head excursion was observed to be reduced by approximately 40 percent [110]. The HANS device utilized in this research exhibited a reduction of approximately 40 – 80 percent in the neck forces, 30 – 50 percent in the *HIC* and 27 percent in the head excursion for all the child models. These observations are consistent with the experimental results [110] with a difference in the magnitudes. This can be attributed to the difference in anatomy of a child and an adult, and the difference in the geometry of the HANS device and the materials used. Incorporation of a HANS device for toddlers in a frontal crash illustrates a reduction in both acceleration induced injuries and excursion based contact injuries.

10. SIDE IMPACT PROTECTION

10.1 Countermeasure development

The complex model employing a Hybrid III 3-year-old dummy has been validated in near side impact, which is detailed in Section 6.5. The numerical model incorporating a rigid wall is illustrated in Figure 109. There are a considerable number of uncertainties in a vehicle crash and child injury mechanisms for side impacts at the present time, which may inhibit the development of a novel device to significantly reduce the possibility of injury. In this research, the use of a rigid ISOFIX system as a means for anchoring the CRS, and energy absorbing foams as methods to attenuate injuries in side impacts, have been investigated. In near-side impact situations, the main cause of injury is contact related [62 and 63]. Therefore a reduction in lateral displacement of the CRS and the child's head may attenuate the amount of injury sustained in near-side crashes.

10.1.1 Rigid ISOFIX system

A rigid ISOFIX system with rectangular cross-section, as outlined in UNECE Regulation 14 [83], was modeled as a method of anchoring the CRS to the vehicle seat using FEM. In addition, a cross-shaped ISOFIX system was also investigated. Figure 150 illustrates the three different anchoring methods used in this research. A cross-shaped ISOFIX system would limit the lateral displacement of the CRS more compared to the rectangular shaped ISOFIX system. Both the ISOFIX systems were modeled using fully integrated shell elements and were assigned material properties of steel (Elastic modulus = 207 GPa, density = 7800 kg/m³, Poisson's ratio = 0.3). An elastic/plastic behaviour was defined for the ISOFIX systems with the yield strength of 210 MPa and the ultimate tensile strength of 475 MPa. The material and sectional properties for the ISOFIX are presented in Appendix D. The linear dimensions of the rectangular section ISOFIX system were 67 mm length, by 30 mm height, by 3 mm thickness. The cross-shaped section ISOFIX system was comprised of two mutually

perpendicular rectangular sections at the center, with the same cross-section dimensions of the individual rectangular section. The ISOFIX was constrained to the CRS and the vehicle seat using a constrained extra nodes card in LS-DYNA. Simulations were completed utilizing a Hybrid III 3-year-old dummy, a Q3s child dummy and the child FE model with all the three anchoring methods under the identical acceleration pulse (Figure 37) for side impact.

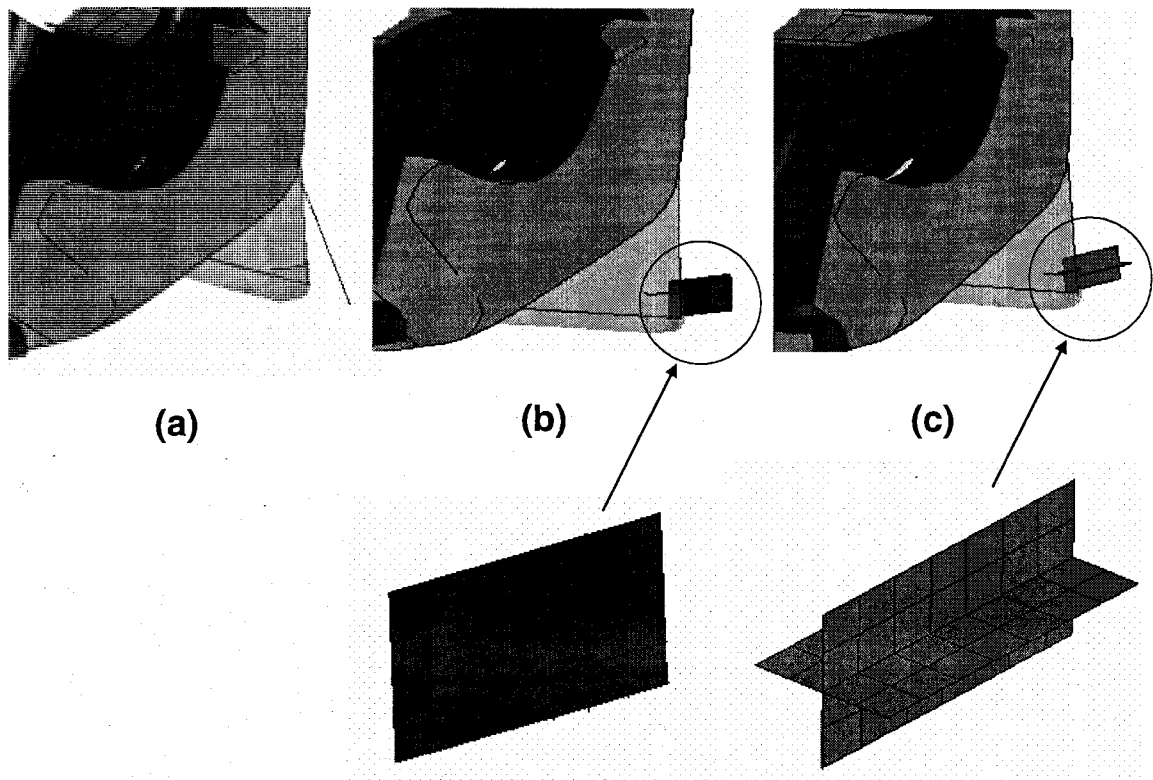


Figure 150. Different anchoring methods: (a) flexible LATCH, (b) rigid ISOFIX rectangular section, and (c) rigid ISOFIX cross-shaped section.

10.1.2 Energy absorbing foam

Wang et al. [117] have investigated the use of energy absorbing foams as a method to attenuate injuries in side impacts. The addition of low-density polymeric energy absorbing foam applied through the entire length of both side wings was considered, with addition of a significant amount of foam in the vicinity of the head/wings of the CRS. In this research a similar concept has been utilized by changing

the geometry and material properties. Energy absorbing foam was added in the region of the CRS where contact between the child's head and the CRS may occur during side impacts. It was expected that during side crashes the dummy's head would contact the energy absorbing foam and the corresponding foam deformation would help minimize the lateral displacement of the head and the injury probability. Material characteristics were identical to the padding on the back of the CRS as taken from Turchi et al. [100 and 101]. Contact between the foam blocks and the CRS (Appendix E) was modeled using a tied nodes to surface contact algorithm in LS-DYNA. The nonlinear stress/strain relationship used for the foam padding was also incorporated into the material model for the foam. Figure 151 depicts the modified CRS with the additional side foam blocks. Simulations were completed with the foam and different configurations of the rigid ISOFIX under the identical acceleration pulse for side impact (Test 4585) for the Hybrid III 3-year-old dummy, the Q3s child dummy and the child FE model for all the three methods of CRS anchoring.

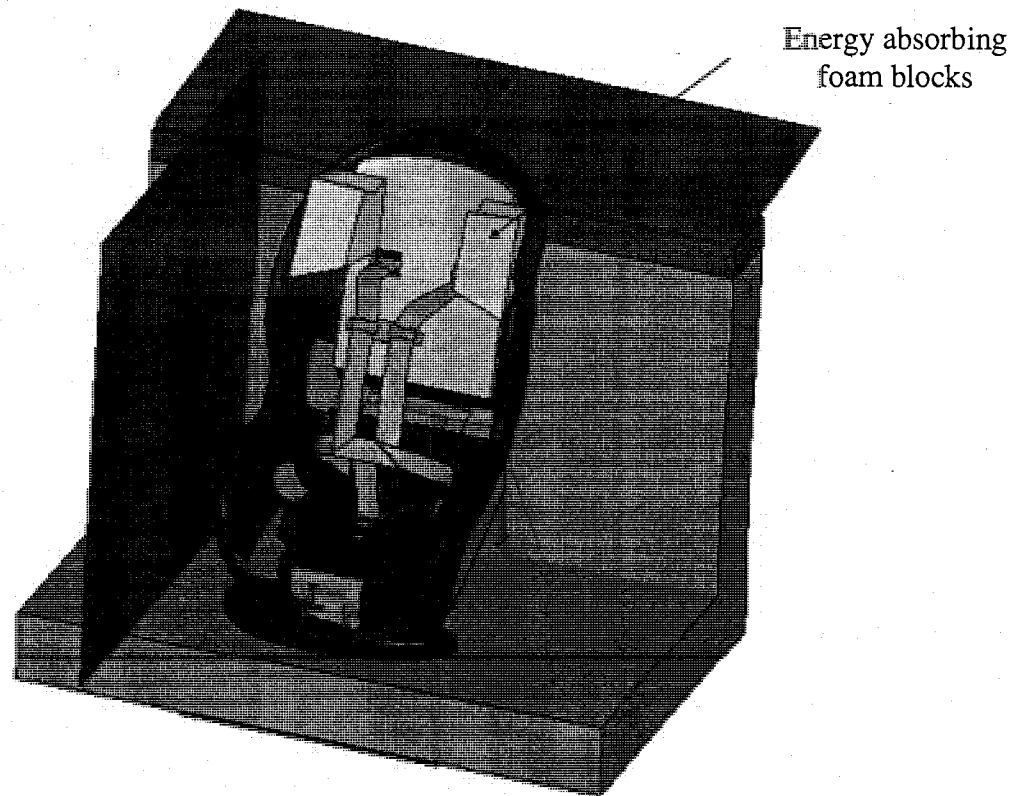


Figure 151. Finite element model of the CRS with additional energy absorbing foam blocks.

An analysis of the injury parameters and kinematics experienced by the Hybrid III and the Q3s dummies, and the child FE model during the simulated side impact was completed. The peak values predicted for the resultant head and chest accelerations, head injury criteria, the upper neck lateral shear and bending as well as the lateral displacement of the center of mass of the head for all the numerical simulations in the absence and presence of foam blocks are tabulated in Tables 18 – 23 (Pages 265 - 266).

10.2 Qualitative analysis

Figures 152, 153 and 154 illustrate the configuration for the Hybrid III 3-year-old, the Q3s child dummies and the child FE model at the times when maximum lateral displacement of the dummy and the CRS was predicted. The flexible LATCH system exhibited the maximum lateral displacement of the CRS and the dummies. For all the child models, CRS contact and foot contact occurred for the flexible LATCH anchoring. Head contact was predicted for the Q3s child dummy and the child FE model for the flexible LATCH configuration. A reduction in lateral head and CRS displacement was predicted for the rigid ISOFIX rectangular section, with minimal CRS contact. Foot contact was predicted for the Q3s child dummy and the child FE model. Use of the rigid ISOFIX system with cross-shaped section further reduced the lateral displacement of the head and the CRS. Contact between the CRS and the rigid wall was not predicted for this configuration for both Hybrid III and Q3s child dummies and the child FE model. A foot contact was predicted for the Q3s child dummy and the child FE model for the rigid ISOFIX with cross-shaped section configuration.

The response of the neck of the Q3s dummy and the child FE model differed considerably from the Hybrid III dummy. For the Q3s dummy and the child FE model, a greater amount of bending in both the lateral and forward directions was predicted. This can be attributed to the geometrical and material differences between the necks of both the dummies and the child FE model. The kinematic response of the Q3s child dummy was predicted to be closer to the response of the child FE model. This is consistent with

the results noted in Section 6.3. Addition of energy absorbing foam illustrated a further reduction in the lateral displacement of the head for all the child models.

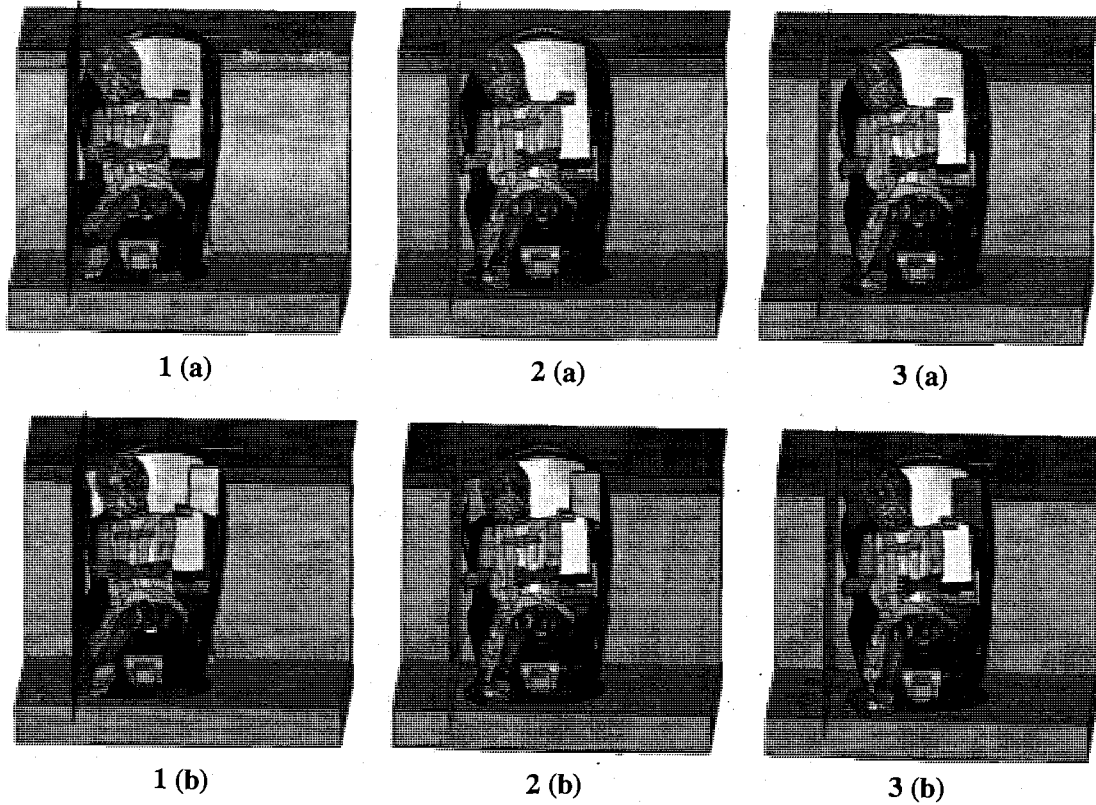


Figure 152. Maximum head and CRS displacement predicted by the Hybrid III 3-year-old dummy for:

1. Flexible LATCH (a) without foam blocks, and (b) with foam blocks
2. Rigid ISOFIX rectangular section (a) without foam blocks, and (b) with foam blocks
3. Rigid ISOFIX cross-shaped section (a) without foam blocks, and (b) with foam blocks

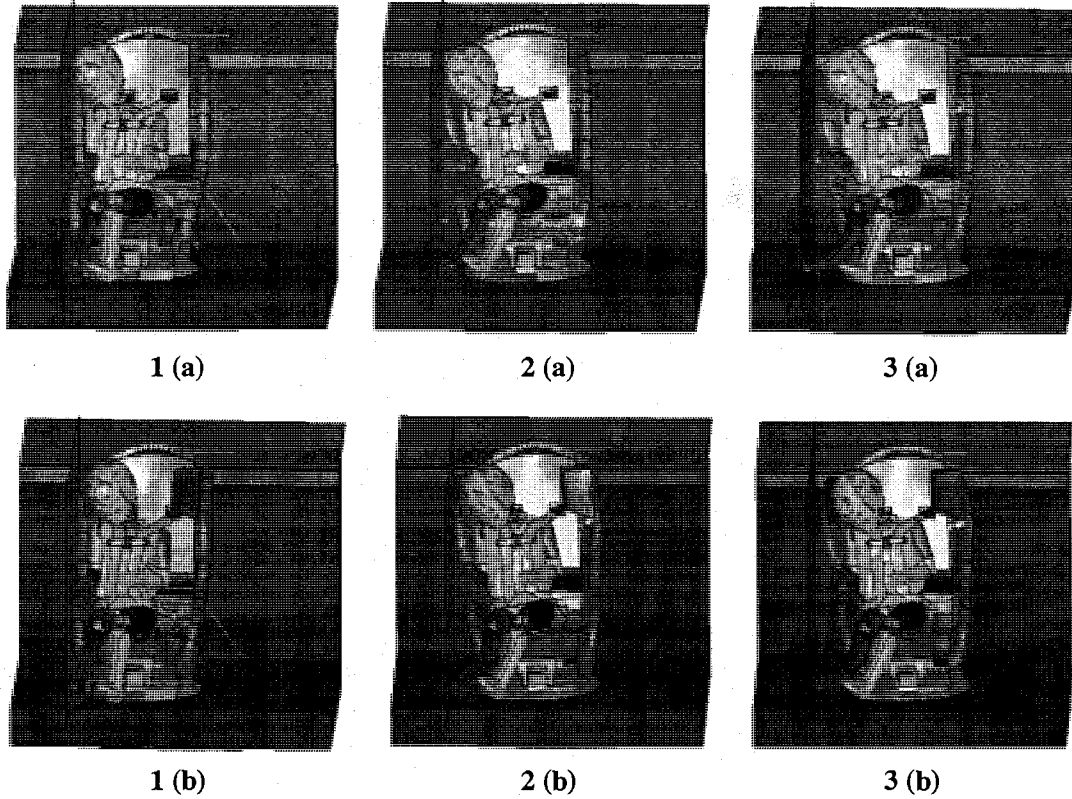


Figure 153. Maximum head and CRS displacement predicted by the Q3s dummy for:

1. Flexible LATCH (a) without foam blocks, and (b) with foam blocks
2. Rigid ISOFIX rectangular section (a) without foam blocks, and (b) with foam blocks
3. Rigid ISOFIX cross-shaped section (a) without foam blocks, and (b) with foam blocks.

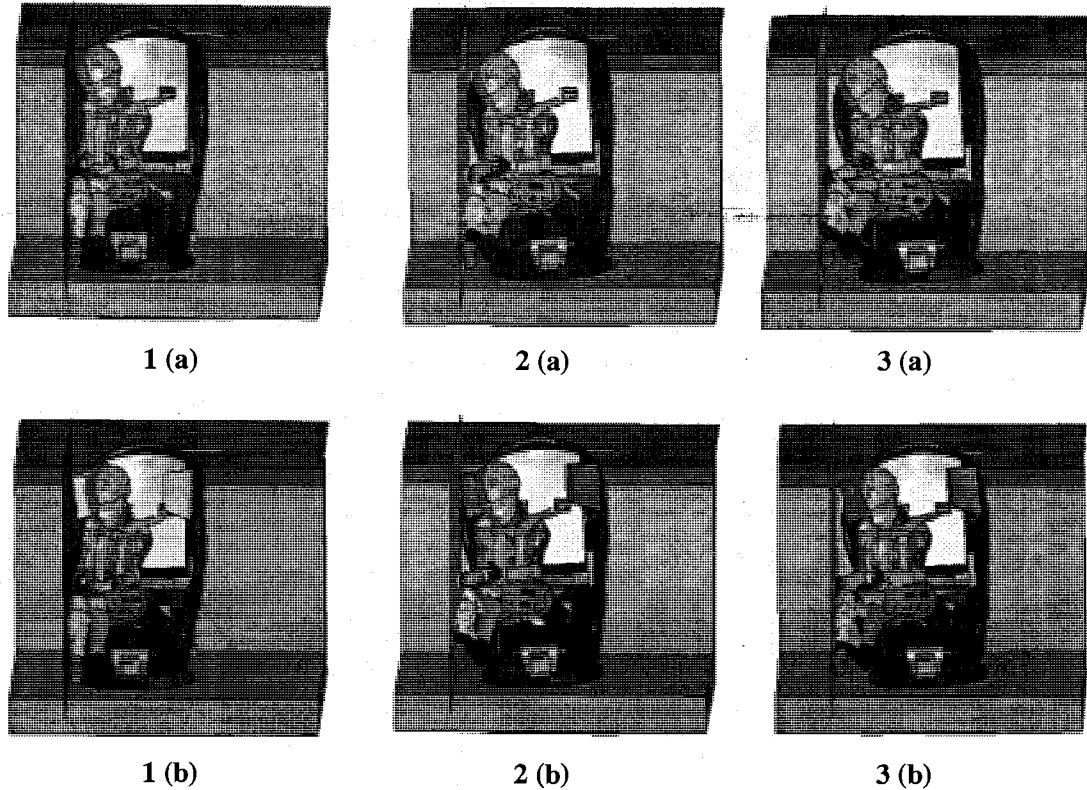


Figure 154. Maximum head and CRS displacement predicted by the child FE model for:

1. Flexible LATCH (a) without foam blocks, and (b) with foam blocks
2. Rigid ISOFIX rectangular section (a) without foam blocks, and (b) with foam blocks
3. Rigid ISOFIX cross-shaped section (a) without foam blocks, and (b) with foam blocks.

10.3 Quantitative analysis

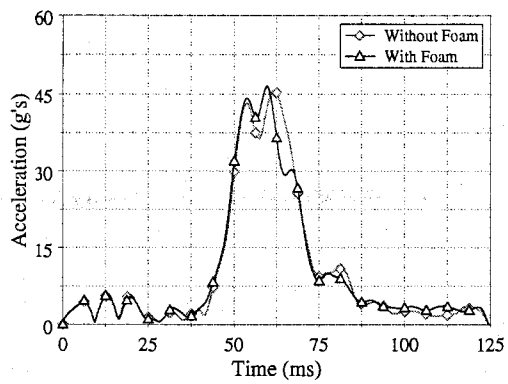
10.3.1 Resultant head accelerations

Figures 155, 156 and 157 illustrate the resultant head acceleration profiles as a function of time for all three anchoring configurations (with and without foam) for both the Hybrid III and the Q3s child dummies, and the child FE model. Similar time profiles with similar peak values were predicted for the resultant head accelerations for the

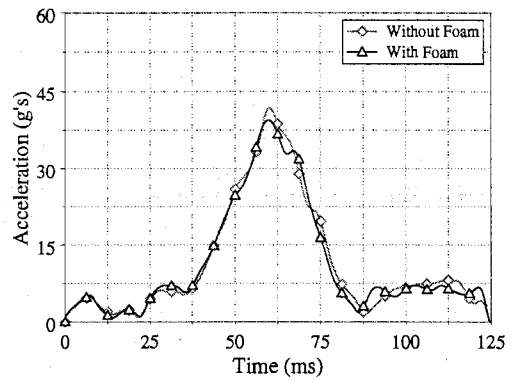
Hybrid III 3-year-old child dummy for all three anchoring configurations. The Q3s dummy and the child FE model exhibited higher peak values for the flexible LATCH configuration. These high values were predicted due to contact of the dummy's head with the rigid wall, which was also predicted in the qualitative analysis. A reduction of approximately 50 percent was predicted in the resultant head accelerations for the Q3s child dummy and the child FE model for both the rigid ISOFIX systems. Addition of foam was effective in reducing the head accelerations further by approximately 10 to 20 percent.

10.3.2 Resultant chest accelerations

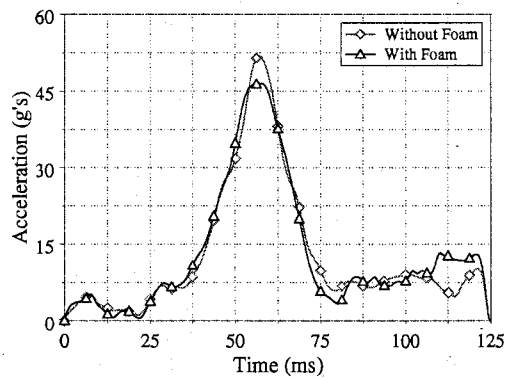
The resultant chest acceleration time profiles are shown in Figures 158, 159 and 160 for both the Hybrid III and Q3s child dummies and the child FE model. It was predicted that the rigid ISOFIX with the rectangular section was effective in reducing the resultant chest accelerations by approximately 50 percent for both the Hybrid III 3-year-old and Q3s child dummies. Whereas the rigid ISOFIX system with cross-shaped section reduced the resultant chest accelerations by 40 percent compared to the values predicted by the flexible LATCH configuration. For the child FE model the resultant chest accelerations were reduced by 30 percent for both the ISOFIX systems. Addition of energy absorbing foam blocks further reduced the chest accelerations by approximately 5 percent for both the child dummies.



(a)

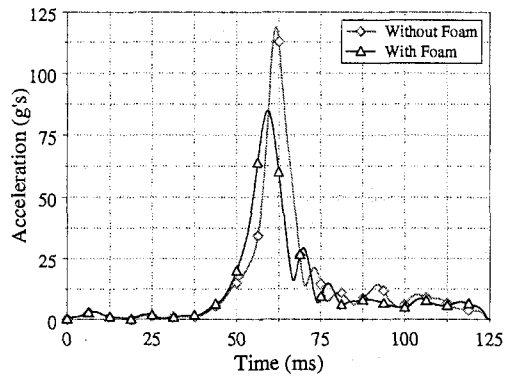


(b)

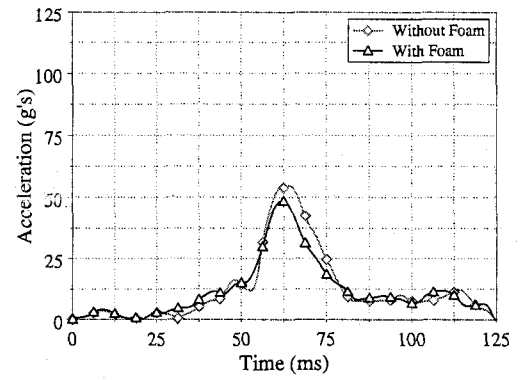


(c)

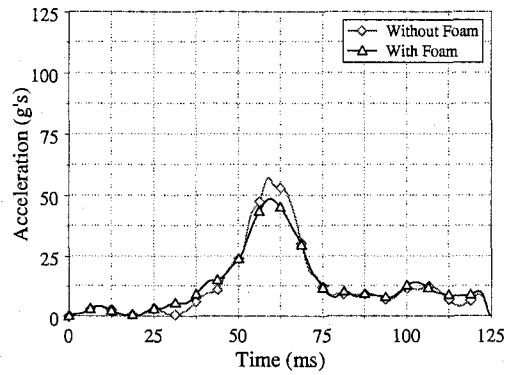
Figure 155. Resultant head acceleration profiles for the Hybrid III 3-year-old dummy as a function of time in the absence and presence of foam blocks for (a) flexible latch, (b) rigid ISOFIX rectangular section and (c) rigid ISOFIX cross-shaped section.



(a)



(b)



(c)

Figure 156. Resultant head acceleration profiles for the Q3s child dummy as a function of time in the absence and presence of foam blocks for (a) flexible latch, (b) rigid ISOFIX rectangular section and (c) rigid ISOFIX cross-shaped section.

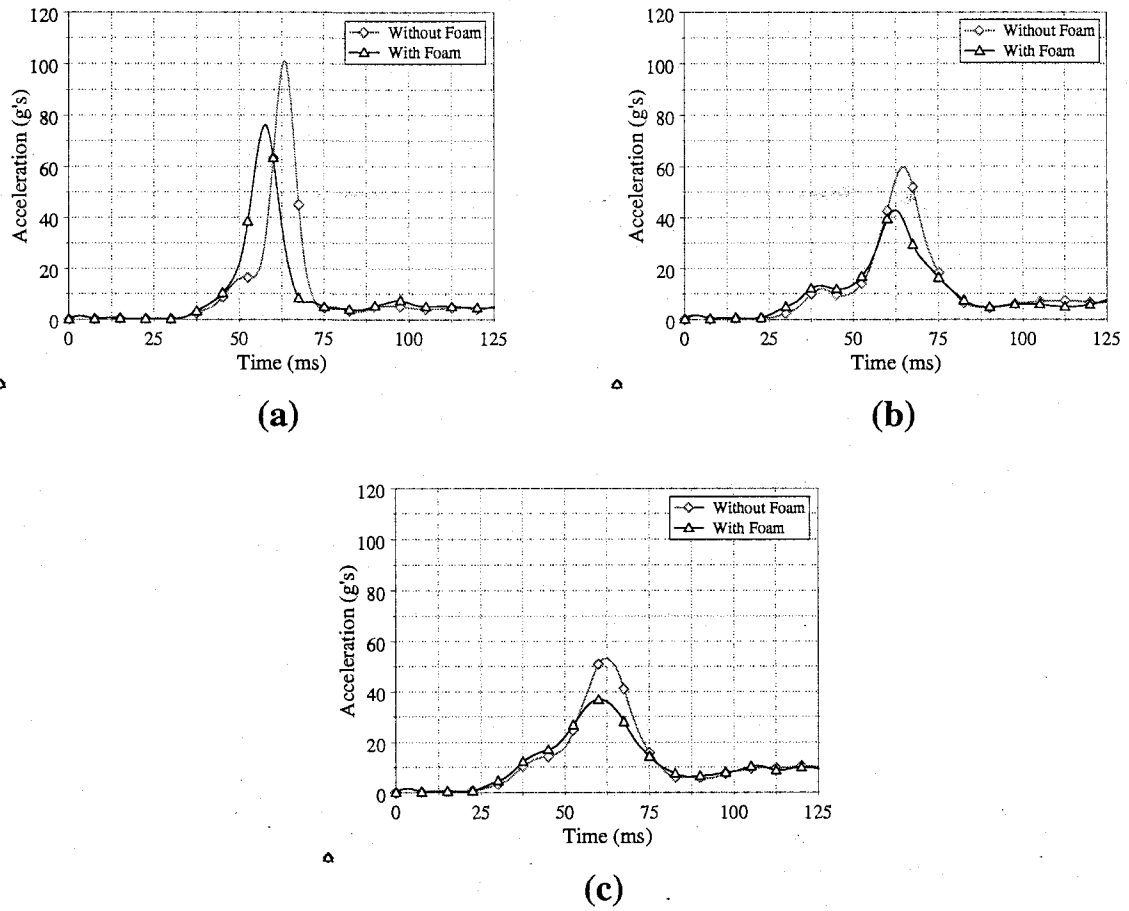
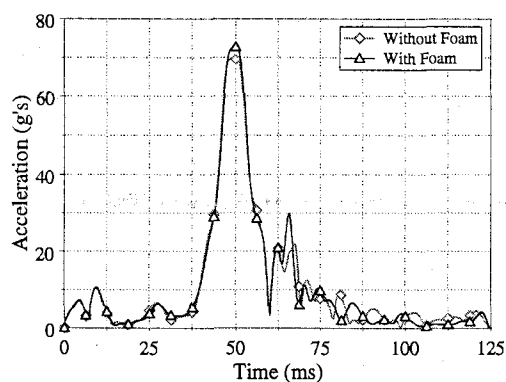
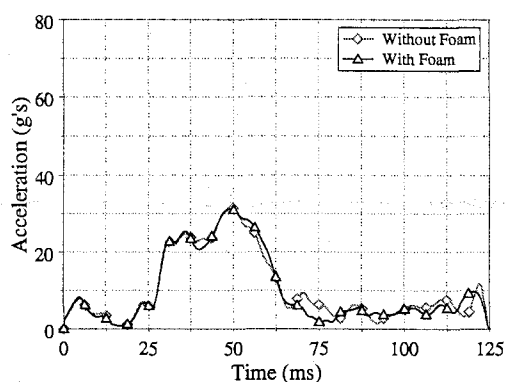


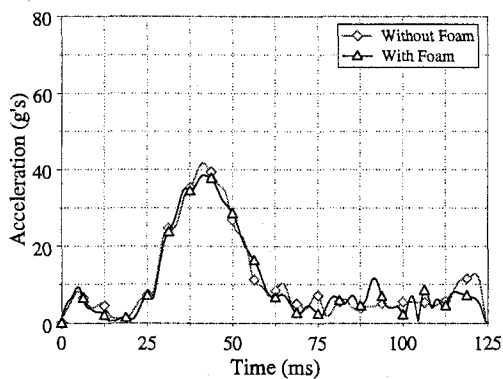
Figure 157. Resultant head acceleration profiles for the child FE model as a function of time in the absence and presence of foam blocks for (a) flexible latch, (b) rigid ISOFIX rectangular section and (c) rigid ISOFIX cross-shaped section.



(a)

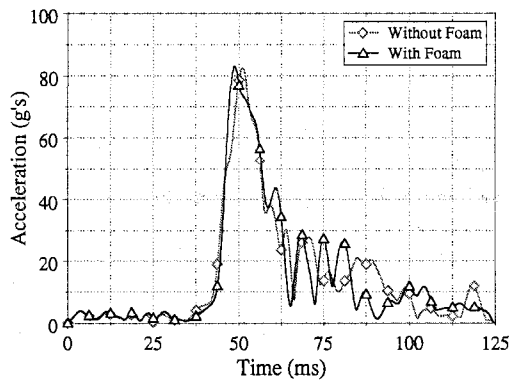


(b)

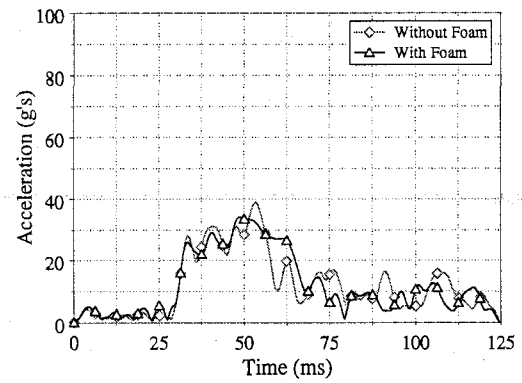


(c)

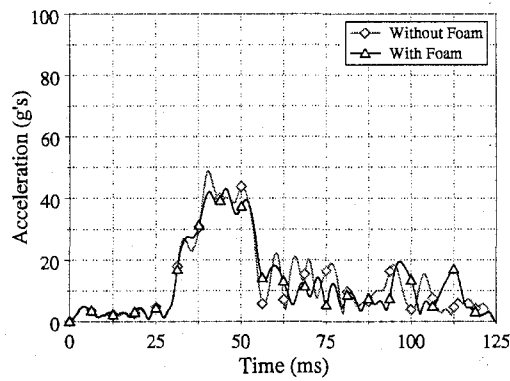
Figure 158. Resultant chest acceleration profiles for the Hybrid III 3-year-old dummy as a function of time in the absence and presence of foam blocks for (a) flexible latch, (b) rigid ISOFIX rectangular section and (c) rigid ISOFIX cross-shaped section.



(a)



(b)



(c)

Figure 159. Resultant chest acceleration profiles for the Q3s dummy as a function of time in the absence and presence of foam blocks for (a) flexible latch, (b) rigid ISOFIX rectangular section and (c) rigid ISOFIX cross-shaped section.

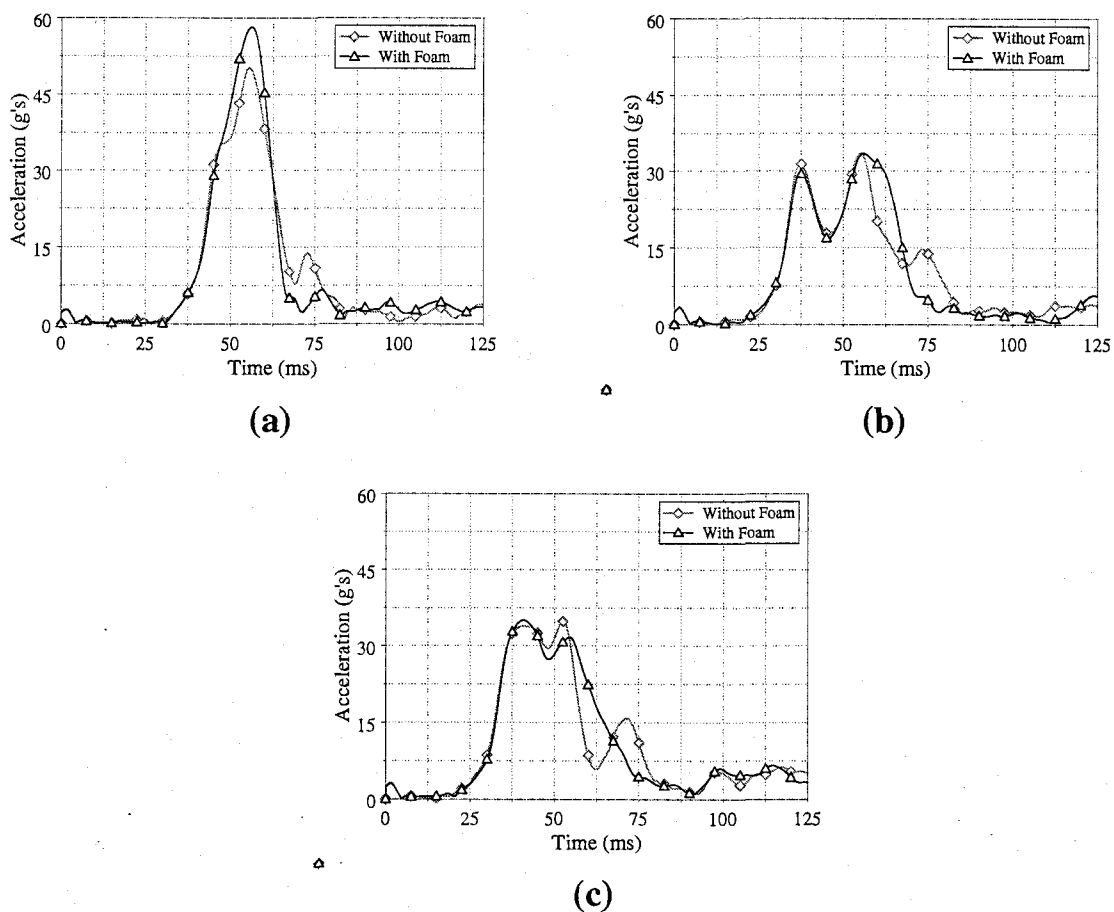


Figure 160. Resultant chest acceleration profiles for the child FE model as a function of time in the absence and presence of foam blocks for (a) flexible latch, (b) rigid ISOFIX rectangular section and (c) rigid ISOFIX cross-shaped section.

10.3.3 Lateral shear

Figures 161 and 162 exhibit the lateral shear (F_y) predicted at the upper neck load cell for both the dummies as a function of time. For the child FE model, the lateral shear (presented in Figure 163) was calculated based on the head acceleration in the local y -axis direction multiplied by the mass of the head (2.79 kg). A reduction of approximately 20 percent was predicted for the Hybrid III child dummy by using a rigid ISOFIX system instead of the flexible LATCH. The rigid ISOFIX system effectively reduced the lateral shear by approximately 45 percent for the child FE model and 57 percent for the Q3s dummy, compared to the flexible LATCH system. Comparatively

higher values of lateral shear were predicted for the Hybrid III 3-year-old dummy and the child FE model compared to the Q3s child dummy. This can be attributed to the difference in the neck characteristics of the three child models. Addition of foam was effective in further reducing the lateral shear by approximately 20 percent for the Hybrid III dummy, 25 percent for the child FE model and 30 percent for the Q3s child dummy respectively.

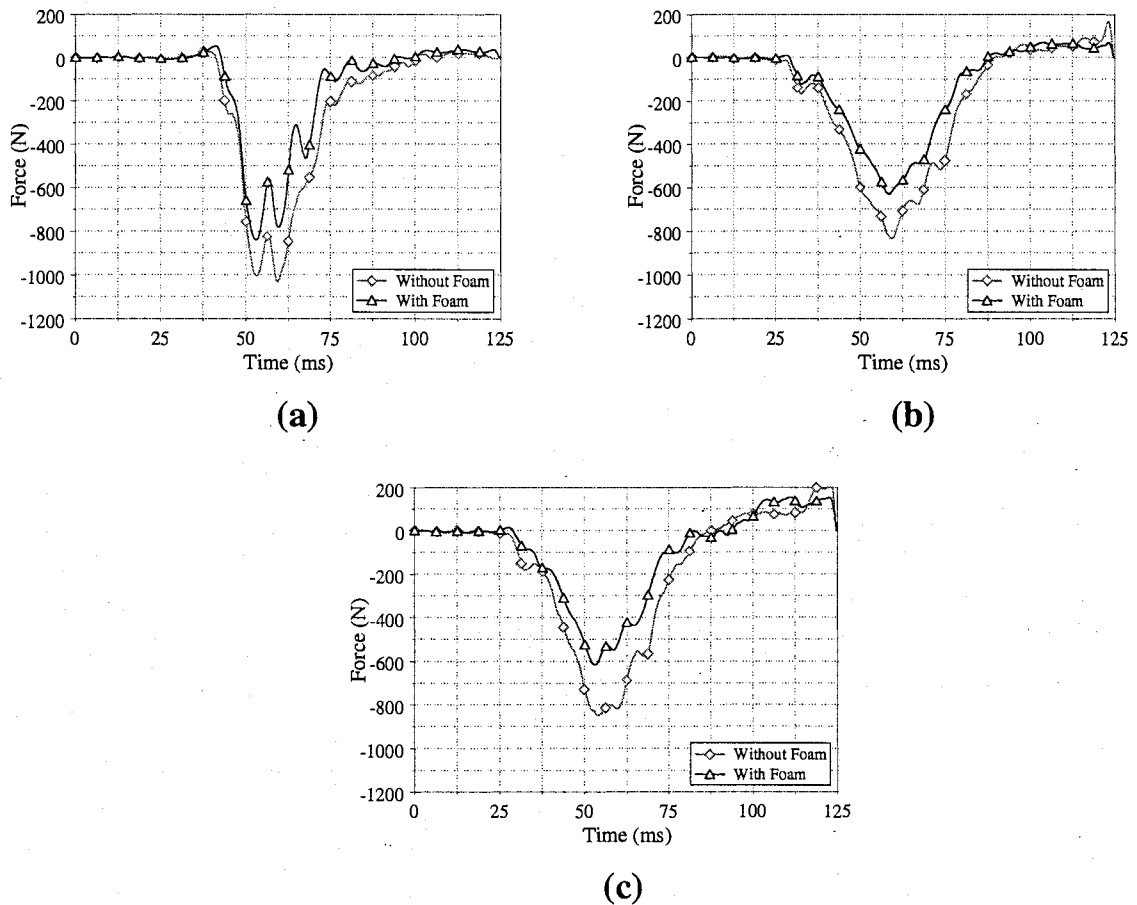
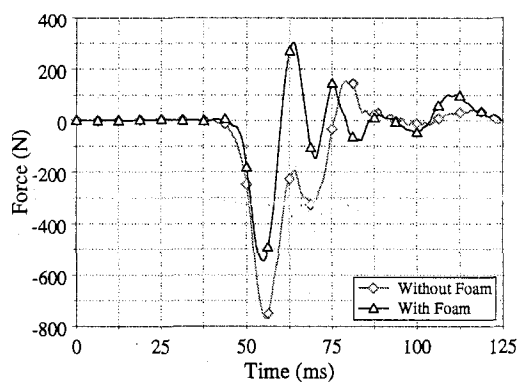
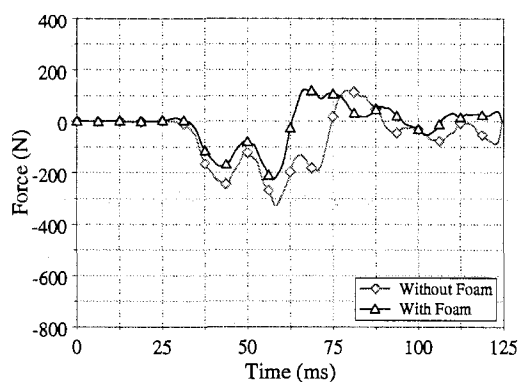


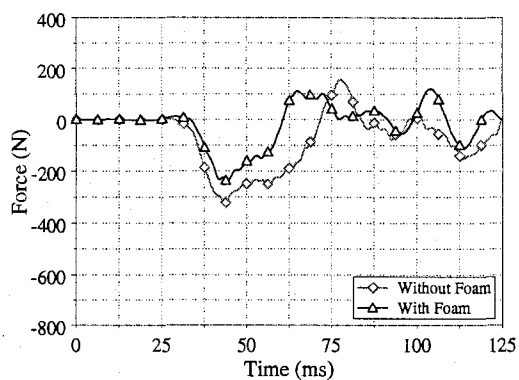
Figure 161. Lateral shear profiles for the Hybrid III child dummy as a function of time in the absence and presence of foam blocks for (a) flexible latch, (b) rigid ISOFIX rectangular section and (c) rigid ISOFIX cross-shaped section.



(a)



(b)



(c)

Figure 162. Lateral shear profiles for the Q3s child dummy as a function of time in the absence and presence of foam blocks for (a) flexible latch, (b) rigid ISOFIX rectangular section and (c) rigid ISOFIX cross-shaped section.

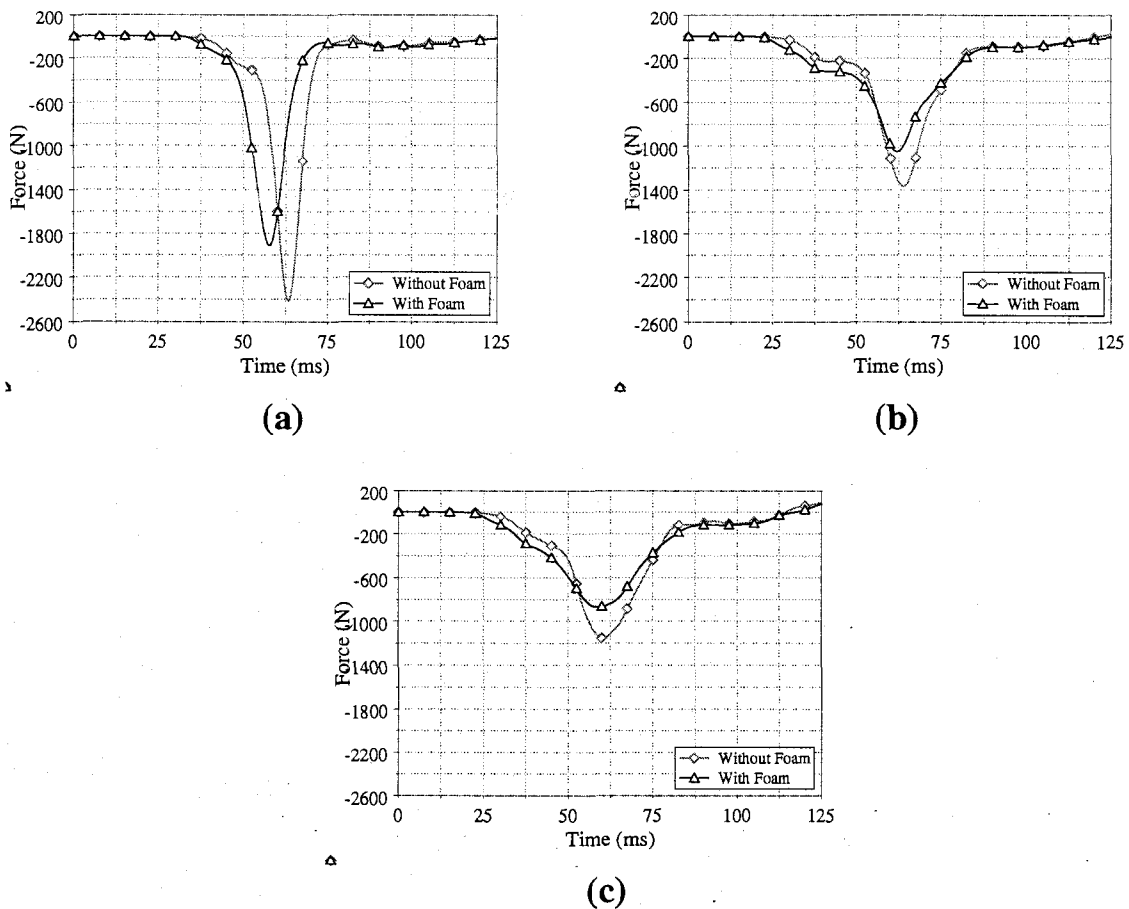


Figure 163. Lateral shear profiles for the child FE model as a function of time in the absence and presence of foam blocks for (a) flexible latch, (b) rigid ISOFIX rectangular section and (c) rigid ISOFIX cross-shaped section.

10.3.4 Lateral bending

Figures 164 and 165 illustrate the lateral bending (M_X) profiles as a function of time for all the three anchoring configurations (with and without foam) for both the Hybrid III and the Q3s child dummies. Bending moments could not be obtained for the child FE model due to the lack of instrumentation. The Hybrid III 3-year-old dummy exhibited similar time profiles for the lateral bending for all three anchoring systems with a difference in peak values. Use of rigid ISOFIX system was predicted to reduce the lateral bending by approximately 35 percent (rectangular section) and 30 percent (cross-shaped section) respectively, compared to the flexible LATCH configuration.

Addition of foam was predicted to further reduce the lateral bending of the Hybrid III dummy's neck by 10 percent. The Q3s dummy illustrated different time profiles for the lateral bending compared to the Hybrid III child dummy. This can be attributed to less stiffness in the Q3s neck which makes the neck more flexible. Both positive and negative moments were predicted for the Q3s dummy due to forward bending of the neck.

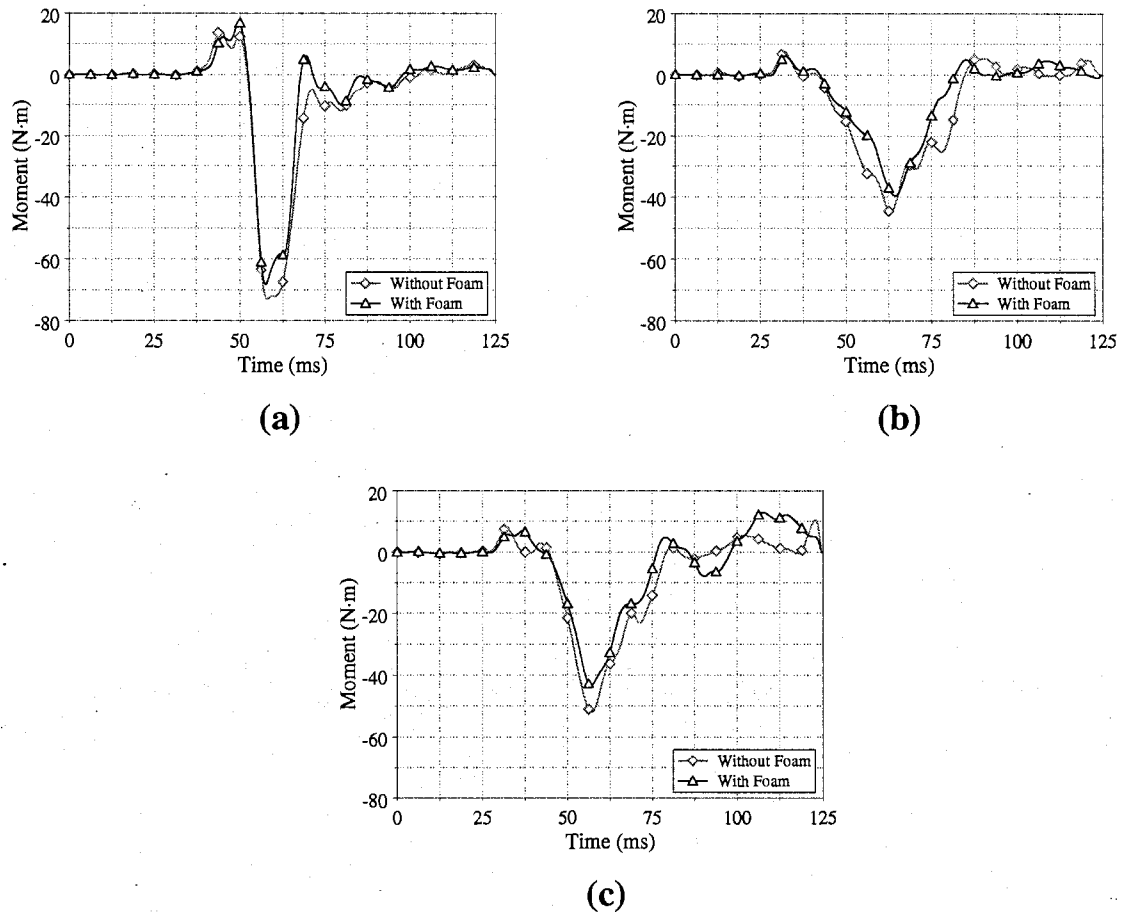


Figure 164. Lateral bending profiles for the Hybrid III child dummy as a function of time in the absence and presence of foam blocks for (a) flexible latch, (b) rigid ISOFIX rectangular section and (c) rigid ISOFIX cross-shaped section.

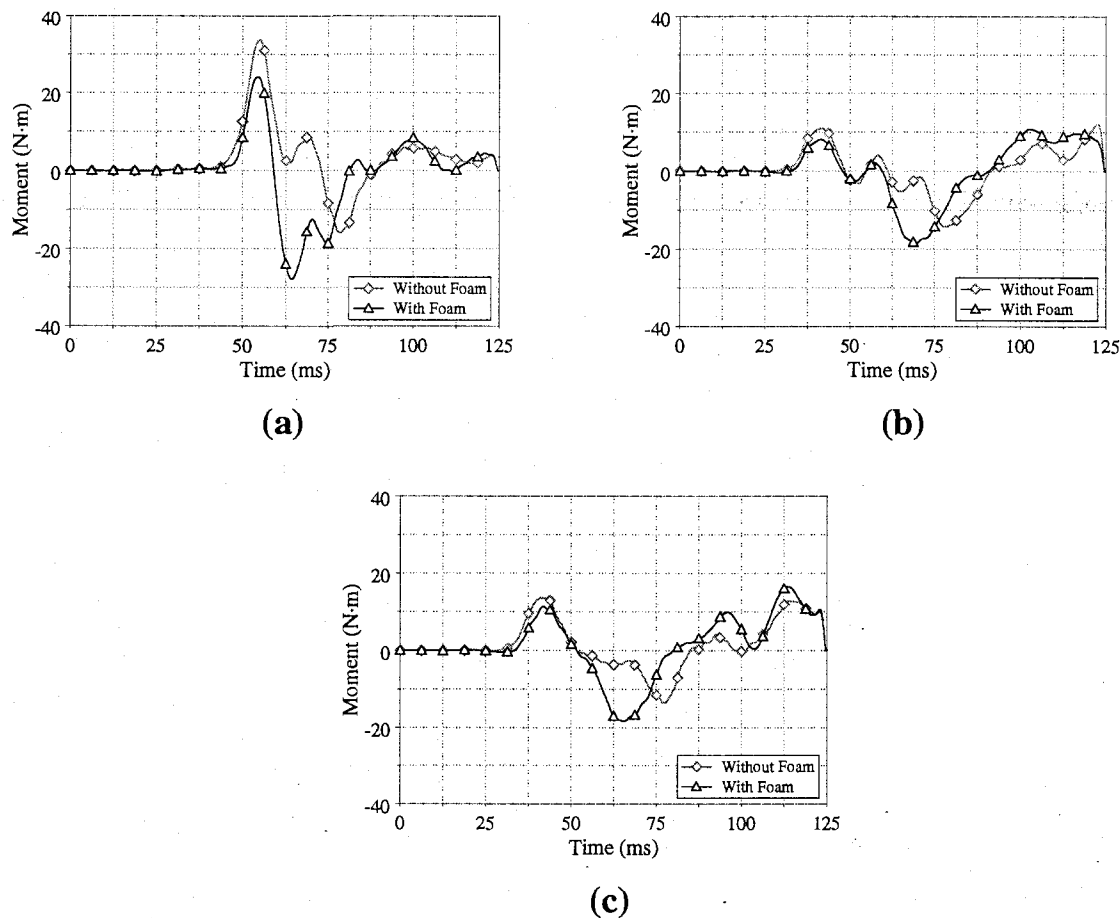


Figure 165. Lateral bending profiles for the Q3s child dummy as a function of time in the absence and presence of foam blocks for (a) flexible latch, (b) rigid ISOFIX rectangular section and (c) rigid ISOFIX cross-shaped section.

Tables 18 – 23 tabulate the peak values of lateral displacement of the center of gravity of the head for both the dummies. The lateral displacement of the head was reduced by 44 mm by using energy absorbing foam blocks with the rectangular section ISOFIX and by 68 mm using the cross-shaped section ISOFIX for the Hybrid III 3-year-old dummy compared to the flexible LATCH configuration. For the Q3s dummy and the child FE model, the lateral displacement of the head was reduced by 27 mm (rectangular section ISOFIX) and 48 mm (cross-shaped section ISOFIX) with the addition of energy absorbing foam blocks compared to the flexible LATCH configuration. Similarly, the lateral displacement of the head was reduced by 40 mm by using energy absorbing foam blocks with the rectangular section ISOFIX and 53 mm by

using cross-shaped section ISOFIX respectively for the child FE model compared to the flexible LATCH configuration.

Table 18. Peak values predicted for the flexible LATCH, rigid ISOFIX (rectangular section) and rigid ISOFIX (cross-shaped section) configurations for the Hybrid III 3-year-old dummy.

	Flexible Latch	Rigid ISOFIX (Rectangular section)	Rigid ISOFIX (Cross-shaped section)
Head y-axis acceleration (g's)	-45.5	-39.5	-49.5
Chest y-axis acceleration (g's)	-68.2	-31.8	-41
Resultant head acceleration (g's)	45.7	41.6	51.8
Resultant chest acceleration (g's)	69	31.8	41.6
Head injury criteria (HIC-15)	161.2	117.6	180.8
Lateral Shear (N)	-1030	-836.6	-848.3
Lateral Bending (N.m)	-73	-44.8	-52
Lateral head cg displacement (mm)	253.6	224.2	202.2

Table 19. Peak values predicted for the flexible LATCH, rigid ISOFIX (rectangular section) and rigid ISOFIX (cross-shaped section) configurations for the Hybrid III 3-year-old dummy in the presence of energy absorbing foam blocks.

	Flexible Latch	Rigid ISOFIX (Rectangular section)	Rigid ISOFIX (Cross-shaped section)
Head y-axis acceleration (g's)	-44.5	-37.5	-44
Chest y-axis acceleration (g's)	-71	-31	-38
Resultant head acceleration (g's)	46	38.9	46.4
Resultant chest acceleration (g's)	72.6	31.2	38.5
Head injury criteria (HIC-15)	157.4	109	171.5
Lateral Shear (N)	-832.2	-625.2	-612.4
Lateral Bending (N.m)	-69	-39.7	-43.5
Lateral head cg displacement (mm)	237.4	209.7	185.8

Table 20. Peak values predicted for the flexible LATCH, rigid ISOFIX (rectangular section) and rigid ISOFIX (cross-shaped section) configurations for the Q3s child dummy.

	Flexible Latch	Rigid ISOFIX (Rectangular section)	Rigid ISOFIX (Cross-shaped section)
Head y-axis acceleration (g's)	-115.67	-47.8	-53.2
Chest y-axis acceleration (g's)	-80.5	-38.8	-48.7
Resultant head acceleration (g's)	118.7	54.7	56.3
Resultant chest acceleration (g's)	82.2	38.9	48.8
Head injury criteria (HIC-15)	543	233	252
Lateral Shear (N)	-766.7	-325	-322.5
Lateral Bending (N.m)	33.7	-14.2	-13.2
Lateral head cg displacement (mm)	226.8	228.3	205.2

Table 21. Peak values predicted for the flexible LATCH, rigid ISOFIX (rectangular section) and rigid ISOFIX (cross-shaped section) configurations for the Q3s dummy in the presence of energy absorbing foam blocks.

	Flexible Latch	Rigid ISOFIX (Rectangular section)	Rigid ISOFIX (Cross-shaped section)
Head y-axis acceleration (g's)	-81.6	-44	-44.2
Chest y-axis acceleration (g's)	-82.5	-33.3	-42.3
Resultant head acceleration (g's)	83.8	48.6	48.6
Resultant chest acceleration (g's)	83	34	42.8
Head injury criteria (HIC-15)	340	150	173.3
Lateral Shear (N)	-544	-227	-235.4
Lateral Bending (N.m)	-27.9	-18.5	-18.32
Lateral head cg displacement (mm)	205.8	200.1	179.6

Table 22. Peak values predicted for the flexible LATCH, rigid ISOFIX (rectangular section) and rigid ISOFIX (cross-shaped section) configurations for the child FE model.

	Flexible Latch	Rigid ISOFIX (Rectangular section)	Rigid ISOFIX (Cross-shaped section)
Head y-axis acceleration (g's)	-88.11	-49.4	-41.8
Chest y-axis acceleration (g's)	-48.6	-32	-33.7
Resultant head acceleration (g's)	100.9	59.8	53.15
Resultant chest acceleration (g's)	50.2	33.6	34.4
Head injury criteria (HIC-15)	373.8	217.4	217.5
Lateral Shear (N)	-2411.9	-1365	-1148
Lateral head cg displacement (mm)	230	215.2	197.7

Table 23. Peak values predicted for the flexible LATCH, rigid ISOFIX (rectangular section) and rigid ISOFIX (cross-shaped section) configurations for the child FE model in the presence of energy absorbing foam blocks.

	Flexible Latch	Rigid ISOFIX (Rectangular section)	Rigid ISOFIX (Cross-shaped section)
Head y-axis acceleration (g's)	-69.6	-38	-31.7
Chest y-axis acceleration (g's)	-54.2	-31.3	-34.7
Resultant head acceleration (g's)	76.2	42.8	36.7
Resultant chest acceleration (g's)	57.7	33.4	35
Head injury criteria (HIC-15)	264.4	104.4	103.8
Lateral Shear (N)	-1898	-1047	-863
Lateral head cg displacement (mm)	197.5	190.8	176.9

10.4 Discussion

The injury risk analysis curve and the protection reference values are applicable only for frontal impacts. No injury criteria are stated in FMVSS for child injury in side impacts, therefore injury risk analysis can not be carried out for side impact simulations. The rectangular-shaped rigid ISOFIX system has previously shown capabilities in side impact protection over a flexible LATCH system [106 - 108]. The far-side impact tests carried out by Charlton et al. [106] illustrated a reduction in lateral displacement of the head with rectangular shaped rigid ISOFIX system compared to the flexible LATCH. The observations from sled testing carried out by CLEPA [107], detailed in Section 2.8.3.3, illustrated that the rectangular shaped rigid ISOFIX results were superior to flexible LATCH. These results illustrated a reduction in head and chest accelerations by approximately 50 percent for the TNO P3 dummies by incorporation of rectangular shaped rigid ISOFIX system compared to the flexible LATCH. The numerical simulations predicted a reduction of approximately 50 percent in resultant head and chest accelerations for both the ISOFIX systems compared to flexible LATCH. These predictions are consistent with the experimental results.

The rectangular cross-section does not completely limit the lateral displacement of the CRS. Therefore the cross-shaped rigid ISOFIX was investigated. The observations illustrate a reduction of approximately 20 mm in the lateral displacement of the head of the child dummy by using a cross-shaped rigid ISOFIX system instead of a rectangular shaped ISOFIX. In near-side impact situations the main cause of injury is contact related [62 and 63]. Therefore a further reduction in the lateral displacement of the CRS and the child's head, by incorporation of cross-shaped ISOFIX system, can attenuate the amount of contact-based injury sustained in near-side crashes. Both the ISOFIX systems efficiently reduced the lateral shear by 40 – 50 percent, and lateral bending by approximately 30 percent. A reduction in neck forces and moments decreases the probability of inertia induces neck injuries and AOD [32 and 40].

Addition of energy absorbing foam blocks further reduced the lateral displacement of the dummy's head by approximately 20 to 30 mm, compared to the simulations with the same anchorage method without foam. The presence of foam in between the child's head and the intruding vehicle provides cushioning which may help in preventing contact based injuries. Therefore the use of energy absorbing foams in conjunction with the cross-shaped rigid ISOFIX system was predicted to be an efficient method of reducing both contact/non-contact based injuries in near-side impacts.

11. CONCLUSION AND FUTURE WORK

Extensive experimental and numerical investigations have been completed incorporating a 3-year-old Hybrid III dummy, 3-year-old Q3/Q3s child dummies and a child FE model in frontal and side impact crashes. Based on the quantitative and qualitative analysis of the experimental and numerical testing, the following conclusions can be stated:

11.1 Experimental Testing

A full width, rigid barrier, frontal crash test was completed in accordance to CMVSS 208. Two Hybrid III 3-year-old dummies were used for the experimental crash test. For the crash test, both CRS units were configured for the forward facing orientation and the child dummies were restrained using a five-point restraint system. The first child dummy was seated behind the driver and was secured to the car seat using the seat lap belt. The second child dummy was seated behind the passenger and was attached to the car seat using the LATCH system. The injury risk analysis conducted using the acquired results from the experimental crash test indicated the following:

- (i) Maximum values of chest accelerations observed for both the anchoring configurations were approximately 40 g's. Peak values for the resultant upper neck forces sustained by both the dummies were observed to be approximately 1700 N. High magnitudes of these forces were observed to occur for approximately 40 to 50 ms. The lower neck moments were observed to be of a higher magnitude than upper neck moments due to the considerable extension of the neck. The peak values of the lower neck moments roughly lied between 95 N·m and 120 N·m.
- (ii) Head injury criteria for both the configurations fell below the critical value. *HIC* calculated over a 36 ms sampling window ranged between 450 and 615. Maximum values of the N_{ij} evaluated at the upper neck load cell for the seat belt

anchorage and the ISOFIX configurations were observed to be 0.8 and 1 respectively. The injury analysis shows that both the dummies would sustain severe neck and chest injuries.

- (iii) Percentage reduction of roughly 10% to 20% was observed in the head and neck injury potential by using an adult seat-belt rather than the ISOFIX, in conjunction with a top tether as a means of anchoring the CRS to the vehicle seat. Based on the injury parameters, mounting of the CRS using the flexible LATCH does not provide any significant safety improvements over the use of seat lap belts as an anchorage device in a frontal impact.

The numerical model validation for both the simple and complex CRS models is presented in Chapter 6. An acceptable correlation in terms of the peak values as well as the dynamic response within the entire time domain between the numerical simulation results and the experimental findings, in accordance with CMVSS 208, FMVSS 213 and ANPRM (FMVSS 213) was observed for the complex CRS model. Therefore the numerical model appropriately predicts the kinematics and kinetics which the Hybrid III 3-year-old child dummy experienced in both frontal and side impact crashes.

A comparative study between the dynamic responses of different child models was also completed under a simulated FMVSS 213 crash test. Taking the child FE model as baseline, it was observed that the Q3/Q3s dummies better predict the kinematic response of a child compared to the Hybrid III 3-year-old dummy. Therefore, Q3/Q3s child dummies are more biofidelic compared to the Hybrid III 3-year-old dummy.

11.2 Countermeasures

11.2.1 Frontal impact protection - rearward facing

The simplified rigid CRS model incorporating a Hybrid III 3-year-old dummy was simulated in accordance with CMVSS 208 conditions in both forward and rearward facing CRS configurations. An analysis of the observations acquired from the numerical simulations indicated the following:

- (i) Maximum values of the resultant forces observed by the upper neck load cell were 1545 N and 1050 N for the forward and rearward facing configurations respectively. Similar maximum values of the resultant forces (approximately 1400 N) were observed by the lower neck load cells in both the rearward and forward-facing configurations. Higher magnitudes of the resultant forces were generally observed for the forward-facing CRS configuration.
- (ii) Peak resultant moments were generally much greater for the lower neck in the forward facing CRS configuration. This was due to the significant neck extension which was observed in the forward facing position. Maximum values of the resultant moments at the upper neck load cell location were 34 N·m and 17 N·m for the forward and rearward CRS configurations respectively. Peak values of the resultant moments at the lower neck load cell location were 142 N·m and 19.5 N·m for the forward and rearward CRS configurations respectively. In general, higher values of the resultant moments at both the lower and upper load cell locations were sustained for longer time periods in the forward facing CRS position.
- (iii) The N_{ij} was substantially lower for the child dummy in the rearward facing CRS configuration. Slightly higher values of the HIC evaluated over 15 ms and 36 ms windows were observed for the forward facing configurations for each evaluation time period.

- (iv) The data analysis of neck forces and moments illustrates that there is a greater chance of acquiring inertia-based neck injuries and AOD in the case of a forward facing configuration compared to the rearward facing configuration. Therefore based upon the injury parameters, a rearward-facing configuration is safer for children older than one year in age compared to the forward-facing configuration.

11.2.2 Frontal impact protection - load limiting of tethers

Values of the load limits for both upper tether and lower LATCH anchors were calculated based on the two approaches, namely, the injury based approach and the energy based approach. Numerical simulations were completed in accordance with FMVSS 213 crash testing conditions incorporating the load limiting behaviour in upper tether and lower LATCH anchors. Based on the data analysis for both the load limiting and no load limiting conditions, the following conclusions were obtained:

- (i) Analysis of the head accelerations from the numerical simulation has illustrated a reduction in the head injury criteria for all the three numerical models by incorporating load limiting behaviour in the upper tether and lower LATCH anchors. A reduction of 75 percent for the Hybrid III 3-year-old child dummy, 70 percent for the Q3 dummy and 60 percent for child FE model was predicted in the HIC_{15} due to load limiting of tethers.
- (ii) A reduction of approximately 45 percent and 35 percent in the upper neck resultant forces was predicted for the Hybrid III dummy and the Q3 child dummy respectively due to load limiting of the tethers. A reduction of approximately 35 percent was predicted in the cross-sectional forces for the child FE model due to load limiting of tethers. The maximum values of resultant forces predicted by the upper neck load cell for the Hybrid III and the Q3 dummies were predicted to be greater than 1800 N. These high forces were observed for approximately 40 ms.

- (iii) Head trajectories for all the three child models were generated for both the load limiting and no load limiting conditions. Greater head excursions were predicted for the load limiting condition. The child FE model and the Q3 dummy exhibited greater head excursions compared to the Hybrid III child dummy for both the load limiting and no load limiting configurations. Through the qualitative comparison it was seen that the child models settled down quicker into the CRS for the no load limiting configurations. Due to load limiting of tethers the maximum neck rotation was predicted to be slightly less than the values observed in the no load limiting case
- (iv) Based on the data analysis of head accelerations and neck forces it can be stated that the proposed implementation of load limiting behaviour into the top tether and lower anchors does illustrate a reduction of acceleration induced injuries in a frontal crash.

11.2.3 Frontal impact protection - head and neck restraining device

The HANS device was comprised of two parts: the HANS collar and the HANS tether. The HANS collar was restrained around the dummy's torso by the seatbelt webbing, and the HANS tether was constrained to the dummy's head, in the proximity of the center of mass of the dummy's head. Numerical simulations were completed in accordance to FMVSS 213 crash testing conditions from which the following conclusions can be stated:

- (i) Similar time profiles for the head accelerations were predicted for both in the absence and presence of the HANS device. The peak values of head accelerations were predicted to be reduced by approximately 40 percent for the Q3 child dummy and 20 percent for the child FE model. Similar time profiles of the resultant chest accelerations were predicted for all the three FE models with a minor difference in peak values.

- (ii) A reduction of approximately 40 percent was predicted for the Hybrid III dummy in the upper neck resultant forces due to the presence of the HANS device. The resultant upper neck forces were predicted to be reduced by approximately 80 percent for the Q3 child dummy. The maximum values for the cross-sectional forces were predicted to be 1110 N for the condition without the HANS device and 546.7 N for the simulation in the presence of the HANS device respectively. Therefore a reduction of approximately 50 percent was predicted in the cross-sectional forces for the child FE model due to the presence of the HANS device. A reduction of approximately 70 percent was predicted in the resultant lower neck moments with the addition of the HANS device for both Hybrid III and Q3 child dummies.
- (iii) For the Hybrid III 3-year-old child dummy the HIC_{15} was predicted to be reduced by approximately 20 percent. The addition of a HANS device resulted in a reduction of approximately 50 percent in HIC_{15} and 40 percent in HIC_{36} for the Q3 child dummy. For the child FE model, a reduction of approximately 30 to 40 percent in the head injury criteria was predicted due to addition of the HANS device. A reduction of approximately 25 percent was predicted for Hybrid III dummy 40 percent for the Q3 dummy, in the peak values for the neck injury criteria evaluated at the upper neck load cell, for the first 100 ms of the numerical simulations.
- (iv) From the qualitative analysis and the analysis of the head trajectories it was predicted that the addition of the HANS device efficiently reduces the forward head excursion and the neck rotation in the event of a frontal impact.
- (v) The data analysis demonstrates that the probability of sustaining severe inertia based head and neck injuries, and AOD is drastically reduced by using the HANS device. In addition, a reduction in the head excursions decreases the probability of the child to acquire excursion based contact injuries. Therefore incorporation of

the HANS device for toddlers in a frontal crash has a great potential of reducing both the contact as well as the non-contact injuries.

11.2.4 Side impact protection

A cross-shaped rigid ISOFIX system as a method for anchoring the CRS to the vehicle seat was investigated. Further energy absorbing foam on the side wings of the CRS in the region near the dummy's head was also examined in order to further reduce the lateral displacement of the dummy's head. Based on the qualitative and quantitative analysis for flexible LATCH, rigid ISOFIX rectangular section and rigid ISOFIX cross-shaped section anchoring conditions, in the absence and presence of foam in the vicinity of the head, the following conclusions can be stated:

- (i) Use of rigid ISOFIX systems effectively reduced the chest accelerations by 50 percent (rectangular section) and 40 percent (cross-shaped) section for both the Hybrid III and Q3s child dummies. For the child FE model, the resultant chest accelerations were reduced by 30 percent for both the ISOFIX systems.
- (ii) Comparatively higher values for neck loads were predicted for the child FE model and the Hybrid III dummy compared with Q3s. A reduction of approximately 20 percent was predicted for the Hybrid III child dummy by using the rigid ISOFIX systems instead of the flexible LATCH. The rigid ISOFIX systems effectively reduced the lateral shear by approximately 45 percent for the child FE model and 57 percent for the Q3s dummy, compared to the flexible LATCH system.
- (iii) The response of the neck of the Q3s dummy and the child FE model differed considerably from the Hybrid III dummy. For both the Q3s dummy and the child FE model, greater amount of bending in both the lateral and forward directions was predicted. This can be attributed to lower degree of stiffness and geometrical differences in the Q3s neck which makes the neck more flexible. Both positive

and negative moments were predicted for the Q3s dummy due to forward bending of the neck. For the Hybrid III dummy, use of rigid ISOFIX systems was observed to reduce the lateral bending by approximately 35 percent (rectangular section) and 30 percent (cross-shaped section) respectively.

- (iv) Addition of energy absorbing foam was effective in further reducing the injury parameters and the lateral displacement of the dummy's head. The lateral displacement of the head was reduced by 44 mm by using energy absorbing foam with rectangular section ISOFIX and 68 mm by using cross-shaped section ISOFIX respectively for the Hybrid III 3-year-old dummy compared to the flexible LATCH configuration. For the Q3s dummy, the lateral displacement of the head was reduced by 27 mm (rectangular section ISOFIX) and 48 mm (cross-shaped section ISOFIX) respectively with the addition of energy absorbing foam compared to the flexible LATCH configuration. Similarly, the lateral displacement of the head was reduced by 40 mm by using energy absorbing foam with rectangular section ISOFIX and 53 mm by using cross-shaped section ISOFIX respectively for the child FE model compared to the flexible LATCH configuration.
- (v) The analysis of neck forces and moments illustrates a reduction in inertia based neck injuries due to incorporation of the rigid ISOFIX system. In addition the cross-shaped rigid ISOFIX system provides more room between the child and the intruding vehicle that reduces the amount of contact based injuries. Therefore the cross-shaped rigid ISOFIX system in the presence of energy absorbing foam exhibits the capability of reducing both contact/non-contact based injury incurred during a near-side impact.

11.3 Limitations

The results presented in this dissertation are based on FE simulation observations, which will contain modeling errors related to discretization, contact and material models (in addition to other potential sources). In addition, these FE simulations represent standardized laboratory testing conditions. Numerical simulations were conducted in accordance with FMVSS 213 and CMVSS 208 standards. Therefore, the predictions are applicable to properly restrained children. Children in different seating positions (OOP) were not considered in this research. The limitations associated with different countermeasures are as follows:

11.3.1 Frontal impact protection – rearward facing

Rearward facing simulations were completed utilizing the simplified rigid CRS model. This model does not incorporate the LATCH system and the vehicle seat buck. Therefore, preloading of top tether and lower LATCH anchors could not be attained. In addition, the simplified rigid model does not consider the relative motion between the CRS and the vehicle. The numerical simulations for the rearward facing CRS were completed utilizing a pure frontal acceleration pulse and the effect of a side pulse was not investigated. Rearward-facing CRS orientation illustrates a reduction in acceleration induced head and neck injuries for the frontal impacts. The lateral displacement of the CRS can be greater in a rearward-facing orientation compared to the forward-facing condition. This can be detrimental in the event of a side impact. Therefore further research is needed to suitably incorporate a rearward-facing CRS inside a vehicle.

11.3.2 Frontal impact protection – load limiting of tethers

The main limitation of the use of load limiting behaviour in tethers is the applicability to frontal impact situations without any secondary impacts. In the event of an impact involving a lateral component of the acceleration pulse, there is an increased probability of injuries due to contact with the vehicle interior. In addition, load limit

values for both the top tether and the lower LATCH anchors were evaluated based on the FMVSS 213 excursion limits. An exhaustive examination of the available leg room space in small passenger vehicles was not completed. Load limiting conditions will result in potentially greater CRS motion (relative to the vehicle), excursion of the child occupant and possible impact with the vehicle interior. This is of concern as the most common injuries sustained by children in child restraints are to the head and extremities during loading as a result of contact. Despite this serious consequence, load limiting research is required as it is documented in this dissertation, although not as prevalent as head contact injuries, that children involved in frontal crash that are properly restrained in a CRS and positioned in the rear seat of the vehicle do sustain acceleration based head injuries. The proposed implementation of load limiting behaviour into the top tether and lower anchors does illustrate possible benefits. Further research is needed to appropriately assess the value of load limitation into real world application.

11.3.3 Frontal impact protection – head and neck restraining device

The material selected for the HANS device is ABS 20 percent glass fiber filled. The mechanical properties of fiber reinforced materials tend to be greater in the direction of the glass fiber orientation as compared to the transverse direction. Uniform material characteristics were assumed for the HANS device utilized in this research. Additionally, for preliminary analysis the HANS tethers have been directly constrained to the head of the dummy. Further research is needed to model the interaction between the tethers and the head of the child.

11.3.4 Side impact protection

The rigid ISOFIX system utilized in this research assume a rigid connection between the ends of the anchor and the vehicle seat. This is not applicable for the vehicles manufactured in North America. The lower anchor points provided in the North American vehicles seat do not rigidly connect the CRS to the vehicle seat.

11.4 Future work

Future work for this research includes an investigation in the rearward facing CRS orientation using the deformable child seat. Current small passenger vehicles do not have enough leg room in the rear in order to comfortably seat a toddler in a rearward facing CRS. Therefore CRS design modifications can be made to appropriately seat a 3-year-old child in a rearward facing child seat.

The current study on the load limiting of tethers has shown possible benefits for reduction of injury potential in frontal impacts. Further research is needed to appropriately assess the value of load limitation into real world application. Additionally, incorporation of directional behaviour, to limit CRS motion in the case of side impact, in the load limiting devices should be investigated in future studies. These devices will permit elongation in the tethers during a frontal impact thereby increasing the head excursion. In the event of a side impact, a mechanism preventing transverse displacements of the CRS will inhibit possible sideward motion and reduce the possibility of contact with the CRS and vehicle interior.

At present the HANS tethers have been directly constrained to the head of the dummy. Further research is needed to model the interaction between the tethers and the head of this child. This can be achieved by designing a cap or a helmet and restraining it around the dummy's head with tethers around the chin. The HANS tethers can be constrained to this cap/helmet.

In-depth studies can be done on the child injury mechanisms in near side seating configurations with vehicle intrusions. Since no injury criteria are stated in FMVSS for child injury in side impacts, some critical values and injury criteria especially for the neck can be suggested to better interpret the injury data obtained from the experimental and numerical tests.

A combination of different countermeasures can be investigated. For example, use of rigid ISOFIX system can be examined in rearward facing CRS configurations for both frontal and side impact situations. Also, use of HANS device with rigid ISOFIX system can be investigated for different impact directions. The testing of out of position child occupants can also be considered. The effect of slouching and sleeping can be taken into account, as children are rarely seated upright in a child safety seat.

REFERENCES

1. Statistics Canada (2003). Major Causes of Death, Government of Canada. <http://142.206.72.67/02/02b/02b_003_e.htm> Accessed February 2007.
2. National Highway Traffic Safety Administration (2005). Traffic Safety Facts 2005 (DOT HS 810 618 pp. 1-6). U.S. Department of Transportation.
3. National Highway Traffic Safety Administration (2006). Traffic Safety Facts 2006 (DOT HS 810 631 pp. 1-224). U.S. Department of Transportation.
4. Transport Canada (2006). Canadian Motor Vehicle Traffic Collision Statistics: 2005. (TP 3322). Catalogue Number T 45-3/2005.
5. Weber K (1995). Rear-Facing Restraint for Small Child Passengers. UMTRI Research Review, Vol. 25, pp. 12 – 17.
6. Gotschall CS, Luchter S (1999). Head Injuries to motor vehicle occupants aged 0-5 years. Children's National Medical Center, Washington DC, USA.
7. Patel JC, Tepas JJ, Mollitt DL and Pieper P (2001). Pediatric cervical spine injuries: Defining the disease. Journal of Pediatric Surgery, Vol. 36, pp. 373-376.
8. Mousny M, Saint-Martin C, Danse E, Rombouts JJ (2001). Unusual upper cervical fracture in a 1 year-old girl. Journal of Pediatric Orthopaedics, Vol. 31, pp. 590 – 593.
9. Arbogast KB, Cornejo RA, Kallan MJ, Winston FK and Durbin DR (2002). Injuries to children in forward facing child restraints. Annual Proceedings of the Association of Advancement of Automotive Medicine, Vol. 46, pp. 212-230.

10. National Highway Traffic Safety Administration (2007). Traffic Safety Facts: Crash statistics (DOT HS 810 856). US Department of Transportation. <<http://www.nhtsa.gov/motorcycles/pdf/TSF810856.htm>> Accessed February 2007.
11. Hospital for Sick Kids, Dr. Andrew Howard. Personal Interview. October 2007.
12. National SAFE KIDS Campaign (2004). Motor Vehicle Occupant Injury Fact Sheet. NSKC, Washington DC.
13. Skold BA (1999). An Improved ISOFIX system for rearward-facing child seats. Child Occupant Protection in Motor Vehicle Crashes, Vol. 3, pp. 161 - 164.
14. Paine M, Griffiths M, Brown J, Case M and Johnstone O (2003). Protecting children in car crashes: the Australian experience. 18th International Technical Conference on the Enhanced Safety of Vehicles, Paper No. 193, Nagoya, Japan.
15. Advance notice of proposed rulemaking (2002). Federal Motor Vehicle Safety Standards 213: Child Restraint Systems. 49 CFR Part 571, Docket No. 02-12151, Federal Register, Vol. 67, No. 84, pp. 1-17.
16. Weber K (2000). Crash protection for child passengers: A review of best practice. UMTRI Research Review, University of Michigan Transportation Research Institute, Vol. 31, pp. 1-28.
17. Read Review of Britax Wizard - Midnight Print Infant Car Seat (2003). <http://www.epinions.com/content_107278929540> Accessed January 2008.
18. World Health Organization (2004). World report on road traffic injury prevention. WHO Library Cataloguing-in-publication Data. World Health Organization, 2002. Global Burden of Disease Project, Version 1.

19. Public Health of Health Canada (2006). Government of Canada. <http://www.phac-aspc.gc.ca/publicat/meas-haut/mu_w_e.html> Accessed October 2006.
20. Chouinard A and Hurley B (2005). Towards the development of a national child restraint survey. Proceedings of Canadian Multidisciplinary Road Safety Conference XV, Fredericton, New Brunswick, June 6-9, 2005.
21. Committee on Trauma Research, Institute of Medicine and National Research Council (1985). Injury in America – A continuing public health problem. National Academy Press, Washington DC.
22. DeSantis-Klinich K, Hulbert GM and Schneider LW (2002). Estimating Infant Head Injury Criteria and Impact Response Using Crash Reconstruction and Finite Element Modeling. Stapp Car Crash Journal, Vol. 46, pp. 2 – 30.
23. Gennarelli TA (1986). Mechanism and pathophysiology of cerebral concussion. Journal of Head Trauma Rehabilitation, Vol. 1, No. 2, pp. 23-29.
24. Gennarelli TA (1993). Mechanisms of brain injury. Emergency Medicine, Vol. 11, pp. 5-11.
25. King AI (2000). Fundamentals of impact biomechanics: Part I – biomechanics of the head, neck and thorax. Annual Review of Biomedical Engineering, Vol. 2, pp. 55-81.
26. McGrory BJ, Klassen RA, and Chao EYS (1993). Acute fractures and dislocations of the cervical spine in children and adolescents. Journal of Bone and Joint Surgery Vol. 75, pp. 988-995.

27. Cirak B, Ziegfeld S, Knight VM, Chang D, Avellino AM and Paidas CN (2004). Spinal injuries in children. *Journal of Pediatric Surgery*, Vol. 39, No. 4, pp. 607-612.
28. Sochor MR, Faust DP, Garton H and Wang SC (2004). Simulation of occipitoatlantoaxial injury using a MADYMO model. *Conference Proceedings of the SAE World Congress, Detroit Michigan, SAE Technical Paper 2004-01-0326*.
29. Dai LY, Ni B and Yuan W (1999). Pediatric cervical spine and spinal cord injuries. *Journal of Pediatric Surgery*, Vol. 20, pp. 96-98.
30. Steinmetz MP, Lechner RM and Anderson JS (2003). Atlantooccipital dislocation in children: Presentation, diagnosis, and management. *Neurosurgical Focus*, Vol. 14, No. 2, pp. 1-7.
31. Tingvall C (1987). Children in cars: Some aspects of the safety of children as car passengers in road traffic accidents. *Acta Paediatrica Scandinavica. Supplement 339*.
32. DeSantis-Klinich K, Saul RA, Auguste G, Backaitis S and Kleinberger M (1996). Techniques for Developing Child Dummy Protection Reference Values. *NHTSA Event Report, Docket Submission # 74-14 Notice 97 Item 069*.
33. Cassan F, Lesirel P, Grant R and Gehre C (2003). Advanced methods for improved CHILD occupant safety in cars. *International Traffic Medicine Association, Budapest, Hungary, 14th to 17th of September 2003*.
34. Eman A, Sennah K, Howard A and Hale I (2003). Multi-body Dynamic Simulations of Forward Facing Child Occupants Under Varying Crash Pulses. *Proceedings of the Canadian Multidisciplinary Road Safety Conference XIII, June 8-11, 2003, Banff, Alberta*.

35. Huelke DF, Mackay GM, Morris A, Bradford M (1992). Car Crashes and Non-Head Impact Cervical Spine Injuries in Infants and Children. Society of Automotive Engineers, 920563.
36. Gray H (1860). Gray's Anatomoy Gray's Anatomy: Descriptive and Surgical. 2nd Edition. <<http://education.yahoo.com/reference/gray/subjects/subject?id=73>> Accessed October 2007.
37. Burdi AR, Huelke DF, Snyder RG and Lowrey GH (1969). Infants and Children in the Adult World of Automobile Safety Design: Pediatric and Anatomical Considerations for Design of Child Restraints. Journal of Biomechanics, Vol. 2, pp. 267 – 280.
38. Yoganandan N, Kumaresan S, Pintar FA and Gennarelli TA (1999). Biomechanical tolerance criteria for paediatric populations. Department of Neurosurgery, Medical college of Wisconsin, USA.
39. Weber K (2002). Child passenger protection. Accidental injury: Biomechanics and Prevention, ed. Nahum et al., ISBN 0-387-98820-3, New York, Springer-Verlang.
40. Dublin AB, Marks WM and Weinstock D (1980). Traumatic dislocation of the atlanto-occipital articulation (AOA) with short-term survival with a radiographic method of measuring the AOA. Journal of Neurosurgery, Vol. 52, pp. 541-546.
41. Thomas DJ and Jessop ME (1983). Experimental head and neck injury, Impact Injury of the Head and Spine, ed. Ewing et al., pp. 177-217, Springfield IL: Thomas.
42. Arbogast K, Durbin DR, Cornejo RA, Kallan MJ and Winston FK (2004). An evaluation of the effectiveness of forward facing child restraint systems. Accident Analysis and Prevention, Vol. 36, pp. 585–589.

43. Zaza S, Sleet DA, Thompson RS, Sosin DM and Bolen JC (2001). Reviews of evidence regarding interventions to increase use of child safety seats. *American Journal of Preventive Medicine*, Vol. 21, pp. 31–43.
44. Eby D and Kostyniuk L (1999). A statewide analysis of child safety seat use and misuse in Michigan. *Accident Analysis and Prevention*, Vol. 31, pp. 555–566.
45. Decina L and Lococo K (2005). Child restraint system use and misuse in six states. *Accident Analysis and Prevention*, Vol. 37, pp. 583–590.
46. Decina L and Knoebel K (1997). Child safety seat misuse patterns in four states. *Accident Analysis and Prevention*, Vol. 29, No.1, pp. 125-132.
47. New York State Police brochure. Child safety seats: Use and Misuse. <http://www.troopers.state.ny.us/Publications/Traffic_Safety/childsafetyseats.pdf> Accessed April 2008.
48. Winston FK, Durbin DR, Kallan MJ and Moll EK (2000). The danger of premature graduation to seat belts for young children. *Pediatrics*, Vol. 105, No. 6, pp. 1179-1183.
49. Howard A (2002). Automobile restraints for children: a review for clinicians. *Canadian Medical Association Journal*, Vol. 167, No.7, pp. 769-73.
50. SAFE KIDS CANADA. Booster seat use in Canada: a national challenge (2004). <http://www.sickkids.ca/SKCFForParents/custom/EnglishReport_BoosterSeats.pdf?s=Safety+Information+by+Topic&sID=10774&ss=Child+Passenger+Safety&ssID=11330&sss=Report%3A+Booster+Seat+Use+in+Canada+%2D+A+National+Challenge&sssID=1156>

51. Ehiri JE, Ejere HOD, Magnussen L, Emusu D, King W and Osberg JS (2006). Interventions for promoting booster seat use in four to eight year olds traveling in motor vehicles. The Cochrane Database of Systematic Reviews 1, 45 pages.
52. Snowdon A, Polgar J, Patrick L and Stamler L (2006). Parents' knowledge and use of safety systems for children in Ontario. Canadian Journal of Nursing Research, Vol. 38, No. 2, pp. 98-114.
53. Snowdon AW, Hussein A, High L, Stamler L, Millar-Polgar J, Patrick L and Ahmed E (2008). The Effectiveness of a Multimedia Intervention on Parents' Knowledge and Use of Vehicle Safety Systems for Children. Journal of Pediatric Nursing. Vol. 23, No. 2, pp. 126-139.
54. Brown J, Bilston L, McCaskill M and Henderson M (2005). Identification of injury mechanisms for child occupants aged 2-8 in motor vehicle accidents. Final Project Report for the Motor Accidents Authority of NSW, pp. 1-71.
55. Sherwood C, Ferguson S and Crandall J (2003). Factors leading to crash fatalities to children in child restraints. Center for Applied Biomechanics, University of Virginia, pp. 1-17.
56. Howard A, McKeag AM, Rothman L, German A, Hale I, Emam A, Altenhof W and Turchi R (2003). Cervical Spine Injuries in Children Restrained in Forward Facing Child Restraints. Proceedings of the Canadian Multidisciplinary Road Safety Conference XIII, June 8-11, 2003, Banff, Alberta.
57. Nance ML, Elliott MR, Arbogast KB, Winston FK and Durbin D R (2006). Delta v as a predictor of significant injury for children involved in frontal motor vehicle crashes. Annals of Surgery, Vol. 243, No. 1, pp. 121-125.

58. Smith K and Cummings P (2004). Passenger seating position and the risk of passenger death or injury in traffic crashes. *Accident Analysis and Prevention*, Vol. 36, pp. 257–260.
59. Evans L and Frick M (1988). Seating position in cars and fatality risk. *Public Health*, Vol. 78, pp. 1456–1458.
60. Lund U (2005). The effect of seating location on the injury of properly restrained children in child safety seats. *Accident Analysis and Prevention*, Vol. 37, pp. 435–439.
61. Williams A and Zador P (1977). Injuries to children in automobiles in relation to seating location and restraint use. *Accident Analysis and Prevention*, Vol. 9, pp. 69–76.
62. Howard A, Rothman L, Moses A, Pazmino-Canizares J, Monk B, Comeau J, Mills D, Beng S, Hale I and German A (2004). Children in Side-Impact Motor Vehicle Crashes: Seating Positions and Injury Mechanisms. *The Journal of TRAUMA Injury, Infection, and Critical Care*, Vol. 56, pp. 1276 –1285.
63. Newgard CD, Lewis RJ, Kraus JF and McConnell KJ (2005) Seat position and the risk of serious thoracoabdominal injury in lateral motor vehicle crashes. *Accident Analysis and Prevention*, Vol. 37, pp. 668-674.
64. Bendjellal F, Nakhla S and Maier D (2006). Investigation into children protection in side impact motor vehicle crashes. 4th International Conference, Protection of children in cars.
65. Glass R, Segui-Gomez M and Graham J (2000). Child passenger safety: decisions about seating location, airbag exposure, and restraint use. *Risk Analysis*, Vol. 20, pp. 521–527.

66. Arbogast KB, Moll EK, Morris SD and Winston FK (2001). Child occupant protection: a summary of current safety recommendations. PREVENTIVE CARE UPDATE, Vol. 8, No. 4, pp. 141-148.
67. German A, Gardner WT, Howard AW, Mackay M and Letts RM (1999). Mechanisms of Lap Belt and Airbag Injuries in Children. Child Occupant Protection in Motor Vehicle Crashes, Vol. 3, pp. 81 - 96.
68. Howard A (2005). Child safety in frontal and side impacts. Presentation at Ford Motor Company, Hospital for Sick Kids, May 2005.
69. 60. Gadd CW (1966). Use of a weighted-impulse criterion for estimating injury hazard. Conference Proceedings 10th Stapp Car Crash Conference, pp. 95-100, Holloman Air Force Base, New Mexico.
70. Versace J (1971). A review of the severity index. Proceedings of the 15th Annual Stapp Car Crash Conference, Paper no. 710881, pp. 771-796, Coronado, California.
71. National Highway Traffic Safety Administration (1998). Federal Motor Vehicle Safety Standards No. 208: Occupant crash protection. Docket No. 571.208, Federal Register, Vol. 63, 28935, pp. 497-580.
72. Schmitt KU, Muser MH and Niederer P (2001). A New Neck Injury Criterion Candidate for Rear-End Collisions Taking Into Account Shear Forces and Bending Moments. 17th Enhanced Safety of vehicles Conference, Paper No. 124, June 4 - 7, 2001, Amsterdam, Netherlands.
73. Eppinger R, Sun E, Bandak F, Haffner M, Khaewpong N, Maltese M, Kuppa S, Nguyen T, Takhounts E, Tannous R, Zhang A and Saul R (1999). Development of

Improved Injury Criteria for the Assessment of Advanced Automotive Restraint Systems – II. National Highway and Traffic Safety Administration.

74. National Highway Traffic Safety Administration (2002). Proposed amendments to FMVSS 213 frontal test procedures. U.S. Department of Transportation. <<http://www.nhtsa.gov/cars/rules/rulings/CPSUpgrade/CPSRevise/PRE/.html>> Accessed January 2008.
75. Transport Canada (1998). Canadian Motor Vehicle Safety Standard No. 213: Child Restraint Systems. Canada Gazette Part II, Vol. 132, No. 7.
76. Transport Canada (2007). Motor Vehicle Safety Act. Government of Canada. <<http://www.tc.gc.ca/acts-regulations/GENERAL/mvsa/regulations/rssr/rssr.htm>>. Accessed November 2007.
77. Arsdell V (2005). The evolution of FMVSS 213: Child restraint Systems. 2005 SAE International, Paper No. 2005-01-1840, pp. 147-158.
78. Final rule (2003). Federal Motor Vehicle Safety Standards 213: Child Restraint Systems. 49 CFR Part 571, Docket No. NHTSA-03-15351, Federal Register, Vol. 68, No. 121, pp. 1-40.
79. Transport Canada (2002). Motor Vehicle Safety Acts. Government of Canada. <<http://www.tc.gc.ca/acts-regulations/mvsa/regulations/mvsrg/210/mvs210.html>> Accessed November 2007.
80. National Highway Safety Administration (2006). Federal Motor Vehicle Safety Standards: Child Restraint Anchorage Systems, 49 CFR Parts 571 and 596, Docket No. 98-3390, Notice 2.

81. National Highway Traffic Safety Administration. Child Protective Services. U.S. Department of Transportation. <<http://www.nhtsa.dot.gov/CPS/newtips/pages/Tip4.htm>>. Accessed November, 2007.
82. National Highway Traffic Safety Administration (2005). Laboratory Test Procedures for FMVSS 213, TP-213-08.
83. United Nations Economic Commission for Europe (2006). Uniform provisions concerning the approval of vehicles with regard to safety-belt anchorages, ISOFIX anchorage systems and ISOFIX top tether anchorages. Rev.1/Add.13/Rev.4. pp. 1-74. < <http://www.unece.org/trans/main/wp29/wp29regs/r014r4e.pdf>> Accessed December 2007.
84. National Highway Traffic Safety Administration. Child Passenger Safety. U.S. Department of Transportation. < <http://www.boosterseat.gov/4StepsFlyer.pdf>> Accessed November 2007.
85. Transport Canada. Keep Kids Safe: Car time 1-2-3-4. TP #13511 <www.tc.gc.ca/roadsafety> Accessed November 2007.
86. Ministry of Transportation. Tips for Installing child car seats. Government of Ontario. <<http://www.mto.gov.on.ca/english/safety/carseat/tips.htm#3>> Accessed January 2008.
87. Car safety website. <<http://www.car-safety.org>> Accessed November 2007.
88. Bois P Du, Chou C, Fileta B, Khalil T, King A, Mahmood H, Mertz H and Wismans J (2004). Vehicle crashworthiness and occupant protection. American Iron and Steel Institute, Southfield, Michigan, pp. 1-388.

89. First Technology Safety Systems website. <<http://www.ftss.com>> Accessed October 2007.
90. Mello TB. Meet the crash test dummies. <<http://www.edmunds.com/ownership/safety/articles/105394/article.html>> Accessed October 2007.
91. National Highway Traffic Safety Administration. Vehicle Research and Test Centre. U.S Department of Transportation. < <http://www-nrd.nhtsa.dot.gov/vrtc/bio/child/child.htm>> Accessed December 2007.
92. Jager K, Ratingen M, Lesire P, Guillemot H, Pastor C, Schnottale B, Tejera G and Lepretre J (2005). Assessing new child dummies and criteria for child occupant protection in frontal impact, 19th Enhanced Safety of vehicles Conference, Paper no. 05-0157, pp. 1-15, June 6-9, 2005, Washington D.C.
93. Saul R, Pritz H, McFadden J, Backaitis S, Hallenbeck H and Rhule D (2001). Description and performance of the Hybrid III three year old, six year old and small female test dummies position air bag environments. 17th Enhanced Safety of vehicles Conference, Paper No. 98-S7-O-01, June 4 - 7, 2001, Amsterdam, Netherlands.
94. Carlson M, Burleigh M, Barnes A, Waagmeester K and Ratingen M (2007). Q3s 3 year old side impact dummy development. 20th Enhanced Safety of vehicles Conference, Paper Number 07-0205, pp. 10-19, June 18-21, 2007, Lyon, France.
95. Safe Car Guide website. < <http://www.safecarguide.com/exp/ncap/idx.htm>> Accessed November 2007.
96. National Highway Traffic Safety Administration (2002). Safety Rating Program for Child Restraint Systems. Docket No. NHTSA 2001-10053, Notice 1.

97. National Highway Traffic safety Administration. Child Restraint System Rating. U.S. Department of Transportation. <<http://www.nhtsa.dot.gov/CPS/CSSRating/QandA.html>> Accessed January 2008.
98. Kallieris D, Barz J, Schmidt G, Heess G and Mattern R (1976). Comparison between child cadavers and child dummy by using child restraint systems in simulated collisions. 20th STAPP Car Crash Conference, SAE paper no. 760815.
99. Cassan, M Page, Y Pincemallie, D Kallieris and C Tarriere (1993). Comparative study of restrained child dummies and cadavers in experimental crashes. SAE Technical Paper Series, SAE paper no. 933105.
100. Turchi R, Altenhof W, Kapoor T and Howard A (2004). An investigation into the head and neck injury potential of three-year-old children in forward and rearward facing child safety seats. International Journal of Crashworthiness, Vol. 10, pp. 1-14.
101. Turchi R (2004). An investigation into the head and neck injury potential of three-year-old children in forward and rearward facing child safety seats. MASc. Thesis, University of Windsor.
102. Bohman K, Bostrom O, Osvalder A and Eriksson M (2007). Rear seat frontal impact protection for children seated on booster cushions – an attitude, handling and safety approach. 20th Enhanced Safety of vehicles conference, Paper No. 07-0268, pp. 41-49, June 18-21, 2007, Lyon, France.
103. Belcher T and Newland C (2007). Investigation of lower anchorage systems for child restraints in Australia. 20th Enhanced Safety of vehicles conference, Paper No. 07-0298, pp. 50-64, June 18-21, 2007, Lyon, France.

104. Rockwell T. Side Impact Vehicle Testing: Development of a Lateral Test Procedure for Child Restraints, ACE Systems Technologies Inc., pp. 1-40, <<http://www-nrd.nhtsa.dot.gov/pdf/nrd-01/SAE/SAE2003/Rockwell.pdf>> Accessed January 2006.
105. NHTSA Vehicle Crash Test Database. Test no. 4585. < <http://www-nrd.nhtsa.dot.gov/database/aspx/vehdb/querytesttable.aspx>> Accessed August 2007.
106. Charlton J, Fildes B, Laemmle R, Smith S and Douglas F (2004). A Preliminary Evaluation of Child Restraint Crash Performance with Three Anchorage Systems in a Holden Commodore. Australasian Road Safety Research, Policing and Education Conference Proceedings, pp. 1-10. <<http://www.rsconference.com/pdf/RS040079.pdf>> Accessed January 2007.
107. CLEPA (2004). Side Impact and Ease of Use Comparison between ISOFIX and LATCH. Presentation to GRSP, Informal Document GRSP-35 -1 9, Geneva, May 2004, pp. 1-31 <<http://www.unece.org/trans/doc/2004/wp29grsp/TRANS-WP29-GRSP-35-inf19e.pdf>> Accessed January 2007.
108. Klinich K, Ritchie N, Manary M, Reed M, Tambora N and Schneider L (2005). Kinematics of the Q3s ATD in a child restraint in a far side impact loading. 19th Enhanced Safety of vehicles Conference, Paper No 05-0262, June 6-9, 2005, Washington D.C.
109. HANS device owner's manual. <<http://hansdevice.com/site/index.html>> Accessed December 2007.
110. Gramling H, Hodgman P and Hubbard R (1998). Development of the HANS Head and Neck Support for Formula One. Motor Sports Engineering Conf, SAE, Paper No. 983060, Ministry of Transportation.

111. Emam A, Howard A, Sennah K, Chapman M and Altenhof W (2004). Rearward and forward facing dynamic behavior of child occupants in frontal collisions. Proceedings of Canadian Multidisciplinary Road Safety Conference XIV, June 2004, Ottawa, Canada.
112. Mizuno K, Iwata K, Deguchi T and Ikami T (2006). Development of a Three-Year-Old Child FE Model. Traffic Injury Prevention, Vol. 6, pp. 361-371.
113. Mizuno K, Iwata K, Namikiri T and Tanaka N (2006). Comparison of human FE model and crash dummy response in various child restraint systems. International Crashworthiness Conference, 2006, Athens, Greece.
114. Mizuno K and Namikiri T (2007). Analysis of child responses in CRS using child human FE model. 20th Enhanced Safety of vehicles conference, Paper No. 07-0145, pp. 1-9, June 18-21, 2007, Lyon, France.
115. Zhang W, Kapoor T, Tot M, Altenhof W, Howard A and Mizuno K (2007). A Comparison of the Kinematics of a Child Finite Element Model and the Hybrid III 3-Year-Old Dummies in Frontal Crashes. SAE World Congress, Paper No. 2007-01-0977, April 2007, Detroit, U.S.A.
116. M Surcel and M Gou (2005). Development of a mathematical model for evaluating child occupant behavior in the case of a vehicle side impact simulation. International journal of crashworthiness, Vol. 10, No. 1, pp. 111-118.
117. Wang Q (2006). Development of a finite element model for Hybrid III three-year-old dummy-based child restraint system safety simulation. MASc. Thesis. University of Windsor.
118. NHTSA vehicle Crash Test Database. Test No. 3629. <http://www-nrd.nhtsa.dot.gov/database/nrd-11/veh_db.html> Accessed June 2006.

119. Transport Canada (1998). Canadian Motor Vehicle Safety Standards 208: Occupant crash protection. Government of Canada. <<http://www.tc.gc.ca/acts-regulations/GENERAL/m/mvsa/regulations/mvsrg/200/mvsr208.html>> Accessed January 2008.
120. SAE J211/1 (2003). Instrumentation for Impact Test - Part 1- Electronic Instrumentation, Society of Automotive Engineers, Warrendale PA.
121. J.O. Hallquist (1998). LS-DYNA Theoretical Manual, Livermore Software Technology Corporation, Livermore CA.
122. American Standard of Testing Methods. (2004). Standard test methods for tensile properties of plastics [Metric]. (Designation: D638M). Annual book of ASTM standards, Philadelphia, PA, USA.
123. LS-DYNA model of the Hybrid III 3 year old child dummy - version 2.3B2 (2000). Users Manual, First Technology Safety Systems, Plymouth, MI.
124. Q3: Advanced 3 Year Old Child Crash Test Dummy (2005). User's Manual, Version Aug. 2005, rev 3.1.
125. LS-DYNA Model of the Q3 Dummy Version 1.0beta (2006). Users Manual, First Technology Safety Systems, Plymouth, MI.
126. LS-DYNA Model of the Q3s Dummy Version 1.0beta (2007). Users Manual, First Technology Safety Systems, Plymouth, MI.
127. Rebba R, Mahadevan S and Huang S (2006). Validation and error estimation of computational models. Reliability Engineering and System Safety, Vol. 91, pp. 1390 – 1397.

128. Oberkampf W and Trucano T (2002). Verification and validation in computational fluid dynamics. Progress in Aerospace Sciences. Vol. 38, pp. 209 – 272.
129. Lau E, Ray R and Parenteau CS (1999). Characteristics of children in rollover collisions.” Child Occupant Protection in Motor Vehicle Crashes, Vol. 3, pp. 3 - 16.
130. Online Materials Information Resource.
<<http://www.matweb.com/search/DataSheet.aspx?MatID=77802andckck=1>>
Accessed November 2007.
131. Medical Dictionary Search Engine. Abbreviated Injury Scale.
<<http://www.books.md/A/dic/abbreviatedinjuryscale.php>>. Accessed January 2008.

APPENDICES

APPENDIX A – Contents of the associated DVD

APPENDIX B – Injury scales and Prasad and Mertz injury risk curves

APPENDIX C – Numerical algorithms

APPENDIX D – Material models and sample input data from LS-Dyna

APPENDIX E – Contact definitions

APPENDIX F – Copyright permission

APPENDIX A

Contents of the associated DVD

Input files for the child FE model:

1. Child_flexible_LATCH_213: Frontal impact with FMVSS 213 acceleration pulse
2. Child_load_limiting_213: Load limiting with FMVSS 213 acceleration pulse
3. Child_HANS: HANS device with FMVSS 213 acceleration pulse
4. Child_4585_rigid_ISOFIX: Rigid ISOFIX (cross-shaped) with 4585 acceleration pulse
5. Child_4585_rigid_ISOFIX_with_foam: Rigid ISOFIX (cross-shaped) in the presence of foam blocks, with 4585 acceleration pulse

Animation files:

1. Experimental videos
 - a. FMVSS 213 sled test
 - b. CMVSS 208 vehicle crash test (front and side view)
2. Numerical videos
 - a. Simplified CRS model
 - (i) Hybrid III forward facing in accordance with CMVSS 208
 - (ii) Hybrid III rearward facing in accordance with CMVSS 208
 - b. Complex CRS model
 - (i) Frontal Impact: Animation files for Hybrid III 3-year-old dummy, Q3 dummy and the child FE model for:
 - Flexible LATCH in accordance with FMVSS 213
 - Load limiting
 - Presence of the HANS device
 - (ii) Side Impact: Animation files for Hybrid III 3-year-old dummy, Q3s dummy and the child FE model for:
 - Flexible LATCH: with and without foam
 - Rigid ISOFIX (rectangular section): with and without foam
 - Rigid ISOFIX (cross shaped): with and without foam

APPENDIX B

Injury scales and Prasad and Mertz injury risk curves

The injury risk curves obtained from the test dummy in the crash demonstrate the probability of injury to a real person in that crash. There are two types of injury scales used to find the probability of injury in an occupant during a crash. They are AIS and MAIS (Maximum Abbreviated Injury Scale) [73, 74 and 131]. The AIS is used for coding single injuries and is a basis for the methods of assessing multiple injuries or for assessing cumulative effects of more than one injury. The assessment of multiple injuries is achieved by the MAIS.

Injuries are ranked on a scale of 1 to 6, with 1 being minor, 5 severe, and 6 an injury which cannot be survived. This represents the threat to life associated with an injury and is not meant to represent a comprehensive measure of severity. The Abbreviated Injury Scale does not grade its ranks as a typical scale does. In other words, the difference between AIS1 and AIS2 is not the same as that between AIS4 and AIS 5.

Table 1 - B. AIS injury scales.

Injury	AIS Score
1	Minor
2	Moderate
3	Serious
4	Severe
5	Critical
6	Unsurvivable

1. Probability of head injury

The HIC_{15} probability curves are used to measure the chances that a vehicle occupant would receive certain head injury at a given HIC value. The HIC_{15} injury probability curves for children represented by the 3-year-old dummy are as follows:

$$\text{AIS 2+ Percent Injury Probability} = [1 / (1 + \exp^{(2.49 + 114/HIC - 0.00847 * HIC)})] \times 100\%.$$

$$\text{AIS 3+ Percent Injury Probability} = [1 / (1 + \exp^{(3.39 + 114/HIC - 0.00653 * HIC)})] \times 100\%.$$

$$\text{AIS 4+ Percent Injury Probability} = [1 / (1 + \exp^{(4.90 + 114/HIC - 0.00616 * HIC)})] \times 100\%.$$

$$\text{AIS 5+ Percent Injury Probability} = [1 / (1 + \exp^{(7.82 + 114/HIC - 0.00753 * HIC)})] \times 100\%.$$

$$\text{Fatality Percent Injury Probability} = [1 / (1 + \exp^{(12.14 + 114/HIC - 0.00991 * HIC)})] \times 100\%.$$

Where HIC refers to the head injury criteria calculated over a 15 ms window.

2. Probability of neck injury

These probability curves are used to evaluate the probability of neck injuries in the occupant. The probability curves used to evaluate these injury criteria are as follows:

$$\text{AIS 2+ Percent Injury Probability} = [1 / (1 + \exp^{(2.0536 - 1.1955 * N_{ij})})] \times 100\%.$$

$$\text{AIS 3+ Percent Injury Probability} = [1 / (1 + \exp^{(3.227 - 1.969 * N_{ij})})] \times 100\%.$$

$$\text{AIS 4+ Percent Injury Probability} = [1 / (1 + \exp^{(2.693 - 1.196 * N_{ij})})] \times 100\%.$$

$$\text{AIS 5+ Percent Injury Probability} = [1 / (1 + \exp^{(3.817 - 1.196 * N_{ij})})] \times 100\%.$$

$$\text{Fatality Percent Injury Probability} = [1 / (1 + \exp^{(3.817 - 1.196 * N_{ij})})] \times 100\%.$$

Where N_{ij} refers to the neck injury criteria calculated at the upper neck load cell.

3. Probability of chest injuries

Injury probability as a function of chest acceleration (chest g's) based on a 3 ms clip of the spinal acceleration on a 3-year-old dummy is listed below.

$$\text{AIS 2+ Percent Injury Probability} = [1 / (1 + \exp (1.2324 - 0.06284*a))] \times 100\%$$

$$\text{AIS 3+ Percent Injury Probability} = [1 / (1 + \exp (3.1493 - 0.06873*a))] \times 100\%$$

$$\text{AIS 4+ Percent Injury Probability} = [1 / (1 + \exp (4.3425 - 0.06873*a))] \times 100\%$$

$$\text{AIS 5+ Percent Injury Probability} = [1 / (1 + \exp (8.7652 - 0.07189*a))] \times 100\%$$

$$\text{Fatality Percent Injury Probability} = [1 / (1 + \exp (8.7652 - 0.07189*a))] \times 100\%$$

Where a refers to the chest acceleration in g's.

APPENDIX C

Numerical algorithms

The following are numerical algorithms that were employed using MathCAD software in order to calculate HIC , N_{ij} , and all average values with respect to time. Also, the numerical algorithm for the SAE J211 2nd order Butterworth filter that was used to filter the experimental and numerical raw data. The numerical algorithms were developed by Dr. William Altenhof.

1. Head injury criteria

$$\begin{array}{l}
 HIC(t, a, w) := \left| \begin{array}{l}
 \text{points} \leftarrow \text{rows}(a) \\
 \delta t \leftarrow t_2 - t_1 \\
 \text{num} \leftarrow \text{floor}\left(\frac{w}{\delta t}\right) \\
 \text{end points} \leftarrow \text{points} - \text{num} \\
 \text{for } j \in 1.. \text{end points} \\
 \left| \begin{array}{l}
 h_j \leftarrow \text{num} \cdot \delta t \cdot \left[\frac{1}{\text{num} \cdot \delta t} \sum_{i=j}^{\text{num}+j-1} \frac{(a_{i+1} + a_i)}{g} \cdot (t_{i+1} - t_i) \right]^{2.5} \\
 th_j \leftarrow \frac{t_{\text{points}-\text{num}} - t_1}{\text{end points} - 1} \cdot j + \frac{(t_1 \cdot \text{end points} - t_{\text{points}-\text{num}})}{(\text{end points} - 1)}
 \end{array} \right. \\
 \text{augment}(th, h)
 \end{array} \right.
 \end{array}$$

2. Neck injury criteria

$$\begin{array}{l}
 NIC(F, M) := \left| \begin{array}{l}
 \text{for } i \in 1.. \text{rows}(F) \\
 \left| \begin{array}{l}
 Fz_{c_i} \leftarrow \text{if}(F_i > 0 \cdot N, 2120 \cdot N, -2120 \cdot N) \\
 Myc_i \leftarrow \text{if}(M_i > 0 \cdot N \cdot m, 68 \cdot N \cdot m, -27 \cdot N \cdot m) \\
 NIC_i \leftarrow \frac{F_i}{Fz_{c_i}} + \frac{M_i}{Myc_i}
 \end{array} \right. \\
 NIC
 \end{array} \right.
 \end{array}$$

3. SAE J211 2nd Order Butterworth Filter

```

SAEJ211(t, Acc, CFC) :=
  n1 ← rows(t)
  sum ← 0·s
  for i ∈ 1..n1 - 1
    Dti ← ti+1 - ti
    sum ← sum + Dti
  T ←  $\frac{\text{sum}}{n1 - 1}$ 
  wd ← 2·π·CFC·2.0775
  wa ←  $\frac{\sin\left(w_d \cdot \frac{T}{2}\right)}{\cos\left(w_d \cdot \frac{T}{2}\right)}$ 
  a0 ←  $\frac{w_a^2}{\left(1.0 + \sqrt{2} \cdot w_a + w_a^2\right)}$ 
  a1 ← 2·a0
  a2 ← a0
  b1 ←  $-2 \cdot \frac{\left(w_a^2 - 1\right)}{\left(1 + \sqrt{2} \cdot w_a + w_a^2\right)}$ 
  b2 ←  $\frac{\left(-1 + \sqrt{2} \cdot w_a - w_a^2\right)}{\left(1 + \sqrt{2} \cdot w_a + w_a^2\right)}$ 
  filter11 ← 0·g
  filter12 ← 0·g
  filter21 ← 0·g
  filter22 ← 0·g
  jend ← n1 - 2
  for j ∈ 3..jend
    filter1j ← a0·Accj + a1·Accj-1 + a2·Accj-2 + b1·filter1j-1 + b2·filter1j-2
  for j ∈ 3..jend
    filter11j ← filter1jend-(j-1)
  for j ∈ 3..jend
    filter2j ← a0·filter11j + a1·filter11j-1 + a2·filter11j-2 + b1·filter2j-1 + b2·filter2j-2
  for j ∈ 3..jend
    filter21j ← filter2jend-(j-1)
  filter21

```

APPENDIX D

Material models and sample input data from LS-Dyna

This section describes in brief detail the material characteristics for different CRS components including the CRS polypropylene, the foam pad and the seatbelt.

1. Material and section properties of the polypropylene CRS

Table 1 - D. Material properties of the polypropylene CRS

Material property	Values
Density	800 kg/m ³
Young's modulus	0.842 GPa
Poisson's ratio	0.3

```

$-----1-----2-----3-----4-----5-----6-----7-----8
$           MATERIAL CARDS           UNITS : MM, KG, MSEC, KN           $
$-----1-----2-----3-----4-----5-----6-----7-----8
*MAT_PIECEWISE_LINEAR_PLASTICITY
$^M-212512
$   MID      RO      E      PR      SIGY      ETAN      FAIL      TDEL
$ 2125120.00000080  0.842  0.30 0.0087644  0.01.0000E+21  0.0
$   C      P      LCSS      LCSR      VP
$   0.0     0.0  12006.0  0.0     0.0
$   EPS1    EPS2    EPS3    EPS4    EPS5    EPS6    EPS7    EPS8
$   0.0     0.0     0.0     0.0     0.0     0.0     0.0     0.0
$   ES1     ES2     ES3     ES4     ES5     ES6     ES7     ES8
$   0.0     0.0     0.0     0.0     0.0     0.0     0.0     0.0
*SECTION_SHELL
$   SECID   ELFORM   SHRF   NIP   PROPT   QR/IRID   ICOMP   SETYP
$ 212482    2        1.0    2     0.0    0.0       0        1
$   T1      T2      T3      T4      NLOC    MAREA
$   3.5     3.5     3.5     3.5     0       0.0
*SECTION_SHELL
$   SECID   ELFORM   SHRF   NIP   PROPT   QR/IRID   ICOMP   SETYP
$ 212484    2        1.0    2     0.0    0.0       0        1
$   T1      T2      T3      T4      NLOC    MAREA
$   4.5     4.5     4.5     4.5     0       0.0
    
```



```

*DEFINE_CURVE
$^SEAT
$   LCID      SIDR      SFA      SFO      OFFA      OFFO      DATTYP
   12006      0        1.0      1.0      0.0      0.0      0
$
      A1        O1
      0.0      0.008764434
      0.001382007 0.01000733
      0.002855826 0.01130735
      0.0050      0.01250856
      0.007814528 0.01355027
      0.01129941 0.01441537
      0.01545465 0.01513364
      0.02028024 0.01575421
      0.02577619 0.01630852
      0.0319425 0.01679455
      0.03877915 0.01719495
      0.04628617 0.01751026
      0.05446354 0.01776919
      0.06331126 0.01799649
      0.07282934 0.01817425
      0.08301777 0.01827228
      0.09387656 0.01835182
      0.1054057 0.01853002
      0.1176052 0.01858846
      0.1304751 0.01871528

```

2. Material and section properties of the seatbelt shell elements

Table 2 - D. Material properties of the seatbelt shell elements

Material property	Values
Density	890.6 kg/m ³
Young's modulus	2.068 GPa
Poisson's ratio	0.3

```

$-----1-----2-----3-----4-----5-----6-----7-----8
$          MATERIAL CARDS          UNITS : MM, KG, MSEC, KN          $
$-----1-----2-----3-----4-----5-----6-----7-----8
*MAT_FABRIC
$^MAT0166
$   MID      RO      EA      EB      EC      PRBA      PRCA      PRCB
   2124948.9060E-07 2.068 0.0 0.0 0.0 0.30 0.0 0.0
$   GAB      GBC      GCA      GSE      EL      PRL      LRATIO      DAMP
   0.0 0.0 0.0 0.0 0.0 0.0 0.0 0.20
$   AOPT      FLC      FAC      ELA      LNRC      FORM      FVOPT      TSRFAC
   0.0 0.0 0.0 0.0 0.0 0.0 0.0
$   BLANK      BLANK      BLANK      A1      A2      A3
$
$   V1      V2      V3      D1      D2      D3      BETA
$
*SECTION_SHELL
$   SECID      ELFORM      SHRF      NIP      PROPT      QR/IRID      ICOMP      SETYP
   212482      2      1.0      2      0.0      0.0      0      1
$   T1      T2      T3      T4      NLOC      MAREA
   3.5 3.5 3.5 3.5 0 0.0

```

3. Material and section properties of the one dimensional seatbelt elements

```

$-----1-----2-----3-----4-----5-----6-----7-----8
$          MATERIAL CARDS          UNITS : MM, KG,  MSEC, KN          $
$-----1-----2-----3-----4-----5-----6-----7-----8
*MAT_SEATBELT
$^M-212516
$      MID      MPUL      LLCID      ULCID      LMIN
      212516  0.000040      12009      12018      0.0
*SECTION_SEATBELT
$      SECID
      212483
*DEFINE_CURVE
$^LCUR_LOAD
$      LCID      SIDR      SFA      SFO      OFFA      OFFO      DATTYP
      12009      0      1.0      1.0      0.0      0.0      0
$      A1
      0.0      0.0
      0.192      17.793
*DEFINE_CURVE
$^LCUR_UNLOAD
$      LCID      SIDR      SFA      SFO      OFFA      OFFO      DATTYP
      12018      0      1.0      1.6      0.0      0.0      0
$      A1
      0.0      0.0
      0.192      17.793

```

4. Material and section properties of the foam

Table 3 - D. Material properties of the foam

Material property	Values
Density	50.2 kg/m ³
Young's modulus	5.463 MPa
Poisson's ratio	0.3

```

$-----1-----2-----3-----4-----5-----6-----7-----8
$          MATERIAL CARDS          UNITS : MM, KG,  MSEC, KN          $
$-----1-----2-----3-----4-----5-----6-----7-----8
*MAT_LOW_DENSITY_FOAM
$^MAT0168
$      MID      RO      E      LCID      TC      HU      BETA      DAMP
      2125115.0170E-08  0.005463      1.0      TC      0.10      0.0      0.50
$      SHAPE      FAIL      BVFLAG      ED      BETA1      KCON      REF
      5.0
*SECTION_SOLID
$      SECID      ELFORM      AET
      212481      2      0

```

*DEFINE_CURVE

\$	LCID	SIDR	SFA	SFO	OFFA	OFFO	DATTYP
\$	1		1.0	0.000025	0.0	0.0	
\$		A1		O1			
		0.0		0.0			
		0.01326531		3.079164			
		0.02653061		6.02553			
		0.03979592		8.220119			
		0.05306122		9.327401			
		0.06632653		9.673192			
		0.07959184		9.893332			
		0.09285714		10.0266			
		0.1061224		10.13375			
		0.1193878		10.30251			
		0.1326531		10.55831			
		0.1459184		10.85381			
		0.1591837		11.13803			
		0.172449		11.38413			
		0.1857143		11.59942			
		0.1989796		11.7938			
		0.2122449		11.97717			
		0.2255102		12.15943			
		0.2387755		12.35048			
		0.2520408		12.56022			
		0.2653061		12.79754			
		0.2785714		13.06231			
		0.2918367		13.34962			
		0.3051021		13.65452			
		0.3183674		13.97205			
		0.3316326		14.29727			
		0.344898		14.62599			
		0.3581633		14.95943			
		0.3714286		15.30114			
		0.3846939		15.65467			
		0.3979592		16.02358			
		0.4112245		16.41142			
		0.4244898		16.82103			
		0.4377551		17.25158			
		0.4510204		17.70102			
		0.4642857		18.16934			
		0.477551		18.66936			
		0.4908163		19.21905			
		0.5040816		19.83478			
		0.5173469		20.52033			
		0.5306122		21.27331			
		0.5438775		22.09189			
		0.5571429		22.98122			
		0.5704082		23.95088			
		0.5836735		25.01052			
		0.5969388		26.16979			
		0.6102041		27.43835			
		0.6234694		28.82586			
		0.6367347		30.34196			
		0.65		31.99632			

5. Material and section properties of the HANS collar

Table 4 - D. Material properties of the HANS collar (ABS 20 percent glass fiber filled)

Material property	Values
Density	1200 kg/m ³
Young's modulus	6.0 GPa
Poisson's ratio	0.3

```

$-----1-----2-----3-----4-----5-----6-----7-----8
$          MATERIAL CARDS          UNITS : MM, KG, MSEC, KN          $
$-----1-----2-----3-----4-----5-----6-----7-----8
*PART
HANS_COLLAR
$  PID      SECID      MID      EOSID      HGID      GRAV      ADPOPT      TMID
   12493    212600    212600
*SECTION_SHELL_TITLE
SEC0170 FOR HANS COLLAR
$  SECID      ELFORM      SHRF      NIP      PROPT      QR/IRID      ICOMP      SETYP
   212600      16    1.000000      5      0      0      0      1
$  T1      T2      T3      T4      NLOC      MAREA
 4.000000  4.000000  4.000000  4.000000
*MAT_PIECEWISE_LINEAR_PLASTICITY_TITLE
M-212600 FOR HANS COLLAR
$  MID      RO      E      PR      SIGY      ETAN      FAIL      TDEL
   212600  1.2000E-6  6.000000  0.300000  0.080000  0.0001.0000E+21
$  C      P      LCSS      LCSR      VP
   0.000    0.000      0      0      0.000
$  EPS1      EPS2      EPS3      EPS4      EPS5      EPS6      EPS7      EPS8
   0.000    0.033450
$  ES1      ES2      ES3      ES4      ES5      ES6      ES7      ES8
 0.081000  0.096600

```

6. Material and section properties of the rigid ISOFIX

Table 5 - D. Material properties of the rigid ISOFIX

Material property	Values
Density	7800 kg/m ³
Young's modulus	207 GPa
Poisson's ratio	0.3

```

$-----1-----2-----3-----4-----5-----6-----7-----8
$           MATERIAL CARDS           UNITS : MM, KG, MSEC, KN           $
$-----1-----2-----3-----4-----5-----6-----7-----8
*PART
ISOFIX
$      PID      SECID      MID      EOSID      HGID      GRAV      ADPOPT      TMID
      37129     449585     449654
*SECTION_SHELL_TITLE
P-237096
$      SECID     ELFORM      SHRF      NIP      PROPT     QR/IRID      ICOMP      SETYP
      449585      16     1.000000      2        0          0          0          1
$      T1        T2        T3        T4        NLOC      MAREA
      3.000000   3.000000   3.000000   3.000000
*MAT_PIECEWISE_LINEAR_PLASTICITY_TITLE
M-237131
$      MID      RO      E      PR      SIGY      ETAN      FAIL      TDEL
      449654   7.8000E-6   207.00000   0.300000   0.210000   0.0001.0000E+21
$      C      P      LCSS      LCSR      VP
      0.040400   5.000000
$      EPS1     EPS2     EPS3     EPS4     EPS5     EPS6     EPS7     EPS8
      0.000     0.220700
$      ES1     ES2     ES3     ES4     ES5     ES6     ES7     ES8
      0.210000   0.475000

```

7. Cross-section plane data for the child FE model

```

$-----1-----2-----3-----4-----5-----6-----7-----8
$          CROSS SECTION CARDS          UNITS : M, KG, SEC          $
$-----1-----2-----3-----4-----5-----6-----7-----8
*DATABASE_CROSS_SECTION_PLANE_ID
$   CSID
   170
$   PSID      XCT      YCT      ZCT      XCH      YCH      ZCH
18980365    1.725    4.998E-2    0.440    1.76000    4.998E-2    0.492144
$   XHEV      YHEV      ZHEV      LENL      LENM      ID      ITYPE
   1.725    -0.95002    0.440    0.15    0.15    8710210    0
$
$ Cross-reference summary for SET_PART 18980365
$ -----
$ DATABASE_CROSS_SECTION 170
$
*SET_PART_LIST
$   SID      DA1      DA2      DA3      DA4
18980365    0.0      0.0      0.0      0.0
$   PID1      PID2      PID3      PID4      PID5      PID6      PID7      PID8
   8730000    8730500    8760240    8760310    8760370    8760430    8760610    8760660
$
*DATABASE_CROSS_SECTION_PLANE_ID
$   CSID
   171
$   PSID      XCT      YCT      ZCT      XCH      YCH      ZCH
18980366    1.737    2.499E-2    0.4060    1.73700    2.499E-2    0.486013
$   XHEV      YHEV      ZHEV      LENL      LENM      ID      ITYPE
   1.737    -0.97501    0.4060    0.1      0.1      8710210    0
$
$ Cross-reference summary for SET_PART 18980366
$ -----
$ DATABASE_CROSS_SECTION 171
$
*SET_PART_LIST
$   SID      DA1      DA2      DA3      DA4
18980366    0.0      0.0      0.0      0.0
$   PID1      PID2      PID3      PID4      PID5      PID6      PID7      PID8
   8720000    8720010    8760010

```

APPENDIX E

Contact definitions

Generally, a dummy model consists of two types of contact algorithms – internal contact surfaces and additional contact surfaces. The internal contact surfaces are those permanent and necessary for the dummy model. The additional contact surfaces are defined by the user and they would vary depending on the analysis. Similar additional contact definitions were modeled for contact between the CRS and the child models. The following contact algorithms correspond to the Hybrid III 3-year-old dummy.

1. General contact algorithms:

```
$-----1-----2-----3-----4-----5-----6-----7-----8
$
$ CONTACT CARDS $
$
$-----1-----2-----3-----4-----5-----6-----7-----8
*CONTACT_AUTOMATIC_SINGLE_SURFACE_ID
$^CRS MODEL
$ CID
12023
$ SSID MSID SSTYP MSTYP SBOXID MBOXID SPR MPR
1520019 0 2
$ FS FD DC VC VDC PENCHK BT DT
0.0 0.0 0.0 0.0 0.0 0 0.01.0000E+20
$ SFS SFM SST MST SFST SFMT FSF VSF
1.0 1.0 0.0 0.0 1.0 1.0 1.0 1.0
$ SOFT SOFSCL LCIDAB MAXPAR SBOPT DEPTH BSORT FRCFRQ
0 0.10 1.025 0.0 2.0 100 1
*CONTACT_AUTOMATIC_NODES_TO_SURFACE_ID
$^ SEATBELT SHELL ELEMENTS AND THE CRS
$ CID
12024
$ SSID MSID SSTYP MSTYP SBOXID MBOXID SPR MPR
1520069 1520019 4 2
$ FS FD DC VC VDC PENCHK BT DT
0.90 0.90 0.0 0.0 0.0 0 0.01.0000E+23
$ SFS SFM SST MST SFST SFMT FSF VSF
30.0 90.0 0.0 0.0 1.0 1.0 1.0 1.0
$ SOFT SOFSCL LCIDAB MAXPAR SBOPT DEPTH BSORT FRCFRQ
0 0.10 1.025 0.0 2.0 0 1
```

*CONTACT_AUTOMATIC_NODES_TO_SURFACE_ID

\$^1D SEATBELT ELEMENTS (PART LATCH) AND THE CRS

\$ CID								
12025								
\$	SSID	MSID	SSTYP	MSTYP	SBOXID	MBOXID	SPR	MPR
	1520022	1520019	4	2			0	0
\$	FS	FD	DC	VC	VDC	PENCHK	BT	DT
	0.90	0.90	0.0	0.0	0.0	0	0.01.0000E+23	
\$	SFS	SFM	SST	MST	SFST	SFMT	FSF	VSF
	50.0	150.0	0.0	0.0	1.0	1.0	1.0	1.0
\$	SOFT	SOFSC	LCIDAB	MAXPAR	SBOPT	DEPTH	BSORT	FRCFRQ
	0	0.10		1.025	0.0	2.0	0	1

*CONTACT_AUTOMATIC_NODES_TO_SURFACE_ID

\$^1D SEATBELT ELEMENTS (PART TOP_TET) AND THE RIGID VEHICLE SEAT

\$ CID								
12026								
\$	SSID	MSID	SSTYP	MSTYP	SBOXID	MBOXID	SPR	MPR
	1520023	13	4	3			0	0
\$	FS	FD	DC	VC	VDC	PENCHK	BT	DT
	0.40	0.40	0.0	0.0	0.0	0	0.01.0000E+23	
\$	SFS	SFM	SST	MST	SFST	SFMT	FSF	VSF
	50.0	100.0	0.0	0.0	1.0	1.0	1.0	1.0
\$	SOFT	SOFSC	LCIDAB	MAXPAR	SBOPT	DEPTH	BSORT	FRCFRQ
	0	0.10		1.025	0.0	2.0	0	1

*CONTACT_TIED_SURFACE_TO_SURFACE_ID_OFFSET

\$^FOAM PADDING AND THE CRS

\$ CID								
12027								
\$	SSID	MSID	SSTYP	MSTYP	SBOXID	MBOXID	SPR	MPR
	1520019	1520011	2	0			0	0
\$	FS	FD	DC	VC	VDC	PENCHK	BT	DT
	0.0	0.0	0.0	0.0	0.0	0	0.01.0000E+23	
\$	SFS	SFM	SST	MST	SFST	SFMT	FSF	VSF
	1.0	1.0	0.0	0.0	1.0	1.0	1.0	1.0
\$	SOFT	SOFSC	LCIDAB	MAXPAR	SBOPT	DEPTH	BSORT	FRCFRQ
	2	0.30		1.025	0.0	2.0	0	1

*CONTACT_AUTOMATIC_SURFACE_TO_SURFACE_ID

\$^FOAM PADDING AND THE CHILD DUMMY

\$ CID								
12028								
\$	SSID	MSID	SSTYP	MSTYP	SBOXID	MBOXID	SPR	MPR
	26	1520018	3	2			0	0
\$	FS	FD	DC	VC	VDC	PENCHK	BT	DT
	0.0	0.0	0.0	0.0	0.0	0	0.01.0000E+20	
\$	SFS	SFM	SST	MST	SFST	SFMT	FSF	VSF
	1.0	0.1	0.0	0.0	1.0	1.0	1.0	1.0
\$	SOFT	SOFSC	LCIDAB	MAXPAR	SBOPT	DEPTH	BSORT	FRCFRQ
	2	0.10		1.025	0.0	3.0	0	1

*CONTACT_AUTOMATIC_NODES_TO_SURFACE_ID

\$^LOCAL CONTACT BETWEEN THE SEATBELT SHELL ELEMENTS AND THE CRS

```

$      CID
      12029
$      SSID      MSID      SSTYP      MSTYP      SBOXID      MBOXID      SPR      MPR
      1520052    1520019         4         2
$      FS        FD        DC        VC        VDC        PENCHK        BT        DT
      0.0        0.0        0.0        0.0        0.0          0      0.01.0000E+23
$      SFS        SFM        SST        MST        SFST        SFMT        FSF        VSF
      50.0       12.5        0.0        0.0        1.0        1.0        1.0        1.0
$      SOFT      SOFSCS  LCIDAB      MAXPAR      SBOPT      DEPTH      BSORT      FRCFRQ
      0         0.10                1.025        0.0        2.0          0          1
    
```

*CONTACT_AUTOMATIC_SURFACE_TO_SURFACE_ID

\$^THE CHILD DUMMY AND THE CRS

```

$      CID
      12030
$      SSID      MSID      SSTYP      MSTYP      SBOXID      MBOXID      SPR      MPR
      1520018    1520019         2         2
$      FS        FD        DC        VC        VDC        PENCHK        BT        DT
      0.40       0.40        0.0        0.0        0.0          0      0.01.0000E+20
$      SFS        SFM        SST        MST        SFST        SFMT        FSF        VSF
      0.2        0.2        0.0        0.0        1.0        1.0        1.0        1.0
$      SOFT      SOFSCS  LCIDAB      MAXPAR      SBOPT      DEPTH      BSORT      FRCFRQ
      2         0.10                1.025        0.0        3.0          0          1
    
```

*CONTACT_AUTOMATIC_SINGLE_SURFACE_ID

\$^SEATBELT SHELL ELEMENTS AND TWO CLASPS

```

$      CID
      12031
$      SSID      MSID      SSTYP      MSTYP      SBOXID      MBOXID      SPR      MPR
      1520020         0         2
$      FS        FD        DC        VC        VDC        PENCHK        BT        DT
      0.20       0.20        0.0        0.0        0.0          0      0.01.0000E+20
$      SFS        SFM        SST        MST        SFST        SFMT        FSF        VSF
      50.0       50.0        0.0        0.0        1.0        1.0        1.0        1.0
$      SOFT      SOFSCS  LCIDAB      MAXPAR      SBOPT      DEPTH      BSORT      FRCFRQ
      0         0.10                1.025        0.0        2.0        100          1
    
```

*CONTACT_AUTOMATIC_SURFACE_TO_SURFACE_ID

\$^SEATBELT, TWO CLASPS AND THE CHILD DUMMY

```

$      CID
      12032
$      SSID      MSID      SSTYP      MSTYP      SBOXID      MBOXID      SPR      MPR
      1520020    1520018         2         2
$      FS        FD        DC        VC        VDC        PENCHK        BT        DT
      0.40       0.40        0.0        0.0        0.0          0      0.01.0000E+23
$      SFS        SFM        SST        MST        SFST        SFMT        FSF        VSF
      0.07       0.2         0.0        0.0        1.0        1.0        1.0        1.0
$      SOFT      SOFSCS  LCIDAB      MAXPAR      SBOPT      DEPTH      BSORT      FRCFRQ
      2         0.10                1.025        0.0        3.0        100          1
    
```

*CONTACT_AUTOMATIC_NODES_TO_SURFACE_ID

\$^TOP_TETHER AND THE CRS

\$ CID									
12033									
\$	SSID	MSID	SSTYP	MSTYP	SBOXID	MBOXID	SPR	MPR	
	1520023	1520019	4	2			0	0	
\$	FS	FD	DC	VC	VDC	PENCHK	BT	DT	
	0.95	0.90	0.0	0.0	0.0	0	0.01.0000E+23		
\$	SFS	SFM	SST	MST	SFST	SFMT	FSF	VSF	
	50.0	150.0	0.0	0.0	1.0	1.0	1.0	1.0	
\$	SOFT	SOFSC	LCIDAB	MAXPAR	SBOPT	DEPTH	BSORT	FRCFRQ	
	0	0.10		1.025	0.0	2.0	0	1	

*CONTACT_AUTOMATIC_NODES_TO_SURFACE_ID

\$^THE SEATBOTTOM AND THE DEFORMABLE VEHICLE SEAT

\$ CID									
12034									
\$	SSID	MSID	SSTYP	MSTYP	SBOXID	MBOXID	SPR	MPR	
	1520053	1520015	4	0			0	0	
\$	FS	FD	DC	VC	VDC	PENCHK	BT	DT	
	0.20	0.10	0.0	0.0	0.0	0	0.01.0000E+23		
\$	SFS	SFM	SST	MST	SFST	SFMT	FSF	VSF	
	10.0	150.0	0.0	0.0	1.0	1.0	1.0	1.0	
\$	SOFT	SOFSC	LCIDAB	MAXPAR	SBOPT	DEPTH	BSORT	FRCFRQ	
	0	0.10		1.025	0.0	2.0	0	1	

*CONTACT_AUTOMATIC_NODES_TO_SURFACE_ID

\$^THE STANDBOTTOM AND THE DEFORMABLE VEHICLE SEAT

\$ CID									
12035									
\$	SSID	MSID	SSTYP	MSTYP	SBOXID	MBOXID	SPR	MPR	
	1520015	1520015	4	0			0	0	
\$	FS	FD	DC	VC	VDC	PENCHK	BT	DT	
	0.9	0.9	0.0	0.0	0.0	0	0.01.0000E+23		
\$	SFS	SFM	SST	MST	SFST	SFMT	FSF	VSF	
	10.0	150.0	0.0	0.0	1.0	1.0	1.0	1.0	
\$	SOFT	SOFSC	LCIDAB	MAXPAR	SBOPT	DEPTH	BSORT	FRCFRQ	
	0	0.10		1.025	0.0	2.0	0	1	

*CONTACT_AUTOMATIC_NODES_TO_SURFACE_ID

\$^THE SEATBACK AND THE DEFORMABLE VEHICLE SEAT

\$ CID									
12036									
\$	SSID	MSID	SSTYP	MSTYP	SBOXID	MBOXID	SPR	MPR	
	1520059	1520015	4	0			0	0	
\$	FS	FD	DC	VC	VDC	PENCHK	BT	DT	
	0.20	0.10	0.0	0.0	0.0	0	0.01.0000E+23		
\$	SFS	SFM	SST	MST	SFST	SFMT	FSF	VSF	
	10.0	150.0	0.0	0.0	1.0	1.0	1.0	1.0	
\$	SOFT	SOFSC	LCIDAB	MAXPAR	SBOPT	DEPTH	BSORT	FRCFRQ	
	0	0.10		1.025	0.0	2.0	0	1	

*CONTACT_AUTOMATIC_NODES_TO_SURFACE_ID

\$^LOCAL CONTACT BETWEEN THE SEATBELT AND THE SEAT

```

$      CID
      12037
$      SSID      MSID      SSTYP      MSTYP      SBOXID      MBOXID      SPR      MPR
      1520052    1520019         4         2
$      FS      FD      DC      VC      VDC      PENCHK      BT      DT
      0.0      0.0      0.0      0.0      0.0      0      0.01.0000E+23
$      SFS      SFM      SST      MST      SFST      SFMT      FSF      VSF
      10.0      1.0      0.0      0.0      1.0      1.0      1.0      1.0
$      SOFT      SOFSC      LCIDAB      MAXPAR      SBOPT      DEPTH      BSORT      FRCFRQ
      0      0.10
      1.025      0.0      2.0      0      1
    
```

*CONTACT_AUTOMATIC_NODES_TO_SURFACE_ID

\$^LOCAL CONTACT BETWEEN THE SEATBELT SHELL ELEMENTS AND THE CRS

```

$      CID
      12038
$      SSID      MSID      SSTYP      MSTYP      SBOXID      MBOXID      SPR      MPR
      1520056    1520014         4         0
$      FS      FD      DC      VC      VDC      PENCHK      BT      DT
      0.0      0.0      0.0      0.0      0.0      0      0.01.0000E+23
$      SFS      SFM      SST      MST      SFST      SFMT      FSF      VSF
      50.0      1.0      0.0      0.0      1.0      1.0      1.0      1.0
$      SOFT      SOFSC      LCIDAB      MAXPAR      SBOPT      DEPTH      BSORT      FRCFRQ
      0      0.10
      1.025      0.0      2.0      0      1
    
```

*CONTACT_AUTOMATIC_NODES_TO_SURFACE_ID

\$^TOP TETHER AND THE DEFORMABLE VEHICLE SEAT

```

$      CID
      12039
$      SSID      MSID      SSTYP      MSTYP      SBOXID      MBOXID      SPR      MPR
      1520023    1520015         4         0
$      FS      FD      DC      VC      VDC      PENCHK      BT      DT
      0.20      0.10      0.0      0.0      0.0      0      0.01.0000E+23
$      SFS      SFM      SST      MST      SFST      SFMT      FSF      VSF
      1.0      150.0      0.0      0.0      1.0      1.0      1.0      1.0
$      SOFT      SOFSC      LCIDAB      MAXPAR      SBOPT      DEPTH      BSORT      FRCFRQ
      0      0.10
      1.025      0.0      2.0      0      1
    
```

*CONTACT_AUTOMATIC_NODES_TO_SURFACE_ID

\$^THE SEATBACK AND THE RIGID VEHICLE SEAT

```

$      CID
      12040
$      SSID      MSID      SSTYP      MSTYP      SBOXID      MBOXID      SPR      MPR
      1520059      13         4         3
$      FS      FD      DC      VC      VDC      PENCHK      BT      DT
      0.40      0.40      0.0      0.0      0.0      0      0.01.0000E+23
$      SFS      SFM      SST      MST      SFST      SFMT      FSF      VSF
      100.0      10.0      0.0      0.0      1.0      1.0      1.0      1.0
$      SOFT      SOFSC      LCIDAB      MAXPAR      SBOPT      DEPTH      BSORT      FRCFRQ
      0      0.10
      1.025      0.0      2.0      0      1
    
```

*CONTACT_AUTOMATIC_SURFACE_TO_SURFACE_ID

\$^CHILD DUMMY'S LEGS

\$ CID

12041

\$	SSID	MSID	SSTYP	MSTYP	SBOXID	MBOXID	SPR	MPR
	1520022	1520023	2	2			0	0
\$	FS	FD	DC	VC	VDC	PENCHK	BT	DT
	0.0	0.0	0.0	0.0	0.0	0	0.01.0000E+23	
\$	SFS	SFM	SST	MST	SFST	SFMT	FSF	VSF
	1.0	1.0	0.0	0.0	1.0	1.0	1.0	1.0
\$	SOFT	SOFSC	LCIDAB	MAXPAR	SBOPT	DEPTH	BSORT	FRCFRQ
	0	0.10		1.025	0.0	2.0	100	1

*CONTACT_AUTOMATIC_SURFACE_TO_SURFACE_ID

\$^THE CHILD DUMMY'S HEAD TO THE CHILD DUMMY'S ARMS

\$ CID

12042

\$	SSID	MSID	SSTYP	MSTYP	SBOXID	MBOXID	SPR	MPR
	1520025	1520026	2	2			0	0
\$	FS	FD	DC	VC	VDC	PENCHK	BT	DT
	0.6	0.5	0.0	0.0	0.0	0	0.01.0000E+20	
\$	SFS	SFM	SST	MST	SFST	SFMT	FSF	VSF
	1.0	1.0	0.0	0.0	1.0	1.0	1.0	1.0
\$	SOFT	SOFSC	LCIDAB	MAXPAR	SBOPT	DEPTH	BSORT	FRCFRQ
	0	0.10		1.025	0.0	2.0	0	1

*CONTACT_AUTOMATIC_SURFACE_TO_SURFACE_ID

\$^THE CHILD DUMMY'S RIGHT UPPER AND LOWER ARMS

\$ CID

12043

\$	SSID	MSID	SSTYP	MSTYP	SBOXID	MBOXID	SPR	MPR
	1520027	1520028	2	2			0	0
\$	FS	FD	DC	VC	VDC	PENCHK	BT	DT
	0.6	0.5	0.0	0.0	0.0	0	0.01.0000E+20	
\$	SFS	SFM	SST	MST	SFST	SFMT	FSF	VSF
	1.0	1.0	0.0	0.0	1.0	1.0	1.0	1.0
\$	SOFT	SOFSC	LCIDAB	MAXPAR	SBOPT	DEPTH	BSORT	FRCFRQ
	0	0.10		1.025	0.0	2.0	0	1

*CONTACT_AUTOMATIC_SURFACE_TO_SURFACE_ID

\$^THE CHILD DUMMY'S LEFT UPPER AND LOWER ARMS

\$ CID

12044

\$	SSID	MSID	SSTYP	MSTYP	SBOXID	MBOXID	SPR	MPR
	1520029	1520030	2	2			0	0
\$	FS	FD	DC	VC	VDC	PENCHK	BT	DT
	0.6	0.5	0.0	0.0	0.0	0	0.01.0000E+20	
\$	SFS	SFM	SST	MST	SFST	SFMT	FSF	VSF
	1.0	1.0	0.0	0.0	1.0	1.0	1.0	1.0
\$	SOFT	SOFSC	LCIDAB	MAXPAR	SBOPT	DEPTH	BSORT	FRCFRQ
	0	0.10		1.025	0.0	2.0	0	1

*CONTACT_AUTOMATIC_SURFACE_TO_SURFACE_ID

^THE CHILD DUMMY'S HEAD AND THE SEAT

\$ CID

12045

\$	SSID	MSID	SSTYP	MSTYP	SBOXID	MBOXID	SPR	MPR
	1520025	1520019	2	2			0	0
\$	FS	FD	DC	VC	VDC	PENCHK	BT	DT
	0.4	0.4	0.0	0.0	0.0	0	0.01.0000E+20	
\$	SFS	SFM	SST	MST	SFST	SFMT	FSF	VSF
	1.0	1.0	0.0	0.0	1.0	1.0	1.0	1.0
\$	SOFT	SOFSC	LCIDAB	MAXPAR	SBOPT	DEPTH	BSORT	FRCFRQ
	0	0.10		1.025	0.0	2.0	0	1

*CONTACT_AUTOMATIC_SURFACE_TO_SURFACE_ID

^THE CHILD DUMMY'S ARMS AND THE CRS

\$ CID

12046

\$	SSID	MSID	SSTYP	MSTYP	SBOXID	MBOXID	SPR	MPR
	1520026	1520019	2	2			0	0
\$	FS	FD	DC	VC	VDC	PENCHK	BT	DT
	0.4	0.4	0.0	0.0	0.0	0	0.01.0000E+20	
\$	SFS	SFM	SST	MST	SFST	SFMT	FSF	VSF
	1.0	1.0	0.0	0.0	1.0	1.0	1.0	1.0
\$	SOFT	SOFSC	LCIDAB	MAXPAR	SBOPT	DEPTH	BSORT	FRCFRQ
	0	0.10		1.025	0.0	2.0	0	1

*CONTACT_AUTOMATIC_SURFACE_TO_SURFACE_ID

^THE CHILD DUMMY'S TORSO AND THE CRS

\$ CID

12047

\$	SSID	MSID	SSTYP	MSTYP	SBOXID	MBOXID	SPR	MPR
	1520031	1520019	2	2			0	0
\$	FS	FD	DC	VC	VDC	PENCHK	BT	DT
	0.4	0.4	0.0	0.0	0.0	0	0.01.0000E+20	
\$	SFS	SFM	SST	MST	SFST	SFMT	FSF	VSF
	1.0	1.0	0.0	0.0	1.0	1.0	1.0	1.0
\$	SOFT	SOFSC	LCIDAB	MAXPAR	SBOPT	DEPTH	BSORT	FRCFRQ
	0	0.10		1.025	0.0	2.0	0	1

*CONTACT_AUTOMATIC_SURFACE_TO_SURFACE_ID

^THE CHILD DUMMY'S RIGHT LEG AND THE CRS

\$ CID

12048

\$	SSID	MSID	SSTYP	MSTYP	SBOXID	MBOXID	SPR	MPR
	1520022	1520019	2	2			0	0
\$	FS	FD	DC	VC	VDC	PENCHK	BT	DT
	0.4	0.4	0.0	0.0	0.0	0	0.01.0000E+20	
\$	SFS	SFM	SST	MST	SFST	SFMT	FSF	VSF
	1.0	1.0	0.0	0.0	1.0	1.0	1.0	1.0
\$	SOFT	SOFSC	LCIDAB	MAXPAR	SBOPT	DEPTH	BSORT	FRCFRQ
	0	0.10		1.025	0.0	2.0	0	1

*CONTACT_AUTOMATIC_SURFACE_TO_SURFACE_ID

\$^THE CHILD DUMMY'S LEFT LEG AND THE CRS

\$ CID

12049

\$	SSID	MSID	SSTYP	MSTYP	SBOXID	MBOXID	SPR	MPR
	1520023	1520019	2	2			0	0
\$	FS	FD	DC	VC	VDC	PENCHK	BT	DT
	0.4	0.4	0.0	0.0	0.0	0	0.01	0.0000E+20
\$	SFS	SFM	SST	MST	SFST	SFMT	FSF	VSF
	1.0	1.0	0.0	0.0	1.0	1.0	1.0	1.0
\$	SOFT	SOFSC	LCIDAB	MAXPAR	SBOPT	DEPTH	BSORT	FRCFRQ
	0	0.10		1.025	0.0	2.0	0	1

2. Dummy contacts for rearward facing model with the vehicle seat:

*CONTACT_AUTOMATIC_NODES_TO_SURFACE_ID

\$^CRS WITH VEHICLE SEAT BACK

\$ CID HEADING

12052CRS WITH VEHICLE SEAT BACK

\$	SSID	MSID	SSTYP	MSTYP	SBOXID	MBOXID	SPR	MPR
	1520059	1520017	4					
\$	FS	FD	DC	VC	VDC	PENCHK	BT	DT
	0.350000	0.300000	0.000	0.000	0.000	0	0.0001	0.0000E+23
\$	SFS	SFM	SST	MST	SFST	SFMT	FSF	VSF
	10.000000	150.000000	0.000	0.000	1.000000	1.000000	1.000000	1.000000
\$	SOFT	SOFSC	LCIDAB	MAXPAR	SBOPT	DEPTH	BSORT	FRCFRQ
	0	0.100000	0	1.025000	0.000	2	0	1

*CONTACT_AUTOMATIC_SURFACE_TO_SURFACE_ID

\$^DUMMY'S HEAD WITH VEHICLE SEAT

\$ CID HEADING

12054DUMMY'S HEAD WITH VEHICLE SEAT

\$	SSID	MSID	SSTYP	MSTYP	SBOXID	MBOXID	SPR	MPR
	1520025	1521040	2	2				
\$	FS	FD	DC	VC	VDC	PENCHK	BT	DT
	0.600000	0.500000	0.000	0.000	0.000	0	0.0001	0.0000E+20
\$	SFS	SFM	SST	MST	SFST	SFMT	FSF	VSF
	1.000000	1.000000	0.000	0.000	1.000000	1.000000	1.000000	1.000000
\$	SOFT	SOFSC	LCIDAB	MAXPAR	SBOPT	DEPTH	BSORT	FRCFRQ
	0	0.100000	0	1.025000	0.000	2	0	1

3. Dummy contacts with the HANS device:

```

*CONTACT_AUTOMATIC_SURFACE_TO_SURFACE_ID
$^DUMMY AND HANS COLLAR
$  SSID      MSID      SSTYP      MSTYP      SBOXID      MBOXID      SPR      MPR
   1520018    12493         2         3
$  FS        FD        DC        VC        VDC        PENCHK      BT        DT
   0.400000  0.400000    0.000    0.000    0.000        0    0.0001.0000E+20
$  SFS       SFM       SST        MST        SFST       SFMT       FSF       VSF
   1.000000  1.000000    0.000    0.000    1.000000    1.000000    1.000000    1.000000
$  SOFT      SOFSCL    LCIDAB     MAXPAR     SBOPT     DEPTH     BSORT     FRCFRQ
       2  0.100000         0  1.025000    0.000        3         0         1

*CONTACT_AUTOMATIC_SURFACE_TO_SURFACE_ID
$^SEATBELT AND HANS COLLAR
$  SSID      MSID      SSTYP      MSTYP      SBOXID      MBOXID      SPR      MPR
   1520020    12493         2         3
$  FS        FD        DC        VC        VDC        PENCHK      BT        DT
   0.400000  0.400000    0.000    0.000    0.000        0    0.0001.0000E+23
$  SFS       SFM       SST        MST        SFST       SFMT       FSF       VSF
   1.000000  1.000000    0.000    0.000    1.000000    1.000000    1.000000    1.000000
$  SOFT      SOFSCL    LCIDAB     MAXPAR     SBOPT     DEPTH     BSORT     FRCFRQ
       2  0.100000         0  1.025000    0.000        3        100         1

*CONTACT_AUTOMATIC_SURFACE_TO_SURFACE_ID
$^FOAM INSERT AND HANS COLLAR
$  SSID      MSID      SSTYP      MSTYP      SBOXID      MBOXID      SPR      MPR
       26    12493         3         3
$  FS        FD        DC        VC        VDC        PENCHK      BT        DT
       0.000    0.000    0.000    0.000    0.000        0    0.0001.0000E+20
$  SFS       SFM       SST        MST        SFST       SFMT       FSF       VSF
   1.000000  1.000000    0.000    0.000    1.000000    1.000000    1.000000    1.000000
$  SOFT      SOFSCL    LCIDAB     MAXPAR     SBOPT     DEPTH     BSORT     FRCFRQ
       2  0.100000         0  1.025000    0.000        3         0         1

*CONTACT_AUTOMATIC_SURFACE_TO_SURFACE_ID
$^CRS AND HANS COLLAR
$  SSID      MSID      SSTYP      MSTYP      SBOXID      MBOXID      SPR      MPR
   1520019    12493         2         3
$  FS        FD        DC        VC        VDC        PENCHK      BT        DT
   0.400000  0.400000    0.000    0.000    0.000        0    0.0001.0000E+20
$  SFS       SFM       SST        MST        SFST       SFMT       FSF       VSF
   1.000000  1.000000    0.000    0.000    1.000000    1.000000    1.000000    1.000000
$  SOFT      SOFSCL    LCIDAB     MAXPAR     SBOPT     DEPTH     BSORT     FRCFRQ
       2  0.100000         0  1.025000    0.000        3         0         1

```

*CONTACT_AUTOMATIC_NODES_TO_SURFACE_ID

\$^HANS TETHER AND DUMMY

\$	SSID	MSID	SSTYP	MSTYP	SBOXID	MBOXID	SPR	MPR
	1520081	1520018	4	2				
\$	FS	FD	DC	VC	VDC	PENCHK	BT	DT
	0.400000	0.400000	0.000	0.000	0.000	0	0.0001.0000E+23	
\$	SFS	SFM	SST	MST	SFST	SFMT	FSF	VSF
	50.000000	100.000000	0.000	0.000	1.000000	1.000000	1.000000	1.000000
\$	SOFT	SOFSC	LCIDAB	MAXPAR	SBOPT	DEPTH	BSORT	FRCFRQ
	0	0.100000	0	1.025000	0.000	2	0	1

*CONTACT_AUTOMATIC_NODES_TO_SURFACE_ID

\$^HANS TETHER AND HANS COLLAR

\$	SSID	MSID	SSTYP	MSTYP	SBOXID	MBOXID	SPR	MPR
	1520081	12493	4	3				
\$	FS	FD	DC	VC	VDC	PENCHK	BT	DT
	0.400000	0.400000	0.000	0.000	0.000	0	0.0001.0000E+23	
\$	SFS	SFM	SST	MST	SFST	SFMT	FSF	VSF
	50.000000	100.000000	0.000	0.000	1.000000	1.000000	1.000000	1.000000
\$	SOFT	SOFSC	LCIDAB	MAXPAR	SBOPT	DEPTH	BSORT	FRCFRQ
	0	0.100000	0	1.025000	0.000	2	0	1

4. Dummy contacts with the side-wall:

*CONTACT_AUTOMATIC_SURFACE_TO_SURFACE_ID

\$ CID HEADING

12050CRS AND SIDE WALL

\$	SSID	MSID	SSTYP	MSTYP	SBOXID	MBOXID	SPR	MPR
	1520019	24980	2	3				
\$	FS	FD	DC	VC	VDC	PENCHK	BT	DT
	0.400000	0.400000	0.000	0.000	0.000	0	0.0001.0000E+20	
\$	SFS	SFM	SST	MST	SFST	SFMT	FSF	VSF
	1.000000	1.000000	0.000	0.000	1.000000	1.000000	1.000000	1.000000
\$	SOFT	SOFSC	LCIDAB	MAXPAR	SBOPT	DEPTH	BSORT	FRCFRQ
	0	0.100000	0	1.025000	0.000	2	0	1

*CONTACT_AUTOMATIC_SURFACE_TO_SURFACE_ID

\$ CID HEADING

12051DUMMY AND SIDE WALL

\$	SSID	MSID	SSTYP	MSTYP	SBOXID	MBOXID	SPR	MPR
	1520018	24980	2	3				
\$	FS	FD	DC	VC	VDC	PENCHK	BT	DT
	0.400000	0.400000	0.000	0.000	0.000	0	0.0001.0000E+20	
\$	SFS	SFM	SST	MST	SFST	SFMT	FSF	VSF
	1.000000	1.000000	0.000	0.000	1.000000	1.000000	1.000000	1.000000
\$	SOFT	SOFSC	LCIDAB	MAXPAR	SBOPT	DEPTH	BSORT	FRCFRQ
	0	0.100000	0	1.025000	0.000	2	0	1

5. Dummy contacts with the energy absorbing foam:

```

*CONTACT_TIED_NODES_TO_SURFACE_OFFSET_ID
$^FOAM BLOCKS AND THE CRS (CONTACT 1)
$  SSID      MSID      SSTYP      MSTYP      SBOXID      MBOXID      SPR      MPR
   1520084   1520019         4         2
$  FS        FD        DC        VC        VDC        PENCHK      BT        DT
   0.000     0.000     0.000     0.000     0.000         0     0.0001.0000E+23
$  SFS       SFM       SST        MST        SFST       SFMT        FSF       VSF
100.00000 100.00000     0.000     0.000  1.000000  1.000000  1.000000  1.000000
$  SOFT      SOFSCS   LCIDAB    MAXPAR    SBOPT     DEPTH      BSORT     FRCFRQ
       2  0.100000         0  1.025000     0.000         2         0         1

*CONTACT_AUTOMATIC_NODES_TO_SURFACE_ID
$^FOAM BLOCKS AND THE CRS (CONTACT 2)
$  SSID      MSID      SSTYP      MSTYP      SBOXID      MBOXID      SPR      MPR
   1520083   1520019         4         2
$  FS        FD        DC        VC        VDC        PENCHK      BT        DT
   0.000     0.000     0.000     0.000     0.000         0     0.0001.0000E+20
$  SFS       SFM       SST        MST        SFST       SFMT        FSF       VSF
100.00000 100.00000     0.000     0.000  1.000000  1.000000  1.000000  1.000000
$  SOFT      SOFSCS   LCIDAB    MAXPAR    SBOPT     DEPTH      BSORT     FRCFRQ
       2  0.100000         0  1.025000     0.000         3         0         1

*CONTACT_AUTOMATIC_SURFACE_TO_SURFACE_ID
$^FOAM BLOCKS AND THE DUMMY
$  SSID      MSID      SSTYP      MSTYP      SBOXID      MBOXID      SPR      MPR
   25040     1520018         3         2
$  FS        FD        DC        VC        VDC        PENCHK      BT        DT
   0.000     0.000     0.000     0.000     0.000         0     0.0001.0000E+20
$  SFS       SFM       SST        MST        SFST       SFMT        FSF       VSF
   1.000000  0.100000     0.000     0.000  1.000000  1.000000  1.000000  1.000000
$  SOFT      SOFSCS   LCIDAB    MAXPAR    SBOPT     DEPTH      BSORT     FRCFRQ
       2  0.100000         0  1.025000     0.000         3         0         1

*CONTACT_AUTOMATIC_SINGLE_SURFACE_ID
$^SELF FOAM (FOAM BLOCKS AND FOAM INSERT OF CRS)
$  SSID      MSID      SSTYP      MSTYP      SBOXID      MBOXID      SPR      MPR
   3040071         0         2
$  FS        FD        DC        VC        VDC        PENCHK      BT        DT
   0.000     0.000     0.000     0.000     0.000         0     0.0001.0000E+20
$  SFS       SFM       SST        MST        SFST       SFMT        FSF       VSF
50.000000 50.000000     0.000     0.000  1.000000  1.000000  1.000000  1.000000
$  SOFT      SOFSCS   LCIDAB    MAXPAR    SBOPT     DEPTH      BSORT     FRCFRQ
       0  0.100000         0  1.025000     0.000         2        100         1

```

*CONTACT_AUTOMATIC_SURFACE_TO_SURFACE_ID

\$^FOAM BLOCKS AND THE SIDE WALL

\$	SSID	MSID	SSTYP	MSTYP	SBOXID	MBOXID	SPR	MPR
	25040	24984	3	3				
\$	FS	FD	DC	VC	VDC	PENCHK	BT	DT
	0.400000	0.400000	0.000	0.000	0.000	0	0.0001	0.0000E+20
\$	SFS	SFM	SST	MST	SFST	SFMT	FSF	VSF
	1.000000	1.000000	0.000	0.000	1.000000	1.000000	1.000000	1.000000
\$	SOFT	SOFSC	LCIDAB	MAXPAR	SBOPT	DEPTH	BSORT	FRCFRQ
	0	0.100000	0	1.025000	0.000	2	0	1

APPENDIX E

Copyright permission

Permission for Reference 106

Tanya
you are welcome to use these figures (see below)
regards
Jude

----- Original Message -----

Subject: Re: Seeking Copyright Permission
Date: Tue, 12 Feb 2008 19:48:44 -0500
From: aaam1@aol.com
To: Judith.Charlton@muarc.monash.edu.au
References: <47B23C18.1090308@muarc.monash.edu.au>

Funny you should send this email. Tanya contacted us about another paper from 2003. She must be going through all of our proceedings for her research. It is absolutely fine to allow her to use the figures, parts of the proceedings for her purposes. I can write to her separate if you like. I'm sure we'd all like her to complete her thesis and get her degree.

Irene

-----Original Message-----

From: Jude Charlton <Judith.Charlton@muarc.monash.edu.au>
To: Irene <AAAM1@aol.com>
Sent: Tue, 12 Feb 2008 6:38 pm
Subject: [Fwd: Seeking Copyright Permission]

Irene

Are you able to advise here, please ? Have you had any experience with such copyright requests for use of material published in AAAM proceedings? The paper referred to here is from 2004 proceedings
thanks
Jude

----- Original Message -----

Subject: Seeking Copyright Permission
Date: Tue, 12 Feb 2008 00:26:39 -0800 (PST)
From: Tanya Kapoor <tanya151181@yahoo.com
<mailto:tanya151181@yahoo.com>>
To: Judith Charlton <judith.charlton@general.monash.edu.au
<mailto:judith.charlton@general.monash.edu.au>>

Dear Judith Charlton,

I have been writing my dissertation for my PhD degree in Mechanical Engineering at the University of Windsor , Ontario , Canada . Within the

Literature Review chapter of my thesis I would like to use Figure 2 in the publication "A Preliminary Evaluation of Child Restraint Crash Performance with Three Anchorage Systems in a Holden Commodore" to illustrate research done by other researches in my research area. I am requesting your permission to use these figures in my literature review

part. My dissertation would be printed in 5 copies. Two copies would be

deposited in the University of Windsor Library . One copy would be deposited in the Mechanical Engineering Department. The other two copies

would be given to individuals. An early response to this e-mail will be greatly appreciated.

Thank you very much!

Best regards,

Tanya Kapoor

Tanya Kapoor, Phd. Candidate
University of Windsor
Department of Mechanical, Automotive and Materials Engineering
401 Sunset Avenue, Windsor, Ontario, Canada N9B 3P4
Cell: +1 (519) 551-8285
Work: +1 (519) 253-3000 ext. 4786
Fax: +1 (519) 973-7007
Email: tanya151181@yahoo.com <mailto:tanya151181@yahoo.com>

-
Looking for last minute shopping deals? Find them fast with Yahoo! Search.

<http://us.rd.yahoo.com/evt=51734/*http://tools.search.yahoo.com/newsearch/category.php?category=shopping>

-- Judith L. Charlton, PhD
Senior Research Fellow
Accident Research Centre
Building 70, Clayton Campus
Monash University VIC 3800 Australia
tel +61 3 9905 1903
fax +61 3 9905 4363

Permission for References 32 and 108

Hi Tanya

I checked, and I believe that since that paper was in the ESV proceedings, which are published by NHTSA, they aren't copyrighted. As

long as you cite them, it's fine with me to use them.

Kathy Klinich

Tanya Kapoor wrote:

> Dear K. Klinich,

>

> I have been writing my dissertation for my PhD degree in Mechanical
> Engineering at the University of Windsor , Ontario , Canada . Within
> the Literature Review chapter of my thesis I would like to use
Figures

> 12 and 18 in the publication "Kinematics of the Q3s ATD in a child
> restraint under far side impact loading" to illustrate research done
> by other researches in my research area. I am requesting your
> permission to use these figures in my literature review part. My
> dissertation would be printed in 5 copies. Two copies would be
> deposited in the University of Windsor Library . One copy would be
> deposited in the Mechanical Engineering Department. The other two
> copies would be given to individuals. An early response to this
e-mail

> will be greatly appreciated.

>

> Thank you very much!

>

> Best regards,

>

> Tanya Kapoor

>

>

> Tanya Kapoor, Phd. Candidate

> University of Windsor

> Department of Mechanical, Automotive and Materials Engineering

> 401 Sunset Avenue, Windsor, Ontario, Canada N9B 3P4

> Cell: +1 (519) 551-8285

> Work: +1 (519) 253-3000 ext. 4786

> Fax: +1 (519) 973-7007

> Email: tanya151181@yahoo.com

Permission for Reference 55

The AAAM gives you permission to use the figures from the article you reference from our AAAM Proceedings in the manner and with the copies mentioned in your email below. However, please acknowledge copyright to AAAM and acknowledge the authors accordingly.

Good luck with your thesis.

Irene Herzau
AAAM Director
Association for the Advancement of Automotive Medicine

Tanya Kapoor wrote:

> Dear Sir/Madam,
>
> I have been writing my dissertation for my PhD degree in Mechanical
> Engineering at the University of Windsor, Ontario, Canada. Within the

> Literature Review chapter of my thesis I would like to use Figure 1
to
> Figure 9 in the publication "Factors leading to crash fatalities to
> children in child restraints" in Annu Proc Assoc Adv Automot Med.
> 2003;47:343-59 to illustrate research done by other researches in my
> research area. I am requesting your permission to use these figures
in
> my literature review part. My dissertation would be printed in 5
> copies. Two copies would be deposited in the University of Windsor
> Library. One copy would be deposited in the Mechanical Engineering
> Department. The other two copies would be given to individuals. An
> early response to this e-mail will be greatly appreciated.
>
> Thank you very much!
>
> Best regards,
>
> Tanya Kapoor/
> /
>
> Tanya Kapoor, Phd. Candidate
> University of Windsor
> Department of Mechanical, Automotive and Materials Engineering
> 401 Sunset Avenue, Windsor, Ontario, Canada N9B 3P4
> Cell: +1 (519) 551-8285
> Work: +1 (519) 253-3000 ext. 4786
> Fax: +1 (519) 973-7007
> Email: tanya151181@yahoo.com

VITA AUCTORIS

Ms. Tanya Kapoor was born on November 15, 1981 in New Delhi, India to Mr. Rakesh Kapoor and Mrs. Poonam Kapoor. She has one younger brother, Tushar Kapoor (b. 1984). She graduated her High school from Bal Bharati Public School, Delhi in 1999. From there she went to the Indira Gandhi Institute of technology, Indraprastha University, Delhi where she obtained a Bachelors of Technology (B.Tech) in Mechanical and Automation Engineering in 2003. She is currently a candidate for the Doctor of Philosophy degree in Mechanical Engineering at the University of Windsor and hopes to graduate in Winter 2008.